Heinrich Heine
Universität
Düsseldorf

Mathematical models of photosynthesis on multiple temporal scales

Inaugural-Dissertation

zur Erlangung des Doktorgrades

der Mathematisch-Naturwissenschaftlichen Fakultät
der Heinrich-Heine-Universität Düsseldorf

vorgelegt von
Tim Nies
aus Wuppertal, Deutschland

Düsseldorf Oktober 2023

aus dem Institut für Quantitative und Theoretische Biologie
der Heinrich-Heine-Universität Düsseldorf

Gedruckt mit der Genehmigung der
Mathematisch-Naturwissenschaftlichen Fakultät der
Heinrich-Heine-Universität Düsseldorf

Berichterstatter:

1. Prof. Dr. Oliver Ebenhöh
2. Dr. Shizue Matsubara

Tag der mündlichen Prüfung: 06.03.2024

Declaration of Authorship

Ich versichere an Eides statt, dass die Dissertation von mir selbstständig und ohne unzulässige fremde Hilfe unter Beachtung der "Grundsätze zur Sicherung guter wissenschaftlicher Praxis an der Heinrich-Heine Universität Düsseldorf" erstellt worden ist. Die Dissertation habe ich in dieser oder in ähnlicher Form noch bei keiner anderen Institution eingereicht. Ich habe bisher keine erfolglosen oder erfolgreichen Promotionsversuche unternommen.

Wuppertal, den

Tim Nies

Abstract

Photosynthesis is a pivotal process for many life forms on Earth, making light energy chemically available and fixing carbon dioxide into biomass. It is, hence, not surprising that many scientific investigations have been dedicated to unraveling the molecular mechanisms of photosynthesis with the aim of biotechnological exploitation or crop enhancement. To dissect these mechanisms, scientists use various experimental and computational methods. However, despite technological improvements and theoretical advancements, science is still far from fully comprehending all parts of photosynthesis. This lack of comprehension is partially due to the multiple time scales on which photosynthesis unfolds, rendering examining it challenging. In this thesis, I use the power of kinetic modeling to construct several frameworks and conduct *in silico* analyses to address questions focused on metabolic control, fluorescence signals, and photoprotection spanning a spectrum of temporal dimensions.

I start my analysis by looking at steady-state phenomena. Employing a model representation that conceptualizes photosynthesis as a supply-demand system, I identify shifts of metabolic control on carbon fixation depending on external conditions. Following this, I introduce a mathematical model of photoinhibition, a long-term (minutes to hours) photosynthetic process. With the developed computational framework, I derive hypotheses elucidating the mechanistic underpinnings of fluorescence changes observed during high light exposure of plants and their connection to photodamage and protection. Subsequently, my focus narrows to shorter temporal scales (microseconds to minutes) governing photosynthesis. By employing moderately rapid (seconds to minutes) non-photochemical quenching phenomena as a case study, I analyze how varying technical parameters in PAM experiments affect *in silico* replication. Finally, I will look at the rapid (microseconds to seconds) processes in photosystem II (PSII) to probe the connection between fluorescence and PSII state changes during measurements using a fast repetition rate technique.

All models of photosynthesis have undergone testing against experimental data. Each model can reproduce characteristic fluorescence traces observed during experimental measurements. Consequently, these models could serve as a critical part of larger modeling projects, representing photosynthesis. The appropriate model choice depends on the temporal scale for observing photosynthetic phenomena. I envisage that the presented use of previously published (steady-state and NPQ analysis) and new mathematical models (photoinhibition and fast repetition rate technique) will contribute to a deeper understanding of photosynthesis on many of its temporal scales and thus open new paths to sustainable agriculture and biotechnological exploitation of photosynthetic organisms.

Zusammenfassung

Die Photosynthese ist ein zentraler Prozess für viele Lebensformen auf der Erde, der Lichtenergie chemisch verfügbar macht und Kohlendioxid in Biomasse bindet. Es ist daher nicht verwunderlich, dass viele wissenschaftliche Untersuchungen der Entschlüsselung der molekularen Mechanismen der Photosynthese gewidmet sind, mit dem Ziel der biotechnologischen Nutzung oder der Verbesserung von Pflanzen. Um diese Mechanismen zu entschlüsseln, setzen Wissenschaftler verschiedene experimentelle und rechnerische Methoden ein. Trotz technologischer Verbesserungen und theoretischer Fortschritte ist die Wissenschaft jedoch noch weit davon entfernt, alle Teile der Photosynthese vollständig zu verstehen. Dies liegt zum Teil daran, dass die Photosynthese auf mehreren Zeitskalen abläuft, was ihre Untersuchung zu einer Herausforderung macht. In dieser Arbeit nutze ich die Möglichkeiten der kinetischen Modellierung, um verschiedene Rahmenwerke zu konstruieren und In-silico-Analysen durchzuführen, um Fragen zur Stoffwechselkontrolle, zu Fluoreszenzsignalen und zur Photoprotektion zu beantworten, die ein Spektrum zeitlicher Dimensionen abdecken.

Ich beginne meine Analyse mit der Betrachtung von stationären Phänomenen. Anhand einer Modelldarstellung, die die Photosynthese als ein System von Angebot und Nachfrage konzipiert, ermittle ich Verschiebungen der metabolischen Kontrolle der Kohlenstofffixierung in Abhängigkeit von äußeren Bedingungen. Anschließend führe ich ein mathematisches Modell der Photoinhibition ein, einem langfristigen (Minuten bis Stunden) photosynthetischen Prozess. Auf der Grundlage des entwickelten mathematischen Rahmens leite ich Hypothesen ab, die die mechanistischen Grundlagen der Fluoreszenzveränderungen, die bei starker Lichtexposition von Pflanzen beobachtet werden, und ihre Verbindung zu Lichtschäden und -schutz aufklären. Anschließend konzentriere ich mich auf kürzere Zeitskalen (Mikrosekunden bis Minuten), die die Photosynthese bestimmen. Indem ich mäßig schnelle (Sekunden bis Minuten) nicht-photochemische Löschphänomene als Fallstudie verwende, analysiere ich, wie sich unterschiedliche technische Parameter in PAM-Experimenten auf die *in silico* Replikation auswirken. Schließlich werde ich mich mit den schnellen (Mikrosekunden bis Sekunden) Prozessen im Photosystem II (PSII) befassen, um den Zusammenhang zwischen Fluoreszenz und PSII-Zustandsänderungen während der Messungen mit einer Technik mit hoher Wiederholrate zu untersuchen.

Alle Photosynthesemodelle wurden anhand experimenteller Daten getestet. Jedes Modell kann charakteristische Fluoreszenzspuren reproduzieren, die bei experimentellen Messungen beobachtet wurden. Folglich könnten diese Modelle als entscheidender Teil größerer

Modellierungsprojekte dienen, die die Photosynthese darstellen. Die Wahl des geeigneten Modells hängt von der zeitlichen Skala für die Beobachtung photosynthetischer Phänomene ab. Ich gehe davon aus, dass die vorgestellte Verwendung bereits veröffentlichter (Steady-State- und NPQ-Analyse) und neuer mathematischer Modelle (Photoinhibition und Fast-Repetition-Rate-Technik) zu einem tieferen Verständnis der Photosynthese auf vielen ihrer zeitlichen Skalen beitragen und somit neue Wege für eine nachhaltige Landwirtschaft und biotechnologische Nutzung photosynthetischer Organismen eröffnen wird.

Acknowledgements

Dum inter homines sumus, colamus humanitatem

Seneca

I want to thank Prof. Dr. Oliver Ebenhöh for being an excellent supervisor. You always were there when I had problems and needed encouragement. You have introduced me to the fascinating realm of photosynthesis and mathematical modeling, and your guidance has helped me along my scientific path. Also, a big thank you to (now) Jun.-Prof. Dr. Anna Matuszyńska. Your hard work and scientific enthusiasm toward nonphotochemical quenching have inspired me to learn more. You have also supported me in writing my first research paper; your assistance has been invaluable.

I want to thank Dr. Shizue Matsubara for your support and guidance provided during our meetings and discussions. My understanding of photosynthesis and fluorescence spectroscopic measurement has significantly increased thanks to your expertise. Moreover, I am incredibly grateful for allowing me to conduct my own experiment as a guest in your group. I would like to extend a big thank you to Ana Carolina dos Santos Sá and Yuxi Niu; with your help, it was much easier for me to get some usable data.

Next, I would like to thank Prof. Dr. Benjamin Stich and Prof. Dr. Berkley J. Walker. You generously provided me with the chance to explore different facets of plant science and offered me guidance during my time spent in your groups. Additionally, I would like to extend my sincerest appreciation to all of the members of your groups who contributed to making my visit a delightful experience.

I want to thank the Deutsche Forschungsgemeinschaft and the DFG-funded International Graduate School for Plant Science (IRTG 2466 "Network, exchange, and training program to understand plant resource allocation", NEXTplant) for their funding and for allowing me to extend my scientific experience on international conferences and research stays. Moreover, I want to thank all my peers in the graduate school. Your support and our exchange really helped along the way.

Then a big shout-out to all the current and former members of the QTB group. Thanks, Ellen and Thomas, for the hilarious conversation. Thanks, Ovidiu, for your help with all the statistical questions and all the wonderful celebrations you organized with Ellen. Also, thank you, Adélaïde, for

your support along the way and all your super delicious desserts. Yvan and Chilperic, talking with you was and is always a pleasure. You helped me improve my French while I maybe made your German worse (...Nachttischlampe). Janina, I cannot say how thankful I was that you were always there when I had problems with my computer. I also really enjoyed all our conversations when I visited your office, and I hope you have a great time in the new place. Thank you, Marvin, for your help with all git-related and modelbase questions. You have the rare skill to make everything funny and seem to be easy. Also, a big shout-out to Nima. Also, you made work much easier, and your stories were always hilarious. Mara, thank you for all your help regarding administrational stuff, without you I would have been lost in bureaucracy.

Last but not least, I thank my family. You helped over the years in numerous instances. Through my yet brightest and darkest times, you were always there. This "Stisel" would never have made it so far without your constant encouragement.

Contents

List of Abbreviations

PAM	**P**ulse **A**mplitude **M**odulation
LIFT	**L**ight **I**induced **F**luorescence **T**ransients
FI	**F**luorescence **I**induction
PSII	**P**hoto**s**ystem II
PSI	**P**hoto**s**ystem I
PETC	**P**hotosynthetic **E**lectron **T**ransport **C**hain
CBB	**C**alvin **B**enson **B**assham cycle
PQ	**P**lasto**q**uinone
PC	**P**lasto**c**yanin
Fd	Ferre**d**oxin
NPQ	**N**on **P**hotochemical **Q**uenching

Dedicated to my family

Preface

Almost all life forms living on Earth depend on the sun's energy. However, the sun's energy that reaches us through radiation is not *per se* helpful in sustaining life. It must be transformed into usable forms that can drive biochemical processes. Most organisms are not able to do this. They depend on photosynthesis-conducting life forms, such as plants, algae, and some bacteria, that use specialized protein-pigment complexes embedded in membranes to capture the radiation energy, which is eventually stored in biochemically accessible energy equivalents. Photosynthetic organisms use the captured energy to fix carbon dioxide into biochemical compounds. These compounds are the building blocks on which new biomass forms. The carbon fixation process happens at most places where life exists on Earth. Whether in deserts, rain forests, or milder climatic zones, photoautotrophic organisms with specialized carbon fixation mechanisms evolved.

Considering light energy capturing (energy supply) and carbon sequestration (energy demand) as both parts of photosynthesis, photosynthesis can be regarded as a so-called supply-demand system. However, to function efficiently, a supply-demand system must be tightly coordinated. Efficient coordination is challenging for photosynthetic organisms because they are constantly exposed to variations in abiotic factors, such as light intensity. Even worse, an imbalance in abiotic factor exposure can lead to stress that eventually damages the molecular machinery of photosynthesis. Thus, processes evolved, facilitating the acclimation to external factors. Because photosynthesis is the basis of new biomass and, hence, the groundstone for agriculture, biotechnological applications, and many pharmaceutical products, it is unsurprising that human society had an early interest in understanding how photosynthetic organisms function. Much work was conducted to understand photosynthesis and research in this area has a long history. However, photosynthesis is challenging to investigate because it combines various biophysical and biochemical phenomena on multiple temporal scales, making a complete understanding difficult.

This thesis uses kinetic modeling to understand photosynthetic processes on multiple temporal scales. All these processes are connected to acclimatory phenomena that help photosynthetic organisms tackle issues they face in continuously changing light environments. In the first part of this thesis, comprising chapters 1, 2, and 3, I will introduce the molecular background

of photosynthesis, fluorescence spectroscopic measurement techniques, and kinetic modeling as my chosen method. The second part presents the scientific work. Here, various models were built and used to investigate the connection between light changes and photosynthetic performance. I investigated the effects of prolonged exposure to high light, inducing photoinhibition, the rapid light changes in the LIFT technique, the moderate light changes in a quencher induction-relaxation analysis using PAM, and long-term/steady-state light exposure on photosynthesis (chapters 4, 5, 6, and 7). This work would not be possible without much collaborative effort that helped me along the way, providing me with computational and experimental resources. The thesis ends with a discussion of the findings obtained in the preceding chapters

Chapter 1

Photosynthesis: basis of life on different temporal scales

Photosynthesis is one of the most critical processes on Earth. By utilizing light energy from the sun in the form of radiation, photosynthesis leads to the formation of ATP and NADPH. These products of the so-called photosynthetic electron transport chain (PETC) are used to fuel, among others, reactions of the Carbon-Benson-Bassham cycle (CBB cycle), which is responsible for carbon sequestration. Classically, photosynthesis is divided into the light reaction, which supplies energy, and the dark reaction, which fixes carbon dioxide (CO_2). However, it is well known today that dark and light reactions are interdependent and both are regulated and driven by light-dependent activities. Therefore, it was proposed by some authors to treat photosynthesis as an energy storage process that consists of four phases. "(1) light absorption and energy delivery by antenna systems, (2) primary electron transfer in reaction centers, (3) energy stabilization by secondary processes, (4) and synthesis and export of stable products" (Blankenship, 2021). To achieve an efficient energy storage process, all parts of photosynthesis must be regulated. Hence, not surprisingly, complex regulatory mechanisms and protein complexes finely tuned to their function evolved. This chapter provides a basic overview of the history, molecular complexes, and processes connected to photosynthesis. It ends with a discussion of the different temporal scales of photosynthesis and the open questions tackled in this thesis.

1.1 History of photosynthesis

The history of photosynthesis research started several centuries ago and deserves a small recapitulation. In the following, I will use the timeline presented in the book "Molecular Mechanisms of Photosynthesis" by Robert E.

Blankenship as a foundation (Blankenship, 2021) of following section. Because photosynthesis is such a rich topic in which many excellent scientists have worked, it is clear that a short presentation of the history of photosynthesis research must be limited to a few key findings. The dismission of some findings is not meant to say that they are less critical for advancing our understanding of photosynthesis but simply due to the necessity to keep this section short. Other excellent reviews can be consulted for a detailed introduction to the history of photosynthesis, such as, e.g., Govindjee, Shevela, and Björn, 2017 or Stirbet et al., 2019.

1.1.1 Early developments

Today, the scientific community knows a lot about photosynthesis and connected processes. However, enormous hard work by many excellent scientists was needed to reach the current state of detailed knowledge with which we can understand and manipulate plants for food security, agriculture, and horticulture. Although already **Aristotle** (384-322 BC) and especially his pupil **Theophrastus** (371–287 BC) wrote about the nature of plants in their writings, the history of modern photosynthesis research only began in the 17^{th} century with the work by the Flemish physician **Jan Baptista van Helmont** (1577-1644). Van Helmont discovered that a willow tree, he had observed over five years, gained around 76 kg while the soil in which the plant lived weighed the same after the experiment. Because only water was added to the willow tree, van Helmont concluded that the tree biomass came from water. Even so, his conclusion was only partially correct from a modern standpoint, van Helmont was the first to investigate plant growth systematically.

The period between 1771 and 1804 led to the first unbalanced chemical equation of photosynthesis:

$$\text{carbon dioxide + water + light} \rightarrow \text{organic matter + oxygen}$$

This equation could be derived from the work of scientists who focused on the importance of oxygen, water, light, and carbon dioxide. The Swedish chemist **Carl Scheele** (1742-1786) was the first to isolate oxygen, but **Joseph Priestly** (1733-1804), an English minister, found the connection between plants and oxygen with his famous candle mouse experiment. The Dutch

physician **Jan Ingenhousz** (1730-1799) and his rival **Jean Senebier** (1742-1809), a Swiss minister, discovered the importance of light and carbon dioxide. The importance of the last part in the unbalanced photosynthetic equation, water, was discovered by **Nicolas de Saussure** (1767-1845). Balancing the chemical equation was only possible when modern chemistry became widespread in the scientific community. **Jean Baptiste Boussingault** (1802-1887) was the first to determine a photosynthetic quotient of 1 and to conclude that the organic matter involved in photosynthetic processes is likely carbohydrates. Following this, the German plant physiologist **Julius van Sachs** (1832-1897) showed that starch, a carbohydrate, accumulates only in illuminated leaves with the help of photography. Using these results, eventually, a minimally balanced equation could be proposed,

$$CO_2 + H_2O \longrightarrow (CH_2O) + O_2.$$

1.1.2 Building a mechanistic understanding

Establishing the chemical equation of photosynthesis was the impetus for further discoveries that were only reachable when the knowledge and technical skills of the plant physiology and biochemistry community became more advanced. An important next step was the idea that photosynthesis is a redox process driven by light. This central idea of photosynthesis, which led to predictions such as that oxygen comes from H_2O and not from CO_2, was introduced by the Dutch microbiologist **Cornelis van Niel** (1887-1985, Van Niel, 1941). This was accompanied by the research of **Robert Hill** (1899-1991), who attempted to separate photosynthesis's reduction and oxidation reaction. Hill's experiment aimed to see whether an isolated chloroplast can conduct photosynthesis (Hill, 1939). However, in doing so, he also introduced the Hill reaction, the reduction of artificial electron acceptors, and O_2 production in photosynthesis research. The following milestones were the Emerson and Arnold experiments. **William Arnold** (1904-2001) and **Robert Emerson** (1903-1959) used very short light flashes, something that new technical advances made possible, and manometry to investigate photosynthesis. They could convincingly show that photosynthesis is divided into two parts: the light and dark stage. While the light or photochemical reactions are rapid, the dark reactions are enzyme-catalyzed and, thus, much slower.

In further experiments, Emerson and Arnold also discovered the light intensity dependence for the photochemical stage of photosynthesis and estimated that only one O_2 is produced for every 2500 chlorophyll molecules (Emerson and Arnold, 1932a; Emerson and Arnold, 1932b). This finding was difficult to interpret during the time in which Emerson and Arnold conducted their experiments. However, it was essential for the later introduction of the so-called photosynthetic unit by Gaffron and Wohl, 1936.

From the 1940s until the 1960s, many aspects of photosynthesis research concentrated on establishing the minimum quantum requirement: the number of photons necessary for photochemistry. While the German biochemist **Otto Warburg** (1883-1970) was convinced that only three to four photons are necessary per O_2, his former student Emerson, and many others, obtained values of 8-10 photons (Nickelsen and Govindjee, 2011). By trying to decide between the two proposed quantum requirements, Emerson and his students discovered the red drop, a decrease in quantum yield (reciprocal of quantum requirement), when light above a specific wavelength in the far-red part of the spectrum is used. However, when this inefficient long-wavelength light is used with short-wavelength light, the photosynthetic rate (O_2-production) is much greater than usually observed (Emerson, Chalmers, and Cederstrand, 1957). The Dutch biophysicist **Louis Duysen** (1921-2015) gave a first clue for interpreting this so-called enhancement effect (Duysens, Amesz, and Kamp, 1961). He could show that far-red light causes cytochrome f to be oxidized while short-wavelength light reduces it.

1.1.3 The Z-scheme and the Calvin-Benson-Bassham cycle

Finally, when **Robert Hill** and **Fay Bendall** published the idea of two tandem photochemical systems in photosynthesis that was based on the redox potentials of cytochromes, H_2O and $NADP^+$ in the chloroplast, the start for the introduction of the modern Z (zigzag) scheme began (Hill and Bendall, 1960). Suddenly, many of the observed phenomena made sense; the observation by Duysen of the effects on photosynthesis by short- and long-wavelength light, the red drop and enhancement effect, could be explained by a different light preference for each photosystem, today known as photosystem II and photosystem I. The concept of two photosystems with different light preferences and electron carriers between them has been tested multiple times in the last 60 years and was repeatedly confirmed.

Parallel to the discoveries in the electron transport of the photochemical electron transport chain (PETC), many scientists worked on understanding the functioning of ATP synthesis after **Daniel Arnon** (1910-1994) showed that chloroplast could produce ATP in light by photophosphorylation (Arnon, Allen, and Whatley, 1954). The understanding of ATP synthesis culminated in the proposal of the chemiosmotic theory by **Peter Mitchell** (1920-1992, Mitchell, 1979). Our understanding of the so-called dark reaction of photosynthesis is based on the work by **Melvin Calvin** (1911-1997), **Andrew Benson** (1917-2015), and **James Bassham** (1922-2012). Using the technique of carbon isotope labeling ($^{14}CO_2$), feeding a labeled probe to algae, and following the formation of products, they could elucidate much of what is known today as the Calvin-Benson-Bassham cycle (CBB cycle, Bassham, Benson, and Calvin, 1950; Bassham et al., 1954).

This short history of photosynthesis is incomplete, and many exciting and essential discoveries were either left out or drastically shortened. For example, I did not mention the critical contributions to interpreting fluorescence changes, energy transfer phenomena, or observed non-photochemical quenching (NPQ) processes. Because some of these findings are critical for the work here, they are postponed to the introduction of the following chapters. The rest of the chapter is devoted to introducing the molecular building blocks of photosynthesis.

1.2 Molecular apparatus of the photosynthetic electron transport chain (PETC) in oxygenic organims

The molecular machinery of photosynthesis is a complex topic with many details. Profound knowledge collected over the last century describes all involved protein complexes' structure, localization, and mechanisms in the PETC and the CBB cycle. The classical representation of the PETC is a chain of protein-complexes inclusive pigments located in the chloroplast thylakoid membrane. Light energy is collected via antennae made from protein-pigment complexes and transferred to the reaction centers by radiation-less physical processes. Speaking in simple terms, due to the light energy, electrons from H_2O become available and are transferred through photosystem

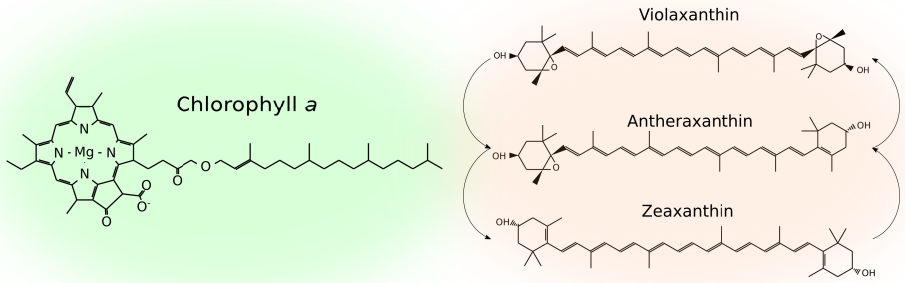

FIGURE 1.1: Two pigments important for photosynthesis: chlorophylls and carotenoids. The molecular structure of chlorophyll *a* and the carotenoids involved in the xanthophyll cycle are shown.

II, cytochrome b_6f, and photosystem I to ferredoxin via the electron carriers plastoquinone, and plastocyanin. The electron on ferredoxin is eventually passed on $NADP^+$ by the activity of the Ferredoxin:$NADP^+$ reductase to form NADPH (two electrons are needed). While the electrons are transferred in the PETC, protons, H^+, are transported from the stroma to the lumen, creating a pH gradient essential for ATP synthesis. ATP and NADPH then drive the carbon fixation mediated by the CBB cycle. This simplified view of the PETC as a linear chain helps to interpret experimental results or perform computer simulations. However, more and more evidence also suggests that the localization in the thylakoid membrane might play a critical role. The thylakoid membrane forms stacks, called grana lamellae, and non-stacked regions, called stroma lamella, in which the parts of the PETC are non-uniformly distributed (Anderson, 2002; Nevo et al., 2012; Kaňa, 2013).

1.2.1 Pigments

Photosynthesis would not be possible without the different pigment molecules connecting to the protein complexes in the PETC. Pigment molecules are an essential part of the antennae surrounding the photosystems and are necessary for multiple photoprotective mechanisms. In organisms like plants or cyanobacteria, we can distinguish two major groups of pigments involved in photosynthesis: chlorophylls and carotenoids.

Chlorophylls, that are denoted with the letter *a* to f, are planar five-ring structures derived from pyrroles, containing an Mg atom coordinated to four nitrogen atoms in the center (Rüdiger and Grimm, 2006; Hörtensteiner, 2013;

Taiz et al., 2015). Especially chlorophyll *a* and chlorophyll *b* are essential for photoautotrophic photosynthesis in plants, algae and some bacteria, that is the topic in this work. Chlorophyll *b* is structurally similar to chlorophyll *a* despite having a formyl group at the C-7 position instead of a methyl group. This difference has spectroscopic consequences, shifting chlorophyll *b*'s maximum absorption. Chlorophyll *b* is not located in the photosystems but is an essential part of the antenna/light-harvesting complexes as it contributes to the spectrum of light that can be absorbed to drive the PETC (Taiz et al., 2015; Blankenship, 2021).

The isoprene-derived carotenoids are prolonged molecules with a delocalized π-electron system, often with ring structures on both ends (Britton, 1995). Most carotenoids are orange-red, with a 400-500 nm absorption band. They function as auxiliary pigments that absorb and transfer light energy to chlorophylls. Additionally, some carotenoids are essential for photoprotective mechanisms, e.g., non-photochemical quenching or the quenching of triplet-excited chlorophylls. Especially zeaxanthin and violaxanthin, as part of the xanthophyll cycle, are involved in the dissipation of light energy as heat (Demmig-Adams and Adams III, 1996).

One of the pigments' most essential roles in photosynthesis is the formation of antennae around the reaction centers. Antennae effectively increase the efficiency of light energy collection. Using energy transfer, according to the Föster theory, (Forster, 1965), antenna complexes guide energy as exciton to the reaction centers, eventually triggering photochemistry. Modulation of the antennae and changes in their size around the photosystems, called state transition, is a photoprotective mechanism (Rochaix, 2011; Minagawa, 2011; Ebenhöh et al., 2014).

1.2.2 Photosystem II, Cytochrome b6f, Photosystem I

After the antennae collect the light energy, it is transferred to the reaction centers/ photosystems as an exciton. In the PETC of plants, two photosystems are involved, photosystems II and I (Fig. 1.2). Photosystem II forms dimeric supercomplexes (two photosystems) and consists of multiple proteins and pigments. Around 40 subunits, more or less depending on the species, with different functions are involved in forming photosystem II. Here, the D1 and D2 proteins are the core of photosystem II. The D1 protein is often damaged and must be repeatedly replaced. The general overall chemical reaction mediated by photosystem II can be formalized as follows:

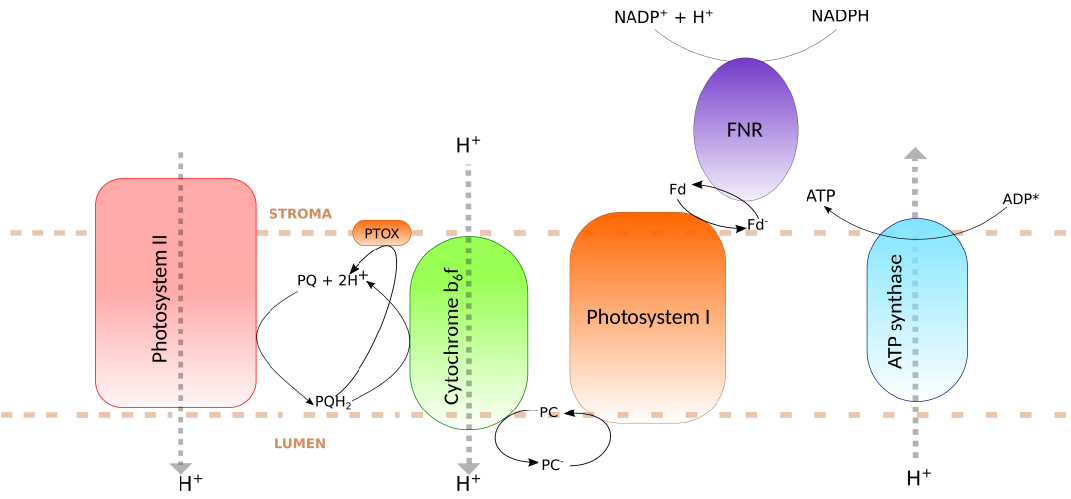

FIGURE 1.2: Simplified scheme of the photosynthetic electron transport chain

$$2\,H_2O + 2\,PQ + 4\,H^+ \longrightarrow O_2 + 4\,H^+ + 2\,PQH_2,$$

here PQ and PQH_2 stand for oxidized and reduced plastoquinone, the first electron carrier that brings electron from photosystem II to cytochrome b_6f. Reduced plastoquinone is also called plastoquinol. Photosystem II is unique in biology because it can oxidize water to molecular oxygen via its oxygen-evolving complex (OEC).

Through the hydrophobic part of the thylakoid membrane, the plastoquinones transport electrons that originate from H_2O to the cytochrome b_6f complex, which is vital for both the linear and cyclic electron flow in the PETC. The cytochrome b_6f complex consists of multiple subunits, including Rieske Fe-S proteins and pigments, and donates electrons to the copper protein plastocyanin (PC). Plasocyanin is located in the lumen of chloroplasts and transfers electrons to photosystem I, reducing the special pigment pair $P700^+$ that lost its electron due to excitation by light energy. The electron from P700 is channeled through three iron-sulfur-clusters and transferred to ferredoxin (Fd), which, together with the protein ferredoxin-NADP reductase (FNR), leads to the reduction of $NADP^+$ to NADPH. The overall reaction for this process is

$$2\,Fd_{red} + NADP^+ + H^+ \longrightarrow 2\,Fd_{ox} + NADPH.$$

Besides its function as an electron carrier, Fd is involved in the redox regulation of the PETC and CBB cycle enzymes via the thioredoxin system or other metabolic processes.

1.2.3 ATP synthesis

Driven by the electron transport through the PETC, protons (H^+) are channeled from the stroma to the lumen, creating a proton gradient. According to the chemiosmotic theory introduced by Peter Mitchell, this proton gradient is an essential part of the proton motive force (Δp), the total energy available for ATP synthesis. Δp consists of a chemical part (proton chemical potential) and a transmembrane electrical potential (Nicholls, 2013). The proton motive force can be written as,

$$\Delta p = \Delta\Phi - 59\Delta pH. \tag{1.1}$$

or

$$\Delta p = -\frac{2.3RT}{F}\Delta pH + \Delta\Phi. \tag{1.2}$$

$\Delta\Phi$ is the transmembrane electrical potential and ΔpH the pH difference across the thylakoid membrane. R is the ideal gas constant, F is the Farraday constant, and T is the temperature in Kelvin.

The protein that performs the ATP synthesis driven by the proton motive force is the ATP synthase. This multisubunit enzyme complex spans the thylakoid membrane and consists of two parts, CF_1 and CF_o (Junge and Nelson, 2015; Kühlbrandt, 2019). CF_1 and CF_o are often compared to a rotor-stator pair. The binding change mechanism proposed by Paul Boyer (Boyer, 2000) describes the formation of ATP. ADP binds at a particular site of the ATP synthase that can switch between multiple conformations necessary for the mechanisms of ATP synthesis. The conformational change is triggered by pumping protons through the ATP synthase. There are three binding sites for ATP, but the number of proton-binding sites (c subunits) is uncertain and currently estimated to be 14, leading to a H^+/ATP ratio of 4.67.

1.3 Calvin-Benson-Bassham (CBB) cycle

While the processes in the PETC lead to the formation of ATP and NADPH, two substances essential for metabolism, the CBB cycle fixes carbon dioxide (CO_2) and thus provides the basis for biomass. Although general principles are the same for most photosynthetic organisms, particularly plants, multiple versions of the same topic evolved. Here, I will focus on the carbon fixation processes found in C_3-plants and refer to other sources for an introduction

to C_4- and Crassulacean acid metabolism (CAM)-photosynthesis (Osmond, 1978; Cushman, 2001; Sage, 2004). For the C_4- and CAM-photosynthesis, the carbon dioxide fixation and formation of the first organic compounds are either spatially or temporally separated.

Many textbooks divide the Calvin-Benson-Bassham cycle into carboxylation, reduction, and regeneration phases (Taiz et al., 2015; Blankenship, 2021). In the carboxylation phase, ribulose-1,5-bisphosphate (RuBP) is carboxylated, forming two molecules of 3-phosphoglycerate. Ribulose-1,5-bisphosphate carboxylase/oxygenase, short RuBisCO, one of the most prominent enzymes in the biology of plants, performs this reaction. Current estimates indicate that over 99% of global carbon dioxide is fixed by RuBisCO (Raven, 2009). It is not surprising, therefore, that in the past, many scientific efforts focused on understanding this particular enzyme's activation, regulation, and control (Andersson, 2008; Parry et al., 2008). Even today, synthetic biology approaches are developed to improve the carbon fixation activity of RuBisCO with the aim of higher crop productivity (Erb and Zarzycki, 2016) and lowering a dangerous site reaction, the oxygenation of ribulose-1,5-bisphosphate. The oxygenation of RuBP results in the formation of one 3-phosphoglycerate and one 2-phosphoglycolate molecule. Especially 2-phosphoglycolate is a potent inhibitor of many CBB cycle enzymes and must be removed quickly to ensure an efficient carbon fixation (Kelly and Latzko, 1976; Flügel et al., 2017). To recycle 2-phosphoglycolate, 2-phosphoglycolate is channeled into a metabolic pathway called photorespiration, which involves reactions in the chloroplast, peroxisome, and mitochondrion. During photorespiration, fixed CO_2 is lost. Photorespiration is essential for C3-photosynthesis, but under the current atmosphere, estimates indicate that up to 30-40% of the total energy in C3-plants is consumed as a result of the photorespiratory pathway, with an additional loss of one-fourth of the net CO2 fixation rate (Sharkey, 1988; Walker et al., 2016).

In the reduction phase, enzymatic reactions utilize the ATP and NADPH from the PETC to form triose-phosphate by reducing 3-phosphoglycerate. Triose-phosphates like glyceraldehyde-3-phosphate and dihydroxyacetone phosphate are essential for the next steps in the CBB cycle but can also be exported to be used in other metabolic processes. The final phase of the

CBB cycle is the regeneration of RuBP. Around ten enzymatic steps are involved, including aldolase, transketolase, and phosphatase-mediated reactions. Computational analyses found that a critical controlling factor for carbon fixation is the regeneration phase reaction mediated by Seduheptolose-1,7-bisphosphatase (SPBase, Poolman, Fell, and Thomas, 2000).

If the triose phosphates are neither exported nor used in starch synthesis, the CBB cycle is autocatalytic. For this case, the overall reaction of the CBB cycle can be summarized as follows:

$$5\,CO_2 + 9\,H_2O + 16\,ATP^{4-} + 10\,NADPH \longrightarrow RuBP^{4-} + 14\,P_i^{2-} + 6\,H^+ + 16\,ADP^{3-} + 10\,NADP^+.$$

However, when triose-phosphates are used in other processes, we can write the following overall equation (compare Blankenship, 2021):

$$3\,CO_2 + 5\,H_2O + 9\,ATP^{4-} + 6\,NADPH \longrightarrow DHAP^{2-} + 8\,P_i^{2-} + 3\,H^+ + 9\,ADP^{3-} + 6\,NADP^+.$$

1.4 Non-photochemical quenching (NPQ) and photoprotection

When light energy falls on an active photosynthetic membrane, different pathways are available for how to process it (Fig. 1.3). In an ideal situation, all light energy is efficiently used in photochemistry, driving the formation of ATP and NADPH. However, this ideal scenario is most of the time not realistic.

Some light energy is re-emitted as fluorescence. Plant physiologists use fluorescence as an indicator of photosynthetic activity with a multitude of different spectroscopic methods (Kalaji et al., 2014; Kalaji et al., 2017). Other parts of the light energy are dissipated as heat and thus unavailable for photosynthesis (Muller, Li, and Niyogi, 2001). This dissipation of light energy as heat plays a critical role in photoprotection. If the energy supply by sun radiation exceeds the photosynthetic organism's demand, triplet excited chlorophyll can be created, forming reactive oxygen species (ROS, Khorobrykh et al., 2020). ROS damage the molecular machinery of the PETC and results in

TABLE 1.1: Reactions in the Calvin Benson Bassham cycle. Abrreviations: RuBisCO — ribulose 1,5-bisphosphate oxgenase/carboxylase; 3-PGA — 3-phosphoglycerate; 1,3-BPGA — 1,3-bisphosphoglycerate; GAP — glyceraldehyde 3-phosphate; DHAP — dihydroxyacetone phosphate; F16BP — fructose 1,6-bisphosphate; F6P — Fructose 6-phosphate; E4P— erythrose 4-phosphate; X5P — xylulose 5-phosphate; S17BP — sedoheptulose 1,7-bisphosphate; S7P — sedoheptulose 7-phosphate; R5P — ribose 5-phosphate; Ru5P — ribulose 5-phosphate; RuBP — ribulose 1,5-bisphosphate.

Enzyme	Reaction
Carboxylation	
1. RuBisCO	$RuBP + CO_2 + H_2O \longrightarrow 2\,3\text{-}PGA$
Reduction	
2. 3-Phosphoglycerate kinase	$3\text{-}PGA + ATP \longrightarrow 1,3-BPGA + ADP$
3. NADP-GAPD	$1,3-BPGA + NADPH + H^+ \longrightarrow GAP + NADP^+ + P_i$
Regeneration	
4. Triose phosphate isomerase	$GAP \longrightarrow DHAP$
5. Aldolase	$GAP + DHAP \longrightarrow F_{16}BP$
6. FBPase	$F_{16}BP + H_2O \longrightarrow F_6P + P_i$
7. Transketolase	$F_6P + GAP \longrightarrow E_4P + X_5P$
8. Aldolase	$E_4P + DHAP \longrightarrow S_{17}BP$
9. SBPase	$S_{17}BP + H_2O \longrightarrow S_7P + P_i$
10. Transketolase	$S_7BP + GAP \longrightarrow R_5P + X_5P$
11. Ribulose 5-phosphate epimerase	$X_5P \longrightarrow Ru_5P$
12. Ribulose 5-phosphate isomerase	$R_5P \longrightarrow Ru_5P$
13. Ru5P kinase	$Ru_5P + ATP \longrightarrow RuBP + ADP + H^+$

lower photosynthetic efficiency. Several protective mechanisms evolved that often dissipate excess light energy as heat to prevent this damage inflicted by ROS.

1.4.1 qE, qT, qI

The quenching of fluorescence due to processes other than photochemistry is collectively termed non-photochemical quenching. When first investigated, scientists classified the observed quenching of fluorescence traces into three modes, depending on their relaxation kinetic in the dark: qE, qT, and qI (Horton and Hague, 1988). Most of the molecular mechanisms behind these different modes of non-photochemical quenching are understood today. The high-energy quenching, qE, functions on a scale of seconds to minutes. The acidification of the lumen due to the action of the PETC triggers the protonation of PsbS and activates the xanthophyll cycle. The combined action of the protonated PsbS and the xanthophyll cycle leads to conformational changes

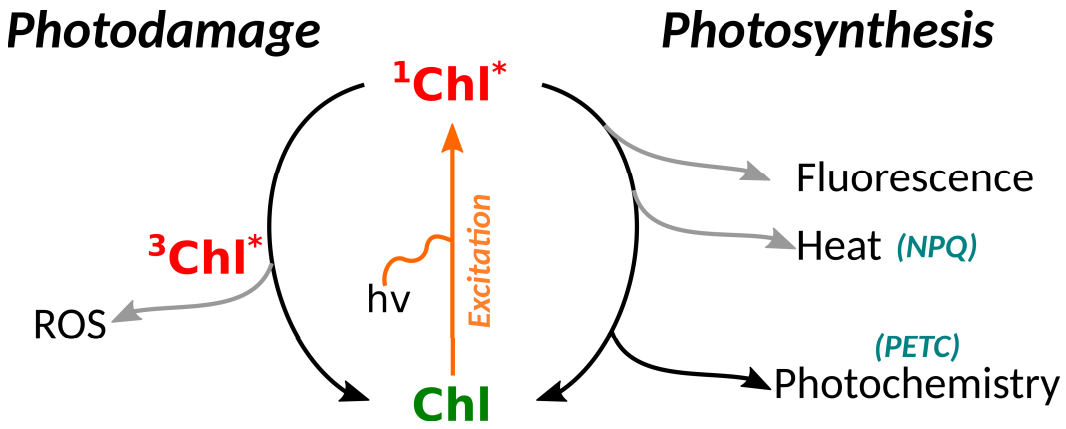

FIGURE 1.3: Ways in which light energy can be processed in photosynthesis. Light energy can be either used to drive photochemistry, is remitted as fluorescence or heat, and can lead to the formation of toxic reactive oxygen species (ROS) when triplet excited chlorophylls are formed from singlet excited chlorophylls. Photosynthetic electron transport chain (PETC) and Non-photochemical quenching (NPQ).

in photosystem II, increasing the dissipation of light energy as heat (Pfundel and Dilley, 1993; Gilmore, 1997; Muller, Li, and Niyogi, 2001). qT or "state transition", which operates over minutes, is the fluorescence quenching induced by redistributing the antenna complexes around photosystem II and photosystem I (Rochaix, 2011). The changes in the antenna sizes around the two photosystems regulate the relative light-absorbing cross-section. qI is the quenching of fluorescence associated with photodamage in photosystem II by excess light energy. Several hours are needed to repair damage in the molecular components of the PETC. This long repair time decreases photosynthetic efficiency (Aro, Kettunen, and Tyystjärvi, 1992).

1.4.2 Photoinhibition and the D1 protein repair cycle

As mentioned above, ROS species damage the molecular machinery of the photosynthetic electron transport chain. Multiple protein complexes are affected that are central to the electron flow. Especially proteins such as the D1 protein in photosystem II, PetD in the cytochrome b_6f, and the zeaxanthin epoxidase are susceptible to high light stress. The best-understood connection between the photodamage inflicted by high light and a high turnover rate ($> 0.5\,d^{-1}$, Li, Aro, and Millar, 2018) is associated with the plastidial genome-encoded D1 protein. Once the D1 protein has been damaged, phosphorylation of the PSII super complex facilitates its disassembly and migration to the stroma lamellae from its usual location in the chloroplast grana (Tikkanen et al., 2008). Several proteases are involved in the

following cleavage of the damaged D1 protein; the best characterized are the thylakoid membrane integral metalloprotease FTSH and DEG proteases (Kato and Sakamoto, 2018). The last step to a fully recovered PSII is translating nascent D1 protein and integrating it into the PSII complex. Recent results suggest that light-induced signals activate D1 protein synthesis via an autoregulatory cycle in which D1 protein damage leads to the mitigation of a repressive interaction of the D1 protein and translational activators (Chotewutmontri and Barkan, 2020). Photodamage repair is a highly costly process with approximately 1300 molecules ATP for replacing one D1 protein (Murata and Nishiyama, 2018; Raven, 2011). Photoinhibition is associated with a significant reduction in the maximum yield of photosystem II (F_v/F_m) when plants are exposed to high light stress for several hours. F_v/F_m is a derived parameter that can be calculated by taking the difference between maximal and minimal fluorescence divided by maximal fluorescence (for a more detailed definition see chapters 4 and 7).

1.5 Time scales of photosynthesis

I close this chapter by discussing the different time scales in photosynthesis. As seen by the broad spectrum of fields dealing with phenomena on different time scales, biology is a discipline investigating life from millions of years to femtoseconds. In this regard, photosynthesis is an interesting example in which rapid and slow processes work together to ensure an efficient energy supply for photosynthetic organisms. Photons excite the pigments located in the antenna complexes. The consequent transfer of the so-formed exciton is usually assumed to be in the range of femto- to picoseconds and is thus a very rapid process. The exciton induces a charge separation in the reaction centers between the specialized pigment pair (P680) and the first electron acceptor, Pheophytin (Pheo), in PSII. Charge separation and following stabilization occurs rapidly and competes with fluorescence emission and non-photochemical quenching. Those processes act on a time scale of pico- to nanosenconds. After charge separation and stabilization, the electron is driven through the PETC. The PETC combines multiple pigment-protein complexes and electron carriers between them. While most likely the processes in the pigment-protein complexes are very fast (see, for example, Khorobrykh et al., 2020), the diffusion of the electron carriers in and around the thylakoid membrane is much slower and thus a potential limiting factor

in terms of speed. Combined, the PETC spans a time range of several pico- to several milliseconds. With turnover rates of several milli-seconds to seconds for intermediates, the CBB cycle can be assumed to be much slower (Arrivault et al., 2009). Photoinhibition/damage leads to the damage of many proteins in the PETC that must be replaced. Some frequently damaged proteins, such as the D1 protein, have a very high turnover rate (Li, Aro, and Millar, 2018). Compared to the fast processes in the PETC, the synthesis and folding of proteins is a rather lengthy process of several seconds to minutes or even hours, leading to the long-lasting effects of photodamage. All theses processes combined, photosynthesis is a formidable example of how life evolved on different temporal scales. Each temporal scale requires differently adapted physical or biochemical processes that work together for the continuous functioning of photosynthesis.

1.6 Aim and Questions

The rate with which science currently progresses is unprecedented in history. Technological improvements in the last three decades allowed scientists to observe nature on previously inaccessible spatial and temporal scales. Upcoming new disciplines, like transcriptomics, genomics, proteomics, and metabolomics, resulted in vast and complex datasets that had to be organized in databases and for which new analysis techniques must be developed. Also, photosynthesis research and fluorescence spectroscopic measurements profited from the increasing technical possibilities, leading to more refined light sources with a high temporal resolution and big-scale phenotyping programs (phenomics). Not only did experiments take advantage of the current technological revolution, but theory also used the new information and computational power to improve its systems and mathematical descriptions of photosynthetic phenomena. However, science is far from a complete understanding of photosynthesis.

The work in this thesis uses kinetic modeling to understand photosynthetic processes on different time scales. Kinetic modeling is an ideal tool where experiments cannot proceed due to technical limitations. Broadly speaking, modeling is a way to formalize and order our knowledge about natural phenomena and derive new hypotheses. These hypotheses can then be tested experimentally. Especially with the new technical advancement, it becomes increasingly possible to measure all temporal scales on which photosynthesis takes place. A systematic understanding of all photosynthetic

processes and their connection to those different temporal scales is necessary to develop new strategies to increase the economic output we can achieve from photosynthetic organisms by biotechnological manipulation. In addition to experiments, theory can help derive hypotheses about potential targets worth testing for, e.g., reaching a higher crop yield. Thus, the connection between experiment and theory will only become tighter in the future of plant science, necessitating better communication between the experimental and theoretical photosynthesis research communities.

With the help of kinetic modeling, the work in this thesis tries to contribute to the following open questions on different temporal scales of photosynthesis:

1.6.1 Long-term time scale: What controls steady-state photosynthesis?

Photosynthesis is a supply-demand system. The PETC represents the supply side, making light energy chemically available as ATP and NADPH. The CBB cycle represents the demand side, fixating carbons into molecular compounds that are the building blocks for biomass. Over the years, multiple models have been created that either implement the PETC/ CBB cycle *in silico* or combine both parts of photosynthesis (e.g., Poolman, Fell, and Thomas, 2000; Morales et al., 2018b; Matuszyńska, Saadat, and Ebenhöh, 2019). By combining the PETC and CBB cycle, it becomes possible to explore the controlling factors for carbon fixation using metabolic control analysis. Various theoretical studies suggested different reactions as the central controlling factor of carbon fixation. Some suggest that the most critical reaction is mediated by RuBisCO, SBPase, or cytochrome b_6f. Others name the photosystems as responsible for the most control. Consequently, it is still not fully resolved what determines steady-state carbon fixation or whether it makes sense to talk of just one controlling factor. I used mathematical modeling to answer the question of the controlling factors for carbon fixation. To do so, I used a previously published model (Saadat et al., 2021) of photosynthesis represented as a supply-demand system and conducted a thorough metabolic control analysis under varying CO_2 and light conditions.

1.6.2 Slow time scale: How does quenching contribute to fluorescence signal changes during high light treatment?

Photosynthetic organisms are exposed to varying external abiotic factors, such as light, humidity, and temperature — especially the fluctuation of light influences photosynthetic performance. When the supply of light energy exceeds the demand of an organism, the molecular machinery of the PETC is damaged, leading to a long-lasting decrease in photosynthesis. The damaged compounds in the PETC must be replaced. However, this is a slow process. Hence, to prevent in advance the damage inflicted by high light, organisms evolved processes to dissipate light energy as heat. Classically, the extent of photodamage is measured using fluorescence spectroscopic devices, recording parameters such as the maximum yield of photosystem II (F_v/F_m), the minimal (F_o), and the maximal fluorescence (F_m). These parameters are not only influenced by the loss of PSII core function but also by quenching phenomena. However, how does quenching influence the observed fluorescence signal concomitantly with photodamage, and what makes the F_m or F_o signal decrease or increase? To find an answer to these questions, I developed and analyzed a mathematical model including the PETC, NPQ, and the D1 protein repair cycle and discussed different fluorescence yield models.

1.6.3 Moderate time scale: How can we overcome the experiment-theory gap in photosynthesis research?: example pulse amplitude modulation experiments

In photosynthesis research, fluorescence spectroscopic techniques have become the standard for evaluating the photosynthetic properties of organisms. Various techniques and devices were developed, enabling the straightforward and fast recording of fluorescence signals. One of the most commonly used techniques is pulse amplitude modulation (PAM), which uses pulsed measuring light and multiple light sources to measure fluorescence signals from photosynthetic organisms (for more details, chapter 2). Combined with saturation light pulses that close the reaction centers and actinic light, PAM is employed to measure critical parameters such as F_v/F_m, Φ_{PSII} and NPQ. It is not surprising, therefore, that multiple models and theories (Zaks et al., 2012; Matuszyńska et al., 2016) were developed that aim to explain the observed

fluorescence changes during a quenching analysis by considering the induction of non-photochemical quenching, a moderately fast process in photosynthesis.

However, to develop a reasonable theory, theoreticians must rely on the information about the experimental procedure provided in publications. While the information in the method sections of many publications is frequently sufficient for experimental replication, *in silico* replication sometimes needs more or other information than provided. This is a classic example of an experiment-theory gap. Here, I tackle the question of which consequences missing information has on the *in silico* replication of quenching analyses. I hypothesize that these consequences also extend to experimental replication (if the missing information is not part of the standard settings of commonly used devices).

I want to emphasize that this analysis to answer this question is not intended to attack established conventions to denote fluorescence spectroscopic experiments. Instead, it aims to encourage better communication between theoretical and experimental communities for improved *in silico* replication and understanding of experimental results.

1.6.4 Fast time scale: What contributes to rapid processes in the PSII during light-induced fluorescence transient experiments?

Fast-repetition rate (FRR)-based fluorescence spectroscopic approaches were developed to acquire photosynthetic parameters quickly. Initially used for aquatic organisms, they are nowadays also frequently used in plant research (see chapter 2). Light-induced fluorescence transients (LIFT) is a FRR-based approach that has been shown to approximate classical measurements of photosynthetic parameters in less time (Keller et al., 2019). Thus, LIFT is an ideal tool for large-scale phenotyping projects. But which processes in photosystem II and the PETC determine and how does quenching influence the LIFT fluorescence signal in its induction and relaxation phase? To answer these questions, I used an extended model of photosystem II based on Lazár et al., 1997 and combined it with a previously published mathematical representation of non-photochemical quenching (Matuszyńska et al., 2016). Using an extended model of photosystem II is necessary because the rapid

processes in photosystem II influence the LIFT fluorescence trace. By systematically varying the parameters associated with photosystem II, I tried to identify the most influential processes for the form of the fluorescence signal.

Chapter 2

Measuring photosynthesis

Photosynthesis is an essential process for the biosphere. It significantly impacts life's existence based on light, CO_2, and oxygen. Also, economically, photosynthesis is of utmost importance in determining, among others, the productivity of crop plants. It is not surprising that humans were, therefore, interested in what is critical for a good harvest and started investigating plants and their connection to light and air. Our current knowledge of photosynthesis is based on multiple theoretical investigations and experiments that elucidated each part of its molecular machinery. Especially chlorophyll *a* fluorescence and gas-exchange measurements helped understand the basic mechanisms of photosynthesis. This work is based on modeling and simulation of photosynthesis models but refers at some points to frequently employed experimental techniques in photosynthesis research. Therefore, this chapter briefly recapitulates the importance of fluorescence spectroscopic measurements in photosynthesis, its physical basis, and its applications. The chapter starts by explaining the physical concepts of fluorescence and mentions frequently employed techniques. It closes with a small recapitulation of the usage of gas exchange for the understanding of photosynthesis.

2.1 Fluorescence of photosynthetic organisms

The photosynthetic electron transport chain in and around chloroplasts' thylakoid membranes consists of pigment-protein complexes. Multiple different chemical species function as pigments. In particular, chlorophylls and carotenoids are the most important for photosynthesis; compare chapter 1. When absorbing light energy, chlorophyll *a* functions as a fluorophore, reemitting a part of the energy in the form of fluorescence. Fluorescence and phosphorescence are two kinds of the same physical concept, luminescence, which is the emission of light from a substance (Lakowicz, 2006). However, the physical details of both kinds of luminescence differ.

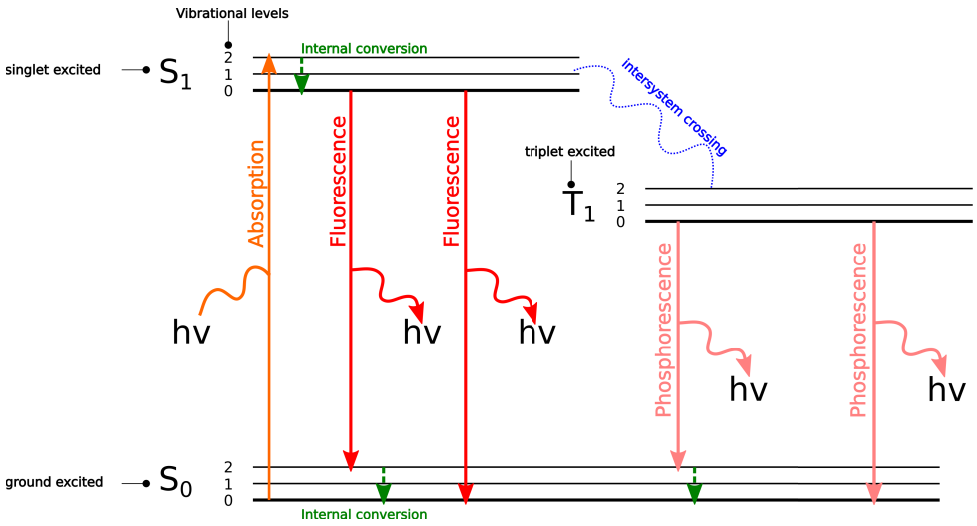

FIGURE 2.1: A Jablonsky diagram depicting the processes involved in fluorescence emission.

2.1.1 Physical basis

Fluorescence and phosphorescence are both kinds of luminescence. When a substance absorbs light energy, it is excited, and electrons are "transferred" to higher energetic orbitals. Fluorescence happens when one electron is in the singlet-state orbital after energy absorbance and paired with an electron with the opposite spin in the ground-state orbital. The return to the ground state is, thus, quantum mechanically allowed and occurs rapidly driven by the emission of photons. Fluorescence has, in general, a lifetime of nanoseconds (Lakowicz, 2006). In contrast to fluorescence, the emission of photons from triplet-excited substances is termed phosphorescence. In triplet-excited states, the higher energetic orbital electron has the same spin as the second electron in the ground state orbital. The return to the ground states is quantum mechanically forbidden, and thus, the emission of photons is slow. Phosphorescence has lifetimes of milliseconds to seconds (Lakowicz, 2006).

So-called Jablonski diagrams depict the ground and excited states of a substance capable of luminescence (Fig. 2.1). After the absorption of light energy, the electron is in a higher electronic state. Each electronic state is subdivided into multiple vibrational levels. After absorption, the electron is usually placed in a higher vibrational level of an excited electronic (energy) state. However, it quickly returns to the lowest vibrational level in a process called internal conversion. When emitting photons, the electron relaxes to the ground state in a high and returns to the lowest vibrational level. By spin-conversion, a molecule in a singlet excited state can be transformed into a triplet-excited state. This transformation from singlet to triplet state is

called intersystem-crossing. The energy of the fluorescence emitted by a substance is less than the energy absorbed. This so-called Stokes shift is based on the loss of energy in the form of heat when the electrons relax from high to low vibrational levels after being excited or returning to a different electronic state.

The quantum yield, a ratio of photons emitted and absorbed, is a number that quantifies the emission of fluorescence. It can be inferred by the rate constants of fluorescence emission (k_f) and other non-radiative decay processes (k_{nr}),

$$\Phi = \frac{k_f}{k_f + k_{nr}}. \tag{2.1}$$

Processes that increase the non-radiative rate constants and lower the fluorescence quantum yield are termed quenching. Quenching can happen in multiple ways, like colliding with other molecules in a reaction solution or forming non-fluorescence complexes. In photosynthesis, non-photochemical quenching is an essential protective mechanism that lowers the chance of photodamage by an over-supply of light energy. Although the activation and regulation of many quenching processes are known today, the molecular details of the quenching itself are often still under debate.

2.1.2 Sources of fluorescence in photosynthesis

In the PETC, chlorophylls and carotenoids absorb light energy as part of the antenna complexes and the photosystems. As a result, chlorophylls are the source of fluorescence, which we can observe with specialized devices. It is often assumed that at room temperature, most of the fluorescence signal originates from the physical processes in and around the chlorophyll *a* molecules associated with photosystem II. However, there is evidence that the pigments connected to photosystem I may contribute to the fluorescence signal after the photosynthetic membrane is exposed to light. Whether the contribution of photosystem I is high or low depends on the wavelength used for excitation and the investigated photosynthetic species (Pfundel and Dilley, 1993).

2.2 Different techniques used in photosynthesis research

The fluorescence emitted by processes associated with photosystem II is a rich source of information about the regulation and internal state of the molecular machinery in the PETC. Many different fluorescence spectroscopic techniques use this so-called variable fluorescence of photosystem II. With the advancement of our knowledge about photosynthesis and the technical possibilities, an increasing number of different devices and protocols were developed that modern scientists use to analyze the photosynthetic performance of organisms in several environmental conditions, sometimes in connection to exposing them to stressors. Using multiple light sources with different wavelengths and flashes of light makes it possible to infer the regulation mechanism for the pigment-protein complexes and redox states of electron carriers in the PETC. After Kautsky and Hirsch discovered the importance of fluorescence for photosynthesis research, many scientists worked on how to use fluorescence to understand plant systems. Today's techniques can be broadly classified into two groups using single turnover flashes (ST) or multiple turnover flashes (MT). Both saturate the Q_A-site of photosystem II using different intensities and lengths of saturating light flashes.

2.2.1 Fluorescence induction

Fluorescence induction (FI) is the most straightforward technique to study fluorescence phenomena in photosynthesis. A characteristic fluorescence trace can be observed when a dark-adapted sample of leaves or other photosynthetic tissue is rapidly transferred to a light environment. In this trace, different phases or characteristic points can be distinguished when plotted with logarithmic time, which we call O, J, I, P, S, M, and T phases (see chapter 7). The O (origin) point is the base fluorescence. After this, the fluorescence increases to the peak (P phase), thereby running through two intermediate inflection points (I and J). In plants and specific light conditions, the fluorescence decreases after the P phase, runs into a small plateau (S phase, semi-steady state), increases slightly (M phase, maximum), and falls to the final endpoint (T phase, terminal). Kautsky and Hirsch first discovered this specific form of the fluorescence trace after exposure to light. Scientists, therefore, call this phenomenon the Kautsky effect, and the corresponding fluorescence signals Kautsky curves (Kautsky and Hirsch, 1931; Kalaji et al., 2012).

With the help of FI experiments, the internal processes in photosystem II became more apparent, and the effect of many photosynthesis inhibitors could be studied.

2.2.2 Pulse amplitude modulation

One of the most frequently used techniques to measure photosynthetic processes connected to the photosynthetic electron transport chain is Pulse Amplitude Modulation (PAM) fluorometry (see chapter 6 and Schreiber, Schliwa, and Bilger, 1986). As described in Schreiber, 2004, devices using the PAM technique combine different beneficial properties that allow obtaining reliable fluorescence yield measurements of photosynthetic samples, e.g., 1) PAM devices have a very low light intensity pulse-modulated measuring light that does not activate photosynthesis, thus allowing fluorescence measurement in dark-adapted samples. 2) PAM devices can selectively distinguish between the measuring and actinic/ ambient light due to an amplifier rejecting non-modulated light. 3) PAM devices can measure rapid changes in the fluorescence signal.

Devices based on the PAM techniques can be used for a range of light protocols to detect different aspects of the electron flow in chloroplasts. One often used technique is the saturation pulse method for quenching analysis. Here, a dark-adapted sample is exposed to a relatively high light-intensity saturation pulse with a predefined duration. This saturation pulse is assumed to close all PSII reaction centers in the dark-adapted sample. Hence, the fluorescence signal should be maximal because no quenching process is yet activated (F_m). After a short period in darkness, actinic light is switched on to activate photosynthesis and concomitant quenching processes. Eventually, the actinic light is switched off, and the experiment continues in dark conditions. During the actinic and following dark phase, saturation pulses are applied to measure maximal fluorescence in light conditions (F_m'). F_m' is determined by the number of closed reaction centers and quenching processes. The obtained fluorescence signal can be used to derive parameters that give information about the extent of non-photochemical quenching or quantum yield of PSII. The light protocol in the saturation pulse method can vary depending on how fine-grained the researcher wants the measurement to be and whether the researcher wants to record quenching relaxation.

2.2.3 Fast repetition rate (FRR) fluorescence and light-induced fluorescence transients

Fast repetition rate (FRR) fluorometry is a technique suited for rapidly acquiring essential fluorescence parameters, giving information on the photosynthetic status of an organism (Kolber, Prášil, and Falkowski, 1998; Kolber et al., 2005). FRR fluorometry is appropriate for the *in situ* measurement of the fluorescence signal and, thus, might be suited for measuring in high-throughput phenotyping experiments. Initially devised for assessing photosynthesis in aquatic environments, FRR has also been used for terrestrial plants (Raesch et al., 2014). It has been shown that the fluorescence parameters measured with FRR agree with those obtained by more classical approaches (Keller et al., 2019).

In FRR fluorometry techniques, such as the light-induced fluorescence transient technique (LIFT), the photosynthetic sample is exposed to a train of subsaturating high-intensity light flashes (flashlets). These flashlets are used to probe fluorescence and excite photosynthetic processes. The duration of the flashlets can vary depending on the experiment and instrumentation but are generally 1.6 µs long. Due to their microsecond application, the flashlets are subsaturating despite their light intensity. In the LIFT technique, two phases can be distinguished. In the induction phase, flashlets are equally spaced and used to progressively close PSII reaction centers (Q_A). The duration of the induction phase varies depending on the protocol but frequently lasts only a few hundred microseconds (e.g., 0.75 ms). In the relaxation phase, the flashlet frequency decreases exponentially. The kinetics of the fluorescence signal is then assumed to rely on the electron transfer processes between the first stable and second electron acceptor (Q_A, and Q_B) and further downstream processes.

2.3 Gas-exchange measurements

Besides fluorescence, gas-exchange measurements are one of the most important means for obtaining more information about photosynthetic activity in plants and aquatic cultures of photosynthetic organisms. Although not the main focus of this thesis, the following paragraph outlines the measurement procedure as it is an integral part of the work of plant physiologists, and many modeling efforts have been built upon gas-exchange experiments.

A plant leaf is an open system constantly exchanging CO_2, O_2, and water vapor with its environment. However, to reach the chloroplast's location where photosynthesis occurs, these gases must diffuse through multiple obstacles, determining their concentration in the intercellular air space of the leaf. Stomatal aperture and mesophyll resistance are the most critical factors limiting the gas concentration in the leaf-air spaces. Much research is ongoing to decipher how and to what extent stomatal and mesophyll conductance (reciprocal of resistance) and their ratio help regulate photosynthetic efficiency and minimize the inevitable water loss associated with leaf gas exchange (Farquhar and Sharkey, 1982; Flexas et al., 2012). In many procedures to measure gas exchange, the leaf is clamped in a leaf chamber connected to a technical device that isolates it from the environment. Plant physiological processes alter the composition of the air flowing into the leaf chamber. The device determines the airflow. Net photosynthesis and leaf transpiration are derived on a leaf area basis by measuring CO_2 and water vapor in the inflowing and the outflowing air stream of the leaf chamber. These derived parameters are then used as a starting point for calculating other variables. The derivation of the net photosynthesis and other quantities is based on model representations of photosynthesis, which can vary in complexity depending on the application and instrument used for the measurement (Farquhar, Caemmerer, and Berry, 1980; Von Caemmerer and Farquhar, 1981).

Chapter 3

Modeling photosynthesis

Understanding the cause and reason of natural phenomena has always been the ultimate goal of science. Recently, we have seen a significant increase in our understanding of nature, thanks to the advancement in technical possibilities and computational power. Nowadays, with the help of genomics, proteomics, and metabolomics, the collection of extensive data sets is possible. However, with experiments' ever-increasing temporal and spatial resolution, interpreting observations has become more challenging. In a sense, science became more complex. Here, mathematical models can help to understand complex processes and connections that are not readily investigated by experimental methods. Today, mathematical modeling has become an integral tool for most of biology. This chapter first introduces the rationale behind modeling in general, followed by a basic introduction to kinetic models. Finally, models of photosynthesis and connected processes are presented that are the foundation for the work in this thesis.

3.1 Modeling: a tool to understand the natural world

The investigation of nature with mathematical models has long been applied in the physical and more recently (within the past approx. 40 years in comparison to several hundred years) in the biological sciences. The key to building a mathematical representation of a natural phenomenon is the reduction to its core components. By doing so, the researcher can ignore superfluous details unnecessary for answering the research question. There are two main approaches to model building. The first is the so-called top-down approach, in which mathematical modeling starts with data from which the metabolic

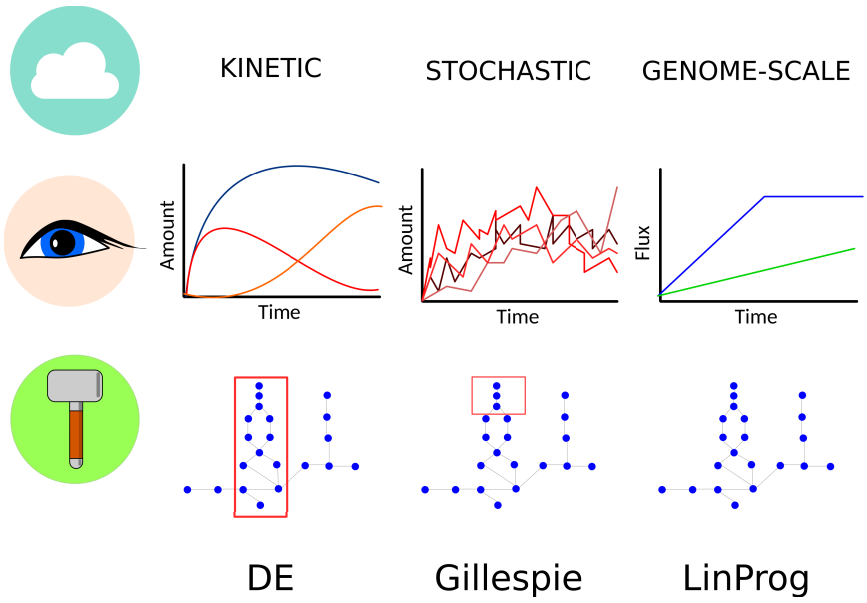

FIGURE 3.1: Visualization of different modeling paradigms, their output, and the underlying mathematical background.

network structure is deduced. The second is the bottom-up approach: inspired by the knowledge about a phenomenon, the researcher builds a mathematical model that qualitatively reproduces some experimental observations. With the so-constructed model, new hypothesis and *in silico* experiments are generated and conducted, respectively.

After choosing the model-building approach, the researcher has to decide on a modeling technique (Figure 3.1). Multiple different mathematical techniques that successfully describe natural phenomena are available. Besides more logic-based approaches, like boolean networks (Wang, Saadatpour, and Albert, 2012), many models in the biological sciences are based on the kinetic, genome-scale, or stochastic paradigm. In the kinetic approach, the researcher constructs computational models with differential equations that describe the change of a variable over time. Due to increasing computational capabilities, several software programs that solve the model in a reasonable time are available today. The second approach is stochastic modeling. Stochastic techniques simulate stochastic movement of biomolecules and reactions, inclusive uncertainties due to thermic effects or other unpredictable influences. Frequently the Gillespie algorithm is used to simulate stochastic phenomena (Gillespie, 2007). However, due to its complexity, the molecular process that can be simulated is limited in size, or high-computational power is needed. In contrast to kinetic or stochastic modeling, the genome-scale approach uses the available information obtained in the whole genome/proteome/metabolome of an organism. This approach

constructs a metabolic network, thereby paying attention to thermodynamic constraints, and eventually solves for an optimal flux distribution using linear programming and a question dependent optimization function that is to maximize or minimize under the assumption of being in a steady state (Palsson, 2015).

3.2 Kinetic modeling

Kinetic models are based on dynamical system theory and differential equations. They produce *in silico* representation of natural phenomena over time. Many different types of differential equations exist. Linear ordinary differential equations are often found to describe gene expression or metabolic models and are the simplest form. When the researcher aims to describe a metabolic network more realistically, enzyme-mechanism-based rate laws are used that introduce nonlinearities in ordinary differential equation systems. This nonlinearity can lead to dynamic behaviors one could not anticipate with linear systems. Besides nonlinearities, time-dependent influxes or perturbations could be included, making the system time-dependent or non-autonomous. The mathematics to understand non-autonomous or/and nonlinear systems used in biological modeling is more involved than for linear systems, meaning that the researcher is often only left with simulation to study the model. Other kinds of differential equations are, for example, differential-algebraic-equations, partial differential equations, or integrodifferential equations that account for algebraic, spatial, or temporal constraints.

The models used in this thesis are kinetic models that either use nonlinear differential or differential-algebraic equations. Modeling metabolic phenomena, such as the PETC or the CBB cycle, often follows a strict structure that consists of three parts: the stoichiometric matrix, the flux vector of rate laws, and the resulting change over time of the involved chemical species. The latter is obtained by multiplying the stoichiometric matrix N by the vector of fluxes v. The model can, thus, be presented with following simple form:

$$\frac{dS}{dt} = Nv \tag{3.1}$$

3.2.1 Stoichiometry

The stoichiometric matrix N describes the structure of the underlying metabolic network. The matrix consists of m rows and n columns corresponding to the numbers of metabolites and reactions, respectively. The stoichiometric matrix contains essential information about the metabolic pathway that considerably constrains the system's dynamic behavior. In the left nullspace, that is, all metabolite vectors for which

$$0 = cN, \tag{3.2}$$

we can find conservation relations — metabolite combinations that are constant when we observe the system. In the right nullspace, that is, all flux vectors for which the steady state assumption is true,

$$0 = Nv, \tag{3.3}$$

we find all steady state flux distributions structurally allowed in the metabolic pathway. Using these fluxes, we can identify strictly coupled metabolic reactions/fluxes in the system using the concept of enzyme subsets or its generalization reaction correlation coefficients. Under the assumption that we are in a steady state, the stoichiometric matrix is also the basis of one of the fundamental analyses for genome-scale models, flux balance analysis.

3.2.2 Rate laws

The vector v contains the rate laws that determine the fluxes through the edges of the metabolic network. In pure chemical or gene expression networks, these rate laws are frequently assumed to be of mass-action form. This form allows, in some cases, a mathematical treatment of the dynamics. However, in mass-action rate laws, second-order interactions also quickly introduce nonlinearities. Chemical networks with mass-action rate laws are investigated in chemical reaction network theory (Feinberg, 2019). By chemical reaction network theory, theorems can be derived that predict the dynamic behavior of the network's metabolites by its structure alone. In a biochemical reaction network, the rate laws often follow saturating functions, such as the Michaelis-Menten, uni-uni, bi-uni, bi-bi, or ping pong form (e.g., see Cleland, 1963). These rate laws are based on the mechanism of the enzyme responsible for the catalysis of the reaction. They are commonly derived using the

King-Altman algorithm (King and Altman, 1956). All rate laws are functions of their substrates and some additional parameters that describe the half-saturation concentrations (K_m) and the maximum velocities (V_m). Also, activation and different inhibition terms can be introduced, increasing the number of necessary parameters and changing the dynamic behavior.

3.2.3 Parameters and Simulations

For the construction of kinetic models, parameters are an essential part. However, the modeler faces the difficulty of sparse information for the concrete numerical values of all parameters in a metabolic network. Therefore, parameters in a kinetic model are often taken from multiple available sources with sometimes varying experimental setups and model organisms. Furthermore, models must often be validated and parameters estimated using fitting procedures to experimental data indirectly connected to the necessary parameters. This fact is not a limitation of the usefulness of models, but the researcher should consider it when interpreting results. The uncertainty about parameter values is a long-lasting topic in the modeling community that is especially severe when the mathematical representations of natural phenomena become more advanced. Therefore, researchers developed techniques that circumvent finding numerical values. One of the most prominent ones is structural kinetic modeling (SKM, Steuer et al., 2006). SKM samples elasticities from predefined distribution and then determines the dynamic stability using dynamic system theory through the Jacobian matrix of the metabolic network.

Having constructed a kinetic model is the first step. Now the metabolic network dynamics have to be investigated using techniques like Metabolic control analysis (MCA).

3.2.4 Metabolic control analysis (MCA)

Metabolic control analysis (MCA) is a concise theoretical framework developed during the last century and an inevitable tool in the toolset of metabolic modelers (Heinrich and Rapoport, 1974; Kacser et al., 1995). It provides precise definitions of controlling factors that determine the long-term dynamics in a biochemical pathway. MCA proposes different metrics for the control a reaction exerts in a metabolic network over the steady state metabolite concentrations or fluxes. The most important ones are the so-called normalized concentration ($C^{S_j}_{v_k}$) and flux control coefficients ($C^{J_j}_{v_k}$), which are system-wide

properties and, hence, depend on the characteristics of the whole metabolic network. They are defined as

$$C_{v_k}^{J_j} = \frac{v_k}{J_j} \frac{\partial J_j / \partial p}{\partial v_k / \partial p}, \tag{3.4}$$

and

$$C_{v_k}^{S_j} = \frac{v_k}{S_j} \frac{\partial S_j / \partial p}{\partial v_k / \partial p}, \tag{3.5}$$

here the steady state fluxes and concentrations are denoted as J_j and S_j, respectively. p is a kinetic parameter affecting only the reaction k with rate v_k directly.

Two of the most essential results in MCA theory are the sum and connectivity theorems. The sum theorems explain how the control on a steady state flux or concentration is distributed in the network:

$$\sum_{k=1}^{r} C_{v_k}^{J_j} = 1, \tag{3.6}$$

and

$$\sum_{k=1}^{r} C_{v_k}^{S_j} = 0. \tag{3.7}$$

The connectivity theorems combine the system-wide properties of the control coefficients with the local enzyme properties of elasticities. Elasticities describe how sensitive a reaction rate is to change in a parameter or concentration. For concentration changes, they are defined as

$$\varepsilon_{S_i}^{v_k} = \frac{S_i}{v_k} \frac{\partial v_k}{\partial S_i}. \tag{3.8}$$

The connectivity theorems are hence,

$$\sum_{k=1}^{r} C_{v_k}^{J_j} \varepsilon_{S_i}^{v_k} = 0, \tag{3.9}$$

and

$$\sum_{k=1}^{r} C_{v_k}^{S_h} \varepsilon_{S_i}^{v_k} = -\delta_{hi}. \tag{3.10}$$

Here δ_{hi} is the Kronecker symbol defined as,

$$\delta_{hi} = \begin{cases} 1, & \text{if } h = i, \\ 0, & \text{if } h \neq i, \end{cases}$$

for a deeper introduction to MCA see also Klipp et al., 2016.

3.3 Modeling in plant physiology

For a relatively short time (approx. last fifty years), models have been an integral part of plant physiological research. After introducing the basics of photosynthesis, its measurements, and modeling, the models used as the foundation for most of the work in this thesis are presented.

3.3.1 Models of the photosynthetic electron transport chain

The basis for most of the models used in this thesis are the mathematical models of the PETC constructed in Ebenhöh et al., 2011 and Ebenhöh et al., 2014. These models were used, changed, and adapted in multiple studies to investigate different aspects of electron flow, quenching, and state transition phenomena in plants and algae (Matuszyńska et al., 2016; Matuszyńska, Saadat, and Ebenhöh, 2019; Saadat et al., 2021). However, these models of the PETC are not the only mathematical description of photosynthesis (e.g., Zaks et al., 2012). Here, I will outline the parts of the photosynthesis model by Ebenhöh et al., 2014 most relevant to this work. Note that I write the equations based on the reduced states of the electron carriers and adapted some of the equations to present them in the form they were later used in Matuszyńska, Saadat, and Ebenhöh, 2019 and Saadat et al., 2021. Also, note that I will omit parts of the original models that are irrelevant to the work in this thesis.

The model by Ebenhöh et al., 2014 consists of multiple differential equations describing the electron carriers (plastoquinone, PQH_2; plastocyanin, PC^-; ferredoxin Fd^-), the lumenal proton concentration (H), and the stromal ATP (A) and NADPH (N) concentration dynamics.

$$\frac{dPQH_2}{dt} = v_{\text{PSII}} + v_{\text{cyc}} + v_{\text{NDH}} - v_{\text{b6f}} - v_{\text{PTOX}} \tag{3.11}$$

$$\frac{dPC^-}{dt} = 2v_{\text{b6f}} - v_{\text{PSI}} \tag{3.12}$$

$$\frac{dFd^-}{dt} = v_{\text{PSI}} - 2v_{\text{FNR}} - 2v_{\text{cyc}} \tag{3.13}$$

$$\frac{dN}{dt} = v_{\text{FNR}} - v_{\text{NADPHconsumption}} \tag{3.14}$$

$$\frac{dA}{dt} = v_{\text{ATPsynthase}} - v_{\text{ATPconsumption}} \tag{3.15}$$

$$b_{\text{H}} \cdot \frac{dH}{dt} = 2v_{\text{PSII}} + 4v_{\text{b6f}} - \frac{14}{3} v_{\text{ATPsynthase}} - v_{\text{leak}} \tag{3.16}$$

Photosystems and Fluorescence

As outlined in Ebenhöh et al., 2014, photosystem II (PSII) and photosystem I (PSI) are assumed to be much faster than the rest of the photosynthetic electron transport chain. This assumption allows us to treat the photosynthetic electron transport chain as a fast-slow system and algebraically solve the equations governing the dynamics in the photosystems under the assumption of being in steady state. Hence, photosystem II is represented as a four-state, and PSI is formulated as a three-state algebraic equation system. PSII includes open non-excited and excited (B_0, B_1) as well as closed non-excited and excited (B_2, B_3) states of PSII

$$-\left(k_{\text{LII}} + \frac{k_{\text{PQred}}}{K_{\text{eq,QAPQ}}} PQH_2\right) B_0 + (k_{\text{H}} + k_{\text{F}}) B_1 + k_{\text{PQred}} PQ \cdot B_2 = 0 \tag{3.17}$$

$$k_{\text{LII}} B_0 - (k_{\text{H}} + k_{\text{F}} + k_{\text{P}}) B_1 = 0 \tag{3.18}$$

$$k_{\text{LII}} B_2 - (k_{\text{H}} + k_{\text{F}}) B_3 = 0 \tag{3.19}$$

$$B_0 + B_1 + B_2 + B_3 = PSII^{\text{tot}}. \tag{3.20}$$

v_{PSII} is (see Matuszyńska, Saadat, and Ebenhöh, 2019,Ebenhöh et al., 2014)

$$v_{\text{PSII}} = c_{\text{PFD}} \cdot k_{\text{P}} \cdot B_1. \tag{3.21}$$

Here, k_{P}, k_{F} and k_{H} are the rate constants of photochemistry, fluorescence, and heat dissipation, respectively. The parameter k_{PQred} describes the reduction of plastoquinone at photosystem II. k_{LII} is the light activation rate constant of PSII that is determined either by the total light intensity alone or in combination with the relative cross-section of PSII. In many models the parameter c_{PFD} is set to be 0.5 (Matuszyńska et al., 2016; Matuszyńska, Saadat, and Ebenhöh, 2019; Saadat et al., 2021)
The fluorescence signal calculates as,

$$F = \frac{k_{\mathrm{F}}}{k_{\mathrm{F}} + k_{\mathrm{H}} \cdot Q + k_{\mathrm{P}}} \cdot B_0 + \frac{k_{\mathrm{F}}}{k_{\mathrm{F}} + k_{\mathrm{H}} \cdot Q} \cdot B_2. \tag{3.22}$$

Note that open and closed PSII are approximate with B_0 and B_2, because B_1 and B_3 acquire only small values during fluorescence transients.

The equation system for PSI is,

$$0 = \frac{dY_0}{dt} = k_{\mathrm{PCox}} \cdot PC^- \cdot Y_2 - \frac{k_{\mathrm{PCox}}}{K_{\mathrm{eq,PCP700}}} \cdot PC \cdot Y_0 - k_{\mathrm{LI}} Y_0 \tag{3.23}$$

$$0 = \frac{dY1}{dt} = k_{\mathrm{LI}} Y_0 - k_{\mathrm{Fdred}} \cdot Fd \cdot Y_1 + \frac{k_{\mathrm{Fdred}}}{K_{\mathrm{eq,PCP700}}} \cdot Fd^- \cdot Y_2 \tag{3.24}$$

Assuming that the total amount of PSI is conserved,

$$PSI^{tot} = Y_0 + Y_1 + Y_2, \tag{3.25}$$

the equation system for PSI can be solved to obtain steady-state expressions of the PSI states.

The rate of PSI is,

$$v_{\mathrm{PSI}} = k_{\mathrm{LI}} \cdot Y_0. \tag{3.26}$$

Here, Y_0, Y_1, Y_2 denote the fraction of open (P_{700}), excited ($P_{700}{}^*$) and oxidized ($P_{700}{}^+$) PSI. k_{PCox} and k_{Fdred} are the oxidation and reduction rate of plastocyanin and ferredoxin at PSI, respectively. k_{LI} is the light activation rate constant of PSI that is determined either by the total light intensity alone or in combination with the relative cross-section of PSI.

Cytochrome b_6f

The reaction mechanism of cytochrome b_6f is formulated as simple mass-action kinetics:

$$v_{\mathrm{b6f}} = max\left(k_{\mathrm{b6f}} \cdot \left(PQH_2 \cdot PC^2 - \frac{PQ \cdot PC^-}{K_{\mathrm{eq,b6f(H)}}}\right), v_{\mathrm{b6f}}^{\mathrm{min}}\right), \tag{3.27}$$

where $K_{\mathrm{eq,b6f(H)}}$ is a pH-dependent equilibrium constant and k_{b6f} the rate constant of the cytochrome b_6f-mediated reaction.

Ferredoxin-NADPH reductase

The Ferredoxin-NADPH is described as convenience kinetics (see Liebermeister and Klipp, 2006; Ebenhöh et al., 2014).

$$v_{FNR} = V_{\text{FNR}}^{\max} \cdot \frac{f^{-2} \cdot n^{+} - (f^2 \cdot n)/K_{\text{eq,FNR}}}{(1 + f^{-} + f^{-2}) \cdot (1 + n^{+}) + (1 + f + f^2) \cdot (1 + n^{+}) - 1} \tag{3.28}$$

here, $K_{\text{eq,FNR}}$ is the equilibrium constant determined by standard potentials. $V_{\text{FNR}}^{\max}$ is the maximum velocity of the FNR-mediated reaction and f, f^{-},n^{+} as well as n are:

$$f = \frac{Fd}{K_{\text{M,F}}},\ f^{-} = \frac{Fd^{-}}{K_{\text{M,F}}},\ n^{+} = \frac{NADP^{+}}{K_{\text{M,N}}},\ n^{=}\frac{NADPH}{K_{\text{M,N}}}, \tag{3.29}$$

where $K_{\text{M,i}}$ are K_M-values for ferredoxin and NADPH.

Cyclic electron flow

The model includes a simplified description of cyclic electron transport around photosystem I.

$$v_{\text{cyc}} = k_{\text{cyc}} \cdot (Fd^{-})^2 \cdot PQ, \tag{3.30}$$

where k_{cyc} is the rate constant of cyclic electron flow around PSI.

ATPsynthase

For the rate of ATP synthase, the description presented in Ebenhöh et al., 2011; Ebenhöh et al., 2014 was used,

$$v_{\text{ATPsyn}} = k_{\text{ATPsyn}} \cdot E \cdot \left(ADP - \frac{ATP}{K_{\text{eq,ATPsyn}}(H)} \right). \tag{3.31}$$

k_{ATPsyn} and $K_{\text{eq,ATPsyn}}$ are the rate constant and the equilibrium constant of the ATP synthase.
A pH-dependent activation ATP synthase was also included (compare Matuszyńska et al., 2016). The activation rate is

$$v_{\text{actATPsyn}} = k_{\text{actATPsyn}} \cdot H(PFD) \cdot (1 - E). \tag{3.32}$$

Deactivation is formulated as

$$v_{\text{deactATPsyn}} = k_{\text{deactATPsyn}} \cdot (1 - H(PFD)) \cdot E. \tag{3.33}$$

Here, H(PFD) is a function that is zero in dark and one in light conditions.

ATP and NADPH consumption

All processes that consume ATP and NADPH are combined into one equation each,

$$v_{\text{ATPcons}} = k_{\text{ATPcons}} \cdot ATP \tag{3.34}$$

and

$$v_{\text{NADPHcons}} = k_{\text{NADPHcons}} \cdot NADPH \tag{3.35}$$

Proton leak

The thylakoid membrane is assumed to be leaky for protons (Ebenhöh et al., 2014; Matuszyńska et al., 2016).

$$v_{\text{leak}} = k_{\text{leak}} \cdot (H - H_{\text{stroma}}) \tag{3.36}$$

PTOX

For the implementation of PTOX, a constant stromal oxygen concentration is assumed (O_2^{ext}).

$$v_{\text{PTOX}} = k_{\text{PTOX}} \cdot O_2^{ext} \cdot PQH_2 \tag{3.37}$$

Equilibrium constants

To include the electrical and pH-dependent contribution of the protonmotive force on the activities of the PETC, we calculated the equilibrium constants as outlined initially in Ebenhöh et al., 2014 and used in Matuszyńska et al., 2016; Matuszyńska, Saadat, and Ebenhöh, 2019; Saadat et al., 2021. I repeat the example outlined in Ebenhöh et al., 2014 for clarification. The overall reaction for cytochrome $_{\text{b6f}}$ is

$$\text{PQH}_2 + 2\,\text{PC} + 2\,\text{H}^+_{\text{stroma}} \rightleftharpoons \text{PQ} + 2\,\text{PC}^- + 4\,\text{H}^+_{\text{lumen}}.$$

We split the reaction into two redox half-reactions and one transport process:

$$\text{(a) } \mathrm{PQ} + 2\,\mathrm{e}^- + 2\,\mathrm{H}^+_{\mathrm{lumen}} \rightleftharpoons \mathrm{PQH_2}$$
$$\text{(b) } \mathrm{PC} + \mathrm{e}^- \rightleftharpoons \mathrm{PC}^-$$
$$\text{(c) } \mathrm{H}^+_{\mathrm{stroma}} \rightleftharpoons \mathrm{H}^+_{\mathrm{lumen}}$$

The overall reaction is the stoichiometric sum

$$-1 \cdot (a) + 2 \cdot (b) + 2 \cdot (c). \tag{3.38}$$

The contributions to the standard Gibbs free energy change are

$$\Delta G^o_1 = -2FE_o(PQ/PQH_2) + 2RT\ ln(10) \cdot pH_{lumen} \tag{3.39}$$
$$\Delta G^o_2 = -2FE_0(PC/PC^-) \tag{3.40}$$
$$\Delta G^o_3 = RT\ ln(10)(pH_{stroma} - pH_{lumen}). \tag{3.41}$$

Hence, according to the stoichiometric sum, the overall standard Gibbs free energy change amounts to

$$\Delta G^o = -\Delta G^o_1 + 2\Delta G^o_2 + 2\Delta G^o_3 \tag{3.42}$$

The equilibrium constant can be easily derived using ΔG^o.

3.3.2 Models of non-photochemical quenching

Light energy, collected by antenna complexes, drives photochemistry. However, when the light energy exceeds the demand for photochemistry, it can become dangerous for the photosynthetic organism and must be rendered harmless in other processes. Two processes are fluorescence emittance and heat dissipation (see chapter 1). Organisms can modulate the latter to deal with variations in external light conditions. Heat dissipation, the so-called non-photochemical quenching (NPQ), can influence crop yield. Hence, much scientific effort was dedicated to understanding quenching and its dynamics. Researchers built various mathematical models of the PETC, including different complex descriptions of non-photochemical quenching (e.g., Matuszyńska et al., 2016). Those models then helped answer questions about the molecular quenching mechanism and plant memory effects influencing the fluorescence signal obtained from photosynthetic organisms. The model by Matuszyńska et al., 2016, used partly in chapter 6 and chapter 7, is based on the description of the PETC in Ebenhöh et al., 2011 and Ebenhöh et al.,

2014. The main advancement of the model is a non-photochemical quenching module based on the combined effects of the xanthophyll cycle (violaxanthin and zeaxanthin) and the protonation of the PsbS protein. Downstream processes like the electron transfer mediated by cytochrome b_6f and photosystem I are combined into one lumped reaction. The ATP synthase is formulated according to Ebenhöh et al., 2011. Cyclic electron flows are implemented as simple mass action kinetics. The equations for quenching used throughout this work follow Matuszyńska et al., 2016:

Xanthophyll cycle

The description of the xanthophyll cycle only considers violaxanthin and zeaxanthin, ignoring antheraxanthin:
the rate of deepoxidation from violaxanthin to zeaxanthin is,

$$v_{\mathrm{VDP}} = k_{\mathrm{deepox}} \cdot \frac{H^{n_H}}{H^{n_H} + pH_{\mathrm{inv}}(K_{\mathrm{pHsatZ}})^{n_H}} \cdot V, \tag{3.43}$$

here pH_{inv} is afunction transforming lumenal pH values into lumenal proton concentrations.
The epoxidation rate from zeaxanthin to violaxanthin is,

$$v_{\mathrm{ZEP}} = k_{\mathrm{epox}} \cdot Z \tag{3.44}$$

PsbS protonation and deprotonation

Equations of protonation and deprotonation of PsbS are used from Matuszyńska et al., 2016,

$$v_{\mathrm{prot}} = k_{\mathrm{prot}} \cdot \frac{H^{n_L}}{H^{n_L} + pH_{\mathrm{inv}}(K_{\mathrm{pHsatLHC}})^{n_L}} PsbS \tag{3.45}$$

and

$$v_{\mathrm{deprot}} = k_{\mathrm{deprot}} \cdot PsbS^{p}. \tag{3.46}$$

Quencher

Quenching is formulated via a four-state quencher module. This module includes the xanthophyll cycle and the protonation state of PsbS. Each state is weighted by a parameter (γ_0, γ_1, γ_2, γ_3) and the Quencher activity is then calculated as,

$$Q = \gamma_0 \cdot (1 - Z_s) \cdot PsbS + \gamma_1 \cdot (1 - Z_s) \cdot PsbS^p + \gamma_2 \cdot Z_s \cdot PsbS^p + \gamma_3 \cdot Z_s \cdot PsbS, \tag{3.47}$$

where the contribution of zeaxanthin (Z_s) is (compare Matuszyńska et al., 2016),

$$Zs = \frac{Z}{Z + Kzsat} \tag{3.48}$$

3.3.3 Models of the Calvin-Benson-Bassham cycle

There are various models of the CBB cycle (Jablonsky, Bauwe, and Wolkenhauer, 2011). One of the most frequently mathematical descriptions of carbon fixation is based on the kinetic model by Pettersson and Ryde-Pettersson, 1988 that was later improved by Poolman, Fell, and Thomas, 2000. The model consists of all enzyme-catalyzed reactions in the CBB cycle. Most of the rates are formulated assuming a rapid equilibrium. Only the rate laws of RuBisCO, SBPase, FBPase and PRK follow a saturating equation with complex inhibition terms in the denominator. The model was successfully used to identify SBPase as one controlling factor in the PETC.

3.3.4 Supply-demand models of photosynthesis

Photosynthesis is a supply-demand system. The PETC represents the supply side by making light energy available as ATP and NADPH. The CBB cycle is the demand side consuming ATP and NADPH to fixate carbon dioxide (CO_2) that is the basis for the building blocks of new biomass. Researchers were interested in building an *in silico* description for the combined effects of the PETC and CBB cycle. One of these descriptions is the mathematical model developed by Saadat et al., 2021. Besides including the PETC and the CBB cycle, the ascorbate-glutathione and the thioredoxin system were implemented. Using this combined representation of the PETC-CBB-ASC network, the importance of cyclic electron flow around photosystem I was studied. Because the model by Saadat et al., 2021 integrates multiple processes involved in the acquisition of chemical energy and carbon fixation, thus encoding various complex relationships, it provides an ideal platform for understanding the control in photosynthesis as a supply-demand system.

This ends the introductory part. In the following, I will present the scientific work carried out in this thesis using the previously mentioned techniques and facts.

Chapter 4

What controls carbon sequestration in plants under which conditions?

This chapter is published in the journal Biosystems (Nies et al., 2023). I was involved in each step of the study. This includes the simulation, data analysis, visualization of the results, and writing all parts of the chapter/manuscript (Introduction, Methods, Results, Discussion). When the original manuscript referred to itself as "paper" or "article" this was changed to "chapter". Additionally, the repository was added to the main text.

Photosynthetic organisms use photosynthesis to harvest sunlight and convert the solar energy into chemical energy, which is then used to reduce atmospheric carbon dioxide into organic molecules. This process forms the basis of all life on Earth, and stands at the beginning of the food chain which feeds the world population. Not surprisingly, many research efforts are currently ongoing aiming at improving growth and product yield of photosynthetic organisms, and several of these activities directly target the photosynthetic pathways. Metabolic Control Analysis (MCA) shows that, in general, the control over a metabolic flux, such as carbon fixation, is distributed among several steps and highly dependent on the external conditions. Therefore, the concept of a single 'rate-limiting' step is hardly ever applicable, and as a consequence, any strategy relying on improving a single molecular process in a complex metabolic system is bound to fail to yield the expected results. In photosynthesis, reports on which processes exert the highest control over carbon fixation are contradictory. This refers to both the photosynthetic 'light' reactions harvesting photons and the 'dark' reactions of the Calvin-Benson-Bassham Cycle (CBB cycle). Here, we employ a recently developed mathematical model, which describes photosynthesis as an interacting supply-demand system, to systematically study how external conditions affect the control over carbon fixation fluxes.

4.1 Introduction

Photosynthesis classically has been divided into two parts. The 'light' reactions supply energy and reduction equivalents to the 'dark' reactions of the Calvin-Benson-Bassham (CBB) cycle (Bassham, Benson, and Calvin, 1950; Bassham et al., 1954), where carbon dioxide is fixed to form reduced carbon compounds used as building blocks in other metabolic processes. The CBB cycle (demand side) is one of the most critical pathways on Earth that plants and many other photosynthetic organisms use. Current estimates indicate that over 99% of global carbon dioxide is fixed by the key enzyme of the CBB cycle ribulose-1,5-bisphosphate carboxylase/oxygenase (RuBisCO) (Raven, 2009). However, the CBB cycle is not the only carbon fixation mechanism employed by photosynthetic organims, especially phototrophic prokaryotes. For instance, green sulfur bacteria fix carbon dioxide via a reversed tricarboxylic acid cycle or filamentous anoxygenic photorophs use a carbon fixation pathway known as hydroxyproprionate pathway for autotrophic growth (Fuchs, 2011). In this chapter, we focus on carbon fixation by the CBB cycle only.

To guarantee efficiency and prevent the formation of toxic reactive oxygen species, the supply (PETC) and demand (CBB cycle) of energy and redox equivalents must be coordinated (Matuszyńska, Saadat, and Ebenhöh, 2019). However, the habitats of photosynthetic organisms are usually characterized by a high fluctuation of abiotic factors, such as light intensity and CO_2 concentration (Kaiser, Morales, and Harbinson, 2018), which makes balancing the photosynthetic electron transport chain (PETC, supply side) and the CBB cycle challenging. Therefore, versatile regulatory mechanisms that coordinate carbon fixation and the PETC and adapt both processes to external conditions have evolved. Examples of regulatory mechanisms include non-photochemical quenching, the thioredoxin-dependent redox control of CBB cycle enzymes, and regulated changes in stomatal conductance (Farquhar and Sharkey, 1982; Muller, Li, and Niyogi, 2001; Geigenberger et al., 2017). These processes are currently targets of research activities aiming to increase plant performance and crop yield (Kaiser, Correa Galvis, and Armbruster, 2019).

Considering the importance of the PETC and CBB cycle it is unsurprising that much effort has been spent studying their kinetics regulation, and control by experimental and theoretical methods. Various mathematical models have been developed aiming at providing a theoretical framework

to analyze which factors determine the efficiency of carbon fixation (Hahn, 1986; Hahn, 1987; Pettersson and Ryde-Pettersson, 1988; Poolman, Fell, and Thomas, 2000; Jablonsky, Bauwe, and Wolkenhauer, 2011). Kinetic models of the CBB cycle established, e.g., the importance of the sedoheptulose-1,7-bisphosphatase (SBPase) for controlling carbon assimilation and provided theoretical explanations for a wide range of observed kinetic properties of RuBisCO (Poolman, Fell, and Thomas, 2000; Raines et al., 2000; Witzel, Götze, and Ebenhöh, 2010). Appropriate theoretical tools are needed to study control in metabolic networks, e.g., the CBB cycle and PETC. Metabolic control analysis (MCA) is a theoretical framework developed in the 1970s, which is continuously improved and generalized (Heinrich and Rapoport, 1974; Kacser et al., 1995; Heinrich and Schuster, 1996; Dourado and Lercher, 2020; Wilken et al., 2022). A major purpose of MCA is to quantify the influence that single enzymes have over the steady-state properties of metabolic networks. A central concept is the *control coefficient* which describes how small changes in activities of single steps affect stationary metabolites and fluxes. Because control coefficients depend on the dynamics of the interactions of all components, they are systemic properties. MCA has been repeatedly applied to study the control of reaction steps in plant metabolic pathways (Rohwer, 2012) with examples including applications to the benzoid pathway, sucrose accumulation, the CBB cycle, the electron transport chain, and combinations of these (Uys et al., 2007; Colón et al., 2010; Ebenhöh et al., 2011; Matuszyńska, Saadat, and Ebenhöh, 2019; Saadat et al., 2021).

Here we present an *in silico* analysis of how external conditions affect the control over carbon fixation fluxes. We focused in particular on the effect of two environmental parameters, light intensity, and CO_2 concentration, to assess how these factors affect the control of carbon fixation. Classically many studies stress the importance of RuBisCO and its activation processes as highly influential on photosynthetic efficiency (Stitt and Schulze, 1994). But is RuBisCO always the main controlling factor? For our analysis, we employ a published kinetic model of photosynthesis (see Fig. 4.6) that combines the PETC, the CBB cycle, and the Ascorbate-Gluthatione (ASC-GSH) cycle implemented in Python using the modelbase software package (Saadat et al., 2021; Aalst, Ebenhöh, and Matuszyńska, 2021). This model was originally used to study the importance of cyclic electron transport around photosystem I for photoprotection and also includes regulatory mechanisms, such as non-photochemical quenching, state transitions between the two photosystems, and redox regulation of CBB cycle enzymes through the thioredoxin

system. We began our analysis by using the stoichiometric structure of this combined model to conduct a reaction correlation analysis (Poolman et al., 2007), followed by the investigation of control on carbon fixation by different key processes in photosynthesis. We identified a condition-dependent shift in control and determined its structural origin using a robustness analysis with sampled parameter sets. Using the results from the robustness analysis, we could show that some reactions exert control in an either-or relationship while others may exert control simultaneously. With this work, we contribute to elucidating the control in photosynthesis and its dependence on external conditions.

4.2 Model and Methods

4.2.1 Model description

For the *in silico* analyses, we used a previously published model of photosynthesis (Saadat et al., 2021). This model (see Fig. 4.6) combines mechanistic descriptions of the PETC, and the CBB cycle, supplying and consuming ATP and NADPH. The model includes the regulation of CBB enzymes via thioredoxin and mechanisms responsible for producing and scavenging ROS around PSI. The scavenging of ROS is mediated by a module representing the ASC-GSH cycle. The analyses can be found in the repository https://gitlab.com/qtb-hhu/photosynthesis-task-force/2023-50-years-of-mca.

4.2.2 Metabolic control analysis

The flux ($C^{J_j}_{v_k}$) and concentration ($C^{S_j}_{v_k}$) coefficients are defined, as

$$C^{J_j}_{v_k} = \frac{v_k}{J_j}\frac{\partial J_j/\partial p}{\partial v_k/\partial p}, \tag{4.1}$$

and

$$C^{S_j}_{v_k} = \frac{v_k}{S_j}\frac{\partial S_j/\partial p}{\partial v_k/\partial p}, \tag{4.2}$$

where the steady state fluxes and concentrations are denoted as J_j and S_j, respectively. p is a kinetic parameter affecting only the reaction k with rate v_k directly. In the computational analyses, the control coefficients were numerically approximated using central difference and varying the parameter p by $\pm 1\%$.

4.2.3 Reaction dendrogram and Reaction correlation coefficients

A set of flux vectors satisfying the steady state condition,

$$\mathbf{Nv} = \mathbf{0}, \tag{4.3}$$

defines the null space of the stoichiometric matrix. A set of base vectors summarised in the kernel matrix **K**, in which they form the columns, span the null space. The kernel matrix can be obtained by the relation,

$$\mathbf{NK} = 0. \tag{4.4}$$

The reaction correlation coefficients were calculated following Poolman et al., 2007. The kernel matrix was orthonormalized using the Gram–Schmidt process implemented in the sympy (Meurer et al., 2017) package. For a pair of reactions and corresponding row vectors in the kernel matrix $\mathbf{k}_i$, and $\mathbf{k}_j$, the reaction correlation coefficients calculate as,

$$\phi_{ij} = \frac{\mathbf{k}_i \mathbf{k}_j^T}{\sqrt{\mathbf{k}_i \mathbf{k}_i^T}\sqrt{\mathbf{k}_j \mathbf{k}_j^T}}. \tag{4.5}$$

The dissimilarity matrix Δ_{ij}, describing the angle between the row vectors of the kernel matrix **K**, was obtained using the reaction correlation matrix

$$\Delta_{ij} = cos^{-1}(\phi_{ij}). \tag{4.6}$$

Hierarchical clustering, using Δ_{ij}, was conducted with the WPGMA algorithm implemented in the scipy package (Virtanen et al., 2020).

4.2.4 Robustness analysis

To analyze whether our previous results were due to the general properties of the system or due to the choice of parameters we performed a control analysis scan over 10000 sets of randomly perturbed parameters. The varied parameters were, 1) the total concentration of photosystem II and 2) photosystem I, 3) the rate constant of cytochrome b6f, 4) the rate constant determining the rate of cyclic electron flow and 5) the Mehler reaction, 6) the maximum velocities of RuBisCO, 7) FBPase, and 8) SBPase, as well as the rate constants of the 9) MDAR and 10) DHAR-catalyzed reactions. The model parameters were randomly multiplied by a factor 2^x, where x was drawn from a uniform

random distribution between -1 and 1. This results in a multiplication by a factor between 0.5 and 2. This analysis was performed for low/high CO2 and light conditions. To reduce the amount of unrealistic simulation we only used those parameter sets that lead to a 5 times higher or lower RuBP steady state concentration for further downstream analyses.

4.3 Results

4.3.1 Reaction correlation analysis

We begin our analysis by studying the constraints on stationary fluxes, which are imposed by the stoichiometry of the network alone. For this, we calculate reaction correlation coefficients (Poolman et al., 2007) for the previously published photosynthesis supply-demand model (Saadat et al., 2021). These coefficients provide a generalization of the concept of enzyme subsets. Reactions within one enzyme subset are strictly coupled in the sense that they always carry fluxes in a fixed proportion. For such reactions, the reaction correlation coefficient is ± 1, and the corresponding row vectors of the kernel matrix of the stoichiometry matrix are parallel. Reaction correlation coefficients generalize this idea by essentially calculating the angle between row vectors of the kernel matrix (for details, see Poolman et al., 2007), and therefore indicate how strong reactions are correlated as a result of structural constraints of a network. Fig. 4.1 presents a metabolic tree constructed by hierarchical clustering using dissimilarities calculated by the reaction correlation coefficients (see Methods). The matrix of reaction correlation coefficients ϕ can be found in the supplement (Fig. 4.7).

There exist ten enzyme subsets containing more than one reaction (table 4.1). Generally, reactions that function as regulatory control mechanisms (such as deprotonation / protonation of PsbS, and the xanthophyll cycle necessary for non-photochemical quenching, or the reactions involved in the redox control by thioredoxin), each form an enzyme subset. Three subsets are connected to the electron transport chain and ROS scavenging. The first subset consists of the reactions mediated by cytochrome b_6f and photosystem I, which are therefore strictly coupled. The second contains the Mehler reaction and ascorbate peroxidase, while the third consists of the remaining reactions of the ASC-GSH cycle. Four subsets can be assigned to the CBB cycle and starch synthesis. The largest subset contains eight reactions, including

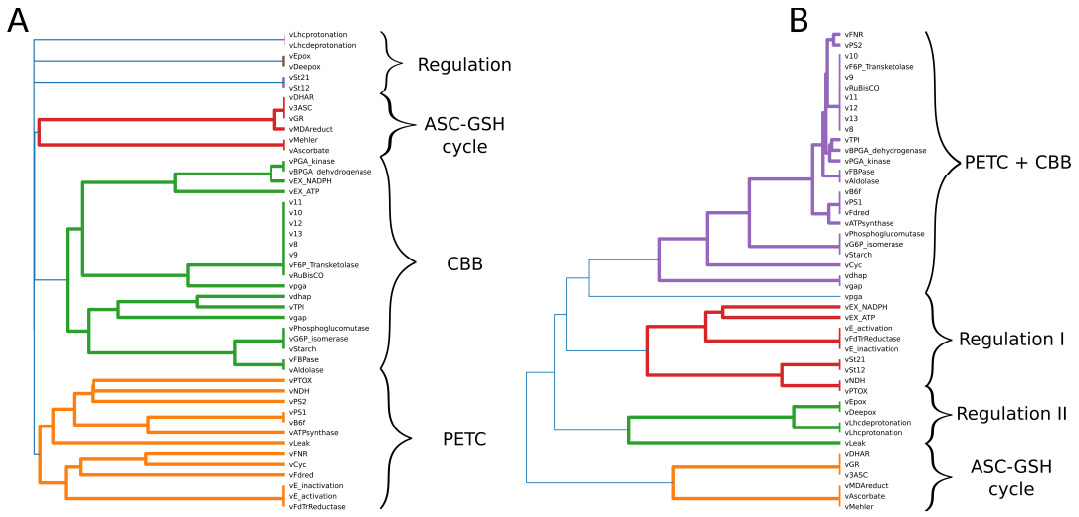

FIGURE 4.1: Metabolic trees, showing different metabolic clusters. The left tree was obtained by reaction correlation analysis. The right tree was obtained by steady-state flux correlation analysis for 10000 random parameter sets in low light intensity and low CO_2 concentration conditions for the kinetic model of photosynthesis. Abbreviations in the cluster annotations: PETC — photosynthetic electron transport chain, CBB — Calvin Benson Bassham cycle, ASC-GSH cycle — ascorbate-glutathione cycle.

RuBisCO, the transketolase reactions, and the reactions of the regeneration phase leading to the formation of ribulose-1,5-bisphosphate.

In Fig. 4.1, clusters of reactions, which are highly correlated but not strictly coupled, are indicated by different colors. We identify clusters that are associated with key metabolic functions, such as the PETC, the ASC-GSH cycle, and the CBB cycle. The CBB cycle is split into two pronounced subclusters, which can be associated with carbon fixation and carbon export, respectively. The same is true for the PETC, for which we can distinguish between the linear (photosystems II/I and cytochrome b_6f) and the cyclic electron flow. Interestingly, RuBisCO and PSII are grouped in different clusters, which suggests that these two processes are decoupled. This is unexpected because the electrons obtained by photosystem II are mainly used by the CBB cycle to fix carbon, therefore, one would expect highly correlated fluxes. This observation can be explained by considering that the stoichiometric analysis applied here is based on the full null space and completely ignores constraints on the stationary flux solutions by the kinetic parameters.

A kinetic model, however, drastically restricts the possible stationary fluxes by the specific parameter values of the dynamic equations. Therefore, actually observable steady-state fluxes will represent only a small subset of the complete null space. The processes decoupling reaction rates of RuBisCO and PSII, such as proton leak, terminal oxidases, etc., are constrained by their

kinetic parameters to carry only relatively small fluxes, such that, in fact, the correlation between RuBisCO and PSII rates should be high for realistic conditions. To test this assumption, we repeated the correlation analysis based on steady-state fluxes sampled from the kinetic model, in which the reference values of the rate constants have been randomly varied by a factor between 0.5 and 2. The rationale behind this is that now the stationary fluxes are restricted to solutions which are close to a reference state and therefore reflect a more physiologically relevant subset of the null space. The resulting tree is depicted in Fig. 4.1B. As expected, the fluxes of the CBB cycle and the PETC are now strongly correlated. We decided to use a factor of 2 as we assume it to be a realistic range achievable for biotechnological manipulation and short-term evolutionary processes. To test whether a higher factor would drastically change our results we repeated all analyses with a factor 5 (see figs. 4.8 to 4.14). Generally the analyses with a higher factor result in similar trends, but show larger variations. This is because, at least for some parameters, a factor of 5 is relatively high, leading to entirely different system behaviors than usually expected.

4.3.2 The control on carbon fixation switches between environmental conditions

We use metabolic control analysis (MCA) to quantify the control that individual molecular processes exert on the performance of the system, measured by the net carbon fixation rate, in different environmental conditions. We found that overall flux control is exerted mostly by one of four steps: photosystem I and II in the electron transport chain and RuBisCO and SBPase in the CBB cycle. In Fig. 4.2 we depict the four flux control coefficients on the overall carbon fixation rate for light intensities ranging from 50 to 1000 $\mu mol\, m^{-2}\, s^{-1}$and for CO_2 concentrations between 6 and 20 µM, corresponding to atmospheric concentrations between approximately 170 and 700 ppm. It is clearly visible that there are two distinct light regimes. A sharp transition between control by the light reactions (low light) to control by the dark reactions (high light) can be observed. Interestingly, the curve separating these two regimes corresponds to the limit where the quenching capacity reaches its maximum, and the lumen becomes highly acidic (see Fig. 4.15). As we observed and discussed previously (Saadat et al., 2021), this transition marks the saturation of the photosynthetic system, above which increasing light no longer facilitates higher carbon fixation rates. At the transition, the carbon

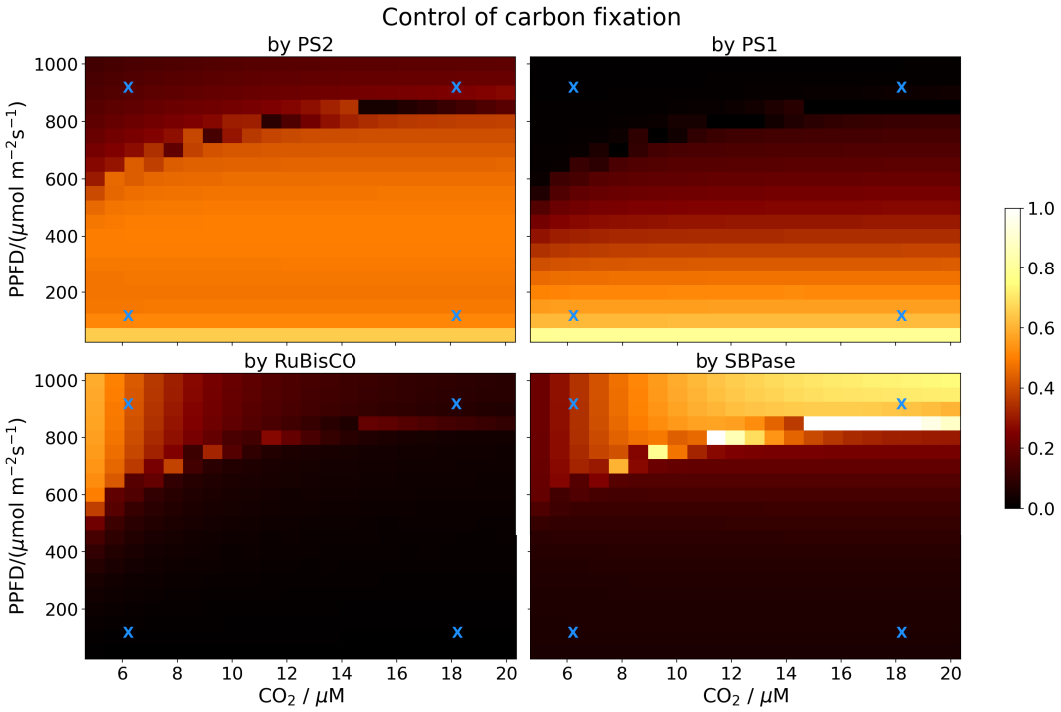

FIGURE 4.2: The flux control of PSII (top left), PSI (top right), RuBisCO (bottom left), and SBPase (bottom right) on carbon fixation in light intensities ranging from 50 to 1000 µmol m^{-2} $s^{-1}$and in CO_2 concentrations ranging from 5 to 20 µM. The control coefficients are indicated by the heat map with dark areas indicating low and light areas high control. The blue crosses are the reference points for the further analyses indicating low CO_2/low light (6 µM, 100 µmol m^{-2} s^{-1}), low CO_2/high light (6 µM, 900 µmol m^{-2} s^{-1}), high CO_2/low light (18 µM, 100 µmol m^{-2} s^{-1}), and high CO_2/high light (18 µM, 900 µmol m^{-2} s^{-1}).

fixation rate (and many other rates and intermediate concentrations) is not a smooth function of the incident light intensity. Therefore, the numerical differentiation employed to calculate the control coefficients may lead to imprecise results and as a consequence, the coefficients very close to the transition should be interpreted with care.

In the low light regime, both photosystems have substantial control whereas the CBB cycle enzymes exert almost no control. This changes drastically for higher light intensities, where PSI exerts practically no control and PSII only a small but distinguishable control, whereas the CBB cycle enzymes now control the carbon fixation rate. In high light, a gradual shift in control from RuBisCO to SBPase can be observed as CO_2 concentrations increase. SBPase has the highest control in high light intensities and high CO_2 concentrations, while RuBisCO is the dominant reaction in high light intensities and low CO_2 concentrations. High control of RuBisCO in high light and low CO_2 concentrations has also been found experimentally (Stitt and Schulze, 1994).

In summary, this analysis shows that the control on carbon fixation switches from photosystem I in low light to photosystem II in medium light intensities to SBPase and RuBisCO in high light intensities, where RuBisCO control dominates in low and SBPase control in high CO_2 concentrations. For our further analyses, we define four reference conditions for low CO_2 / low light (6 µM, 100 µmol m^{-2} s^{-1}), low CO_2 / high light (6 µM, 900 µmol m^{-2} s^{-1}), high CO_2 / low light (18 µM, 100 µmol m^{-2} s^{-1}), and high CO_2 / high light (18 µM, 900 µmol m^{-2} s^{-1}). These conditions are indicated by blue crosses in Fig. 4.2.

4.3.3 Control of photosynthetic intermediates

Besides the carbon fixation rate, also the states of the intermediates in the photosynthetic electron transport chain and the CBB cycle are important determinants for the efficiency and status of the photosynthetic system at large. In particular, poised redox levels of the electron carriers are indicative of the efficient functioning of the PETC, the concentrations of ATP and NADPH are important as ubiquitous energy and redox equivalents, and the CBB cycle intermediates must be above a certain level to ensure the cycle runs efficiently (Matuszyńska, Saadat, and Ebenhöh, 2019). Moreover, various mechanisms ensure that in particular in high light, photodamage by reactive oxygen species (ROS) is minimized.

The electron carriers behave as expected (see figs. 4.16 to 4.19). In general, upstream reactions have a positive control on their redox state, while downstream reactions exert a negative control. For example, the redox state of plastoquinone is strongly positively controlled by PSII, slightly positive by the cyclic electron flow (which feeds back electrons from ferredoxin to plastoquinone), and negatively or not at all by downstream processes, such as PSI or the CBB enzymes (see figure 4.16). The only electron carrier that is more reduced when the CBB cycle enzymes are increased is plastocyanin, which is in agreement with previous model analyses (Saadat et al., 2021) (Fig. 4.17). An interesting observation is that under low light, both ferredoxin and NADPH are less reduced if PSI activity is enhanced, although ferredoxin is a direct product of PSI (Figs. 4.18 and 4.19). A possible explanation for this counter-intuitive finding is that the cyclic electron flow is strongly increased with increasing PSI activity (Fig. 4.20) and that, together with the increased CBB activity (see above) this leads to a slight reduction of these two electron carriers. The control of ATP levels is complex (Fig. 4.21). For example, increased PSII leads to reduced ATP levels in very low light, increased in intermediate light (still below the quencher saturation threshold), and a slight reduction again for high light conditions. However, steady-state energy levels range between 0.6 and 0.8 (fraction of ATP in the adenosine phosphate pool), which are in the range of measured values (Stitt, Lilley, and Heldt, 1982). An interesting effect is observed when calculating the control on the total phosphates in CBB intermediates. Apparently, enhancing the fixation process (RuBisCO) leads to a reduction in CBB intermediates, whereas enhancing the recycling phase (SBPase) leads to an increase, except for very low light intensities (Fig. 4.22). ROS (simulated as stationary H_2O_2 concentrations) levels respond as expected. Increasing the photosystems leads to higher levels while increasing the cyclic electron flow the b_6f complex activity or the CBB cycle lead to reduced levels (Fig. 4.23).

4.3.4 Robustness of the control on carbon fixation in multiple environmental conditions

Control coefficients quantify the strength of control of individual processes in a metabolic network. They are system-wide properties and as such depend on the specific values of the kinetic parameters of the involved enzymatic reactions. Therefore, they should not be considered a rigid value independent

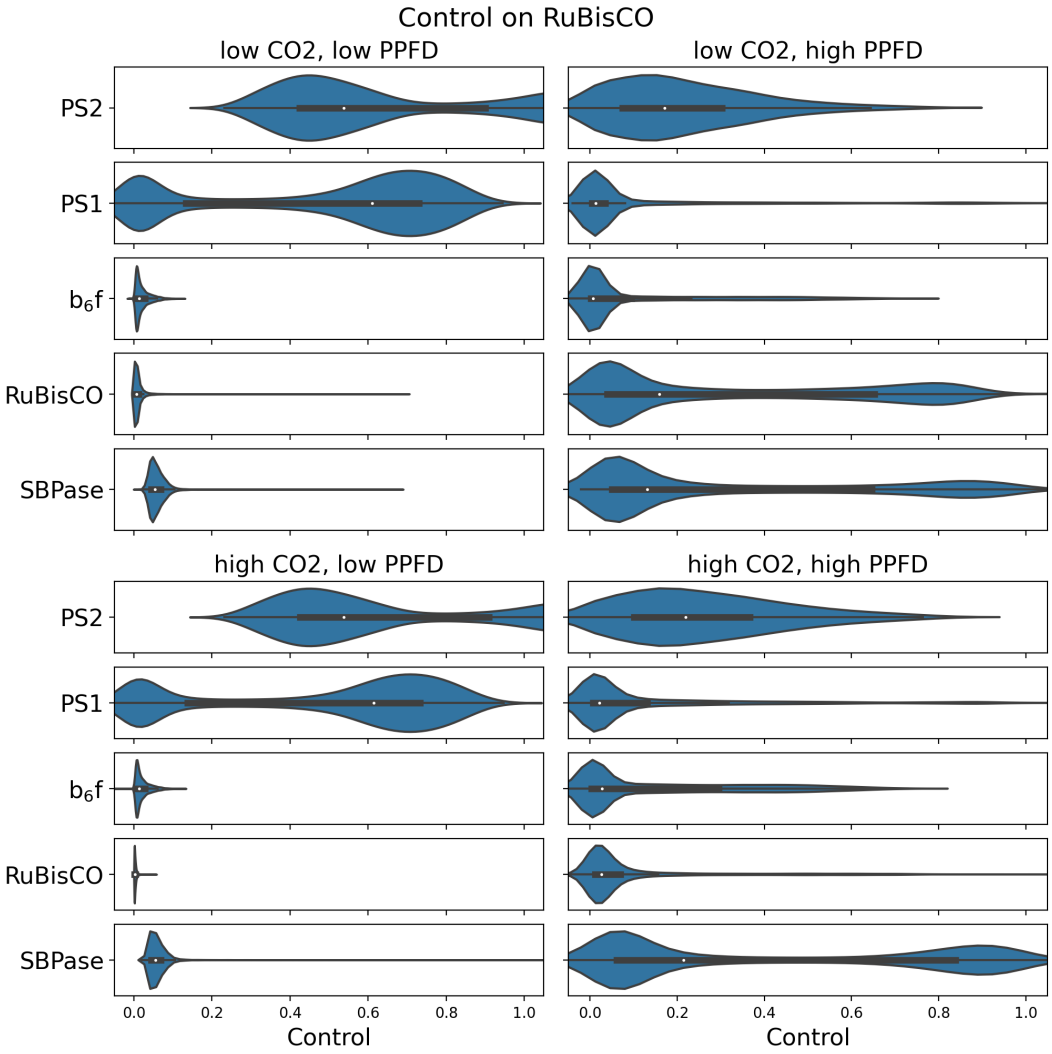

FIGURE 4.3: Distribution of flux control coefficients of key reactions in the PETC and CBB cycle on carbon fixation over 10000 sets of randomly perturbed parameters with a factor between 0.5 and 2. The shaded area shows the frequency of flux control coefficients. In all cases, the area was scaled to the maximum (including values outside the shown range) for clarity. The white dot indicates the median of the distribution and the bold part of the central line denotes the range between upper and lower quartile. Top left shows results under low CO_2 / low light conditions, top right under low CO_2 / high light, bottom left under high CO_2 / low light and bottom right under CO_2 / high light conditions. Only flux control coefficients between 0 and 1 are shown.

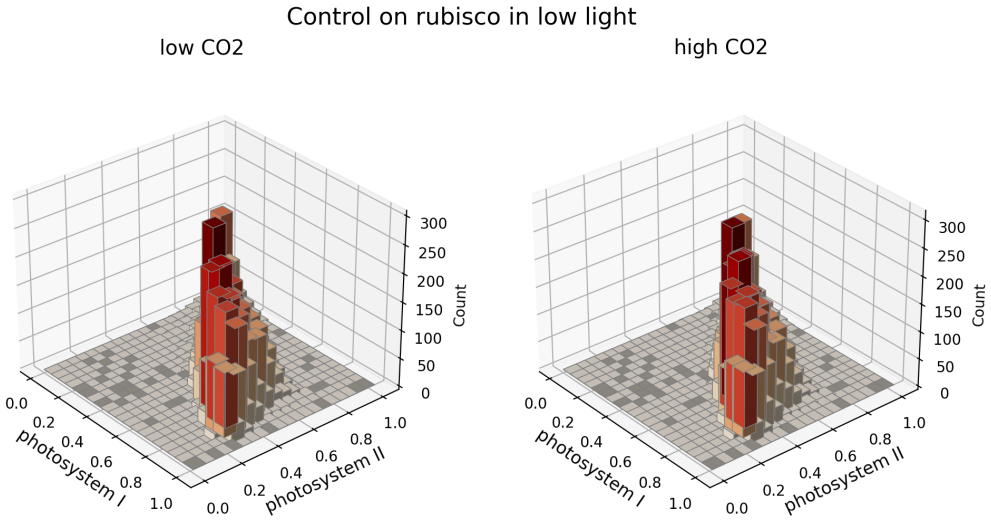

FIGURE 4.4: Correlation of control coefficients for both photosystems on carbon fixation under low-light conditions represented as a 3D histogram. The z-axis indicates the how many control coefficients fall into a specific numerical range. The calculation is based on 10000 randomly generated parameter sets as described in the text.

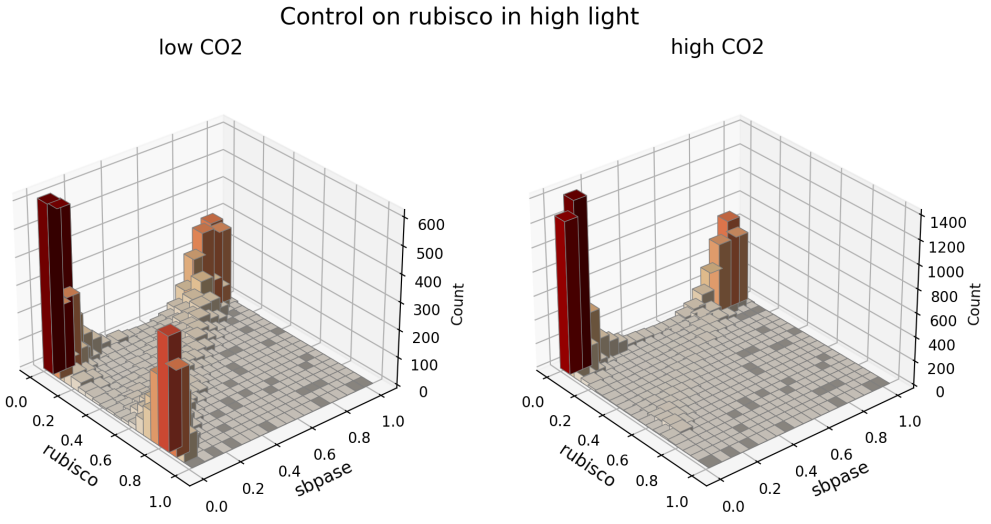

FIGURE 4.5: Control coefficients of carbon fixation by RuBisCO vs. SBPase under high-light conditions represented as a 3D histogram. The z-axis indicates the how many control coefficients fall into a specific numerical range. The calculation is based on 10000 randomly generated parameter sets as described in the text.

of all choices in the model-building process or of varying external conditions. The control on RuBisCO, an essential enzyme for carbon fixation, by other reaction steps in the CBB cycle, PETC, or ASC-GSH cycle, is interesting for broadening our understanding of sequestering carbon in photosynthetic organisms.

In order to determine if the previously observed shift in control (Fig. 4.2) is a consequence of the structural design of the PETC and the CBB, we performed a robustness analysis. For this, we varied parameters by multiplying a randomly selected factor between 0.5 and 2 to generate 10000 perturbed parameter sets. For each parameter set, we analyzed the control exerted by PSII, cytochrome b_6f, RuBisCO, FBPase, and SBPase on carbon fixation in the four reference conditions for low/high CO_2/light as defined above. Figure 4.3 shows the distributions of flux control coefficients on carbon fixation by selected reactions. With most parameter sets, the photosystems had a much higher control on carbon fixation in low light intensities in both CO_2 concentration conditions than reactions in the CBB cycle. In low light intensity, cytochrome b_6f and RuBisCO have almost no control, and SBPase, while detectable, has only a minor influence. Investigating the correlation of control coefficients for both photosystems under low-light conditions reveals that these two processes indeed share the main flux control in a proportion, which depends on the exact parameter values (Fig. 4.4).

The control of photosystems on carbon fixation is drastically reduced in high-light conditions. Especially photosystem I has lost almost all its control. As a general trend, the distribution of flux control coefficients in high light is broader than in low light. The main controlling steps are now on the demand side of photosynthesis, in particular on RuBisCO and SBPase. SBPase is, besides photosystem II, the controlling reaction for carbon fixation in high light intensity and high CO_2 conditions. At the same time, RuBisCO and SBPase are the main factors in high light intensity and low CO_2 concentrations, with RuBisCO having a slightly higher influence. Correlating the control coefficients of these two central CBB enzymes shows for most randomly selected parameter sets RuBisCO does not exert any considerable control under high light and high CO_2 concentrations, while under high light but low CO_2 the control can be on either of these enzymes (or none of the two) but only for a few parameter sets the control is shared between the two enzymes (Fig. 4.5).

Overall, our robustness analysis, in which we randomly varied parameters by a factor between 0.5 and 2, confirms our previous observations, namely that the control shifts from the photosystems in low light to the CBB

cycle enzymes in high light. Under the latter conditions, RuBisCO exerts a higher control if ambient CO_2 concentrations are low, while SBPase is the controlling step under high CO_2 concentrations. This indicates that the shift in control is less a kinetic, parameter-dependent, effect but rather a structural property of photosynthesis.

4.4 Discussion and Outlook

Photosynthesis is a supply-demand system. The supply (PETC) and demand (CBB cycle) sides must be coordinated to ensure efficient photosynthesis. Considering the often rapidly and unpredictably changing light intensities (Kaiser, Morales, and Harbinson, 2018) plants are exposed to in natural environments, maintaining such coordination appears challenging. It is plausible to assume that the present environmental-dependent regulatory mechanisms controlling carbon fixation have evolved to be highly efficient, considering the direct effect that carbon capture has on plant growth and fitness. This work presents an *in silico* analysis of the control over carbon fixation in different environmental conditions. For this, we used a published model of photosynthesis that combines the supply side (PETC), the demand side (CBB cycle), and the Ascorbate-Glutathion cycle (Saadat et al., 2021).

Such a supply-demand photosynthesis model allows for quantifying the control that individual processes have on the overall carbon fixation rate. We focused in particular on photosystems I and II, cytochrome b_6f, RuBisCO, and SBPase, which were reported to exert control on carbon fixation under several conditions (Poolman, Fell, and Thomas, 2000; Johnson and Berry, 2021; Raines et al., 2000). Using Metabolic Control Analysis, we quantified the control of these single steps on carbon fixation for different simulated environmental conditions. By simultaneously varying the light intensity and CO_2 concentration, we could show that the control shifts from the photosystems in low light intensities to RuBisCO and SBPase in high light intensities but then from RuBisCO in low to SBPase in high CO_2 concentrations (Fig. 4.2). The shift of the control confirms that most of the reactions previously reported to control the flux are indeed critical for regulating carbon fixation. However, whether PSII, PSI, RuBisCO, or SBPase is the main controlling factor strongly depends on the external conditions. In our photosynthesis model, a relatively sharp threshold marks the transition between a

supply- and a demand-controlled situation (see Fig. 4.2). This threshold, separating 'low' and 'high' light conditions, occurs when the quenching mechanism reaches its maximal capacity (see Fig. 4.15). This results in a reduction of most electron carriers and a sharp accumulation of protons in the lumen. The PETC still operates at a fast rate, so ATP and NADPH production is no longer limiting carbon fixation. It is an open question whether this sharp transition is a feature of the specific model that was used for this analysis or whether this is actually a systemic property of photosynthesis. We assume that the transition from non-saturated to saturated quencher is not as sharp *in vivo* as suggested by the model, but that the principle feature, namely that high light intensity results in a shift of control to the demand reactions of the CBB cycle, is a structural feature of the photosynthetic supply-demand system. The continuous transition under high light between the RuBisCO and SBPase-mediated control suggests that at high CO_2 concentrations, the carboxylation by RuBisCO is not determining carbon fixation rate, but rather the distribution of the intermediates in the CBB cycle through SBPase. To test whether the shift in control is a kinetic property of the rates in photosynthesis or follows from the structure resulting from the interconnections of the PETC and CBB cycle, we performed a robustness analysis by randomly varying kinetic parameters by a factor between 0.5 and 2. Figure 4.3 illustrates that, at least in our model representation, the control shift is a property that occurs with many parameter sets. This observation indicates that the shift of control indeed seems to be a structural feature, and rather independent of the specific parameter values.

Interesting patterns emerge by correlating the flux control coefficients obtained by the robustness analysis. In the low light regime, the control is shared mostly among the two photosystems (Fig. 4.4 and Fig. 4.24), where often one of the photosystems exhibits a higher control than the other. Which photosystem exerts the higher control apparently depends on the specific numerical parameter values. Additionally, the fact that both photosystems always have clearly non-zero control for all parameter sets in low light underlines the importance of the PETC for carbon fixation as a limiting factor in these conditions. The light-driven photosystems ultimately determine the flow of electrons through the PETC and the translocation of protons into the lumen, hence the production of ATP and reduction equivalents required by the CBB cycle. Correlating the control coefficients quantifying the importance of RuBisCO and SBPase under high light shows a drastically different picture. Fig. 4.5 reveals that typically carbon fixation is either controlled by

RuBisCO or by SBPase, but the control is rarely shared. This is especially pronounced in high light intensity and low CO_2 concentration conditions. Fig. 4.5 also reveals that for a substantial number of parameter combinations, neither RuBisCO nor SBPase exerts control over the carbon fixation rate. A closer inspection reveals that in these cases, the control lies, in fact, with the photosystems. In fact, correlating the total control (sum of control coefficients of the individual processes) of the supply reactions with the total control of the demand reactions reveals that the control lies either on the supply side or on the demand side, but is rarely shared between both sides (Fig. 4.25). An interesting observation is that even in high light conditions, the model exhibited control by the light reactions for a substantial fraction of parameter sets. A possible explanation for the observation that also in high light for many parameter sets the control lies on the photosystems is that variations of the parameters can lead to scenarios where our selected 'high light' condition is actually not perceived as saturating light. In order to test this hypothesis, we relate the control exhibited by the dark reaction to the simulated stationary lumen pH (Fig. 4.26). This analysis shows that whenever the control is on the dark reactions, the pH is low, indicating that light (and the quencher) is saturated, whereas low control by the dark reactions is associated with a high lumenal pH, indicating non-saturating conditions.

Some experimental and theoretical studies claim that cytochrome b_6f controls the photosynthetic flux (Stiehl and Witt, 1969; Johnson and Berry, 2021). In contrast, our analysis suggests that cytochrome b_6f exhibits a considerable control only for very few parameter sets (Fig. 4.3). However, when we systematically decrease the activity of cytochrome b_6f, also in our model cytochrome b_6f can become a rate-controlling step (Fig. 4.27). These considerations show that seemingly conflicting reports on the control of cytochrome b_6f are not necessarily contradictory. In fact, the parameters describing the composition and kinetic properties of the photosynthetic apparatus have an important influence on the strength of control.

Most concentration control coefficients behave as expected. For the electron carriers, upstream reactions exert positive and downstream reactions negative control. We obtained an initially counter-intuitive result only for ferredoxin and NADPH, as they are both less reduced when PSI activity is enhanced in low light. This observation might be explained through an increased cyclic electron flow with a concomitant increase in CBB cycle activity. The cyclic electron flow is an integral part of the photosynthetic machinery

adjusting the ATP/NADPH ratio in the PETC and, hence, is an essential regulatory mechanism. Responding to the ATP/NADPH ratio required by the demand reactions, the effects of other processes can be reduced or even reverted, when compared to a system without cyclic electron flow. The regulatory effects of CEF may also explain the complex patterns in the control that some processes have on ATP concentrations. These results demonstrate that control in a complex system is often non-trivial, and altering reaction rates may result in counterintuitive effects.

Exploring a previously published supply-demand photosynthesis model with metabolic control analysis, we could resolve seemingly contradictory statements about which reactions have the strongest control on carbon fixation. We showed that basically all reactions previously reported exerting a strong control can indeed have high flux control under some conditions. It is important to note that all results have been obtained from a single, imperfect model. The model does not, for example, include the important process of photorespiration or stomatal aperture. It is unclear how far the interpretation of the results and the derived conclusions can be generalized. Still, the strength of theoretical analyses is that also with simplified and imperfect models, general features can be identified and novel hypotheses derived. For example, the general pattern observed in our analysis of how the control shifts between key enzymes and complexes depending on light intensity and CO_2 concentrations is plausible and generally applicable. By understanding the principles of how regulation depends on environmental conditions, new data can be interpreted in a highly informed manner. Additionally, the existence of different physiological states and the fact that the control in photosynthesis shifts might necessitate the adaption of experimental protocols aiming for the improvement of photosynthesis. For instance, improvement strategies could differ depending on the typical physiological states of the photosynthetic organism. With our study, we aimed at demonstrating the usefulness of systematic model analyses with Metabolic Control Analysis in understanding metabolic regulation in complex networks.

4.5 Concluding remarks

In this chapter, we looked into the steady state behavior of photosynthesis (far long-term process) using metabolic control theory. With this, we could identify shifts in the control exerted by various CBB and PETC steps on carbon fixation. Photosynthetic organisms are, in nature, constantly exposed to

changes in abiotic factors. Only in strictly controlled environments, such as greenhouses, can constant steady-state photosynthesis be guaranteed. However, the knowledge about the control in a steady state, besides being beneficial for crop growth in greenhouses, can be used to build a hypothesis about what controls photosynthesis in natural environments.

4.6 Supplementary figures

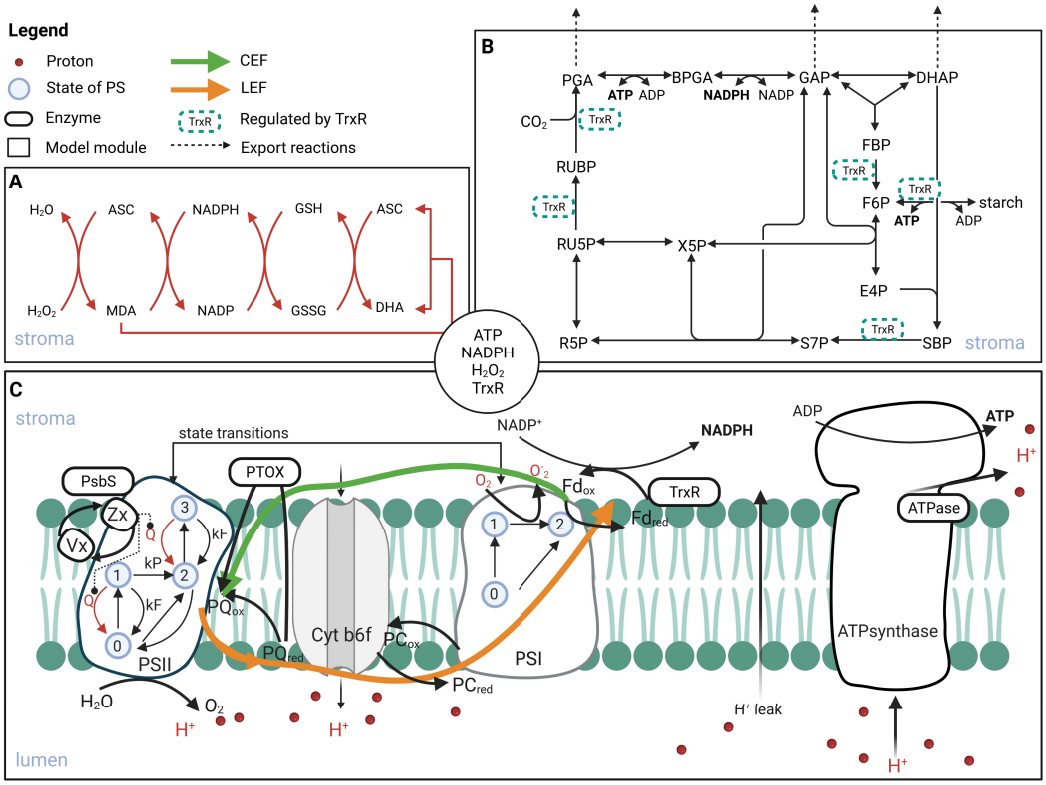

FIGURE 4.6: Schematic representation of the processes included in the computational model of photosynthesis. The model consists of three modules: ascorbate-glutathione (ASC-GSH) cycle (A), CBB with TrxR regulated reactions (B), and PETC (C). The compounds in the circle in the centre are the ones exchanged between the compartments. Taken with permission from Saadat et al., 2021.

TABLE 4.1: Enzyme subsets

Reaction abbreviations	Reaction names

Table 4.1 – *Continued from previous page*

Reaction abbreviations	Reaction names
1. vG6P_isomerase, vPhosphoglucomutase, vStarch	glucose-6-phosphate isomerase, phosphoglucomutase, starch synthesis
2. vdhap	dihydroxyacetone phosphate exporter
3. vpga	3-phosphoglycerate exporter
4. vNDH	NADH reductase
5. vMDAreduct	NADH:monodehydroascorbate oxidoreductase
6. vgap	glyceraldehyde-3-phosphate exporter
7. vE_activation, vE_inactivation, vFdTrReductase	ATP synthse activation and deactivation, Ferredoxin-Thioredoxin reductase
8. vCyc	cyclic electron flow
9. vLeak	proton leak over thylakoid membrane
10. vSt12, vSt21	state transition reactions
11. vDeepox, vEpox	xanthophyll cycle reactions
12. v10, v11, v12, v13, v8, v9, vF6P_Transketolase, vRuBisCO	transketolase (S7P reaction), ribose-5-phosphate isomerase, xylose-5-phosphate epimerase, ribulose-5-phosphate kinase, aldolase (SBP reaction), sedoheptulose bisphosphatase, transketolase (F6P reaction) , ribulose-1,5-bisphosphate carboxylase/oxygenase
13. vAldolase , vFBPase	aldolase (FBP reaction), fructose-1,6-bisphosphotase
14. v3ASC, vDHAR, vGR	spontaneous disproportion of monodehydroascorbate radicals, glutathione:dehydroascorbate oxidoreductase, glutathione:NADP+ oxidoreductase
15. vATPsynthase	ATP synthase
16. vFNR	ferredoxin-NADP reductase

Table 4.1 – *Continued from previous page*

Reaction abbreviations	Reaction names
17. vAscorbate, vMehler	ascorbate peroxidase, Mehler reaction
18. vBPGA_dehydrogenase, vPGA_kinase	1,3-bisphosphoglycerate dehydrogenase, phosphoglycerate kinase (PGA kinase)
19. vPS2	photosystem II
20. vTPI	triose phosphate isomerase
21. vB6f, vPS1	cytochrome b_6f, photosystem I
22. vLhcdeprotonation, vLhcprotonation	PsbS de- and protonation
23. vEX_ATP	ATP export
24. vEX_NADPH	NADPH export
25. vFdred	ferredoxin reduction in photosystem I
26. vPTOX	plastid terminal oxidase

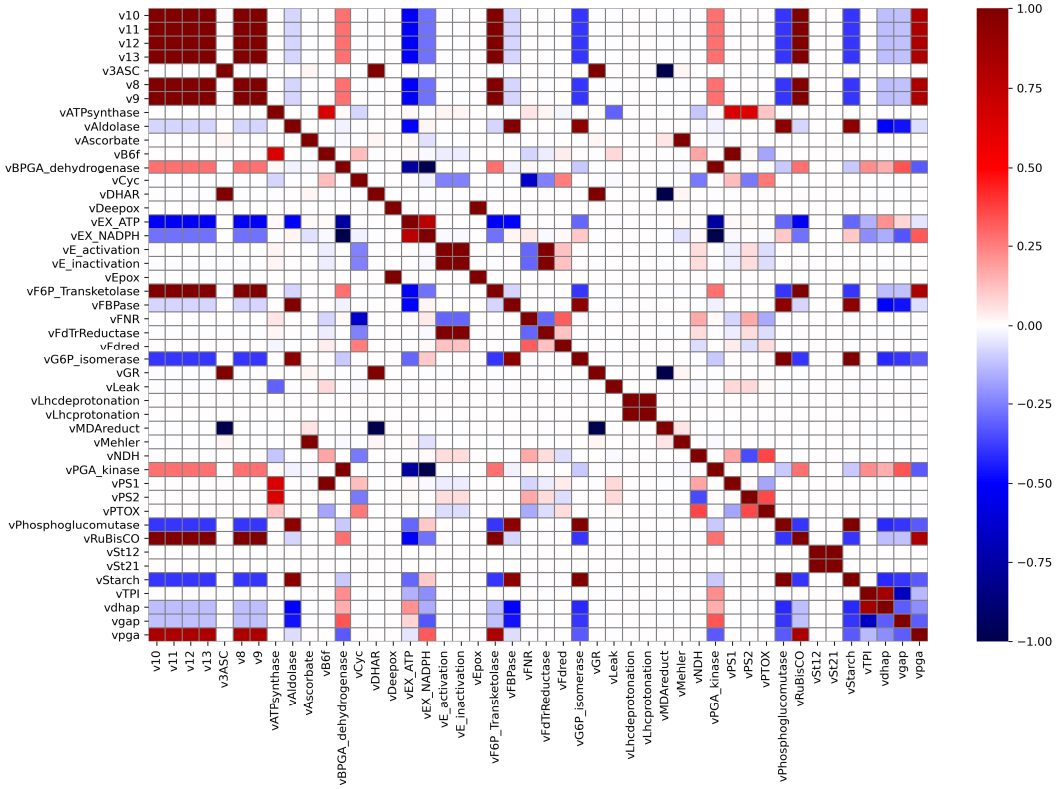

FIGURE 4.7: Reaction correlation coefficient matrix. The correlation was calculated by using the null space of the stoichiometric matrix (see method section). Red indicates positive, blue negative correlation.

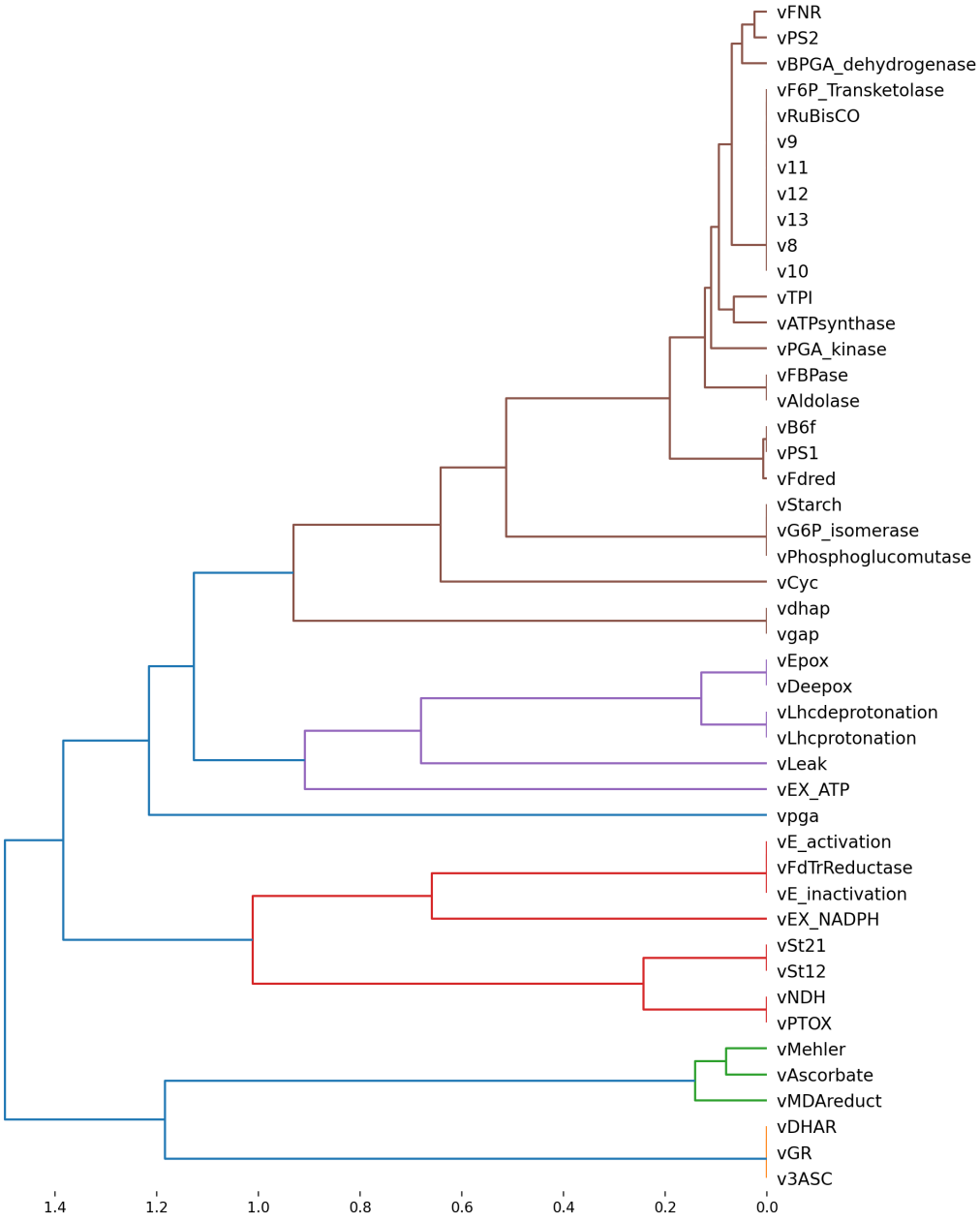

FIGURE 4.8: The tree was obtained by steady-state flux correlation analysis for 10000 random parameter sets in low light intensity and low CO_2 concentration conditions for the kinetic model of photosynthesis. Parameters were varied using a factor of 5. Abbreviations in the cluster annotations: PETC — photosynthetic electron transport chain, CBB — Calvin Benson Bassham cycle, ASC-GSH cycle — ascorbate-glutathione cycle.

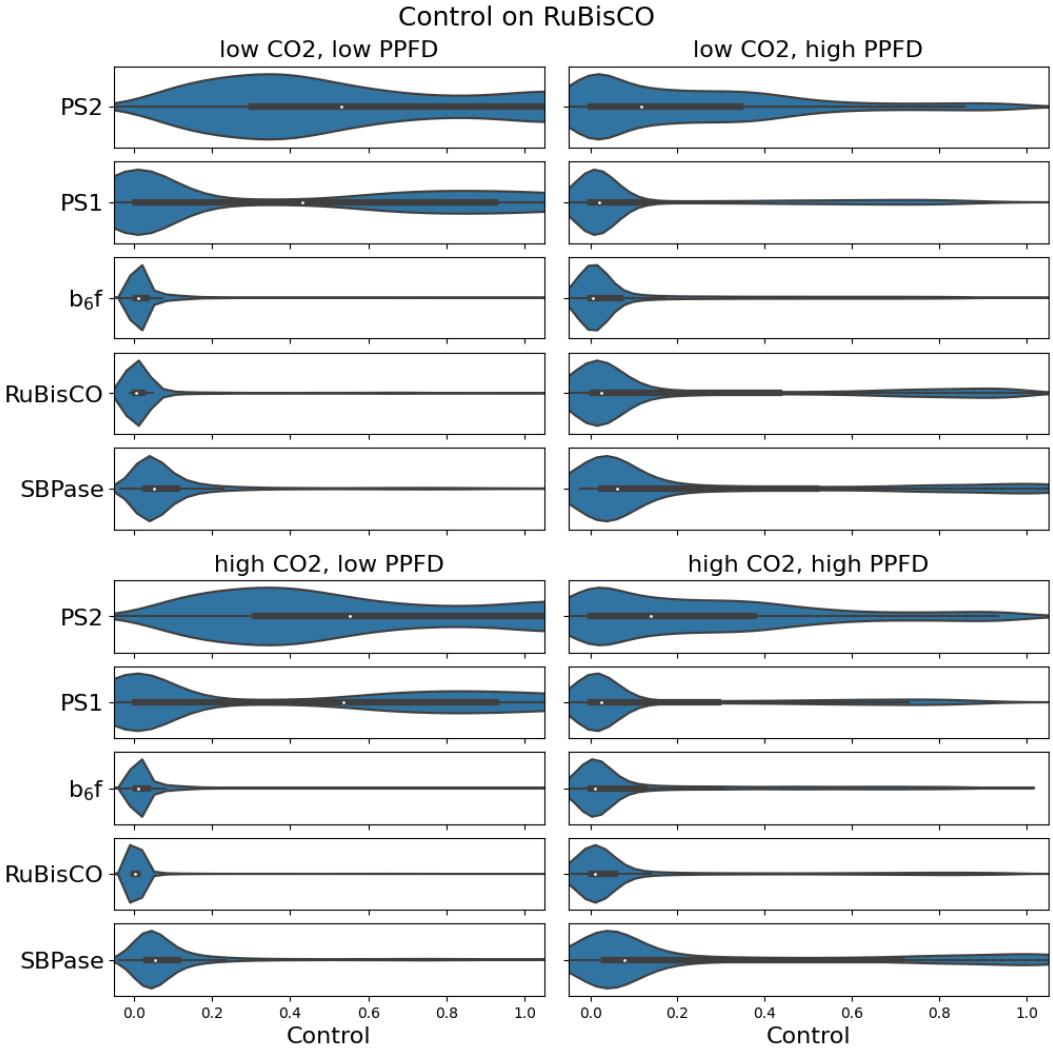

FIGURE 4.9: Distribution of flux control coefficients of key reactions in the PETC and CBB cycle on carbon fixation over 10000 sets of randomly perturbed parameters with a factor between 0.2 and 5. The shaded area shows the frequency of flux control coefficients. In all cases, the area was scaled to the maximum (including values outside the shown range) for clarity. Top left shows results under low CO_2 / low light conditions, top right under low CO_2 / high light, bottom left under high CO_2 / low light and bottom right under CO_2 / high light conditions. Only flux control coefficients between 0 and 1 are shown.

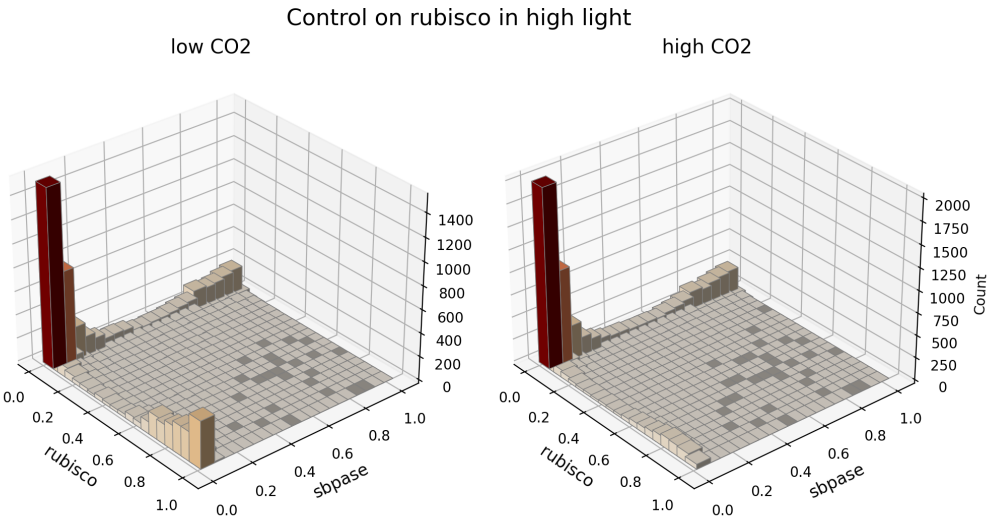

FIGURE 4.10: Control coefficients of carbon fixation by RuBisCO vs. SBPase under high-light conditions represented as a 3D histogram. Parameters were varied using a factor of 5. The z-axis indicates the how many control coefficients fall into a specific numerical range. The calculation is based on 10000 randomly generated parameter sets as described in the text.

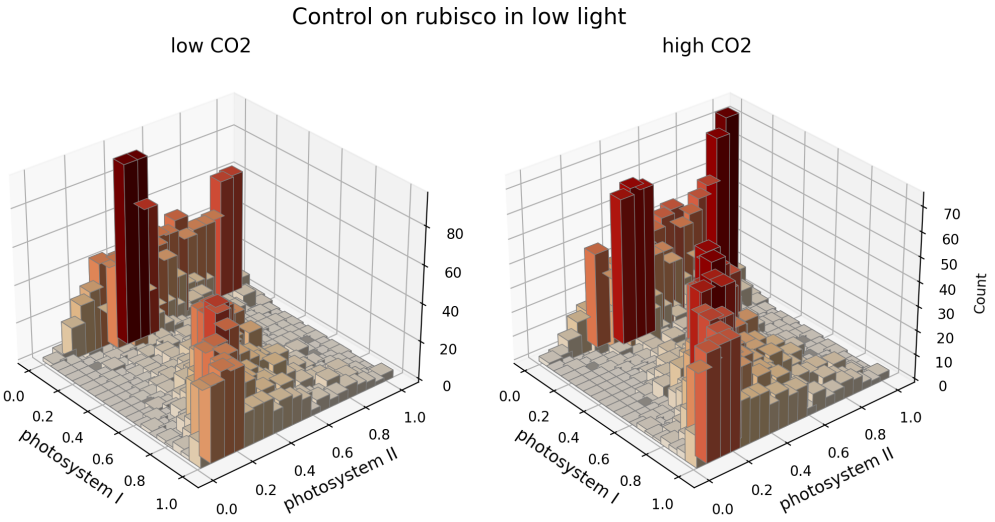

FIGURE 4.11: Correlation of control coefficients for both photosystems on carbon fixation under low-light conditions represented as a 3D histogram. Parameters were varied using a factor of 5. The z-axis indicates the how many control coefficients fall into a specific numerical range. The calculation is based on 10000 randomly generated parameter sets as described in the text.

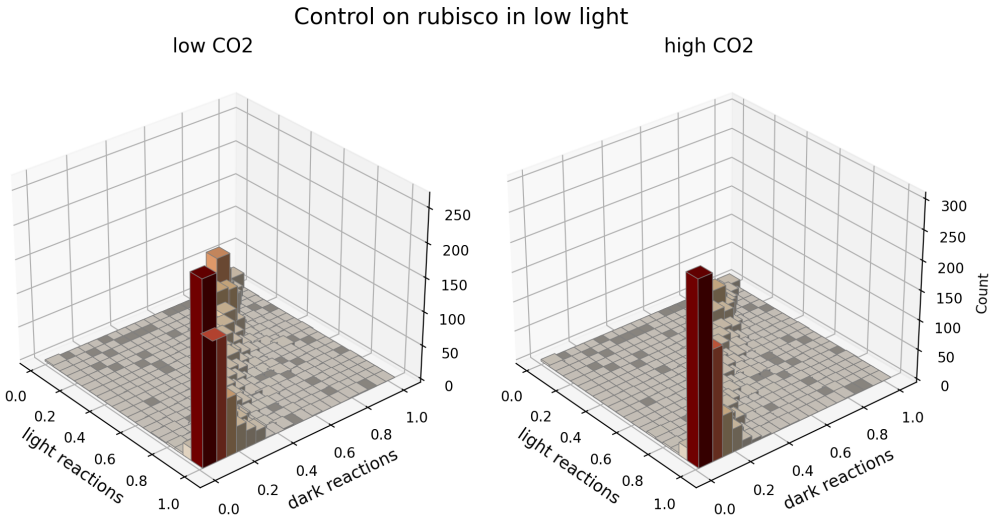

FIGURE 4.12: Control coefficients of carbon fixation by light vs. dark reactions in photosynthesis under low-light conditions represented as a 3D histogram. Parameters were varied using a factor of 5. The z-axis indicates the how many control coefficients fall into a specific numerical range.

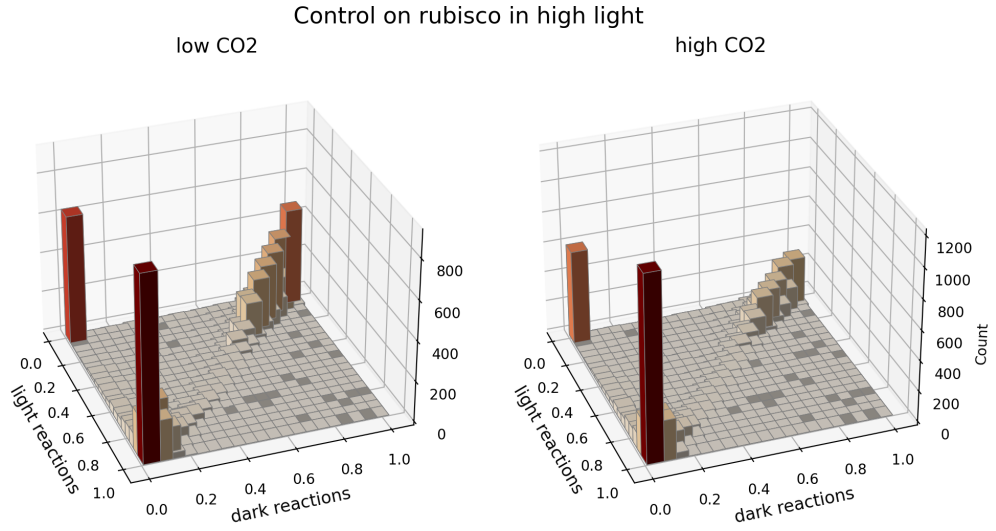

FIGURE 4.13: Control coefficients of carbon fixation by light vs. dark reactions in photosynthesis under high-light conditions represented as a 3D histogram. Parameters were varied using a factor of 5. The z-axis indicates the how many control coefficients fall into a specific numerical range.

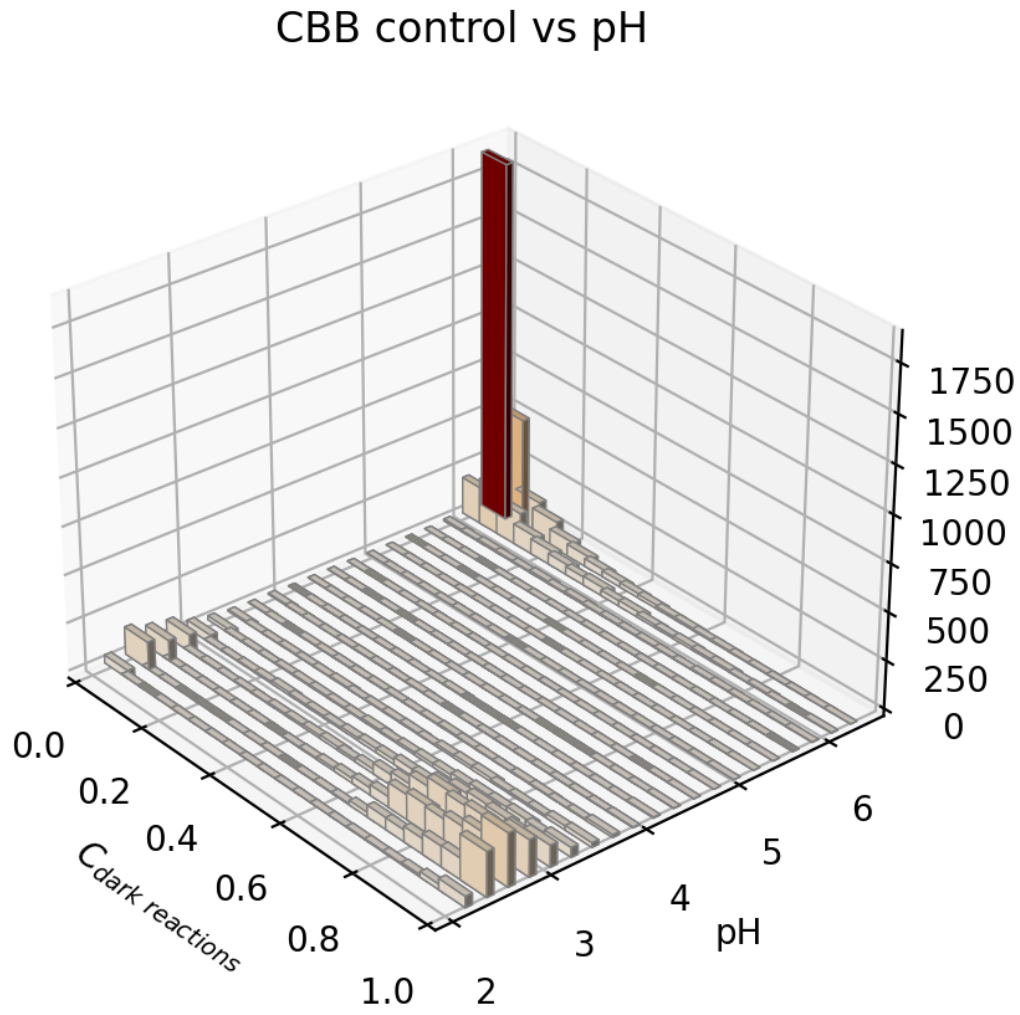

FIGURE 4.14: 3D histogram of steady state lumenal pH vs. control coefficients of dark reaction on carbon fixation. Parameters were varied using a factor of 5. The z-axis indicates the how many control coefficients fall into a specific numerical range.

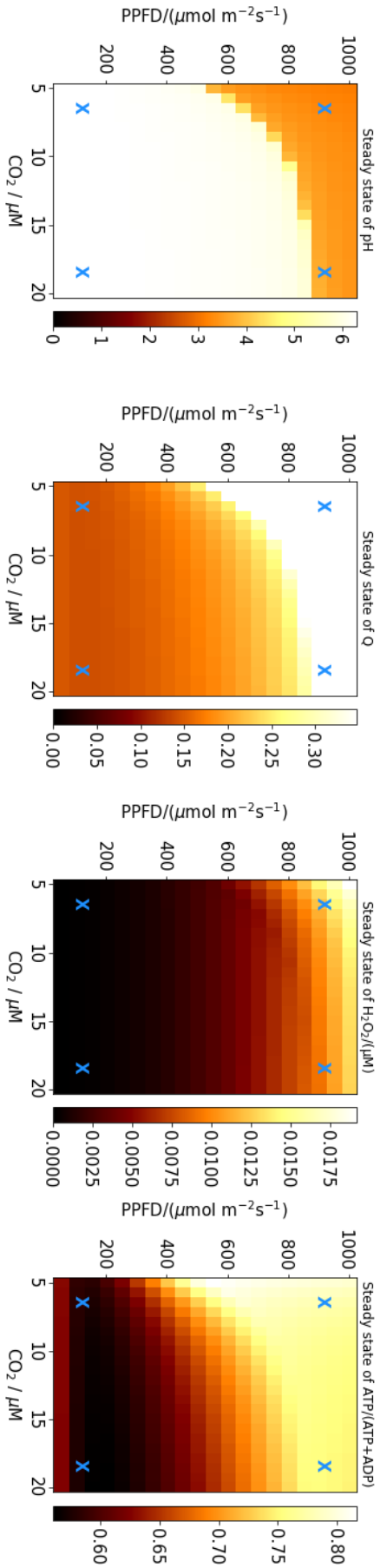

FIGURE 4.15: Steady state scan over light intensities and carbon dioxide concentration. Shown are (from left to right) the pH, quencher state, H_2O_2 concentration, and ATP/(ATP+ADP) fraction.

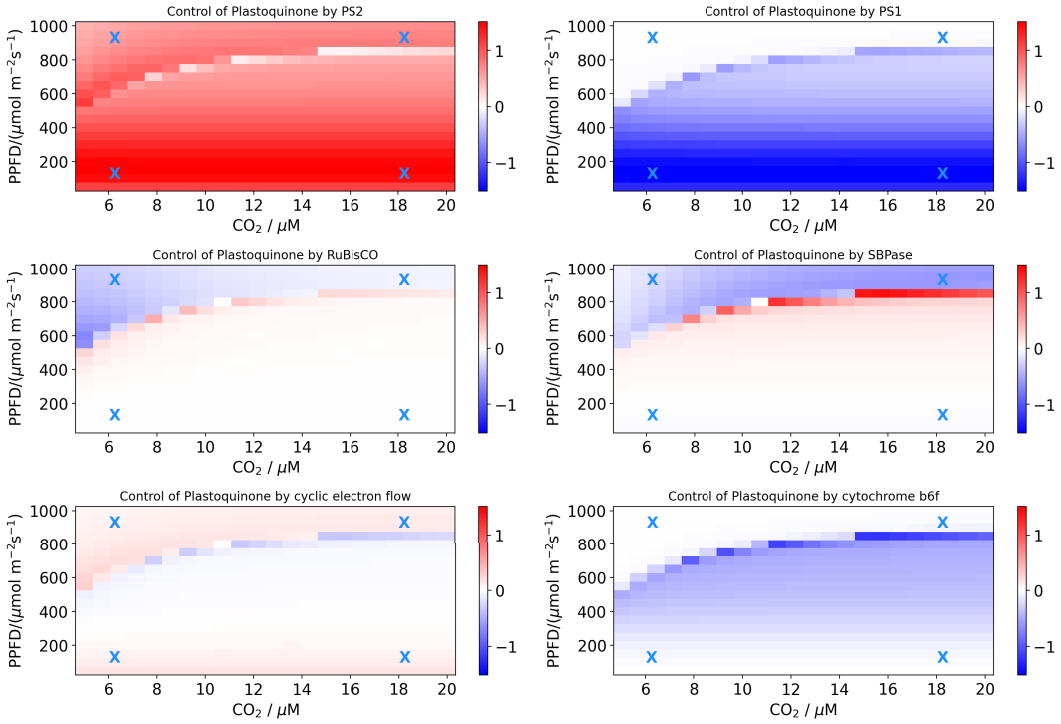

FIGURE 4.16: Concentration control coefficients of plastoquinone steady state concentration by photosystem II and I, RuBisCO, SBPase, cyclic electron flow, and cytochrome b_6f under varying light intensities and carbon dioxide concentrations.

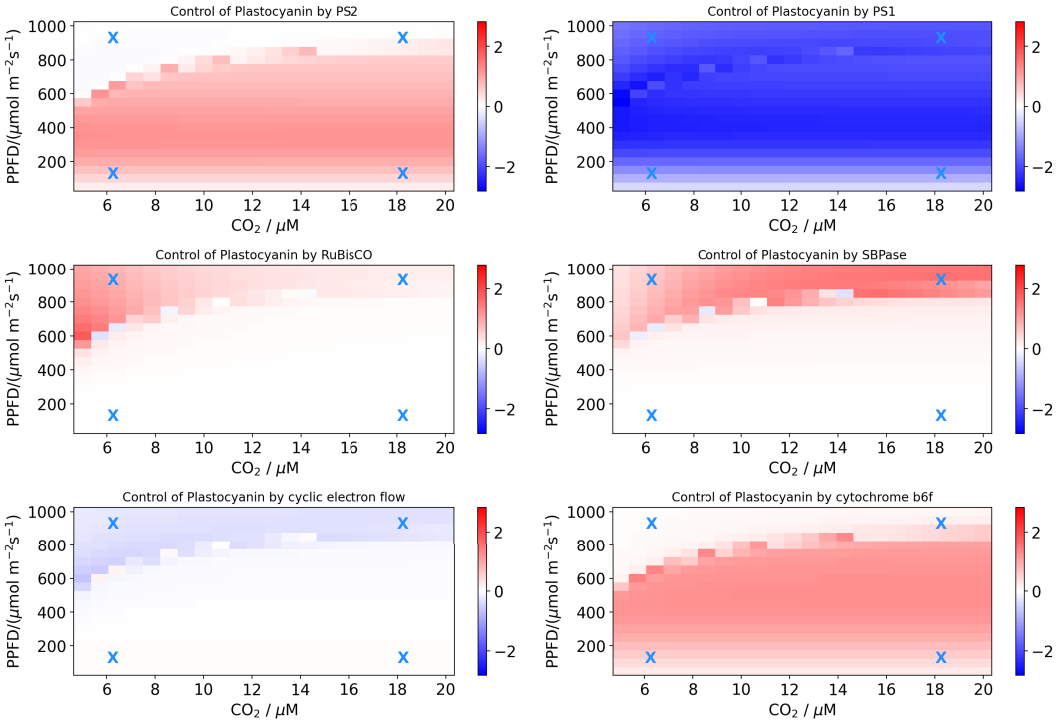

FIGURE 4.17: Concentration control coefficients of plastocyanin steady state concentration by photosystem II and I, RuBisCO, SBPase, cyclic electron flow, and cytochrome b_6f under varying light intensities and carbon dioxide concentrations.

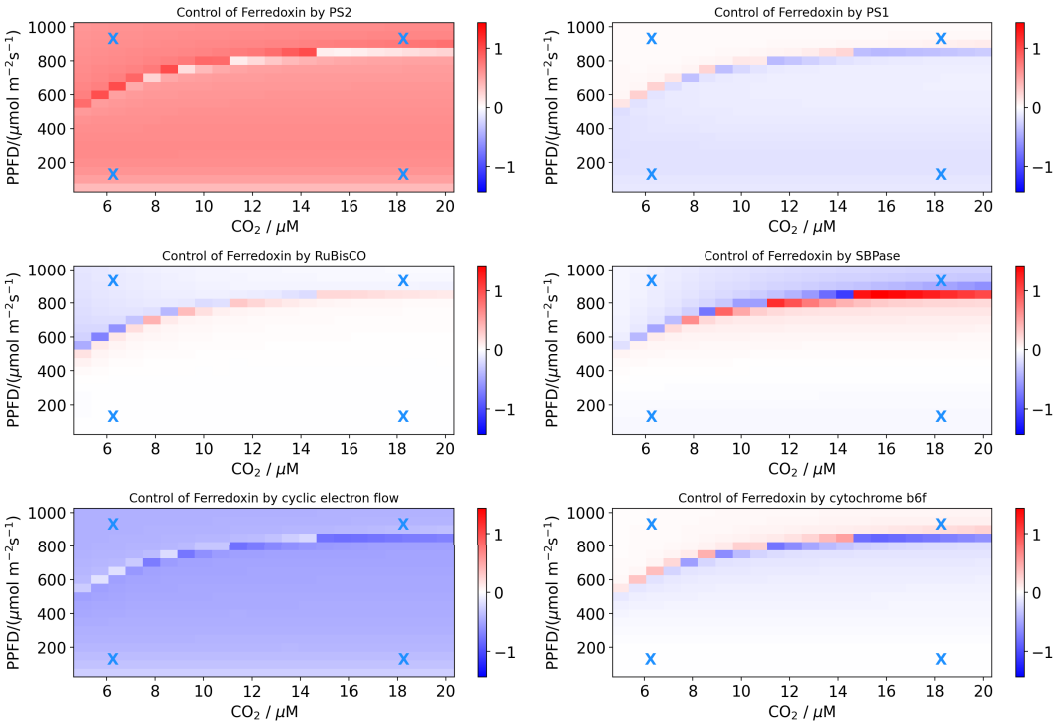

FIGURE 4.18: Concentration control coefficients of ferredoxin steady state concentration by photosystem II and I, RuBisCO, SBPase, cyclic electron flow, and cytochrome b_6f under varying light intensities and carbon dioxide concentrations.

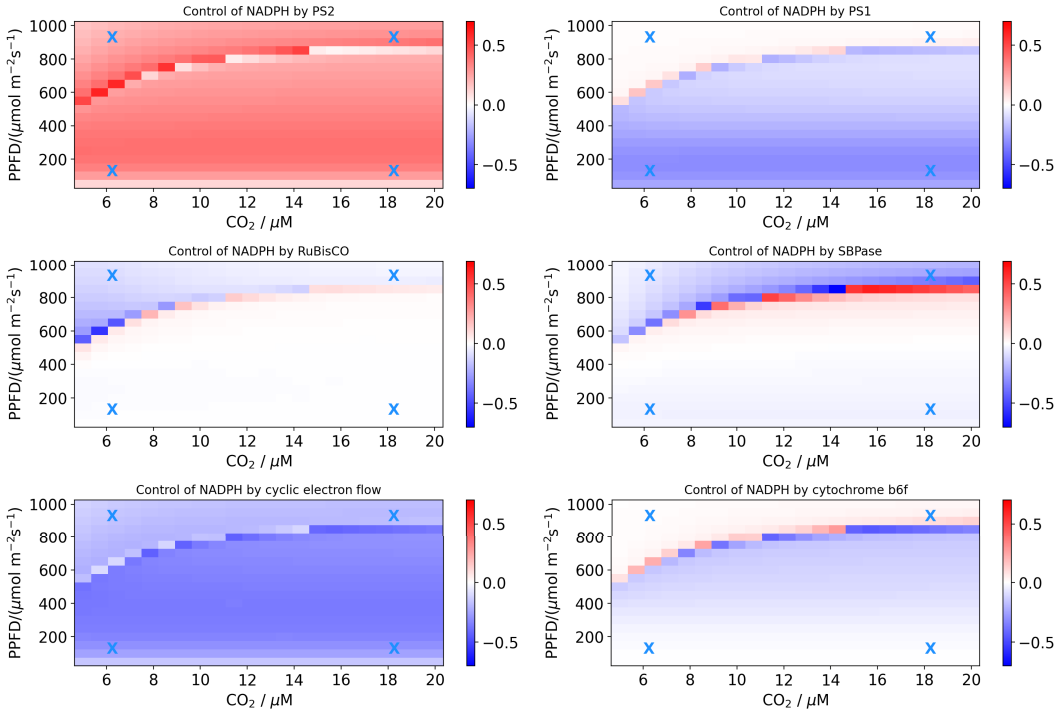

FIGURE 4.19: Concentration control coefficients of NADPH steady state concentration by photosystem II and I, RuBisCO, SBPase, cyclic electron flow, and cytochrome b_6f under varying light intensities and carbon dioxide concentrations.

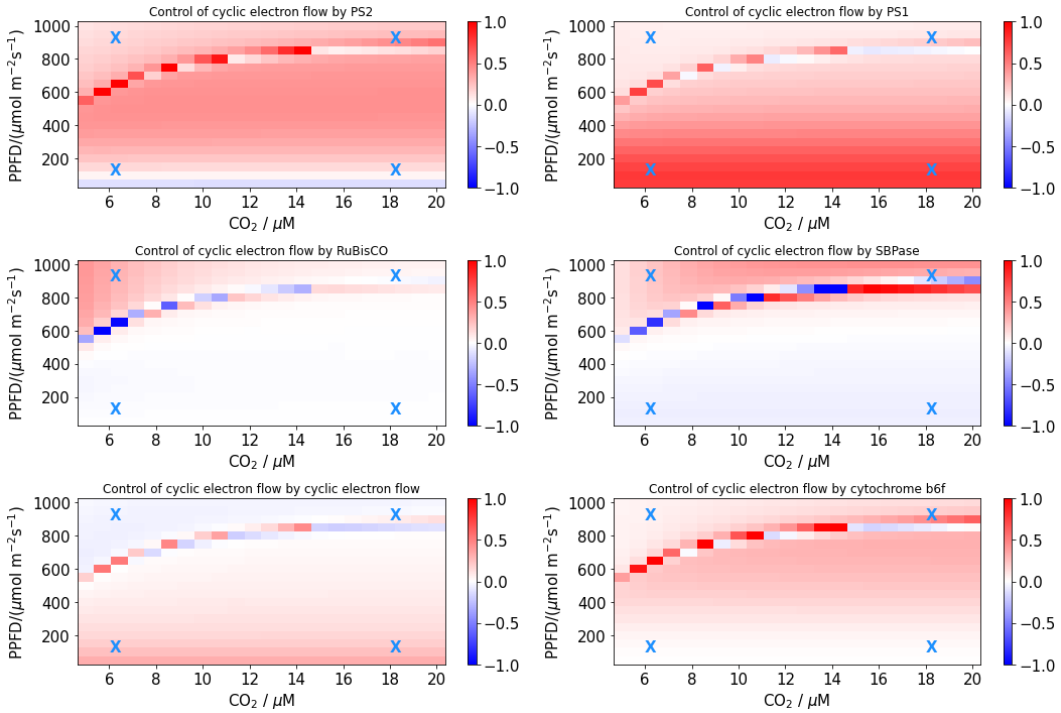

FIGURE 4.20: Flux control coefficients of cyclic electron flow by photosystem II and I, RuBisCO, SBPase, cyclic electron flow, and cytochrome b_6f under varying light intensities and carbon dioxide concentrations.

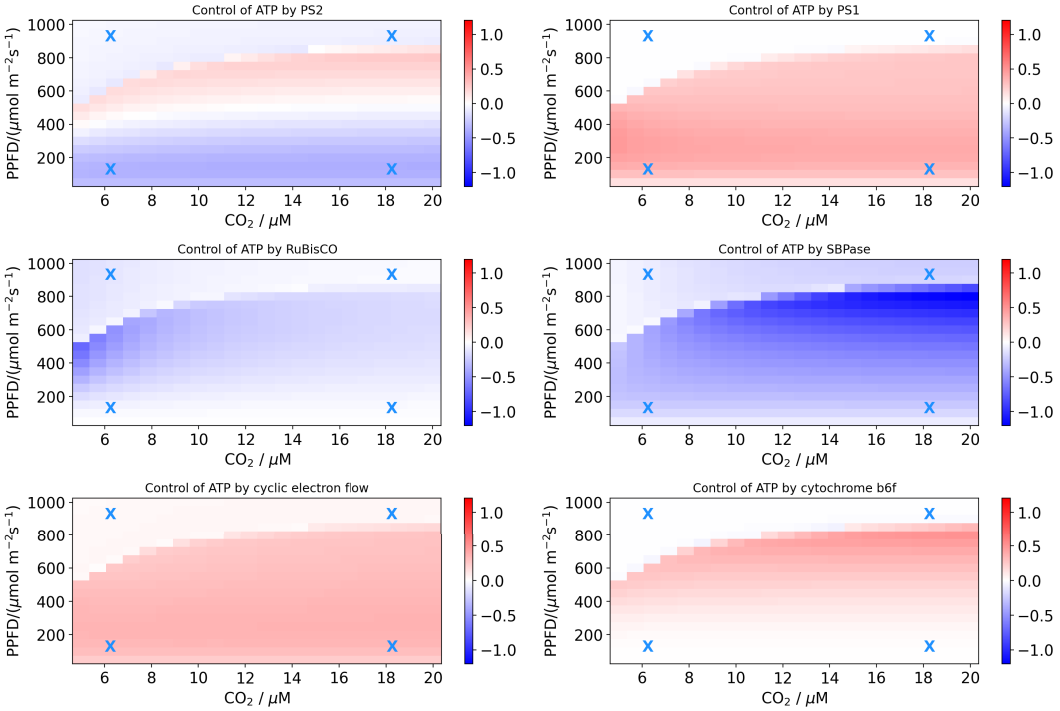

FIGURE 4.21: Concentration control coefficients of ATP by photosystem II and I, RuBisCO, SBPase, cyclic electron flow, and cytochrome b_6f under varying light intensities and carbon dioxide concentrations.

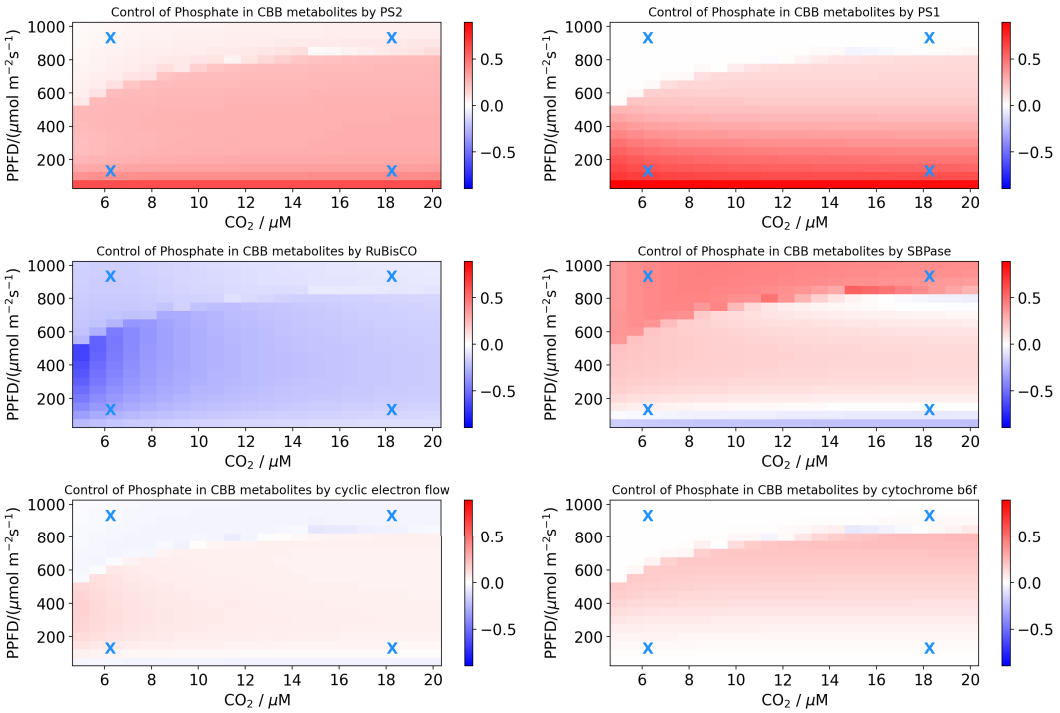

FIGURE 4.22: Concentration control coefficients of phosphate in CBB cycle intermediates by photosystem II and I, RuBisCO, SBPase, cyclic electron flow, and cytochrome b_6f under varying light intensities and carbon dioxide concentrations.

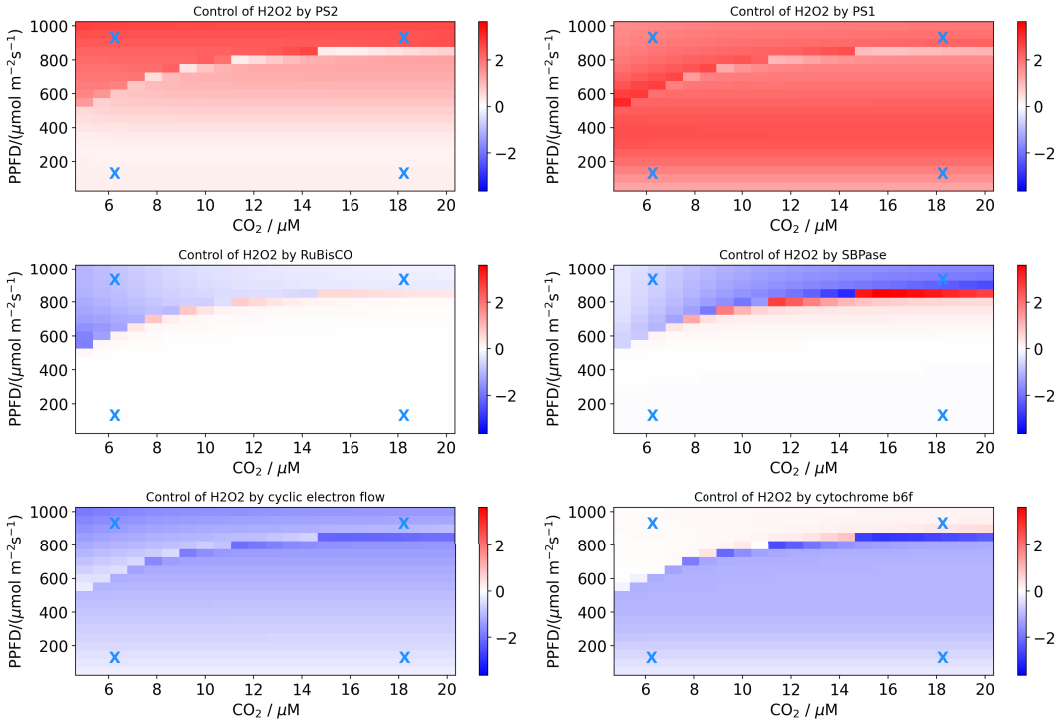

FIGURE 4.23: Concentration control coefficients of H_2O_2 steady state concentration by photosystem II and I, RuBisCO, SBPase, cyclic electron flow, and cytochrome b_6f under varying light intensities and carbon dioxide concentrations.

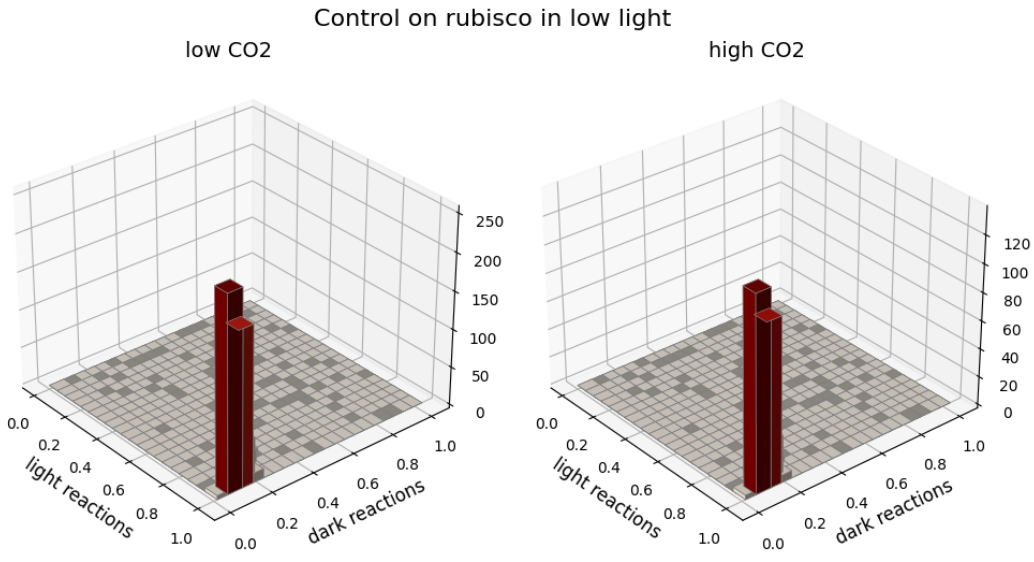

FIGURE 4.24: Control coefficients of carbon fixation by light vs. dark reactions in photosynthesis under low-light conditions represented as a 3D histogram. The z-axis indicates the how many control coefficients fall into a specific numerical range.

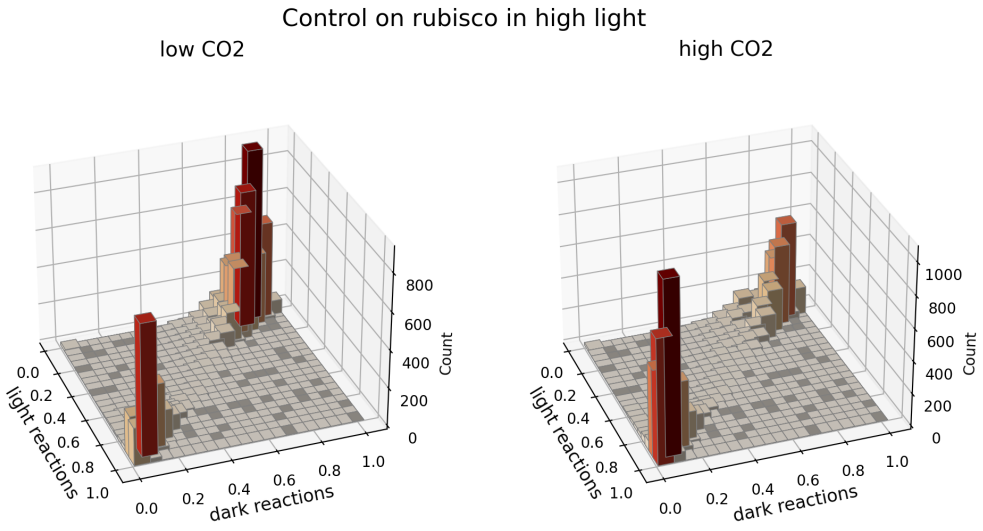

FIGURE 4.25: Control coefficients of carbon fixation by light vs. dark reactions in photosynthesis under high-light conditions represented as a 3D histogram. The z-axis indicates the how many control coefficients fall into a specific numerical range.

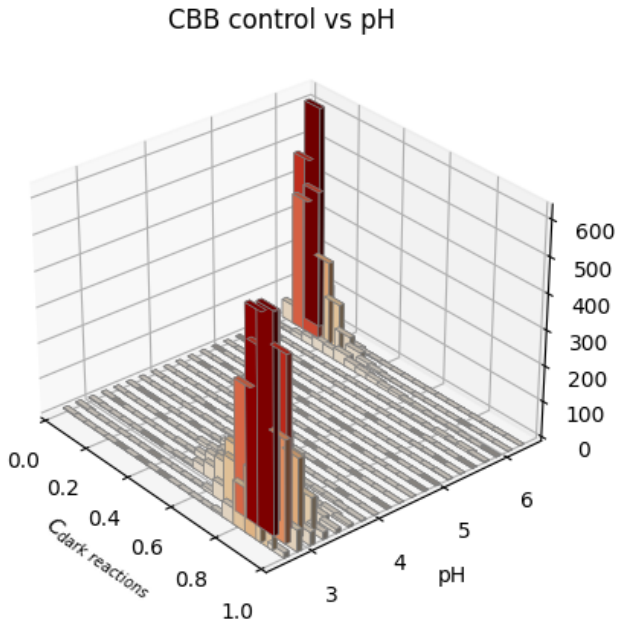

FIGURE 4.26: 3D histogram of steady state lumenal pH vs. control coefficients of dark reaction on carbon fixation. The z-axis indicates the how many control coefficients fall into a specific numerical range.

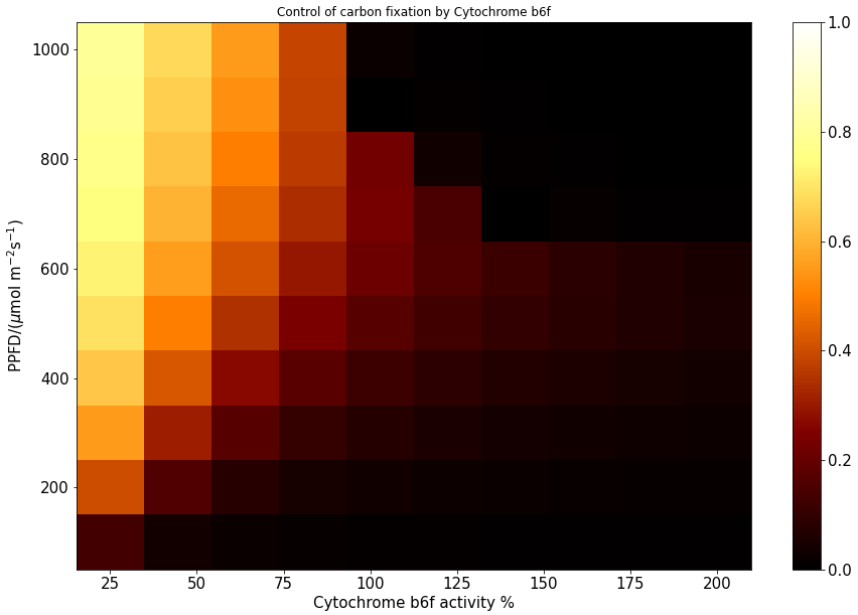

FIGURE 4.27: Flux control coefficients of carbon fixation by cytochrome b_6f under varying light intensities and cytochrome b_6f activities in high CO_2 conditions.

Chapter 5

Modeling of photoinhibition: exploring the impact of quenching processes

This chapter is published on biorxiv (Nies, Matsubara, and Ebenhoeh, 2023) . I was involved in each step of the study. This includes the simulation, data analysis, visualization of the results, and writing all parts of the chapter/manuscript (Introduction, Methods, Results, Discussion). The description of the model, which was initially placed in the supplement, was placed in the method section to create a similar structure for all chapters. In case of a duplication of the model description (original versions in main texts or in supplement), it was decided to use the description that was more informative.

Plants are constantly exposed to changing environments, sometimes leading to extreme conditions and stress. For example, sudden exposure to high light leads to excess absorbed light energy, causing reactive oxygen species (ROS) formation. ROS damage the photosynthetic machinery, particularly the D1 protein in photosystem II (PSII), which therefore needs to be continuously repaired and replaced. The effect of the damage inflicted by high light is a prolonged decrease in photosynthetic efficiency. Hence, it is not surprising that photoinhibition has been subject to numerous experimental studies investigating its effects in the context of crop productivity. However, it has become apparent that classical measures of photoinhibition, i.e., changes in the chlorophyll fluorescence parameter F_v/F_m, are not only determined by the loss of PSII core function but also by processes such as energy transfer and quenching. Mathematical models can help dissect the influences on such fluorescence signals and quantify the contributions of various interacting mechanisms. We present a mathematical model with a dynamic description of the photosynthetic electron transport chain (PETC),

non-photochemical quenching, and photoinhibition. With our model, we investigate the interconnection between quenching, photoprotection, and fluorescence using simulations and experimental data. We found that different energy-dissipating properties of intact and damaged PSIIs, as well as energy transfer between PSIIs, are critical components that need to be included in the model to ensure a satisfactory fit to the experimental data. We envisage that our model provides a framework for future investigations of photoinhibition dynamics and its importance for plant growth and yield.

5.1 Introduction

Photosynthesis is one of the main processes that make energy available to the biosphere (Ksenzhek and Volkov, 1998). By capturing light, photosynthetic organisms convert solar energy into usable chemical energy, which is then used to drive metabolic processes, including the formation of biomass. Plants, algae, and other photosynthetic organisms exist in a wide range of environments, ranging from deserts to tropical forests. These environments can exhibit drastically and rapidly changing external conditions, considering, e.g. light intensity, temperature, and humidity. Plants, as sessile organisms, must adapt to the conditions they are exposed to (Kaiser, Morales, and Harbinson, 2018). However, such fluctuating conditions make the coordination of the photosynthetic electron transport chain (PETC), supplying light energy in the form of ATP and NADPH, and the Calvin Benson Bassham cycle (CBB cycle), which uses ATP and NADPH to sequester CO_2, a challenging task (Nies et al., 2023). Antenna complexes in chloroplast thylakoid membranes collect light energy and channel it to the reaction centers of the PETC. This captured energy is used to drive photochemistry, but the excited states can also dissipate energy as heat or re-emit it as fluorescence (Muller, Li, and Niyogi, 2001). Due to variations in external conditions, the light energy supply can frequently exceed the demand, which leads to the formation of reactive oxygen species (ROS) at multiple sites of the PETC. ROS are highly reactive compounds that can damage the molecular machinery of the PETC (Khorobrykh et al., 2020).

The photodamage induced by ROS affects various proteins, with the D1 subunit of photosystem II (PSII) being the most susceptible. In fact, with a turnover rate of $> 0.5\ \mathrm{d}^{-1}$, the D1 subunit exhibits one of the shortest protein lifetimes in the PETC (Li, Aro, and Millar, 2018). For functional photosynthesis, it is therefore essential that this protein is constantly resynthesized and

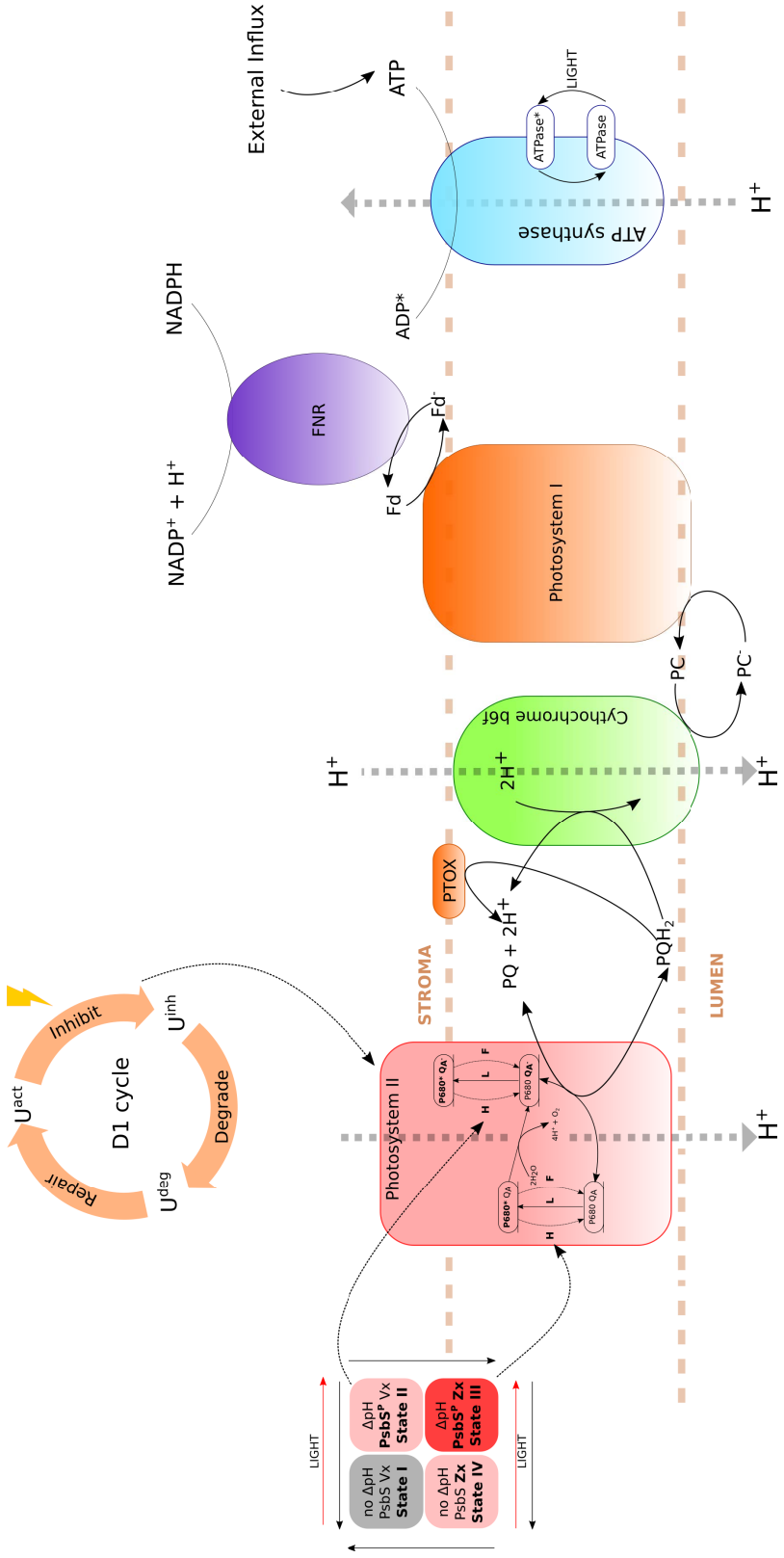

FIGURE 5.1: Schematic depiction of the model of photoinhibition (compare also Ebenhöh et al., 2014; Matuszyńska et al., 2016). Not shown for clarity but included are the cyclic electron flows around photosystem I.

replaced. This is realized by the so-called D1 protein repair cycle, which involves the degradation and synthesis of damaged D1 protein. This cycle has a very high energy demand, with an estimated 1304 ATP per subunit repaired (Murata and Nishiyama, 2018). Despite considerable advances in our understanding of photoinhibition, the exact mechanism of how high-light stress inflicts damage on the photosynthetic machinery is still under debate, and various hypotheses have been proposed (Zavafer, 2021).

Classically, photoinhibition is quantified by measuring F_v/F_m after prolonged exposure to strong irradiance. This was justified because of the almost linear relationship between F_v/F_m and the loss of photosynthetic O_2 evolution (see, e.g. Pätsikkä, Aro, and Tyystjärvi, 1998). It has recently become increasingly apparent that the F_v/F_m, derived from the fluorescence signal, might not be ideal for assessing photoinhibition. The fluorescence signal that a photosynthetic tissue, such as a leaf, emits is influenced by multiple factors, such as non-photochemical quenching, the efficiency of photochemistry, and the three-dimensional structure of the leaf. Hence, F_v/F_m might be determined not only by the loss of the PSII core function but also by other dissipating processes (Malnoë, 2018). Moreover, also theoretical studies have suggested an inherently nonlinear relationship between inactive PSII and the fluorescence signal (Giersch and Krause, 1991).

Over the last decades, various mathematical models of photosynthesis were developed (Stirbet et al., 2019). Some of them focus on the PETC (Ebenhöh et al., 2014; Matuszyńska et al., 2016; Zaks et al., 2012) or the CBB cycle (Pettersson and Ryde-Pettersson, 1988; Poolman, Fell, and Thomas, 2000), and others try integrating both into one mathematical description (Morales et al., 2018b; Matuszyńska, Saadat, and Ebenhöh, 2019; Saadat et al., 2021). Other models focused on detailed processes in PSII (Belyaeva et al., 2016). Many of these models calculate how the fluorescence signal derives from the molecular processes of the PETC. Most of the calculations depend on equations that describe the fluorescence yield associated with closed and open reaction centers of PSII. The difference in how these models determine fluorescence yield primarily arises from different simplified or extended versions of these equations. These equations are based on the current understanding regarding the source of the fluorescence signal, derived from the work conducted during the last sixty years (Joliot, 1964; Butler and Kitajima, 1975; Kitajima and Butler, 1975; Giersch and Krause, 1991; Bernhardt and Trissl, 1999). However, despite much effort, it still needs to be clarified which of the

classical equations and which model representation of the thylakoid membrane (e.g., lake, single unit, domain model, see Bernhardt and Trissl, 1999) is most realistic.

Here we expanded a published model of the PETC and non-photochemical quenching (NPQ) (Ebenhöh et al., 2014; Matuszyńska et al., 2016; Saadat et al., 2021) by integrating a mechanistic description of photoinhibition and the D1 repair cycle. For this, we build upon previous models of the D1 damage-repair cycle and an expansion of the energy transfer theory (Giersch and Krause, 1991; Tyystjärvi, Mäenpää, and Aro, 1994; Pätsikkä, Aro, and Tyystjärvi, 1998). The goal of our model is to quantitatively reproduce experimental data measuring photodamage as changes in F_v/F_m, F_m, and F_o in wildtype *Arabidopsis thaliana* and the *npq1* mutant. The *npq1* mutant lacks violaxanthin de-epoxidase and, thus, zeaxanthin. However, zeaxanthin has been shown to play a critical role in the induction of short- (qE) and long-term (qZ) quenching processes, potentially protecting against high light-induced damage (Horton et al., 2008; Nilkens et al., 2010). Our model provides a theoretical framework in which we discuss different formulations for the fluorescence yield based on previous work and assess how these agree with experimental data. In particular, we focus on the effects of different heat dissipation capabilities and quenching activities on the fluorescence signal under photoinhibtory conditions. This work helps to clarify which processes contribute to the dynamic changes of photosynthesis under high-light stress. Moreover, we provide a quantitative and mechanistic explanation of the observed changes in F_v/F_m, F_o, and F_m in fluorescence measurements.

5.2 Model and Methods

A mathematical model was developed that combines non-photochemical quenching, the D1 protein repair cycle, and the main protein complexes in the PETC. The model is based on published mathematical descriptions that successfully simulated experimental data in the past (Tyystjärvi, Mäenpää, and Aro, 1994; Ebenhöh et al., 2014; Matuszyńska et al., 2016). Most parameter values were obtained from the literature. The model was tested against published data from various plant species and experimentally measured F_v/F_m values (*Arabidopsis thaliana* ecotype Columbia-0 and the *npq1* mutant).

5.2.1 Experimental approach

Arabidopsis thaliana (Columbia-0 and *npq1*) seeds were sown on commercial soil (Pikier, Balster Einheitserdewerk, Fröndenberg, Germany) and stratified for three days in the dark at 4 °C. After that, they were transferred to the climate chamber with 12 h/12 h light/dark photoperiod, 26 °C/20 °C day/night air temperature and 60% relative air humidity. The photosynthetically active radiation was provided by fluorescent lamps (Fluora L58 W/77; Osram, Munich, Germany) with an intensity of approximately 100 µmol m^{-2} s^{-1}at plant height. Finally, seedlings were transferred to pots (7× 7 × 8 cm, one plant per pot) filled with soil (Lignostrat Dachgarten extensive, HAWITA, Vechta, Germany). Care was taken to avoid soil drying during cultivation. Six to seven weeks old plants were used for measuring.

Leaves of *A.thaliana* plants were detached, and petioles were submerged in a 5 mM lincomycin solution in reaction tubes for 3 h in dim light under ventilation. After incubation in the lincomycin solution, leaf discs with a diameter of 1.1 cm were punched out and floated on a water bath to keep the leaf temperature constant at 20 °C. The floating leaf discs were exposed to white LED light (SL 3500-W-G, Photon Systems Instruments) with an intensity of 800 µmol m^{-2} s^{-1}. After 0 h, 0.5 h, 1 h, 3 h, 5 h, and 6 h hours, F_v/F_m was measured on six replicate leaf discs using a DUAL-KLAS-NIR system (Heinz Walz GmbH, Effeltrich, Germany). Each leaf was dark-adapted 20 minutes before a red saturation pulse (635 nm, 0.8 seconds) of >10000 µmol m^{-2} $s^{-1}$was applied from both upper and lower sides of the leaf. Fluorescence was detected on the lower leaf surface to determine F_m.

5.2.2 Model description

Simulations were based on previous models of photosynthesis (Ebenhöh et al., 2014; Matuszyńska et al., 2016) and the D1 protein repair cycle. The photosynthetic electron transport chain in the thylakoid membrane of chloroplasts is implemented according to Ebenhöh et al., 2014. A four-state Photosystem II (PSII) description (B_0 - open and non-excited, B_1 - open and excited, B_2 - closed and non-excited, B_3 - closed and excited) was used. The rate of cytochrome b_6f complex is described via mass-action kinetics. Photosystem I (PSI) is a three-state system similar to PSII. Convenience kinetics describes the activities of the ferredoxin-NADPH-reductase (FNR) (Liebermeister and

Klipp, 2006). The proton leak across the thylakoid membrane, ATP synthesis, and cyclic electron flow around PSI are modeled via mass action kinetics. Reversible reactions are included by calculating lumenal pH-dependent equilibrium constants. Similar to Matuszyńska, Saadat, and Ebenhöh, 2019 and Saadat et al., 2021, a four-state quencher module, based on the xanthophyll cycle and the protonation of PsbS, was integrated (see Fig. 5.1). The model is detailed in the following sections.

5.3 Model

The mathematical model of the photosynthetic electron transport chain, including non-photochemical quenching and the D1 protein repair cycle, is represented as a system of twelve ordinary differential equations. The equations describe the temporal evolution of twelve system variables. These variables are the reduced fraction of plastoquinone (P), plastocyanin (PC), and ferredoxin (Fd), the stromal concentration of ATP (A) and NADPH (N), the lumenal proton concentration (H), the oxidized fraction of PsbS and the fraction of Violaxanthin, the active (U_a), damaged (U_i), and D1 protein less (U_d) form of photosystem II as well as an activator of the ATP synthase (E). Most of the equations are taken from previous work (Tyystjärvi, Mäenpää, and Aro, 1994; Ebenhöh et al., 2014; Matuszyńska et al., 2016). The system of equations reads,

$$\frac{dPQH_2}{dt} = v_{\text{PSII}} + v_{\text{cyc}} - v_{\text{b6f}} - v_{\text{PTOX}} \tag{5.1}$$

$$\frac{dPC^-}{dt} = 2\, v_{\text{b6f}} - v_{\text{PSI}} \tag{5.2}$$

$$\frac{dFd^-}{dt} = v_{\text{PSI}} - 2\, v_{\text{FNR}} - 2\, v_{\text{cyc}} \tag{5.3}$$

$$\frac{dN}{dt} = v_{\text{FNR}} - v_{\text{NADPHconsumption}} \tag{5.4}$$

$$\frac{dA}{dt} = v_{\text{ATPsynthase}} + v_{\text{mito}} - v_{\text{ATPconsumption}} - 231\, v_{\text{deg}} - 1059\, v_{\text{rep}} \tag{5.5}$$

$$b_{\text{H}} \cdot \frac{dH}{dt} = 2\, v_{\text{PSII}} + 4\, v_{\text{b6f}} - \frac{14}{3}\, v_{\text{ATPsynthase}} - v_{\text{leak}} \tag{5.6}$$

$$\frac{dPsbS}{dt} = v_{\text{Deprot}} - v_{\text{Prot}} \tag{5.7}$$

$$\frac{dV}{dt} = v_{\text{EpoxZ}} - v_{\text{DeepoxV}} \tag{5.8}$$

$$\frac{dU_a}{dt} = v_{\text{rep}} - v_{\text{inh}} \tag{5.9}$$

$$\frac{dU_i}{dt} = v_{\text{inh}} - v_{\text{deg}} \tag{5.10}$$

$$\frac{dU_d}{dt} = v_{\text{deg}} - v_{\text{rep}} \tag{5.11}$$

$$\frac{dE}{dt} = v_{\text{actATPsyn}} - v_{\text{deactATPsyn}} \tag{5.12}$$

5.3.1 Photosystems

As outlined in Ebenhöh et al., 2014, we assume processes in photosystem II (PSII) and photosystem I (PSI) to be much faster than the rest of the photosynthetic electron transport chain. This assumption allows us to treat the photosynthetic electron transport chain as a fast-slow system and algebraically solve the equations governing the dynamics in the photosystems. Hence, Photosystem II is represented as a four-state, and PSI is formulated as a three-state algebraic equation system under the assumption of being in steady state. The equation system for PSII, in the case **without energy transfer** between inactive and active PSII, is

$$-\left(k_{\text{LII}} + \frac{k_{\text{PQred}}}{K_{\text{eq,QAPQ}}} PQH_2\right) B_0 + (k_{\text{H}} + k_{\text{F}}) B_1 + k_{\text{PQred}} PQ \cdot B_2 = 0 \tag{5.13}$$

$$k_{\text{LII}} B_0 - (k_{\text{H}} + k_{\text{F}} + k_{\text{P}}) B_1 = 0 \tag{5.14}$$

$$k_{\text{LII}} B_2 - (k_{\text{H}} + k_{\text{F}}) B_3 = 0 \tag{5.15}$$

$$B_0 + B_1 + B_2 + B_3 = U_{\text{a}}. \tag{5.16}$$

Thus, v_{PSII} is (see Matuszyńska, Saadat, and Ebenhöh, 2019)

$$v_{\text{PSII}} = 0.5 \cdot k_{\text{P}} \cdot B_1. \tag{5.17}$$

Here k_{P}, k_{F} and k_{H} are the rate constants of photochemistry, fluorescence, and heat dissipation, respectively. The parameter k_{PQred} describes the plastoquinone reduction at photosystem II and k_{LII} is the light activation rate of PSII, which is set proportional to the total light intensity.
Four states of active Photosystem II (U_{a}) are considered in the solution of the PSII equation system: two ground and two excited states of open (B_0, B_1) and closed (B_2, B_3) reaction centers. The states differ in the ways they use light energy.
The equations governing the dynamics in a system **with energy transfer** between active and inactive PSII reads,

$$-\left(k_{\mathrm{LII}}+\frac{k_{\mathrm{PQred}}}{K_{\mathrm{eq,QAPQ}}}PQH_2\right)B_0+(k_{\mathrm{H}}\cdot Q+k_{\mathrm{F}})B_1+k_{\mathrm{PQred}}PQ\cdot B_2=0 \tag{5.18}$$

$$k_{\mathrm{LII}}B_0-(k_{\mathrm{H}}\cdot Q+k_{\mathrm{F}}+k_{\mathrm{P}})B_1=0 \tag{5.19}$$

$$(k_{\mathrm{H}}\cdot Q+k_{\mathrm{F}})B_3+k_{\mathrm{P}}B_1+\frac{k_{\mathrm{PQred}}}{K_{\mathrm{eq,QAPQ}}}PQH_2B_0 \tag{5.20}$$

$$-(k_{\mathrm{PQred}}PQ+k_{\mathrm{LII}})B_2+k_{\mathrm{T}}(U_{\mathrm{in}}+U_{\mathrm{dn}})B_3=0$$

$$B_0+B_1+B_2+B_3=U_{\mathrm{a}} \tag{5.21}$$

$$k_{\mathrm{LII}}U_{\mathrm{in}}-(\rho\cdot k_{\mathrm{H}}\cdot Q+k_{\mathrm{F}})U_{\mathrm{ip}}+k_{\mathrm{T}}B_3U_{\mathrm{in}}=0 \tag{5.22}$$

$$U_{\mathrm{ip}}+U_{\mathrm{in}}=U_{\mathrm{i}} \tag{5.23}$$

$$k_{\mathrm{LII}}U_{\mathrm{dn}}-(\rho\cdot k_{\mathrm{H}}\cdot Q+k_{\mathrm{F}})U_{\mathrm{dp}}+k_{\mathrm{T}}B_3U_{\mathrm{dn}}=0 \tag{5.24}$$

$$U_{\mathrm{dp}}+U_{\mathrm{dn}}=U_{\mathrm{d}}, \tag{5.25}$$

here k_{T} is the rate of energy transfer. U_{dp} or U_{ip} are the excited, and U_{dn} or U_{in} the non-excited inactive photosystems. The fluorescence signal calculates as,
The equation system for PSI is,

$$0=\frac{dY_0}{dt}=k_{\mathrm{PCox}}\cdot PC^{-}\cdot Y_2-\frac{k_{\mathrm{PCox}}}{K_{\mathrm{eq,PCP700}}}\cdot PC\cdot Y_0-k_{\mathrm{LI}}Y_0 \tag{5.26}$$

$$0=\frac{dY_1}{dt}=k_{\mathrm{LI}}Y_0-k_{\mathrm{Fdred}}\cdot Fd\cdot Y_1+\frac{k_{\mathrm{Fdred}}}{K_{\mathrm{eq,P700Fd}}}\cdot Fd^{-}\cdot Y_2. \tag{5.27}$$

Here, k_{PCox} is the rate constant of oxidation of plastocyanin at P_{700}, k_{Fdred} is the rate for the reduction of ferredoxin by PSI and k_{LI} is the light activation rate of PSI, which is set to the total light intensity.
Assuming that the total amount of PSI is conserved,

$$PSI^{\mathrm{tot}}=Y_0+Y_1+Y_2, \tag{5.28}$$

The equation system for PSI can be solved to obtain steady state expressions of the PSI states.
The rate of PSI is,

$$v_{\mathrm{PSI}}=k_{\mathrm{LI}}\cdot Y_0. \tag{5.29}$$

Here, Y_0, Y_1, and Y_2 is the fraction of open (P_{700}), excited ($P_{700}{}^{*}$) and oxidized ($P_{700}{}^{+}$) PSI.

5.3.2 Fluorescence

We assume that inactive PSII can dissipate excitation energy as heat and emit fluorescence. The fluorescence emitted by these PSII states is still affected by quenching.

Isolated PSII

Assuming no energy transfer between active and inactive PSII, the yield of fluorescence is described as (see Giersch and Krause, 1991; Ebenhöh et al., 2014),

$$F = \frac{k_\mathrm{F}}{k_\mathrm{F} + k_\mathrm{H} \cdot Q + k_\mathrm{P}} \cdot B_0 + \frac{k_\mathrm{F}}{k_\mathrm{F} + k_\mathrm{H} \cdot Q} \cdot B_2 + \frac{k_\mathrm{F}}{k_\mathrm{F} + \rho \cdot k_\mathrm{H} \cdot Q} \cdot (U_\mathrm{i} + U_\mathrm{d}) \tag{5.30}$$

Here k_F, k_P, and k_H are the rate constant of fluorescence, photochemistry, and dissipitation of light energy other than fluorescence and photochemistry. B_0 and B_2 are open and closed states of active PSII (U_a). The parameter ρ has been introduced to account for different heat dissipation properties between active and inactive PSII. Specifically, it describes the ratio of energy dissipation rates as heat between inactive ($U_\mathrm{i} + U_\mathrm{d}$) and active ($U_\mathrm{a}$) states of PSII. Q is the quencher activity.
Minimal fluorescence (F_o) is observed in a dark-adapted state, where $B_0 \approx U_a$. Thus,

$$F_o = \frac{k_\mathrm{F}}{k_\mathrm{F} + k_\mathrm{H} \cdot Q + k_\mathrm{P}} \cdot U_\mathrm{a} + \frac{k_\mathrm{F}}{k_\mathrm{F} + \rho \cdot k_\mathrm{H} \cdot Q} \cdot (U_\mathrm{i} + U_\mathrm{d}). \tag{5.31}$$

Assuming there are no inactive photosystems, Eq. (5.31) becomes,

$$F_{o,a} = \frac{k_\mathrm{F}}{k_\mathrm{F} + k_\mathrm{H} \cdot Q + k_\mathrm{P}} \cdot PSII^\mathrm{tot}. \tag{5.32}$$

This is the expected F_o signal at the beginning of an experiment before high-light treatment started.
The maximal fluorescence yield is obtained in saturating light conditions, where $B_2 \approx U_a$. Therefore,

$$F_m = \frac{k_\mathrm{F}}{k_\mathrm{F} + k_\mathrm{H} \cdot Q} \cdot U_\mathrm{a} + \frac{k_\mathrm{F}}{k_\mathrm{F} + \rho \cdot k_\mathrm{H} \cdot Q} \cdot (U_\mathrm{i} + U_\mathrm{d}), \tag{5.33}$$

and without inactive PSII, representing the signal at the beginning of high-light treatment,

$$F_{m,a} = \frac{k_\mathrm{F}}{k_\mathrm{F} + k_\mathrm{H} \cdot Q} \cdot PSII^\mathrm{tot}. \tag{5.34}$$

To quantify the response of F_o and F_m to high-light stress, we determine the derivatives of the relative fluorescence signals with respect to the active reaction centres, U_a. The non-inhibited state corresponds to $U_a = \mathrm{PSII}^{\mathrm{tot}}$. We define

$$\varphi_o := \frac{d}{dU_\mathrm{a}}\left(\frac{F_o}{F_{o,a}}\right) = \frac{Q \cdot k_\mathrm{H}\,(\rho - 1) - k_\mathrm{P}}{PSII^{\mathrm{tot}}\,(Q \cdot k_\mathrm{H} \cdot \rho + k_\mathrm{F})}, \tag{5.35}$$

and

$$\varphi_m := \frac{d}{dU_\mathrm{a}}\left(\frac{F_m}{F_{m,a}}\right) = \frac{Q \cdot k_\mathrm{H}\,(\rho - 1)}{PSII^{\mathrm{tot}}\,(Q \cdot k_\mathrm{H} \cdot \rho + k_\mathrm{F})}, \tag{5.36}$$

and the ratio of these two values,

$$\gamma := \frac{\varphi_o}{\varphi_m} = \frac{Q \cdot k_\mathrm{H}\,(\rho - 1) - k_\mathrm{P}}{Q \cdot k_\mathrm{H}\,(\rho - 1)} \tag{5.37}$$

For a non-photoinhibited state, we get with Eqs. (5.32) and (5.34)

$$\frac{F_v}{F_m} = 1 - \frac{F_o}{F_m} = 1 - \frac{k_\mathrm{F} + k_\mathrm{H} \cdot Q}{k_\mathrm{F} + k_\mathrm{H} \cdot Q + k_\mathrm{P}} = \frac{k_\mathrm{P}}{k_\mathrm{F} + k_\mathrm{H} \cdot Q + k_\mathrm{P}}, \tag{5.38}$$

and, likewise using Eqs. (5.31) and (5.33), for a photoinhibited state

$$\left(\frac{F_v}{F_m}\right)^i = U_\mathrm{a} \cdot \frac{F_v}{F_m} \cdot \frac{k_\mathrm{H} \cdot Q \cdot \rho + k_\mathrm{F}}{U_\mathrm{a} \cdot k_\mathrm{H} \cdot Q \cdot (\rho - 1) + PSII^{\mathrm{tot}}(k_\mathrm{H} \cdot Q + k_\mathrm{F})}. \tag{5.39}$$

Eq. 5.39 becomes Eq. 5.38 when $U_\mathrm{a} = PSII^{\mathrm{tot}}$.

Connected inactive and active PSII

In a second model, we assume that active closed PSII can transfer excitation energy to damaged PSII, see Giersch and Krause, 1991. We describe this energy transfer rate as a first order process with rate constant k_T. This leads to the following description of the fluorescence signal,

$$F = \frac{k_\mathrm{F}}{k_\mathrm{F} + k_\mathrm{H} \cdot Q + k_\mathrm{P}} \cdot B_0 + \frac{k_\mathrm{F}}{k_\mathrm{F} + k_\mathrm{H} \cdot Q + k_\mathrm{T} \cdot (U_\mathrm{i} + U_\mathrm{d})} \cdot B_2 + \frac{k_\mathrm{F}}{k_\mathrm{F} + \rho \cdot k_\mathrm{H} \cdot Q} \cdot (U_\mathrm{i} + U_\mathrm{d}). \tag{5.40}$$

Hence,

$$F_o = \frac{k_F}{k_F + k_H \cdot Q + k_P} \cdot U_a + \frac{k_F}{k_F + \rho \cdot k_H \cdot Q} \cdot (U_i + U_d), \tag{5.41}$$

and

$$F_m = \frac{k_F}{k_F + k_H \cdot Q + k_T \cdot (U_i + U_d)} \cdot U_a + \frac{k_F}{k_F + \rho \cdot k_H \cdot Q} \cdot (U_i + U_d). \tag{5.42}$$

The expression for F_m is a rational function of active PSII ($U_i + U_d = PSII^{tot} - U_a$). This function has a singularity at,

$$U_a = \frac{PSII^{tot} k_T + Q k_H + k_F}{k_T}, \tag{5.43}$$

and extrema at,

$$U_a = \frac{PSII^{tot} k_T + Q k_H + k_F - \sqrt{(Q k_H \rho + k_F)\,(PSII^{tot} k_T + Q k_H + k_F)}}{k_T} \tag{5.44}$$

as well as,

$$U_a = \frac{PSII^{tot} k_T + Q k_H + k_F + \sqrt{(Q k_H \rho + k_F)\,(PSII^{tot} k_T + Q k_H + k_F)}}{k_T} \tag{5.45}$$

Note that for k_T=0 the expressions for F_m and F_o are identical to the isolated case. Using Eqs. 5.41 and 5.42 we can derive an expression for F_v/F_m,

$$\left(\frac{F_v}{F_m}\right)^{i,T} = K \cdot U_a \cdot \left(\frac{F_v}{F_m} - \frac{k_T (PSII^{tot} - U_a)}{k_F + k_H \cdot Q + k_P}\right), \tag{5.46}$$

where K

$$K = \frac{k_H \cdot Q \cdot \rho + k_F}{U_a (k_F + k_H \cdot Q \cdot \rho) + (PSII^{tot} - U_a) \cdot (k_F + k_H \cdot Q + k_T \cdot (PSII^{tot} - U_a))}. \tag{5.47}$$

For k_T=0 Eq. 5.46 becomes identical to Eq. 5.39.

5.3.3 Photosynthetic electron transport chain

Cytochrome b_6f

The reaction mechanism of cytochrome b_6f is formulated as simple mass-action kinetics (Ebenhöh et al., 2014):

$$v_{\mathrm{b6f}} = \max\left(k_{\mathrm{b6f}} \cdot \left(PQH_2 \cdot PC^2 - \frac{PQ \cdot PC^{-2}}{K_{\mathrm{eq,b6f(H)}}}\right), v_{\mathrm{b6f}}^{min}\right) \tag{5.48}$$

Ferredoxin-NADPH reductase

The Ferredoxin-NADPH is described as convenience kinetics (see Liebermeister and Klipp, 2006; Ebenhöh et al., 2014).

$$v_{\mathrm{FNR}} = V_{\mathrm{FNR}}^{max} \cdot \frac{f^{-2} \cdot n^{+} - (f^2 \cdot n)/K_{\mathrm{eq,FNR}}}{(1 + f^{-} + f^{-2}) \cdot (1 + n^{+}) + (1 + f + f^2) \cdot (1 + n^{+}) - 1} \tag{5.49}$$

here, f, f^{-},n^{+} and n are:

$$f = \frac{Fd}{K_{\mathrm{M,F}}},\ f^{-} = \frac{Fd^{-}}{K_{\mathrm{M,F}}},\ n^{+} = \frac{NADP^{+}}{K_{\mathrm{M,N}}},\ n^{=}\frac{NADPH}{K_{\mathrm{M,N}}} \tag{5.50}$$

Cyclic electron flow

The model includes a simplified description of cyclic electron transport around photosystem I.

$$v_{\mathrm{cyc}} = k_{\mathrm{cyc}} \cdot (Fd^{-})^2 \cdot PQ, \tag{5.51}$$

Following Ebenhöh et al., 2014 we assume the cyclic electron flow via the reduction of the plastoquinone pool by ferredoxin to be irreversible and for various cyclic electron flow reactions one combined reaction.

ATPsynthase

For the rate of ATP synthase, the description presented in Ebenhöh et al., 2011; Ebenhöh et al., 2014 was used,

$$v_{\mathrm{ATPsyn}} = k_{\mathrm{ATPsyn}} \cdot E \cdot \left(ADP - \frac{ATP}{K_{\mathrm{eq,ATPsyn}}(H)}\right). \tag{5.52}$$

A pH-dependent activation of ATP synthase was also included (compare Matuszyńska et al., 2016).

The activation rate is

$$v_{\text{actATPsyn}} = k_{\text{actATPsyn}} \cdot H(\text{PFD}) \cdot (1 - E). \tag{5.53}$$

Deactivation is formulated as

$$v_{\text{deactATPsyn}} = k_{\text{deactATPsyn}} \cdot (1 - H(\text{PFD})) \cdot E. \tag{5.54}$$

Here H(PFD) is a function that is zero in dark and one in light (PFD $\geq$ 1) conditions.

D1 protein repair cycle

The repair and synthesis of the D1 protein of PSII were implemented by first-order equations governing the dynamics of three states of PSII (Tyystjärvi, Mäenpää, and Aro, 1994). These are PSII with intact D1 protein (U_a), PSII with damaged D1 protein (U_i), and PSII without D1 protein (U_d). Here $U_a = \sum_{i=1\ldots4} B_i$ comprises the four states of the model without photoinhibition.

$$\frac{dU_a}{dt} = k_{\text{REP}} \cdot \frac{A}{A + K_{\text{pi,m}}} \cdot U_d - (B_1 + B_3) \cdot k_{\text{PI0}} \tag{5.55}$$

$$\frac{dU_i}{dt} = (B_1 + B_3) \cdot k_{\text{PI0}} - k_{\text{DEG}} \cdot \frac{A}{A + K_{\text{pi,m}}} \cdot U_i \tag{5.56}$$

$$\frac{dU_d}{dt} = k_{\text{DEG}} \cdot \frac{A}{A + K_{\text{pi,m}}} \cdot U_i - k_{\text{REP}} \cdot \frac{A}{A + K_{\text{pi,m}}} \cdot U_d. \tag{5.57}$$

Here k_{REP} and k_{DEG} are the rate constants for the insertion of newly synthesized and degradation of damaged D1 protein. k_0^{PI} is the rate constant of photoinhibition. Several studies indicate that photoinhibition is a costly, energy-consuming process (Raven, 2011; Murata and Nishiyama, 2018). Hence, degradation and insertion (PSII repair) of the D1 protein is proportional to the ATP concentration.

Xanthophyll cycle

The representation of the xanthophyll cycle follows Matuszyńska et al., 2016. This description of the xanthophyll cycle only considers violaxanthin and zeaxanthin while ignoring antheraxanthin.
The deepoxidation from violaxanthin to zeaxanthin is,

$$v_{\mathrm{VDP}} = k_{\mathrm{deepox}} \cdot \frac{H^{n_{\mathrm{HX}}}}{H^{n_{\mathrm{HX}}} + pH_{\mathrm{inv}}(K_{\mathrm{pHsatZ}})^{n_{\mathrm{HX}}}} \cdot V, \tag{5.58}$$

where pH_{inv} is a function transforming lumenal pH in lumenal proton concentrations.
The epoxidation rate from zeaxanthin to violaxanthin is,

$$v_{ZEP} = k_{\mathrm{epox}} \cdot Z \tag{5.59}$$

PsbS protonation and deprotonation

Equations of protonation and deprotonation of PsbS are used from Matuszyńska et al., 2016,

$$v_{\mathrm{prot}} = k_{\mathrm{prot}} \cdot \frac{H^{n_{\mathrm{HL}}}}{H^{n_{\mathrm{HL}}} + pH_{\mathrm{inv}}(K_{\mathrm{pHsatLHC}})^{n_{\mathrm{HL}}}} PsbS \tag{5.60}$$

and

$$v_{\mathrm{deprot}} = k_{\mathrm{deprot}} PsbS^{p}. \tag{5.61}$$

Quencher

Quenching is formulated via a four-state quencher module. This module includes the Xanthophyll cycle and the protonation state of PsbS. Each state is weighted by a parameter (γ_0, γ_1, γ_2, γ_3) and the Quencher activity is then calculated as,

$$Q = \gamma_0 \cdot (1 - Z_s) \cdot PsbS + \gamma_1 \cdot (1 - Z_s) \cdot PsbS^{p} + \gamma_2 \cdot Z_s \cdot PsbS^{p} + \gamma_3 \cdot Z_s \cdot PsbS, \tag{5.62}$$

where the contribution of zeaxanthin (Z_s) is (compare Matuszyńska et al., 2016),

$$Zs = \frac{Z}{Z + Kzsat} \tag{5.63}$$

Additionally, when considering a long-term quenching compound, the simplified assumption was made that this compound's activity is proportional to the fraction of inactive PSII, resulting in a fifth term for the quencher's activity.

$$\gamma_4 \cdot \left(1 - \frac{U_a}{PSII^{tot}}\right). \tag{5.64}$$

ATP and NADPH consumption

All processes that consume ATP and NADPH (except the resynthesis of the D1 protein) are combined into one term each,

$$v_{\text{ATPcons}} = k_{\text{ATPcons}} \cdot ATP \tag{5.65}$$

and

$$v_{\text{NADPHcons}} = k_{\text{NADPHcons}} \cdot NADPH \tag{5.66}$$

In previous models (Ebenhöh et al., 2014; Matuszyńska, Saadat, and Ebenhöh, 2019), an external influx of ATP into the chloroplast is not included. However, several studies have shown that the metabolism of chloroplasts and mitochondria are interconnected and can influence each other (Hoefnagel, Atkin, and Wiskich, 1998; Watanabe et al., 2016; Yamada, Ozaki, and Noguchi, 2020). We assumed that during light conditions, the external influx of ATP into the chloroplast is negligible, and the activity of the PETC provides all ATP. We model the external influx of ATP as constant flux with a light switch to ensure the resynthesis of the D1 protein in darkness.

$$v_{\text{mito}} = k_{\text{mito}} \cdot \frac{K_{\text{PFD}}^{\text{nL}}}{K_{\text{PFD}}^{\text{nL}} + \text{PFD}^{\text{nL}}} \tag{5.67}$$

Proton leak

The thylakoid membrane is assumed to be leaky for protons (Ebenhöh et al., 2014; Matuszyńska et al., 2016).

$$v_{\text{leak}} = k_{\text{leak}} \cdot (H - H_{\text{stroma}}) \tag{5.68}$$

PTOX

For the implementation of PTOX a constant stromal oxygen concentration is assumed (O_2^{ext}).

$$v_{\text{PTOX}} = k_{\text{PTOX}} \cdot O_2^{\text{ext}} \cdot PQH_2 \tag{5.69}$$

5.3.4 Equilibrium constants

To include the electrical and pH-dependent contribution of the protonmotive force on the activities of the PETC, we calculated the equilibrium constants as outlined initially in Ebenhöh et al., 2014 and used in Matuszyńska et al., 2016; Matuszyńska, Saadat, and Ebenhöh, 2019; Saadat et al., 2021. We repeat the example as outlined in Ebenhöh et al., 2014 for clarification. the overall reaction for cytchrome b_6f is

$$PQH_2 + 2\,PC + 2\,H^+_{stroma} \rightleftharpoons PQ + 2\,PC^- + 4\,H^+_{lumen}.$$

We split the reaction into two redox half-reactions and one transport process:

$$\text{(a) } PQ + 2\,e^- + 2\,H^+_{lumen} \rightleftharpoons PQH_2$$
$$\text{(b) } PC + e^- \rightleftharpoons PC^-$$
$$\text{(c) } H^+_{stroma} \rightleftharpoons H^+_{lumen}$$

The overall reaction is the stoichiometric sum

$$-1 \cdot (a) + 2 \cdot (b) + 2 \cdot (c). \tag{5.70}$$

The contribution to the standard Gibbs free energy change are

$$\Delta G^o_1 = -2FE_o(PQ/PQH_2) + 2RT\ ln(10) \cdot pH_{lumen} \tag{5.71}$$
$$\Delta G^o_2 = -2FE_0(PC/PC^-) \tag{5.72}$$
$$\Delta G^o_3 = RT\ ln(10)(pH_{stroma} - pH_{lumen}). \tag{5.73}$$

Hence, according to the stoichiometric sum the overall standard Gibbs free energy change amounts to

$$\Delta G^o = -\Delta G^o_1 + 2\Delta G^o_2 + 2\Delta G^o_3 \tag{5.74}$$

The equilibrium constant can be easily derived using ΔG^o.

5.3.5 Computational analysis

The model was implemented in the Python-based software `modelbase` version 1.3.8 (Aalst, Ebenhöh, and Matuszyńska, 2021). For simulations the cvode solver implemented in Assimulo (Andersson, Führer, and Akesson, 2015) was used. Python files containing the model and analyses can be found in the Gitlab repository https://gitlab.com/qtb-hhu/models/2023-photoinhibition.

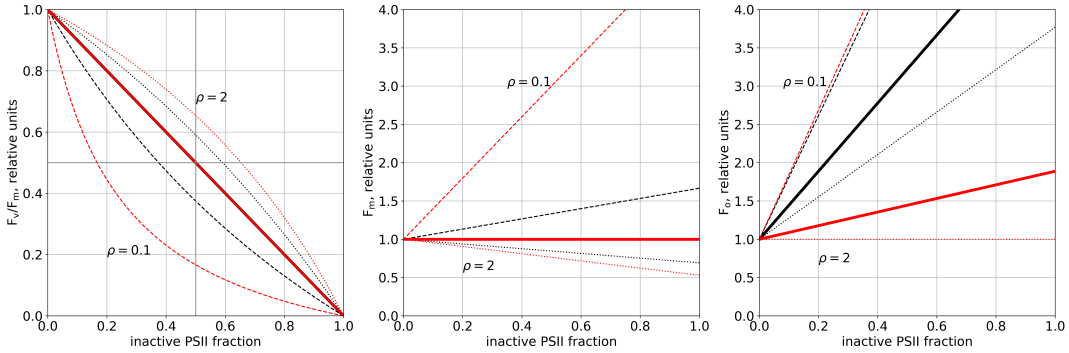

FIGURE 5.2: Relationship between F_v/F_m, F_m, and F_o and fraction of inactive photosystem II based on Eq. 5.30. The dashed, continuous, and dotted lines indicate scenarios in which the ratio of heat dissipation between inactive and active PSII is 0.1, 1, and 2, respectively. Black lines signify a low quenching, while red lines denote high quenching activity (Q = 0.1 and 1). Parameter values used for the calculations can be found in the supplement table 5.1

5.4 Result

For our analysis, we constructed a mathematical model that combines the description of the PETC as in (Ebenhöh et al., 2014; Matuszyńska et al., 2016) and the D1 damage-repair cycle from (Tyystjärvi, Mäenpää, and Aro, 1994) (for details, see Methods and Supplement). In the following, we describe the development of hypotheses about mechanistic aspects of the fluorescence signal during photoinhibition and compare model predictions with experimental observations. Guided by discrepancies between experiment and simulations, we iteratively refine our hypotheses to arrive at a realistic description of the fluorescence signal.

5.4.1 Experimental dynamics of fluorescence signals

The data (see Fig. 5.8) comprises F_v/F_m, F_m and F_o measurements for *Arabidopsis thaliana* wildtype and *npq1* mutant plants for different exposure times to high light and with or without treatment with lincomycin, which inhibits chloroplast protein synthesis and thus the D1 repair (see Methods). The experimental data suggest that the *npq1* mutant, which lacks violaxanthin deepoxidase enzyme and thus cannot form zeaxanthin in the so-called xanthophyll cycle, reacts more sensitively to high-light stress in water (control) and lincomycin treatment. Fig. 5.8 shows that the relative reduction of F_m is generally more pronounced than the increase of F_o, indicating F_m to be the main factor determining the changes in F_v/F_m in this experiment. While the differences between the water and lincomycin treatment are clearly discernible

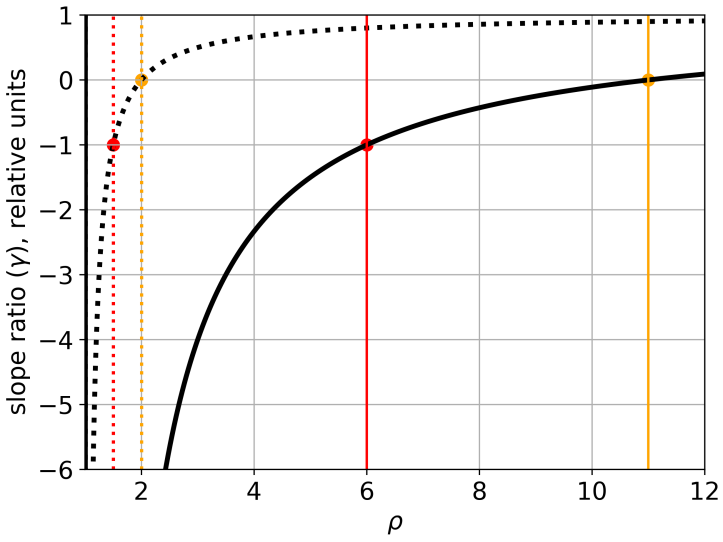

FIGURE 5.3: The slope ratio γ for model without energy transfer in a high (dotted line) and low quenching scenario (continuous line). Vertical lines indicate the points at which the slope ratio is -1 or 0. Parameters are the same as for Fig. 5.2.

for the wildtype and *npq1* mutant in the F_m and F_v/F_m signal, this is not the case for F_o.

5.4.2 Changes in the F_v/F_m signal

We started our computational analysis with the most simple assumptions for the model extended with photoinhibition: We assume that 1) the duration and intensity of the high-light treatment determine the amount of inactive PSII; 2) inactive PSII contributes to fluorescence and has the same quenching properties as active PSII and; 3) there is no energy transfer between active and inactive reaction centers. With these assumptions, our model of photoinhibtion cannot reproduce the experimentally observed data (see Fig. 5.8). The increase of F_o with prolonged high-light treatment is much higher than in the experiment, while there is only little or no effect for simulated F_m. Interestingly, the F_v/F_m signal can be described by the model, indicating that the F_v/F_m signal alone does not provide sufficient information to understand the underlying mechanisms.

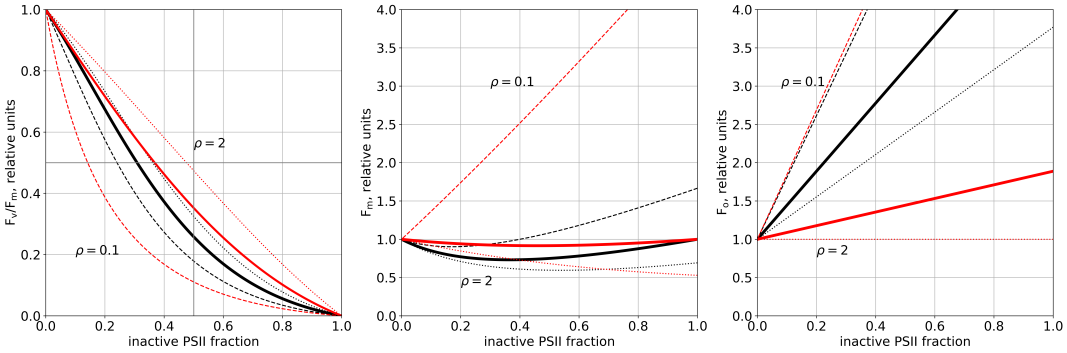

FIGURE 5.4: Relationship between F_v/F_m, F_m, and F_o and fraction of inactive photosystem II based on Eq. 5.40. The dashed, continuous, and dotted lines indicate scenarios in which the ratio of heat dissipation between inactive and active PSII is 0.1, 1, and 2, respectively. Black lines signify a low quenching, while red lines denote high quenching activity (Q = 0.1 and 1). Parameter values used for the calculations can be found in the supplement table 5.1. Energy transfer was set to $8 \cdot 10^8$ mmol^{-1} (mol Chl) s^{-1}.

5.4.3 Fluorescence signal in photoinhibtion

Motivated by this observation, we modified our model similar to Giersch and Krause, 1991 by assuming that the fluorescence signal and heat dissipation properties of active and inactive PSII can differ. This means we relax assumption 2 stated above. To quantify the different behaviour, we introduce the parameter ρ as the ratio of heat dissipation rate constants between inactive and active states of PSII – see Eq.(5.30). This means that $\rho = 1$ corresponds to the previous model, $\rho < 1$ denotes a model in which inactive PSII dissipate heat less effectively and thus yield more fluorescence than active PSII, and $\rho > 1$ describes the opposite scenario.

Using Eqs. (5.31) and (5.33), we can predict the qualitative changes of F_m and F_o as a response to photodamage:

$$\rho = \begin{cases} 0 < \rho < 1, & F_m \text{ increases, } F_o \text{ increases,} \\ 1 < \rho < \frac{k_P}{k_H \cdot Q} + 1, & F_m \text{ decreases, } F_o \text{ increases, } . \\ \rho > \frac{k_P}{k_H \cdot Q} + 1, & F_m \text{ decreases, } F_o \text{ decreases,} \end{cases} \tag{5.75}$$

An increase or decrease of F_m depends only on whether ρ is larger or smaller than 1. In contrast, the F_o behavior (increase or decrease) depends not only on the value of ρ but also on the quenching activity Q.

Fig. 5.2 shows that for the case in which the heat dissipation of active and inactive photosystems is identical (ρ =1, continuous lines), F_v/F_m follows a linear relationship with the fraction of active PSII, both in a low and

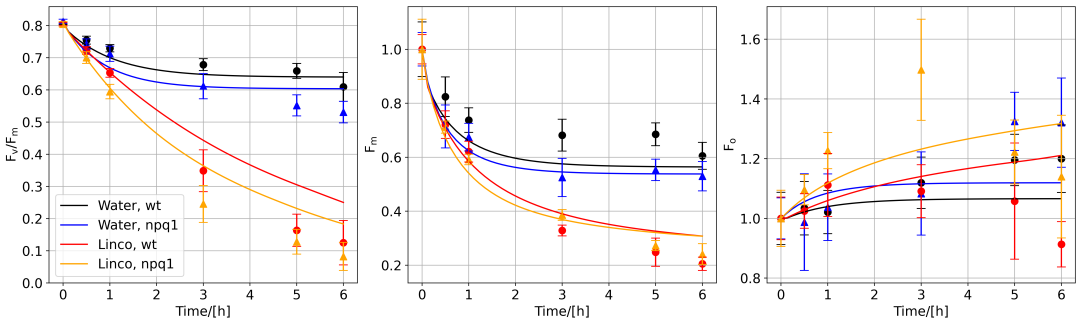

FIGURE 5.5: Experimental measurement and simulated changes in F_v/F_m, F_m, and F_o in high-light treatment of *A.thaliana* plants for 6 hours. The plants were either treated with water (black and blue lines) or lincomycin (red and orange line) inhibiting protein synthesis. Light intensity was 800 µmol m^{-2} s^{-1}.

high quenching scenario (black, and red lines). However, the relationship becomes nonlinear when the active and inactive PSII differ in their heat dissipation capabilities. We further observe that ρ determines the curvature of the relationship between F_v/F_m and active PSII fraction, while an active quencher makes the non-linearity more pronounced. The dependence of F_m and F_o on active PSII is linear in all cases. However, the slope is affected both by ρ and Q. Note that F_m is not affected by photoinhibition for $\rho = 1$ (original model, Fig. 5.8, see also Giersch and Krause, 1991).

For a fluorescence yield model without energy transfer, the ratio of the slopes of relative values of F_o and F_m as functions of active PSII is given by Eq. (5.37). The slope ratio has a singularity at $\rho = 1$ where the slope of F_m becomes zero. The slope ratio is zero at $\rho = k_P/(k_H \cdot Q) + 1$, when the slope of F_o is zero. In our fluorescence measurements for *A. thaliana* during high-light treatment, we observed that the realtive increase of F_o is smaller than the relative decrease of F_m. To reproduce this behavior, the slope ratio must be negative, in the range between -1 and 0. For this, ρ must be constrained to the interval

$$\frac{k_P}{2k_H \cdot Q} + 1 \leq \rho \leq \frac{k_P}{k_H \cdot Q} + 1. \tag{5.76}$$

Fig. 5.3 depicts the slope ratio for the parameter values in the model for two different quenching activities. In a low quenching scenario ($Q = 0.1$, solid line), the parameter ρ is predicted to lie in the range between 6 and 11. This means that, in order to reproduce the experimentally observed slope ratio, damaged PSII needs to dissipate heat with a rate at least six times larger than that at which intact PSII does. Similarly, in a high quenching scenario ($Q = 1$, dotted line) we find $1.5 \leq \rho \leq 2$, which means a one- to twofold

faster heat dissipation for damaged vs. active PSII.

We used these constraints to fit our model to the experimental data. We find that the data could be considerably better explained than in the model with $\rho = 1$ (see Suppplementary Figs. 5.9 and 5.10). With the parameter ρ in the range determined above, all qualitative features of the fluorescence traces could be reproduced. However, there are still quantitative discrepancies, which could not be resolved using this model.

We therefore expanded the model to include excitation energy transfer between closed active and damaged PSII, following the example in Giersch and Krause, 1991. This leads to a modified formula to describe F_m, whereas the description for F_o remains the same as in the case without energy transfer (see Eqs. 5.41 and 5.42). Consequently, the relation between F_m and active PSII becomes nonlinear (see Fig. 5.4). The effect of an excitation energy transfer between active and inactive PSII leads to a faster decrease of the F_v/F_m value in response to lowering the active PSII fraction. Moreover, the effect of the energy transfer seems to be larger in a low quenching than a high quenching state (compare Figs. 5.2 and 5.4). Because the description of F_o does not change compared to the isolated case, ρ and the quencher activity are still the determining factor for the behavior of F_o. However, the behavior of F_m is a nonlinear function of the active PSII fraction, and therefore a slope ratio can no longer be uniquely defined.

5.4.4 Model predictions

Guided by comparison of model predictions and experimental data, we have iteratively refined a model of the photosynthetic electron transport chain. The resulting model includes the assumption that energy quenching differs between active and damaged photosystems. Morever, energy can be transferred from active to damaged photosystems. This model version can satisfactorily reproduce our experimental data for *A. thaliana* (see Fig. 5.5). In the following, we employ our model to make novel predictions how photoinhibition affects key photosynthetic parameters.

Quenching shifts the fraction of closed and open PSII during photoinhibition

To describe internal processes of photosystem II, we used a simplified mathematical representation that has been applied successfully for modeling fluorescence signal changes in connection to state transition and non-photochemical quenching (Ebenhöh et al., 2014; Matuszyńska et al., 2016; Matuszyńska, Saadat, and Ebenhöh, 2019). This representation of PSII can be approximated by a two-state system consisting of the open and closed active PSII states.

Fig. 5.6 shows the changes of closed and open active PSII states during exposure to various light intensities for four hours as phase-space trajectories. We investigate four model versions with (right column) and without (left column) dynamic quencher activity as well as with non-constantly (top row) and constantly active (bottom row) ATP synthase. The version with non-constantly active ATP synthase and dynamic quencher is our original model (top left). For all four versions, the phase-space provides information about the different stages we observe during the onset of photoinhibition. These stages are characterised by the different time-scales on which they operate. The simulation starts with a dark-adapted state and, hence, with no closed PSII. When the light is switched on, the system almost instantaneously changes to a state where both closed, and open PSII are present. The ratio of open to closed PSII depends on the light intensity. A light intensity of around 1000 $\mu mol\, m^{-2}\, s^{-1}$results in approximately 85% of PSII in the closed state. This initial stage is driven by the rapid processes in photosystem II.

The first stage is followed by the second stage, which operates on a time-scale of seconds to minutes. In this phase, two effects dominate. Firstly, ATP synthase is activated (arrows marked as "Q + ATPsyn." and "ATPsyn".). Secondly, the fast component of the quencher is rapidly activated, leading to a slower activation of PSII and thus a smaller fraction of closed states (compare top row with bottom row). Comparing the left (dyanmic quencher) and right (no quencher) columns as well as the top (non-constantly active ATP synthase) and bottom (constantly active ATP synthase) rows of Fig. 5.6 illustrates the effect of these two processes individually. In this stage, photoinhibition starts to become active but photodamage is still negligible.

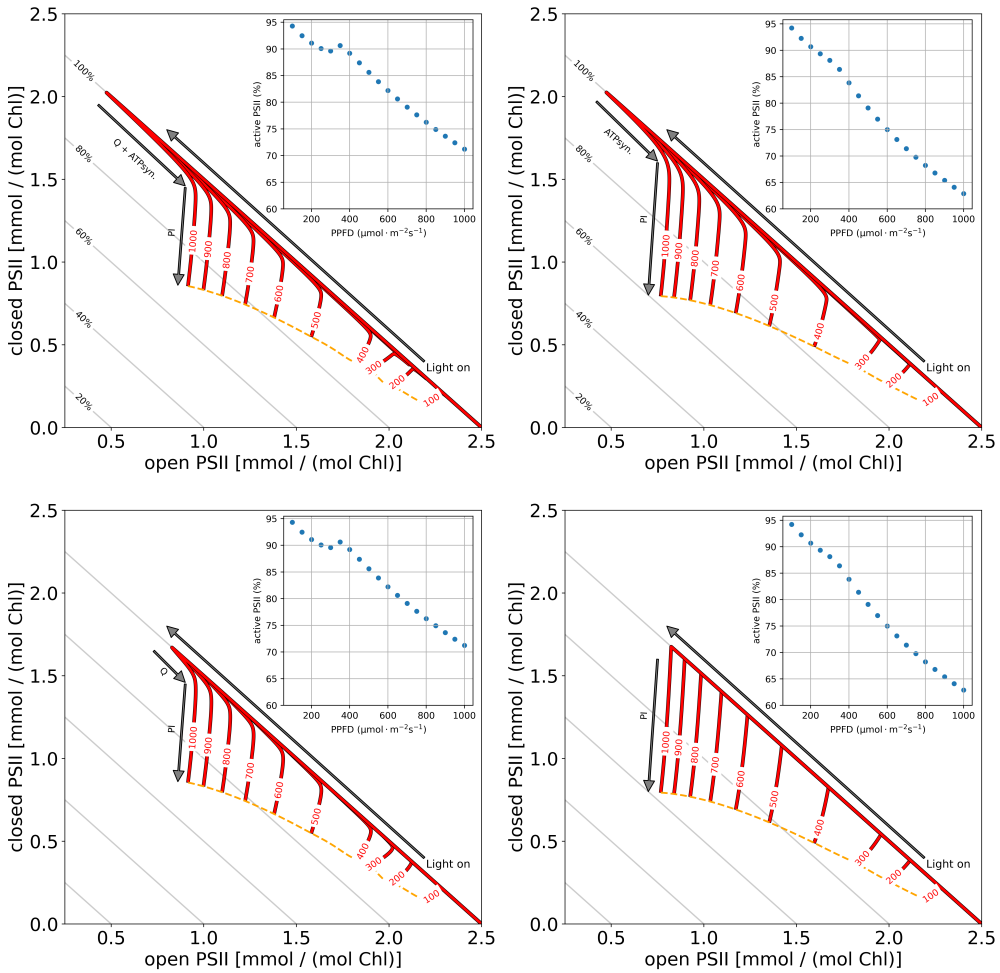

FIGURE 5.6: phase-space of open (B_0) and closed (B_2) active PSII states during photoinhibtory treatment in various light intensities (100 — 1000 µmol m^{-2} s^{-1}). Red lines indicate changes in open and closed PSII. The orange dashed line connects all points in the phase-space reached after 4 hours of light treatment. Grey lines indicate the fraction of total active PSII. Inset shows the fraction of active PSII as a function of applied light intensity at the end of the simulation. The top left and top right panel show the phase-space of a model version with and without a dynamic quencher. The bottom left and bottom right show the phase-space of a model version with and without a dynamic quencher and without ATP synthase activation.

This stage is followed by the slower stage of photoinhibition, which extends over several hours. Here, the active amount of PSII is gradually reduced due to photodamage. In the phase-space this is reflected by the downward pointing red lines. This phase continues until repair processes compensate for the extent of the light-induced damage, indicated by the dashed yellow lines. By comparing the four model versions with and without a dynamic quencher and with non-constantly and constantly active ATP synthase, it becomes apparent that quenching not only leads to more open PSII but also reduces the extent of photodamage, visible by the shorter downward trajectories for the model with active quencher. In our model simulation and with our chosen parameters, the quenching activity leads to almost 10% more active PSII after four hours of light treatment with an intensity of 1000 µmol m^{-2} s^{-1}(see inset in Fig. 5.6).

Steady state photoinhibition analysis

We observed that dynamic quenching, associated with PsbS and the xanthophyll cycle (Fig. 5.5), is a key determinant for the extent of high-light stress-induced photodamage. We employed our model to systematically analyze the connection between quenching and the steady-state behavior for different light intensities. For this, rate constants associated with non-photochemical quenching were set to zero, and the quenching activity was fixed to be a constant value. Subsequently, the system was simulated until it reached a steady state. Fig. 5.7 displays the computed steady state photoinhibition rate.

In low quenching regimes, we observe a slightly sigmoidal transition between high and low photoinhibition rates with increasing light intensities. For very low quenching activities, the photoinhibition rate increases quickly, having a disproportionally high increase at around 400 µmol m^{-2} s^{-1}. This demonstrates that small light intensity changes can already have strong photoinhibitory effects in low light regimes. By contrast, when quenching is active, we observe a smooth transition from low to high-light intensities, indicating greater tolerance against high-light stress.

5.5 Discussion and Outlook

We have presented a model of the PETC integrating non-photochemical quenching and photoinhibitory processes. The model aims to a) investigate

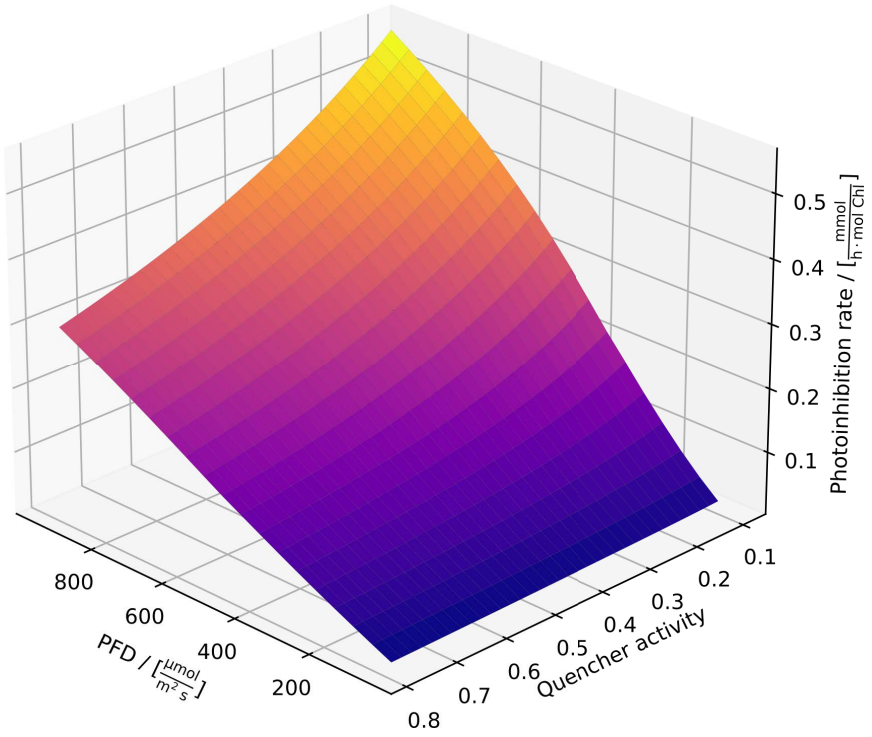

FIGURE 5.7: The predicted stationary flux of photoinhibition for different light intensities and different quencher activities. Quenching activities were modeled for these predictions by imposing fixed values (x-axis) between 0.1, representing almost no quencher activity, and 0.8., representing double the quencher activity typically observed in our model simulations. Light intensity (x-axis) was varied. The system was simulated for each combination of light intensity and quenching activity until a steady state was reached. On the z-axis, the stationary photoinhibition rate is plotted. For low quenching activities, a sigmoidal transition between high and low photoinhibition rates is observed with light intensities. This demonstrates that small light intensity changes can already have strong photoinhibitory effects in low light regimes. For higher quenching activities, the transition is smoother, almost linear, indicating higher flexibility, as expected, more flexibility against high-light stress.

how fluorescence signals (F_m and F_o) in response to photoinhibition can be explained, b) explore which assumptions are sufficient to reproduce experimental data, c) study the effects of different modes of energy quenching, and d) quantify stationary photoinhibtory rates. To do so, we followed a reductionist approach. Our initial model version of photodamage in the PETC was built on the simple assumptions that 1) photoinhibition is proportional to intensity and duration of light treatment, 2) there is no difference between heat dissipation properties of active and damaged photosystems, and 3) there is no energy transfer between photosystems. However, this version could not reproduce the experimental data; see Fig. 5.8. Motivated by differences between simulations and experimental data, we systematically increased the complexity of the model representation by firstly introducing differences in heat dissipation properties of active and inactive photosystems (Fig. 5.2) and secondly an energy transfer between closed active and inactive photosystems in the description of the fluorescence signal (Fig. 5.4).

Both additions are realistic and have previously been used to study fluorescence changes after high-light treatment (Giersch and Krause, 1991) with fluorescence yield models. This previous investigation did not include a dynamic lumenal pH-induced quenching component. Our model implements quenching based on the four state model introduced by Horton et al., 2008, which is also included in Matuszyńska et al., 2016. In comparison to Matuszyńska et al., 2016, in our model version the influence of the qZ component (zeaxanthin concentration high, no PsbS protonation) is reduced. This modification was necessary to realistically simulate differences between the wildtype and *npq1* mutant. After introducing all these changes to our initial model version, the fit agreed with experimental data (Fig. 5.5), supporting the assumptions that heat dissipation properties differ between intact and damaged photosystems and that energy transfer occurs.

Whereas the F_v/F_m and F_m signals could be very well reproduced with deviations in the range of experimental errors, the experimental F_o signal slightly deviates from our simulated fluorescence traces. We hypothesized that a long-term quencher independent of the xanthophyll cycle and PsbS protonation, not yet implemented, could improve the model fit. To test this, we implemented an additional component in the quencher description of Matuszyńska et al., 2016 proportional to inactive PSII to our first model version (without heat dissipation differences and energy transfer). This should mimic a quenching process proportional to high-light stress that is still strongly active after dark adaption. Although the changes in the F_m,

F_v/F_m and F_o signal are now primarily products of the long-term quencher (compare Fig. 5.8 and Fig. 5.11), the agreement between simulated and experimental fluorescence traces improved, even reproducing the decrease of the F_o signal in lincomycin treatment (Fig. 5.11). However, the conditions under which we recorded the experimental data should not induce any additional strong long-term quenching component, motivating us to discard this long-term quencher hypothesis and instead to to focus on the initial simple description of fluorescence yield based on Giersch and Krause, 1991.

Besides replicating experimental data, the value of a model lies in providing a way to investigate biological phenomena not easily accessible by experiments. Here, we specifically focused on the changes in excited and non-excited active PSII during photoinhibition. We used a phase-space visualization to observe the dynamic response of the system to different light conditions (Fig. 5.6). Our results show that one effect of the quencher is to actively push PSII to more open states, leading to a long-term reduction of high-light induced photodamage. The changes in active PSII shown in Fig. 5.6 is probably due the activation of the ATP synthase and the saturation of the quencher. Additionally, we investigated the effects of quenching for steady-state rates of photodamage and found a disproportionally strong effect of high-light stress in low-quenching scenarios Fig 5.7. In high-quenching scenarios, the response becomes linear, indicating that quenching might be essential for the flexible behavior of photosynthetic organisms under high-light stress.

Combining the previous observations, we might speculate that fluorescence changes induced by high-light stress are caused by a combination of various processes, including the reduction of PSII core functionality and multiple long- and short-term quenching mechanisms. Our simulations indicate that, to explain observed changes in the F_v/F_m, F_m and F_o signals, three components are essential: 1) the amount of active and inactive PSII, 2) the difference between their heat dissipation properties and 3) quenching phenomena. For the latter, it is essential to distinguish between short- and long-lived quencher components. While short-lived quenchers influence the decrease of the active PSII fraction but not the fluorescence signal measured after dark-adaption, long-lived quenchers influence both.

There is a continuous discussion about whether inactive PSII is photoprotective (Matsubara and Chow, 2004; Sarvikas, Tyystjärvi, and Tyystjärvi, 2010; Kou et al., 2012). This hypothesis was based on the observation that an active PSII pool remained even after prolonged high-light treatment and

repair inhibited by lincomycin (Lee, Hong, and Chow, 2001). However, later studies did not support these findings and it was speculated that the observed active pools resulted from the specific experimental setup (Kou et al., 2012). Regarding the mechanism, it was hypothesized that photoprotection is caused by an energy transfer from active to inactive photosystems, which are more efficient energy quenchers (Matsubara and Chow, 2004). It was argued that without energy transfer photoinhibition is a first-order process, and that the existence of an energy transfer and photoprotection should be detectable by a deviation from an exponential kinetics (Matsubara and Chow, 2004; Sarvikas, Tyystjärvi, and Tyystjärvi, 2010).

With our model, we can test these hypotheses by simulating the respective scenarios. Fig. 5.12 shows the dynamics of PSII simulated with (red) and without (orange) assumed energy transfer. We observe that in both cases the dynamics of active PSII closely resemble a simple exponential, and thus may be interpreted as a first-order process. However, even in the case without energy transfer, small discrepancies from the exponential behavior are visible. Although such small differences are unlikely to be experimentally detectable, they can be theoretically explained. An exact exponential decay would entail that the fraction of excited PSII (relative to active PSII) remains constant. However, in our simulations this is not precisely the case (see Fig. 5.13). The cause for this is that the redox state of the plastoquinone pool and the state of the quencher depend on the rate of electrons provided by PSII, and thus on the amount of active PSII itself, leading to a non-trivial dynamics which is only approximately exponential. Interestingly, even the decay of PSII under the assumption of energy transfer closely resembles an exponential. We therefore conclude that observing discrepancies from an exponential behaviour might not be the best suited method to discriminate between the two hypotheses.

This is especially the case when using F_v/F_m as a measure of photoinhibition. Our calculations have shown that, in a scenario without energy transfer, changes in F_v/F_m only follow the active PSII decay proportionally if the active and inactive PSII have identical heat dissipation properties ($\rho = 1$, see Fig. 5.2). However, because we used F_m and F_o, besides F_v/F_m, to guide our simulations, we could show that the experimental observations can only be explained if $\rho > 1$, which means that inactive PSII quench energy more efficiently than active PSII. This in turn means that F_v/F_m is a nonlinear function of inactive PSII, and as a consequence the F_v/F_m signal displays a slightly different kinetic than the active PSII pool (see Figs. 5.12 and 5.14). Nonetheless,

without energy transfer also a value of $\rho > 1$ results in simulated F_v/F_m that is too large compared to the experiment (see Figs. 5.9 and 5.10). Assuming an energy transfer, leads to reduced simulated F_v/F_m values and allows quantitative reproduction of the measured signal (Figs. 5.4 and 5.5). Interestingly, energy transfer leads to a more linear response of the F_v/F_m signal to inactive/active PSII (see Fig. 5.14), resulting in a F_v/F_m dynamics that follows the response of the approximately simulated exponential decay of PSII more closely. Thus, our theoretical analysis allowed discrimination between the effects of higher energy quenching of inactive PSII and energy transfer. Our results support the existence of energy transfer processes from active to inactive PSII.

In conclusion, we used a mathematical model of the PETC to investigate the fluorescence signal during photoinhibition and identified key factors that need to be included in order to realistically explain experimental fluorescence data. In addition to the hypotheses explored in this work, there are many other conceivable extensions and improvements. One possible extension is to include PSI fluorescence, as was done in Stirbet and Govindjee, 2016. We speculate that the PSI contribution might lead to a more realistic reproduction of the F_o signal. In addition, it may become important to include a description of PSII heterogeneity. The PSII pool consists of so called PSIIα and PSIIβ complexes. Both differ in their antenna size and localization in the thylakoid membrane (Melis, 1985; Black, Brearley, and Horton, 1986). In preliminary investigations we found that including such a heterogeneity does not change the slope ratio as defined in Eq. (5.37), which is a key indicator for the model response (see supplement). However, a full and realistic implementation of PSIIα and PSIIβ and their different properties into our dynamic model is a future project. So far, also spatial effects have been ignored, in order to reduce the complexity of the *in silico* analysis. However, considering the complex three-dimensional structure of thylakoid membranes, these may be important to consider for more realistic models (Kirchhoff, 2013). Additionally, it has been shown that the spatial architecture of leaves and the place of measurement (ad-, abaxial, or within leaves) influence the fluorescence signal obtained by spectroscopic techniques during photoinhibition (Oguchi et al., 2011). Because we used a Dual-KLAS-NIR device for our measurements that records fluorescence on the abaxial leaf surface, future model versions should account for different local origins of the fluorescence signal. This is because the changes in the fluorescence signal obtained by devices measuring the abaxial surface, such as a Dual-KLAS-NIR, might correlate more with

changes in chloroplasts in the lower than in the upper layers of the leaf. We envisage that our model can be used as a platform for the investigation of photoinhbitory effects, with several applications in mind. These include the study of long-term extinction phenomena (qZ and qH), which could support experimental efforts to identify the molecular mechanisms responsible for such quenching phenomena (Malnoë, 2018). Moreover, our model also opens the possibility of investigating evolutionary questions. For example, by modifying the appropriate parameters, it can be used to explore the quenching capacities of a wide range of plant and algal species, thus supporting the generation of hypotheses explaining the enormous natural variation found in photoprotective processes (Matuszyńska et al., 2016; Rungrat et al., 2019).

5.6 Concluding remarks

This chapter looked at photoinhibition a long-term process connected to photosynthesis. Photoinhibition is a natural process that happens constantly when photosynthetic organisms are exposed to light. Understanding how we can monitor photoinhibition via spectroscopic methods and what molecular processes influence the obtained fluorescence signal is essential for building future strategies that could alleviate the effects of photoinhibition. This is especially important when considering the increasing demand for food that humanity will face in the next few decades. Moreover, understanding the mechanisms behind photodamage and protection will provide new targets to reduce the extent of the damage or speed up the repair. With this chapter, we contributed to obtaining a deeper understanding of photoinhibition. For this, we looked at the absolute and relative changes between characteristic fluorescence signals, allowing us to pinpoint the differences between the damaged and active PSII pool and their different behaviors in terms of amount of inactive photosystems and heat dissipation.

5.7 Supplementary figures and texts

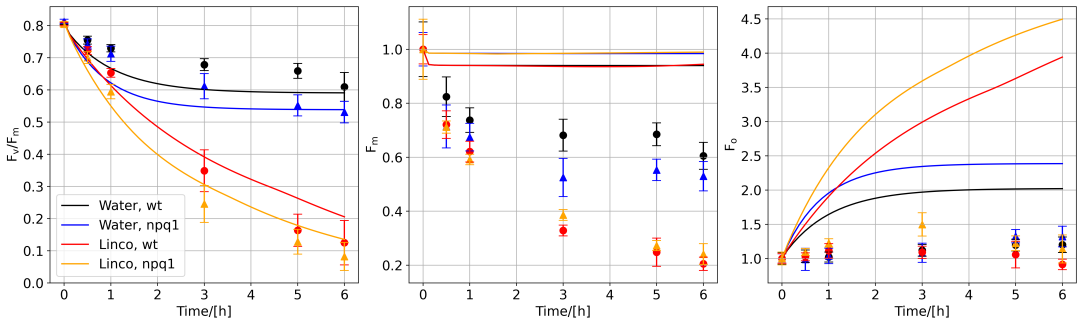

FIGURE 5.8: Experimental measurement and simulated changes in F_v/F_m, F_m, and F_o in high light treatment of *A.thaliana* plants for 6 hours. The plants were treated with water (black and blue lines) or lincomycin (red and orange lines), inhibiting protein synthesis. Light intensity was 800 $\mu mol\, m^{-2}\, s^{-1}$. The model did not include energy transfer processes and difference in heat dissipation properties between active and inactive PSII.

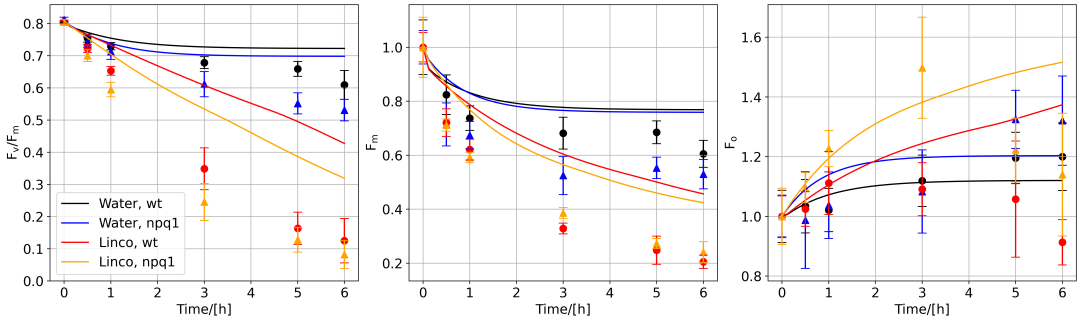

FIGURE 5.9: Experimental measurement and simulated changes in F_v/F_m, F_m, and F_o in high light treatment of *A.thaliana* plants for 6 hours. The plants were treated with water (black and blue lines) or lincomycin (red and orange lines), inhibiting protein synthesis. Light intensity was 800 $\mu mol\, m^{-2}\, s^{-1}$. The model did include differences in heat dissipation properties between active and inactive PSII (ρ=6).

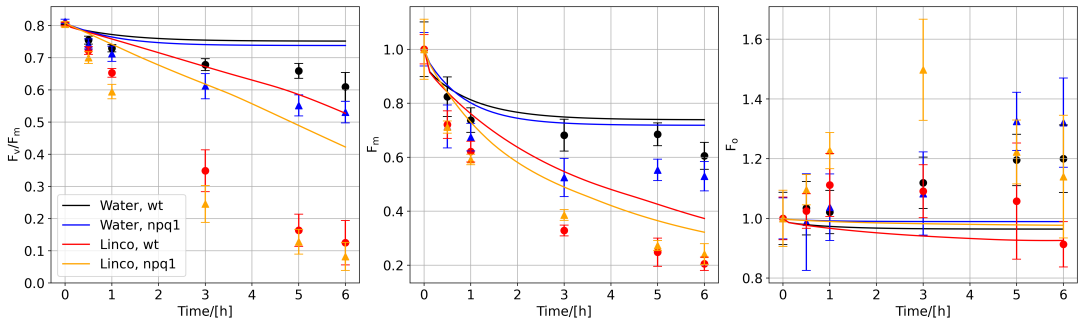

FIGURE 5.10: Experimental measurement and simulated changes in F_v/F_m, F_m, and F_o in high light treatment of *A.thaliana* plants for 6 hours. The plants were treated with water (black and blue lines) or lincomycin (red and orange lines), inhibiting protein synthesis. Light intensity was 800 µmol m^{-2} s^{-1}. The model did include differences in heat dissipation properties between active and inactive PSII (ρ=11).

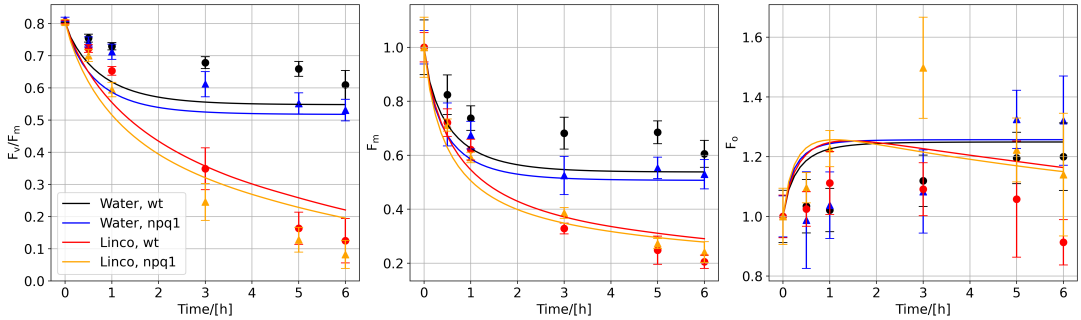

FIGURE 5.11: Experimental measurement and simulated changes in F_v/F_m, F_m, and F_o in high light treatment of *A.thaliana* plants for 6 hours. The plants were either treated with water (black and blue lines) or lincomycin (red and orange line) inhibiting protein synthesis. Light intensity was 800 µmol m^{-2} s^{-1}. $\rho = 1$, $kT = 0$, and slow quenching was used.

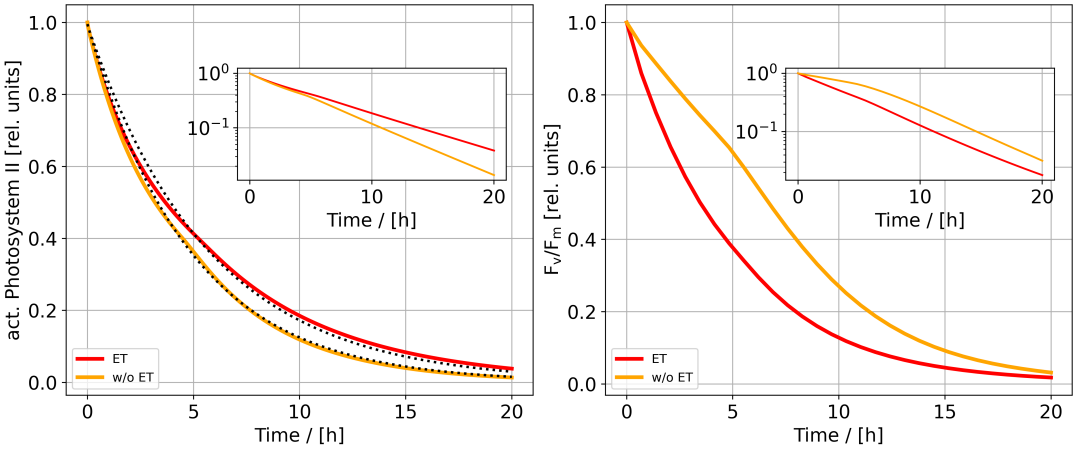

FIGURE 5.12: Simulated changes of active PSII and F_v/F_m in a model version with (red) and without (orange) energy transfer between active and inactive PSII (k_T=0) during high light treatment (800 µmol m^{-2} s^{-1}). The simulation were supposed to happen in lincomycin-treated tissue. Dotted lines indicate a fit to exponential function. Insets show the same data but on logarithmic scale.

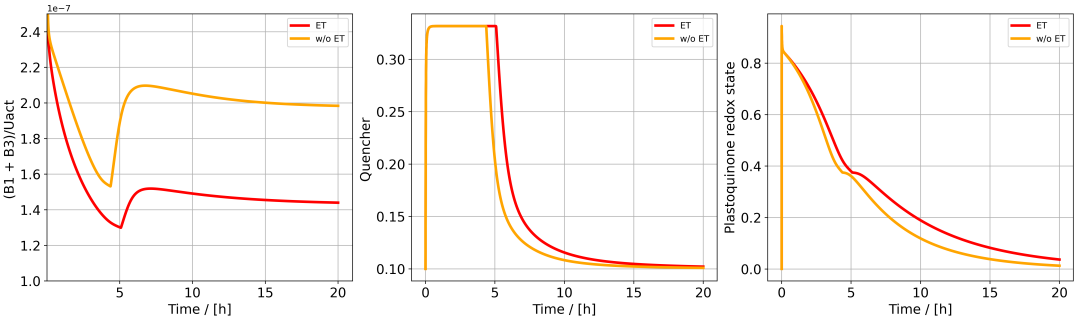

FIGURE 5.13: Simulated changes of excited active PSII states (B1 and B3), quencher activity and plastoquinone redox state in a model version with (red) and without (orange) energy transfer between active and inactive PSII (k_T=0) during high light treatment (800 µmol m^{-2} s^{-1}). The simulation were supposed to happen in lincomycin-treated tissue.

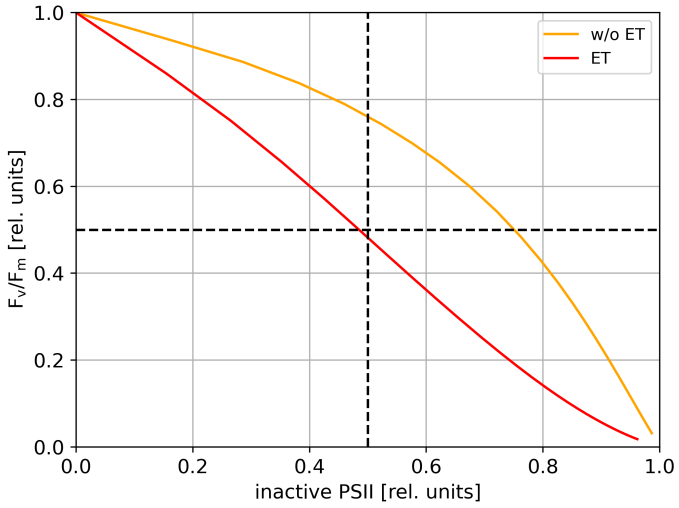

FIGURE 5.14: Simulated changes of F_v/F_m as function of inactive PSII in a model version with (red) and without (orange) energy transfer between active and inactive PSII (k_T=0) during high light treatment (800 µmol m^{-2} s^{-1}). The simulation were supposed to happen in lincomycin-treated tissue.

5.7.1 Connected units with forth- and back transfer of energy between active and damaged PSII

For our theoretical approach, we assume that energy transfer can happen between closed and open reaction centers and between damaged and active reaction center no matter in which state they are. For simplicity we assume that energy transfer does not happen for active open reaction centers and the energy transfer between the active closed reaction centers and damaged reaction centers is the same in both directions. This leads to following description of the fluorescence signal,

$$F = \frac{k_F}{k_F + k_H \cdot Q + k_P} \cdot B_0 + \frac{k_F}{k_F + k_H \cdot Q + k_{T2} \cdot (U_i + U_d)} \cdot B_2 + \tag{5.77}$$

$$\frac{k_F}{k_F + \rho \cdot k_H \cdot Q + k_{T2} \cdot (B_0 + B_2)} \cdot (U_i + U_d). \tag{5.78}$$

Hence, F_o is,

$$F_o = \frac{k_F}{k_F + k_H \cdot Q + k_P} \cdot U_a + \frac{k_F}{k_F + \rho \cdot k_H \cdot Q + k_{T2} \cdot U_a} \cdot (U_i + U_d), \tag{5.79}$$

and F_m,

$$F_{\mathrm{m}} = \frac{k_{\mathrm{F}}}{k_{\mathrm{F}} + k_{\mathrm{H}} \cdot Q + k_{\mathrm{T2}} \cdot (U_{\mathrm{i}} + U_{\mathrm{d}})} \cdot U_{\mathrm{a}} + \frac{k_{\mathrm{F}}}{k_{\mathrm{F}} + \rho \cdot k_{\mathrm{H}} \cdot Q + k_{\mathrm{T2}} \cdot U_{\mathrm{a}}} \cdot (U_{\mathrm{i}} + U_{\mathrm{d}}). \tag{5.80}$$

Using equation 5.79 and 5.80 we can derive an expression for F_v/F_m,

$$\left(\frac{F_v}{F_m}\right)^{\mathrm{i,T}} = K \cdot U_{\mathrm{a}} \cdot \left(\frac{F_v}{F_m} - \frac{k_{\mathrm{T2}}(PSII - U_{\mathrm{a}})}{k_{\mathrm{F}} + k_{\mathrm{H}} \cdot Q + k_{\mathrm{P}}}\right), \tag{5.81}$$

where K

$$K = \frac{k_{\mathrm{H}} \cdot Q \cdot \rho + U_{\mathrm{a}} \cdot k_{\mathrm{T2}} + k_{\mathrm{F}}}{U_{\mathrm{a}}(k_{\mathrm{F}} + k_{\mathrm{H}} \cdot Q \cdot \rho + k_{\mathrm{T2}} \cdot U_{\mathrm{a}}) + (PSII - U_{\mathrm{a}}) \cdot (k_{\mathrm{F}} + k_{\mathrm{H}} \cdot Q + k_{\mathrm{T2}} \cdot (PSII - U_{\mathrm{a}}))}. \tag{5.82}$$

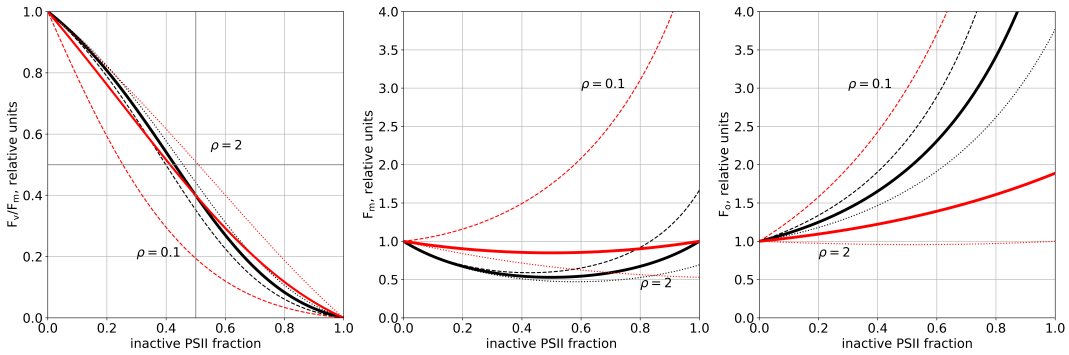

FIGURE 5.15: Relationship between F_v/F_m, F_m, and F_o and fraction of active photosystem II in a model with energy transfer. The dashed, continuous, and dotted lines indicate scenarios in which the ratio of heat dissipation between active and inactive PSII is 0.1, 1, and 2, respectively. Black lines signify a low quenching, while red lines denote a high quenching activity (Q = 0.1 and 1). Parameter values used for the calculations can be found in the parameter table.

5.7.2 PSII heterogeneity

According to Giersch and Krause, 1991, PSII heterogeneity could influence the fluorescence signal observed during photoinhibitory treatment. To check how the relation between F_o, F_m and F_v/F_m and inactive PSI changes when we assume a mixed population of PSIIα and PSIIβ we repeated our analysis in the main text (without energy transfer) implementing PSII heterogeneity according to Giersch and Krause, 1991, in which it was assumed that only PSIIα contributes to inhibited PSII.

Hence, F_o is,

$$F_o^H = PSII^{\text{tot}}\,(1-a)\,\frac{k_\text{F}}{k_\text{F}+k_\text{H}\cdot Q+k_\text{P}} + a\left(\frac{k_\text{F}}{k_\text{F}+k_\text{H}\cdot Q+k_\text{P}}\cdot U_\text{a} + \frac{k_\text{F}}{k_\text{F}+\rho\cdot k_\text{H}\cdot Q}\cdot(U_\text{i}+U_\text{d})\right), \tag{5.83}$$

and F_m,

$$F_m^H = PSII^{\text{tot}}\,(1-a)\,\frac{k_\text{F}}{k_\text{F}+k_\text{H}\cdot Q} + a\left(\frac{k_\text{F}}{k_\text{F}+k_\text{H}\cdot Q}\cdot U_\text{a} + \frac{k_\text{F}}{k_\text{F}+\rho\cdot k_\text{H}\cdot Q}\cdot(U_\text{i}+U_\text{d})\right)., \tag{5.84}$$

where a is the fraction PSIIα.
Using the fact that $U_\text{i}+U_\text{d} = PSII^{\text{tot}} - U_\text{a}$, we can derive a formula for F_v/F_m

$$\left(\frac{F_v}{F_m}\right)^{i,H} = (a\,U_\text{a} + (1-a)\,PSII^{\text{tot}})\cdot\frac{F_v}{F_m}\cdot K, \tag{5.85}$$

where K is

$$\frac{k_\text{H}\cdot Q\cdot\rho+k_\text{F}}{PSII^{\text{tot}}\,(1-a)\,(\rho\cdot k_\text{H}\cdot Q+k_\text{F}) + a\,(U_\text{a}\,(\rho\cdot k_\text{H}\cdot Q+k_\text{F}) + (PSII^{\text{tot}}-U_a)\,(k_\text{H}\cdot Q+k_\text{F}))}. \tag{5.86}$$

The slopes of the relative minimal (F_o) and maximal fluorescence (F_m) regarding active PSII (U_a) are

$$\varphi_o^H := \frac{d}{dU_\text{a}}\left(\frac{F_o^H}{F_{o,a}}\right) = \frac{a\,(Q\cdot k_\text{H}\,(\rho-1)-k_\text{P})}{PSII^{tot}\,(Q\cdot k_\text{H}\cdot\rho+k_\text{F})}, \tag{5.87}$$

and

$$\varphi_m^H := \frac{d}{dU_\text{a}}\left(\frac{F_m^H}{F_{m,a}}\right) = \frac{a\cdot Q\cdot k_\text{H}\,(\rho-1)}{PSII^{\text{tot}}\,(Q\cdot k_\text{H}r+k_\text{F})}. \tag{5.88}$$

Hence, the slope ratio is

$$\gamma^H := \frac{\varphi_o^H}{\varphi_m^H} = \frac{Q\cdot k_\text{H}\,(\rho-1)-k_\text{P}}{Q\cdot k_\text{H}\,(\rho-1)}, \tag{5.89}$$

which is the same as in the isolated case (compare main text).

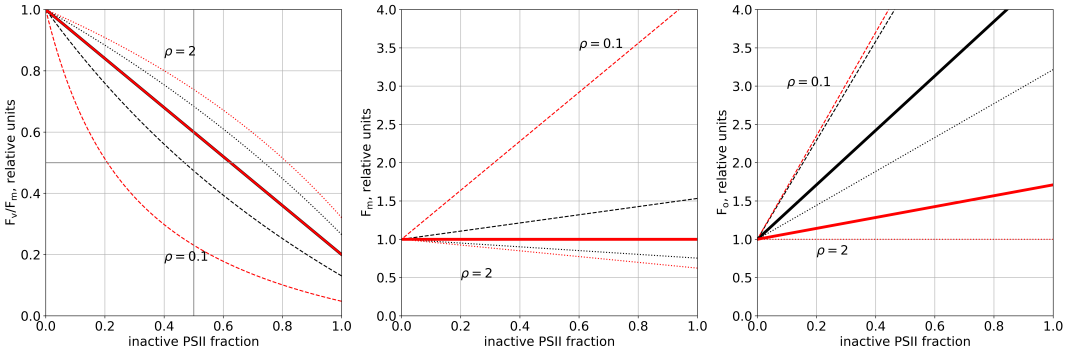

FIGURE 5.16: Relationship between F_v/F_m, F_m, and F_o and fraction of active photosystem II in a model with energy transfer and PSII heterogeneity. The dashed, continuous, and dotted lines indicate scenarios in which the ratio of heat dissipation between active and inactive PSII is 0.1, 1, and 2, respectively. Black lines signify a low quenching, while red lines denote a high quenching activity (Q = 0.1 and 1). Parameter values used for the calculations can be found in the table parameter table. a is set to 0.8.

TABLE 5.1: Parameters used throughout the *in silico* analyses

parameter	value	reference/comment
Pool sizes		
$PSII^{tot}$	2.5 mmol $(\text{mol Chl})^{-1}$	PSII reaction centers Schöttler, Kirchhoff, and Weis, 2004
PSI^{tot}	2.5 mmol $(\text{mol Chl})^{-1}$	PSII reaction centers Schöttler, Kirchhoff, and Weis, 2004
PQ^{tot}	20 mmol $(\text{mol Chl})^{-1}$	total plastoquinone pool Kirchhoff, Mukherjee, and Galla, 2002
PC^{tot}	4 mmol $(\text{mol Chl})^{-1}$	total plastocyanin pool Böhme, 1978
Fd^{tot}	5 mmol $(\text{mol Chl})^{-1}$	total ferredoxin pool Böhme, 1978
ATP^{tot}	50 mmol $(\text{mol Chl})^{-1}$	total adenosine phosphate pool Heineke et al., 1991
$NADP^{tot}$	25 mmol $(\text{mol Chl})^{-1}$	$NADP^+ + NADPH$ pool Heineke et al., 1991
$PsbS^{tot}$	1	normalized PsbS pool, after Matuszyńska et al., 2016
X^{tot}	1	normalized total pool of xanthophylls, afetre Matuszyńska et al., 2016
Rate constants		

Table 5.1 – *Continued from previous page*

parameter	value	reference/comment
$k_{ActATPase}$	0.01 s^{-1}	activation of ATP synthase, after Matuszyńska et al., 2016
$k_{DeactATPase}$	0.002 s^{-1}	deactivation of ATP synthase, after Matuszyńska et al., 2016
$k_{ATPsynthase}$	20 s^{-1}	unchanged from Ebenhöh et al., 2014
$k_{ATPconsumption}$	10 s^{-1}	unchanged from Ebenhöh et al., 2014
$k_{NADPHconsumption}$	20 s^{-1}	after Ebenhöh et al., 2014
k_H	$5 \cdot 10^9$ s^{-1}	rate of non-radiative decay, after Matuszyńska et al., 2016
k_F	$6.25 \cdot 10^8$ s^{-1}	rate of fluorescence, after Matuszyńska et al., 2016
k_P	$5 \cdot 10^9$ s^{-1}	rate of photochemistry, after Matuszyńska et al., 2016
k_{PTOX}	0.01 $mmol^{-1}$ (mol Chl) s^{-1}	after Ebenhöh et al., 2014
k_{cyc}	1 $mmol^{-2}$ $(mol\,Chl)^2$ s^{-1}	after Ebenhöh et al., 2014
k_{leak}	100 s^{-1}	
k_{b6f}	2.5 $mmol^{-2}$ $(mol\,Chl)^2$ s^{-1}	after Ebenhöh et al., 2014
v_{b6f}^{min}	-2.5 mmol $(mol\,Chl)^{-1}s^{-1}$	after Ebenhöh et al., 2014
k_{PCox}	2500 $mmol^{-1}$ (mol Chl) s^{-1}	after Ebenhöh et al., 2014
k_{Fdred}	$2.5 \cdot 10^5$ $mmol^{-1}$ (mol Chl) s^{-1}	after Ebenhöh et al., 2014
k_{PQred}	250 $mmol^{-1}$ (mol Chl) s^{-1}	after Ebenhöh et al., 2014
k_{PTOX}	0.01$mmol^{-1}$ (mol Chl) s^{-1}	after Ebenhöh et al., 2014
V_{FNR}^{max}	1500 mmol $(mol\,Chl)^{-1}s^{-1}$	after Ebenhöh et al., 2014
k_H	$5 \cdot 10^9$ s^{-1}	after Matuszyńska et al., 2016
k_F	$6.25 \cdot 10^8$ s^{-1}	after Matuszyńska et al., 2016
k_P	$5 \cdot 10^9$ s^{-1}	after Matuszyńska et al., 2016
k_{Deepox}	0.0024 s^{-1}	rate of de-epoxidation, unchanged from Matuszyńska et al., 2016
k_{Epox}	0.00024 s^{-1}	rate of epoxidation, unchanged from Matuszyńska et al., 2016
k_{Deprot}	0.0096 s^{-1}	rate of PsbS de-protonation, unchanged from Matuszyńska et al., 2016
k_{Prot}	0.0096 s^{-1}	rate of PsbS protonation, unchanged from Matuszyńska et al., 2016
k_{DEG}	0.0000833s^{-1}	based on a degradation rate of 0.3/h Pätsikkä, Aro, and Tyystjärvi, 1998

Table 5.1 – *Continued from previous page*

parameter	value	reference/comment
k_{PI0}	300 s^{-1}	ad-hoc estimation based on achieving comparable rates as when using the whole PSII pool and k_{PI0}=0.0044 min^{-1} Tyystjärvi, Mäenpää, and Aro, 1994
k_{REP}	0.00833 s^{-1}	based on the observation that U_d concentration is small in WT Pätsikkä, Aro, and Tyystjärvi, 1998
K_{mPI}	16 mmol $(\text{mol Chl})^{-1}$	
k_T	$9 \cdot 10^8$ mmol^{-1} (mol Chl) s^{-1}	fitted to F_v/F_m changes in high light
ρ	7	fitted to F_v/F_m changes in high light
nL	2	ad-hoc value to use a reasonable switch behavior
K_{PFD}	100	ad-hoc value to use a reasonable switch behavior
$mito$	100 mmol $(\text{mol Chl})^{-1}s^{-1}$	ad-hoc value, needs to be refined as model becomes more elaborate
Michaelis constants		
K_{pHsatz}	5.8	half-saturation pH for deepoxidase activity, after Matuszyńska et al., 2016
$K_{pHsatLHC}$	5.8	pKa of PsbS activation, after Matuszyńska et al., 2016
K_{Zsat}	0.12	after Matuszyńska et al., 2016
K_{MF}	1.56 mmol $(\text{mol Chl})^{-1}$	after Ebenhöh et al., 2014
K_{MN}	0.22 mmol $(\text{mol Chl})^{-1}$	after Ebenhöh et al., 2014
External concentrations		
O_2^{ex}	8 mmol $(\text{mol Chl})^{-1}$	external oxygen pool after Ebenhöh et al., 2014
P_i	0.01	internal pool of phosphates after Ebenhöh et al., 2014

Table 5.1 – *Continued from previous page*

parameter	value	reference/comment
Other constants		
F	96.485 kJ	Farraday constant
R	$8.3 \cdot 10^{-3}$ kJ K^{-1} mol^{-1}	universal gas constant
T	298 K	temperature
γ_0	0.1	base quenching Matuszyńska et al., 2016
γ_1	0.25	fast quenching due to protonation Matuszyńska et al., 2016
γ_2	0.6	fastest possible quenching Matuszyńska et al., 2016
γ_3	0.105	slow quenching by Zx Matuszyńska et al., 2016
γ_4	1.01	test long-term quencher
n_{HL}	3	Hill-coefficient for activity of deprotonation, after Matuszyńska et al., 2016
n_{HX}	5	Hill-coefficient for deepoxidase activity, after Matuszyńska et al., 2016
b_H	100	protonation buffering constant Zaks et al., 2012
pHstroma	7.8	
Standard potentials		
$E_0(Q_A/Q_A^-)$	-0.140 V	unchanged from Ebenhöh et al., 2014; Allakhverdiev et al., 2011
$E_0(PQ/PQH_2)$	0.354 V	unchanged from Ebenhöh et al., 2014; Okayama, 1976
$E_0(PC/PC^-)$	0.380 V	unchanged from Ebenhöh et al., 2014; Suzuki, Sakurai, and Nakajima, 1987
$E_0(FA/FA^-)$	-0.550 V	unchanged from Ebenhöh et al., 2014; Evans and Heathcote, 1980
$E_0(Fd/Fd^-)$	-0.430 V	unchanged from Ebenhöh et al., 2014; Cammack et al., 1977
$E_0(P700^+/P700)$	0.480 V	unchanged from Ebenhöh et al., 2014; Witt et al., 2003

Table 5.1 – *Continued from previous page*

parameter	value	reference/comment
$E_0(NADP^+/NADPH)$	-0.113 V	unchanged fromEbenhöh et al., 2014; Nicholls, 2013

Chapter 6

Assessing how technical parameters influence fluorescence measurements

This chapter is published on bioarxiv (Nies et al., 2021). I was involved in each step of the study. This includes the simulation, data analysis, visualization of the results, and writing all parts of the chapter/manuscript (Introduction, Methods, Results, Discussion). The text was slightly adapted to fit into the reading flow of the thesis. This means when the original manuscript referred to itself as "paper" or "article" this was changed to "chapter".

Chlorophyll *a* fluorescence is a powerful indicator of photosynthetic energy conversion in plants and photosynthetic microorganisms. One of the most widely used measurement techniques is Pulse Amplitude Modulation (PAM) fluorometry. Unfortunately, parameter settings of PAM instruments are often not completely described in scientific articles although their variations, however small these may seem, can influence measurements. In this chapter we show the effects of parameter settings on PAM measurements. We first simulated fluorescence signals using a previously published computational model of photosynthesis. Then, we validated our findings experimentally. Our analysis demonstrates how the kinetics of non-photochemical quenching (NPQ) induction and relaxation are affected by different settings of PAM instrument parameters. Neglecting these parameters may mislead data interpretation and derived hypotheses, hamper independent validation of the results, and cause problems for mathematical formulation of underlying processes. Given the uncertainties inflicted by this neglect, we urge PAM users to provide detailed documentation of measurement protocols. Moreover, to ensure accessibility to the required information, we advocate minimum information standards that can serve both experimental and computational biologists in our efforts to advance system-wide understanding of biological

processes. Such specification will enable launching a standardized database for plant and data science communities.

6.1 Introduction

Oxygenic photosynthesis is one of the most essential processes on Earth. It drives the formation of oxygen and provides an energetic basis for carbon dioxide fixation. Due to its pivotal role in biomass production, the last decade has seen an increasing focus on engineering and manipulating photosynthesis in an attempt to improve plant productivity (Ort et al., 2015; Kromdijk et al., 2016; Kaiser, Morales, and Harbinson, 2018; Flexas and Carriquí, 2020). Methods of quantifying the photosynthetic activity *in vivo*, in particular, the electron transport chain (Rochaix, 2011) allow inspection of dynamic changes in photosynthesis under variable environments. Foremost, measurement techniques based on chlorophyll *a* (Chl *a*) fluorescence have provided a broad range of information about reactions in photosystem II (PSII) and thylakoid membranes, leading to an upsurge in the understanding of photosynthesis (Kalaji et al., 2014; Kalaji et al., 2017).

A popular and important technique in photosynthesis research is Pulse Amplitude Modulation (PAM) Fluorometry (Schreiber, Schliwa, and Bilger, 1986). In combination with the saturation pulse method, it provides a minimally invasive system for the determination and quantification of the PSII activity (Schreiber, 2004). For detailed explanations of the method, its practical applications, and limitations, readers are directed to the excellent reviews published over the decades (Maxwell and Johnson, 2000; Baker, 2008; Murchie and Lawson, 2013). The basic principle of Chl *a* fluorescence and an example of induction measurement using PAM are shown in Fig. 6.1.

Non-photochemical quenching of Chl *a* fluorescence (NPQ) is one of the processes that can be quantified by analysing changes in fluorescence emission (Muller, Li, and Niyogi, 2001). The introduction of the PAM fluorometry opened up new opportunities for simple *in vivo* assessment of its dynamics. Under unfavourable conditions, NPQ serves as an important photoprotective mechanism, on one hand lowering the light use efficiency of photosynthesis, on the other protecting the photosynthetic apparatus from long term photodamage (Ruban, 2016). The NPQ parameter is associated with the fraction of the light energy absorbed by PSII that is not used for photochemistry and is dissipated as heat.

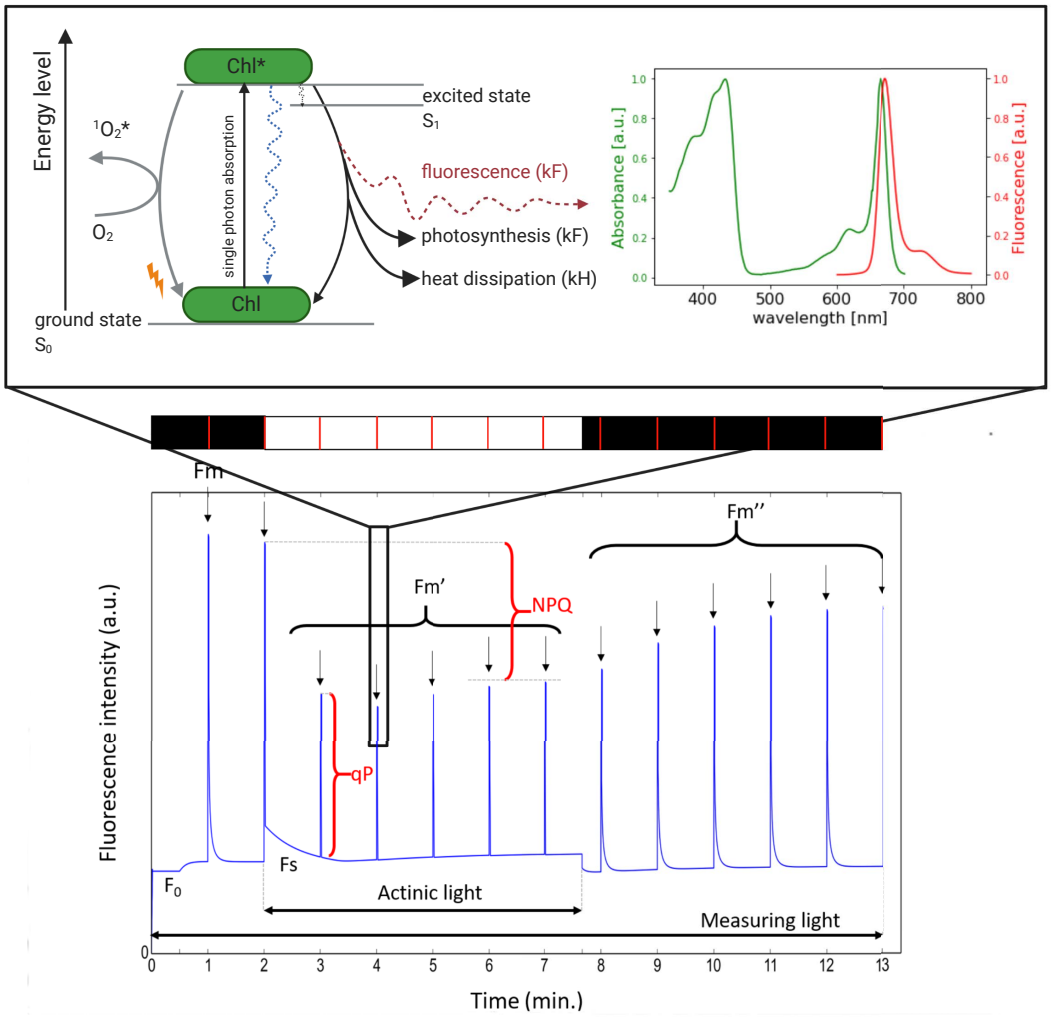

FIGURE 6.1: The basic principle of fluorescence and PAM induction measurement. In this protocol, a dark-adapted plant is exposed to actinic light (AL, white area shown in the light bar, L) followed by dark recovery (black area in L). Multiple saturating light flashes (saturation pulses, SP) are applied before, during and after the actinic illumination to measure the maximal fluorescence F_m, F_m', F_m'', respectively. Light energy absorption brings chlorophyll molecules to the first excited state (S_1, see the simplified Jablonsky diagram in the upper panel on the left). For chlorophylls to return to the ground state (S_0), the absorbed energy can be used for charge separation and photosynthesis (photochemical quenching, qP), dissipated as heat (non-photochemical quenching, NPQ), or re-emitted as fluorescence. The fluorescence emission spectra are red-shifted from the absorption spectra (upper panel on the right) and can be detected using fluorometers with corresponding optical filters. The emitted fluorescence signal is recorded, as shown in the lower panel with key readouts. Based on Muller, Li, and Niyogi, 2001; Lichtman and Conchello, 2006; Murchie and Lawson, 2013. Created with BioRender.com

Computational models serve as powerful tools for predicting systems' responses to various changes and quantifying this effect. Their results help identify the reactions and mechanisms limiting photosynthetic productivity, to improve crop yield (Long et al., 2006; Zhao et al., 2020). Aspiring to make a similar impact through our research, our groups develop mathematical models of photosynthesis and actively search available fluorescence data to test computational models. Unfortunately, many articles presenting PAM fluorescence traces and data do not report detailed experimental protocols that were used to obtain these results. Such omission makes it challenging to reproduce fluorescence measurements by other groups but also *in silico*.

This unintentional concealment of the experimental protocol is inevitably revealed once a computational approach is employed to replicate the experiment.

While simulating fluorescence traces using computational models we noted that our work required guessing some of the parameters used to conduct the experiment, as they were not explicitly stated in publications. This is not unexpected as incomplete reporting of experimental procedures has been identified as one of the factors responsible for the "reproducibility crisis" in science (Baker, 2016; National Academies of Sciences, Engineering, and Medicine, 2019; Jessop-Fabre and Sonnenschein, 2019). Most articles, in which PAM measurements were reported, included information about the type of fluorometer used (Sekulska-Nalewajko et al., 2019; Kalmatskaya et al., 2020) and the intensity of the saturation pulses (SP) (Vieira et al., 2013). Some, to our delight, attached the spectrum of actinic light used for fluorescence quenching analyses (Quero et al., 2020). But in many, values of the following four parameters were missing: i) the time interval (delay) between the determination of the maximum fluorescence (F_m) in darkness and switching on the actinic light (AL), ii) the intensity of the applied AL, iii) the time interval between the SPs, and iv) the duration of the SPs.

To systematically assess the effects of small variations in PAM parameters on the fluorescence traces, we simulated various PAM protocols using a mathematical model of NPQ published by our group (Matuszyńska et al., 2016). We analysed the quantitative dependence of NPQ and PSII yield (Φ_{PSII}) on the technical parameters that were mentioned above. Further, we validated the *in silico* findings by conducting two *in vivo* experiments in which the duration of the saturation pulse and the time point of switching on the actinic light were varied.

With this chapter underlining the importance of full disclosure of PAM

protocols in scientific publications, we hope to raise the awareness of authors, reviewers, and readers and thus to improve the knowledge transfer between the experimental and theoretical communities in plant physiology and photosynthesis. The findings presented here urges PAM users and the plant science community to consider facilitating broader exploitation of their data for modeling and meta-analysis studies while communicating their experimental procedures and results.

6.2 Model and Methods

6.2.1 The model used for simulations

We use a mathematical model (Matuszyńska et al., 2016) to predict how changes in the values of four technical parameters of PAM measurement affect the fluorescence trace. For this, we simulate PAM experiments and systematically vary each of these parameters, quantifying the effect of each perturbation on NPQ and photosynthetic yield (Φ_{PSII}). Table 6.1 contains descriptions of the standard variables derived from fluorescence signals, which are used to calculate NPQ and Φ_{PSII}. The model comprises six ordinary differential equations (ODE) including a detailed description of NPQ. It has been parametrised for *Arabidopsis thaliana* and verified to accurately simulate fluorescence traces also for other higher plants. To reproduce the experimental results that are presented in this chapter we had to change three parameters. These are a coefficient of the light function transforming the photon flux density into the rate of excitation of PSII, the contribution of the protonated PsbS and zeaxanthin to the NPQ mechanism, and the proton leakage from the lumen in the stroma (a, γ_2, k_{leak}). All source code used to perform the presented analysis, together with the model implemented using the Python package `modelbase` developed by our group (Aalst, Ebenhöh, and Matuszyńska, 2021), can be downloaded from our git repository https://gitlab.com/qtb-hhu/fluopam.

6.2.2 Standard PAM light induction protocol

We designed a quenching analysis using PAM measurement that represents a generic experimental setup used with standard PAM fluorometers. Table 6.2 contains descriptions of the reference parameters. We have used 500 $\mu mol\, m^{-2}\, s^{-1}$as the default light intensity of AL. In the following analysis,

TABLE 6.1: Parameters and descriptions of quantities derived from PAM fluorescence measurements in photosyhthetic organisms (Maxwell and Johnson, 2000; Murchie and Lawson, 2013).

Parameter	Description
F_m	maximal fluorescence in a dark-adapted state
$F_{m'}$	maximal fluorescence in a light-exposed state
F_o	minimal fluorescence in a dark-adapted state
F_s	steady-state fluorescence level in a light-exposed state
NPQ	non-photochemical quenching $\frac{F_m - F_{m'}}{F_{m'}}$
Φ_{PSII}	Quantum yield of photosystem II calculated as $\frac{F_{m'} - F_s}{F_{m'}}$

TABLE 6.2: Parameters of the reference PAM protocol used for the simulations.

Technical parameter	Value
Time point of F_m	1 s after the beginning of the measurement
Time point of switching on actinic light	60 s after the beginning of the measurement
Time interval between switching on the actinic light and the first determination of Fm′	10 s
Actinic light intensity	500 µmol m^{-2} s^{-1}
Saturation pulse intensity	5000 µmol m^{-2} s^{-1}
Duration of saturation pulses	0.8 s
Number of saturation pulses during actinic illumination	10
Interval between saturation pulses	60 s
Number of saturation pulses during dark recovery	6
Interval between the last saturation pulse in actinic light and the first saturation pulse in dark recovery	70 s

we systematically varied the time point of switching on and off the AL, the intensity of the AL and SPs, and the duration and interval between SPs. We record the effect on the quenching capacity (NPQ) and photosynthetic yield (Φ_{PSII}). Fig. 6.2 illustrates the basic idea behind our inquiries. We construct the light protocol (upper panel top) and solve the system of ODEs, from which we then calculate the fluorescence signal and plot it over time (upper panel bottom). From the fluorescence signal, we derive further the NPQ value (lower panel left) and quantum yield of photosynthesis (lower panel right).

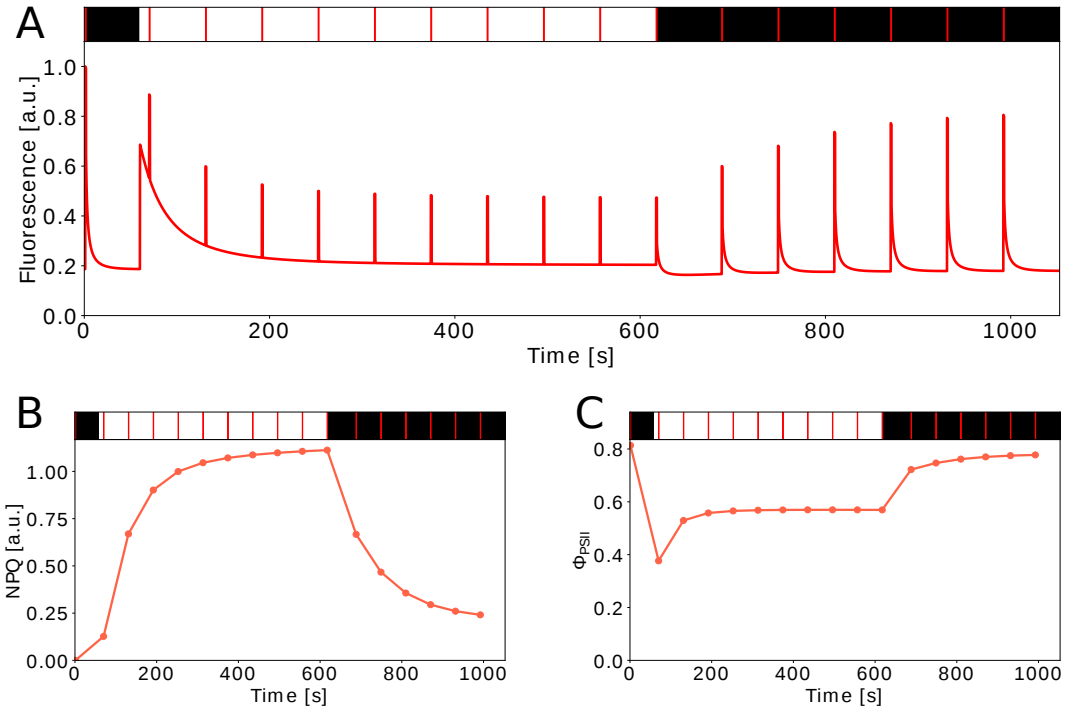

FIGURE 6.2: Example of the simulated PAM induction measurement with a saturation pulse protocol used in this work. Fig. 6.2A: the output of a typical simulated PAM fluorescence trace obtained for the reference parameters from Table 6.2. The dark/light/dark phases and times points of saturation pulses (in red) are indicated in the upper panel. Fig. 6.2B and 6.2C: the variables NPQ and Φ_{PSII}, respectively, which are both derived from the simulated fluorescence

6.2.3 Experimental methods

Plant Material and Growth Conditions

Seeds of *Arabidopsis thaliana* (Columbia-0) were sown on moist commercial soil (Pikier, Balster Einheitserdewerk, Fröndenberg, Germany) and incubated at 4 °C in the dark. After three days they were transferred to a climate chamber with a 12 h/12 h light/dark photoperiod, 60% relative air humidity and 26 °C/20 °C day/night air temperature. The intensity of photosynthetically active radiation provided by fluorescent lamps (Fluora L58 W/77; Osram, Munich) was approx. 100 $^{-}$mol $m^{-2}s^{-1}$ at the plant height. Seedlings were transferred to pots ($7 \times 7 \times 8$ cm, one plant per pot) filled with soil (Lignostrat Dachgarten extensive, HAWITA, Vechta, Germany) on the 15^{th} day after sowing. Plants were watered from the bottom to keep soil moisture throughout the cultivation and during the experiments.

PAM induction curve measurement

In the sixth week after sowing, Chl fluorescence measurements were performed in overnight dark-adapted plants using PAM-2500 (Walz, Effeltrich, Germany) equipped with leaf clip 2030-B. Before determination of the maximal PSII efficiency (F_v/F_m), 5 s of far-red light illumination (peak at 750 nm) was given to oxidize the electron transport chain and PSII. The intensity of red AL (peak at 630 nm) was set at approx. 457 µmol m^{-2} s^{-1}. The default settings (10) were used for the intensity of both measuring light and SP. After 10 min of light induction, during which SP was applied every 60 s starting 1 s after the onset of AL illumination, AL was turned off and dark recovery was monitored for 13 min, during which seven SPs were applied with increasing time intervals as programmed in the protocol provided in the PamWin_3 software (Walz). In the experiment with varying time delay between the F_v/F_m measurement and starting of the AL (10, 30, 40, 50, or 70 s), the width (duration) of SP was fixed at 800 ms (default). In the experiment with a varying width of SP (200, 400, 600, or 800 ms), the time delay was kept at 40 s (default). Four measurements were performed in four replicate plants (one measurement per plant) for each combination of the settings.

6.3 Results

6.3.1 Time Point of switching on and off the AL

In published protocols, we often encountered descriptions such as: "a dark-adapted plant has been exposed to a SP of light to measure the F_{max} and pulses were repeated every 30 seconds. After 12 minutes the light was switched off". Such formulations, upon first reading, suggest that the plant has been exposed to AL immediately after the dark measurement of F_m. However, by comparing our predicted fluorescence traces with the experimental data, we have noticed that in some of the experiments the initial "dark phase" must have continued after the first SP, sometimes even until the time point of the second SP. In Fig. 6.3A we illustrate the effect of the precise timing of switching on the AL on the predicted fluorescence. The time points of SPs are at seconds: 1 s, 70 s, 130.8 s, 191.6 s, 252.4 s, 313.2 s, 374 s, 434.8 s, 495.6 s, 556.4 s, 617.2 s, 688 s, 748.8 s, 809.6 s, 870.4 s, 931.2 s, 992 s. Naturally, the timing of switching on the AL has implications for the NPQ induction while the subsequent dark relaxation is not affected (Fig. 6.3B). The time course of F_s quenching under the AL is unaffected although the F_s level

at a given time point changes (Fig. 6.3A). As expected, the longer the dark phase between the first two SPs, the lower the initial NPQ determined by the second SP applied. These simulations demonstrate that, without precise knowledge of this parameter, a rigorous model interpretation of the NPQ induction kinetics is difficult.

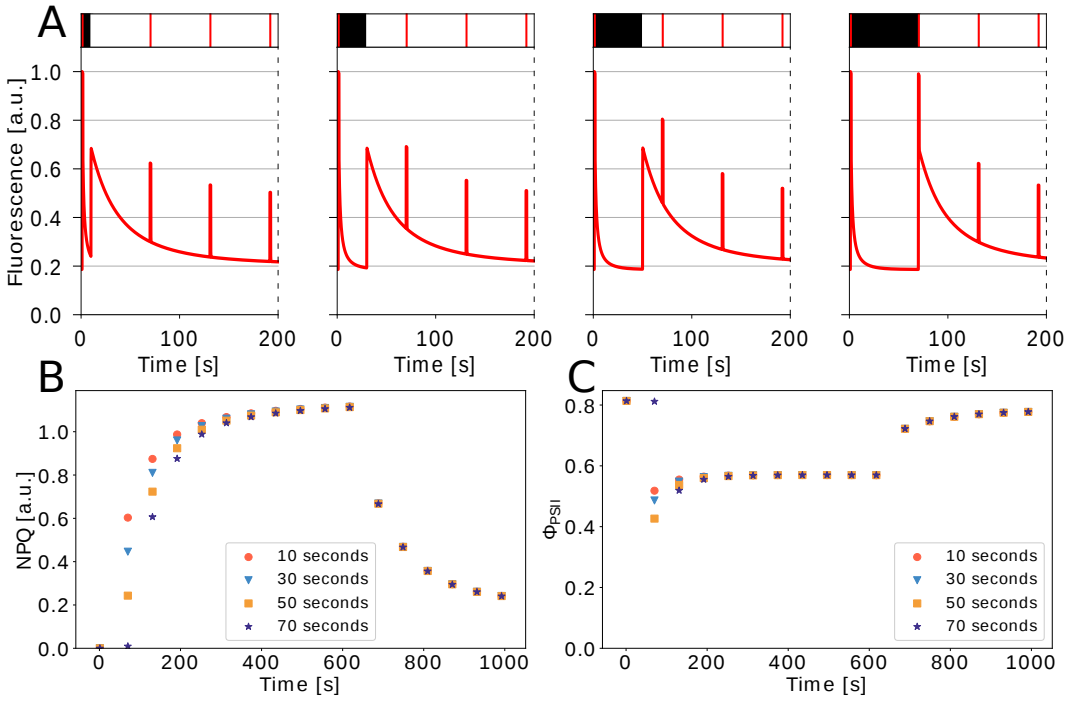

FIGURE 6.3: Variation of the time point of switching on the AL. Fig 6.3A: excerpts of full fluorescence traces. The time point of switching on the AL is varied while the time points of applying SP are kept unchanged. From left to right: 10 s, 30 s, 50 s, and 70 s after the first SP to determine F_m. The vertical dashed lines indicate that the fluorescence traces continue. Fig. 6.3B: derived NPQ values. Fig. 6.3C: yield of photosystem II (Φ_{PSII}).

Likewise, the exact time of switching off the AL is also not described in publications. In Fig. 6.4 we have additionally varied the time point of switching off the AL in a similar manner as done above for switching on the AL while maintaining the overall duration of the AL. In the upper panel the four light-to-dark transition phases are plotted and in the lower panels the derived NPQ and Φ_{PSII}. Additionally to the apparently altered induction kinetics of NPQ observed before, now significant variations in the dark relaxation kinetics can be clearly seen in Fig. 6.4B.

It is observed that whilst the relaxation kinetics of the NPQ is not affected by the precise switching on point of the AL, the induction kinetics of the NPQ varies significantly.

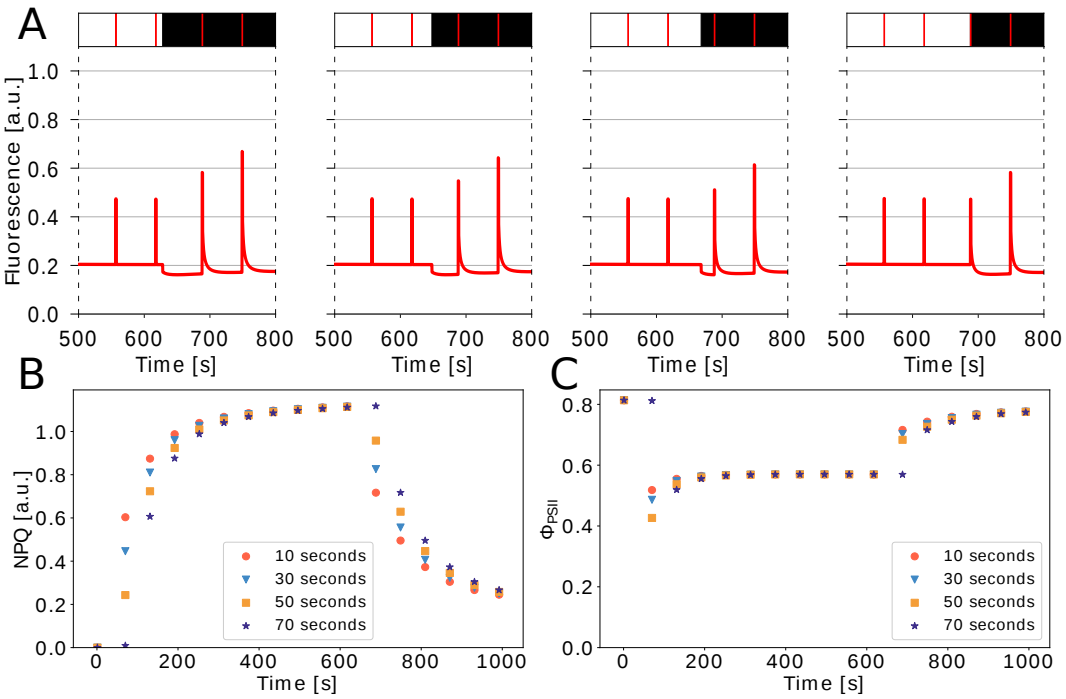

FIGURE 6.4: Variation of the time point of switching on and off the AL. Fig. 6.4A: excerpts of full fluorescence traces. The time point of switching on and off the AL is varied while the time points of applying SP are kept unchanged. From left to right 10 s, 30 s, 50 s, and 70 s after first SP for F_m and a corresponding shift of the last SP in the AL, respectively. Vertical dashed lines indicate that the fluorescence traces continue. Fig. 6.4B: derived NPQ values. Fig. 6.4C: yield of photosystem II (Φ_{PSII}).

6.3.2 AL and SP intensity

The precise definition of the AL is essential for an accurate interpretation of raw fluorescence traces, as well as other dynamic variables derived from them. Commonly used expressions such as 'moderate light' or 'low light intensity' are not informative. Light activation depends on certain physical, biochemical, and structural parameters that vary between photosynthetic organisms depending on e.g. the chlorophyll content, the three-dimensional structure of the chloroplast, and the composition of the thylakoid membrane.

In our model, these differences are accounted for in the light activation function. In this analysis, we systematically increased the AL from intensity 100 to 1000 µmol m^{-2} $s^{-1}$to examine the effect on the derived steady-state NPQ value. As shown in Fig. 6.5, the intensity of AL influences the steady-state NPQ level significantly, in this example up to 350 µmol m^{-2} $s^{-1}$where it reaches saturation.

Besides the intensity of AL, the intensity of the SPs also plays a crucial role in the reproducibility of PAM experiments. To study possible consequences of different SP intensities, we altered the values between 1000 and 9000 µmol m^{-2} s^{-1}. The calculated steady-state NPQ values are higher for SP intensities below 3000 µmol m^{-2} s^{-1}, suggesting that only for intensities over 4000 µmol m^{-2} $s^{-1}$the SP is really saturating. This is an interesting finding of our analysis, where with the simulations we could identify the theoretical minimal intensity of the SP which, in this example, was about 10-fold higher than the lowest AL intensity to induce the maximal NPQ (Fig. 6.5).

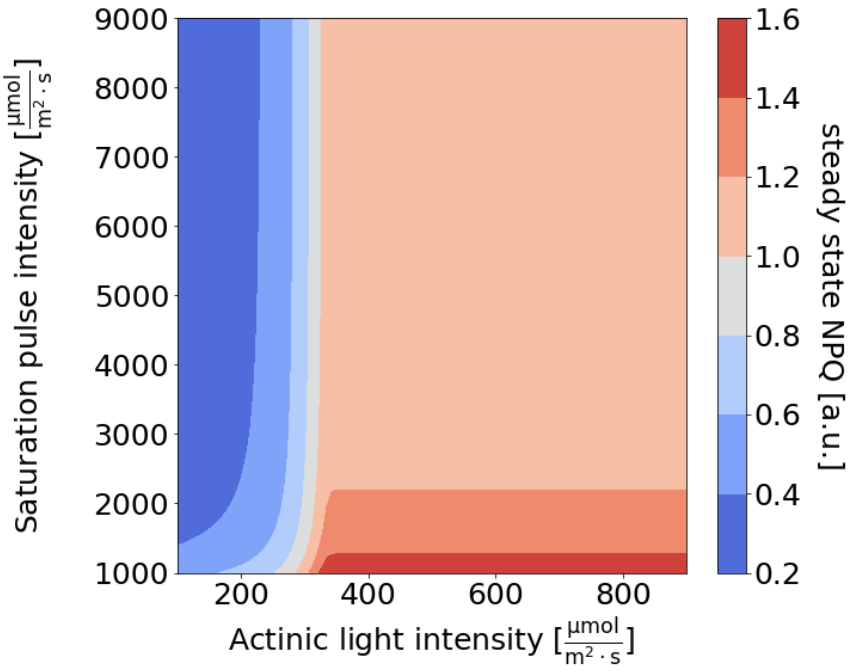

FIGURE 6.5: Steady-state NPQ values (derived at the last SP in the AL environment) simulated for various combinations of AL and SP intensities.

6.3.3 Interval between SPs

Next, we investigated the effect of the time interval between the SPs. From our experience, the value of this parameter is explicitly mentioned in far more articles than for instance the time of switching on the AL, indicating

the importance given to this parameter. Fig. 6.6 shows derived NPQ and Φ_{PSII} values from the PAM protocols with varying intervals between the SPs. Based on the results shown in Fig. 6.6 one could conclude that this technical parameter, if it is within the range typically used by many groups in laboratory experiments (30, 60, 120 s), may not alter the induction and relaxation kinetics or the steady-state level of NPQ. However, when we repeated the analysis for a lower AL intensity of 100 µmol m^{-2} s^{-1}, a tendency of increased NPQ by short-interval SPs could be observed under the AL as well as in the subsequent darkness (Fig. 6.6C).

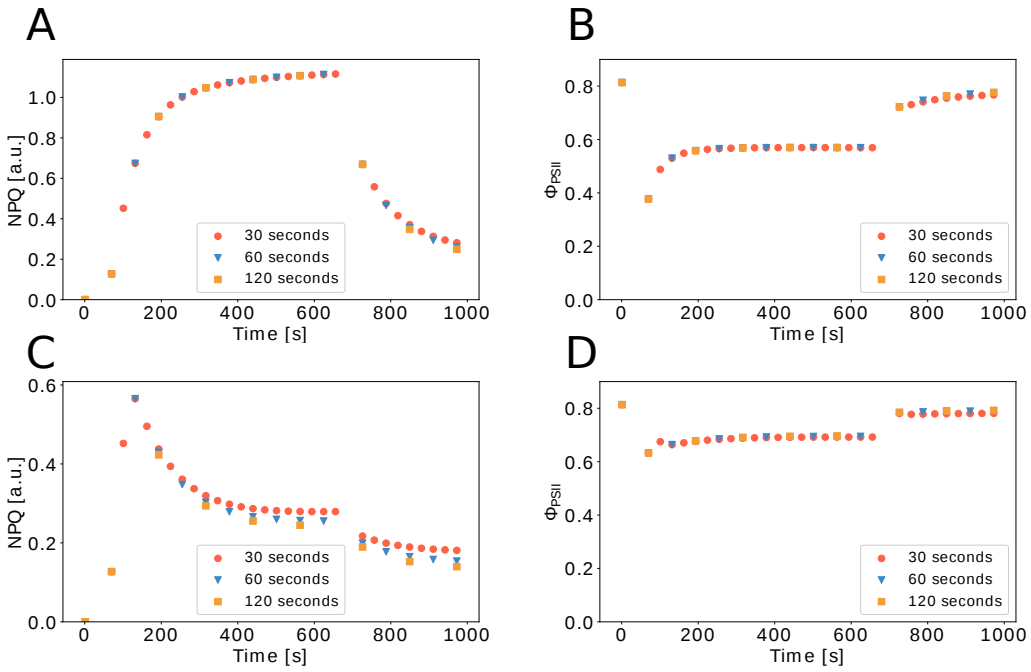

FIGURE 6.6: NPQ and Φ_{PSII} values simulated for the standard PAM induction protocol with varying time intervals between two consecutive SPs. 6.6A and 6.6A: with AL intensity of 500 µmol m^{-2} s^{-1}. 6.6C and 6.6D: with AL intensity of 100 µmol m^{-2} s^{-1}

6.3.4 Duration of SP

Lastly, we investigated the effect of the SP duration. It is often assumed that the SPs of light have no lasting effect on the photosynthetic system, as long as they are 'short' (Schreiber, 2004). To verify this claim, we examined the effect of the SP length from 0.2 s to 2.8 s (Fig. 6.7). Our simulation confirmed no effect of the duration of the SP at 5000 µmol m^{-2} $s^{-1}$and all investigated

intervals on NPQ under the used AL intensity. Interestingly, this technical parameter was among those that are most regularly and explicitly mentioned in the method sections. Despite the special attention and notes, however, there seems to be only a minor immediate effect of altering this parameter, as indicated by our analysis in Fig. 6.7.

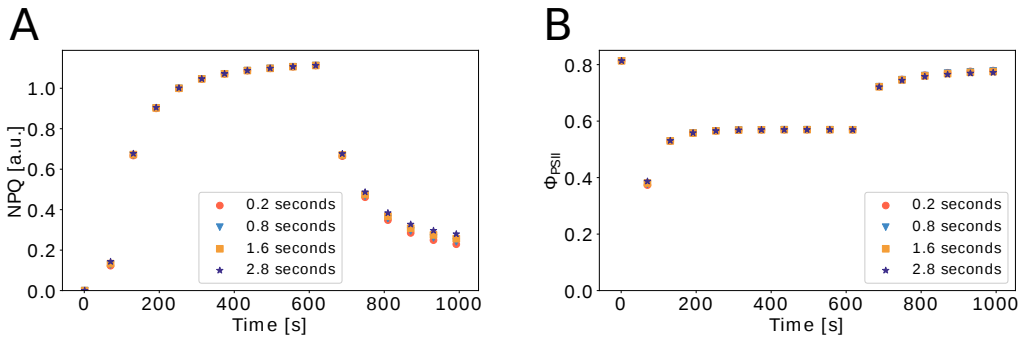

FIGURE 6.7: NPQ and Φ_{PSII} values simulated for the standard PAM induction protocol with varying length of the saturation light pulses.

6.3.5 Model validation

To validate and support our *in silico* analyses we conducted two experiments using plants grown as described in the Method section. The first experiment investigates the impact of the duration of the SP (referred to as SP experiment). The second one focuses on the time point of switching on the AL with the first SP in light-triggered after 1 s (referred to as Delay experiment). As Figs. 6.8 and 6.9 show, our simulations are qualitatively in good agreement with the experimental data of NPQ and Φ_{PSII} in both experiments.

In the SP experiment the model could reproduce some, yet not all features of the NPQ and Φ_{PSII} traces (figs. 6.8A to 6.8D). The duration of SP played only a minor role for both experimental determination and simulation of Φ_{PSII} (figs. 6.8C and 6.8D). The model and experimental results are in good accordance for Φ_{PSII} (see section 6.3.4), with exception of somewhat faster kinetics of increase predicted by the model compared to the observation made in overnight dark-adapted plants. For NPQ the computational analysis deviated from the experiment during light induction whereas dark relaxation could be well reproduced (figs. 6.8A and 6.8B). In addition, the experimental data, albeit showing large variations among the replicate plants,

indicated that the NPQ value might be influenced by the duration of SP while the simulation did not show such influence (Fig. 6.8A)

These deviations may imply that the model parameters, despite the adjustments described in the Materials and Methods (6.2.1 Model used for simulations), are still suboptimal for the plants used for the experiments and/or that some mechanisms are not taken into account in the model. However, looking at the 0.8 s pulse data of the SP experiment and the 40 s delay data of the Delay experiment (Fig. 6.9), for which the same combination of SP duration (0.8 s) and delay (40 s) was used, it becomes evident that the plants in the latter experiment showed NPQ induction and fluorescence traces that were more similar to the simulation (Figs. 6.8 and 6.9). We do not know what factor(s) might have led to the different NPQ induction patterns in the two experiments. One possibility is that reactions in photosynthetic induction, which give rise to a highly variable PMST wave of the fluorescence induction curve (Papageorgiou and Govindjee, 1968; Stirbet et al., 2014), contributed to the NPQ variations. It has been suggested that this slow phase of the fluorescence induction curve has multiple complex causes including the activation of the Calvin-Benson-Bassham cycle and state transition between the two photosystems induced by red and far-red light (Stirbet and Govindjee, 2016), both of which are not included in the simplified model used in this analysis. Since we used red AL in our experiments, the effect of blue light-induced chloroplast movement on NPQ induction (Cazzaniga et al., 2013) can be ruled out. Clearly, the quality (wavelength) of AL is another important information needed to interpret and simulate NPQ induction. Also the length of dark adaptation prior to the initial F_m measurement likely plays a role in the systematically different kinetics of Φ_{PSII} increase upon AL illumination found between the experiment and simulation (Fig. 6.8).

In the Delay experiment the expected changes in NPQ and Φ_{PSII} at the beginning and at the end of the AL phase were observed in the experiment as well as in the simulation (Figs.figs. 6.8E to 6.8H). These changes are only temporal shifts and do not indicate changes in NPQ activation or relaxation kinetics. Yet, as shown in the computational part, when SPs are not bound to the time of AL but fixed at given time points, the length of delay has an effect on NPQ (Figs. 6.3B and 6.4B). Hence, information about the time point of switching on the AL needs to be provided together with the information about the time point of the first SP. Overall, the comparisons between the experimental data and the model simulation shown in Figs. 6.8 and 6.9 support the main message of the simulation analysis presented in the sections 6.3.1

to 6.3.4, namely the importance to report all the details of the PAM experiment protocol for the sake of reproducibility and data interpretation as well as reusage of the experimental results. Furthermore, Figs. 6.8 and 6.9 show that the model (Matuszyńska et al., 2016) adequately reproduces the effects of small changes in technical PAM parameters and is able to give hints about which technical details are more important for the description of PAM protocols. When these details are known, deviations of simulations from experimental data can help us in the search for missing factors and mechanisms to improve the model.

In the Delay experiment changes between the NPQ and Φ_{PSII} traces can be detected at the beginning of the experiment as well as at the end of the AL phase. Nevertheless, these changes are only temporal shifts and do not indicate changes in NPQ activation or relaxation kinetics. Yet, as shown in the computational part, when pulses are not bound to the time of AL but fixed at given time points, an effect on NPQ was observed. Hence, information about the time point for switching on the AL has to be mentioned together with the information when is the first pulse of light taken.

In conclusion the experimental findings are in good agreement with one of the messages that is conveyed in this chapter: it is important to note all details of the PAM experiment for the sake of reproducibility and reusage of the experimental results. Furthermore, the comparison between the model and the simulation indicates that the NPQ model (Matuszyńska et al., 2016) is adequate to investigate the effects of small changes in technical PAM parameters and is able to give hints which technical details are highly important in the description of PAM protocols.

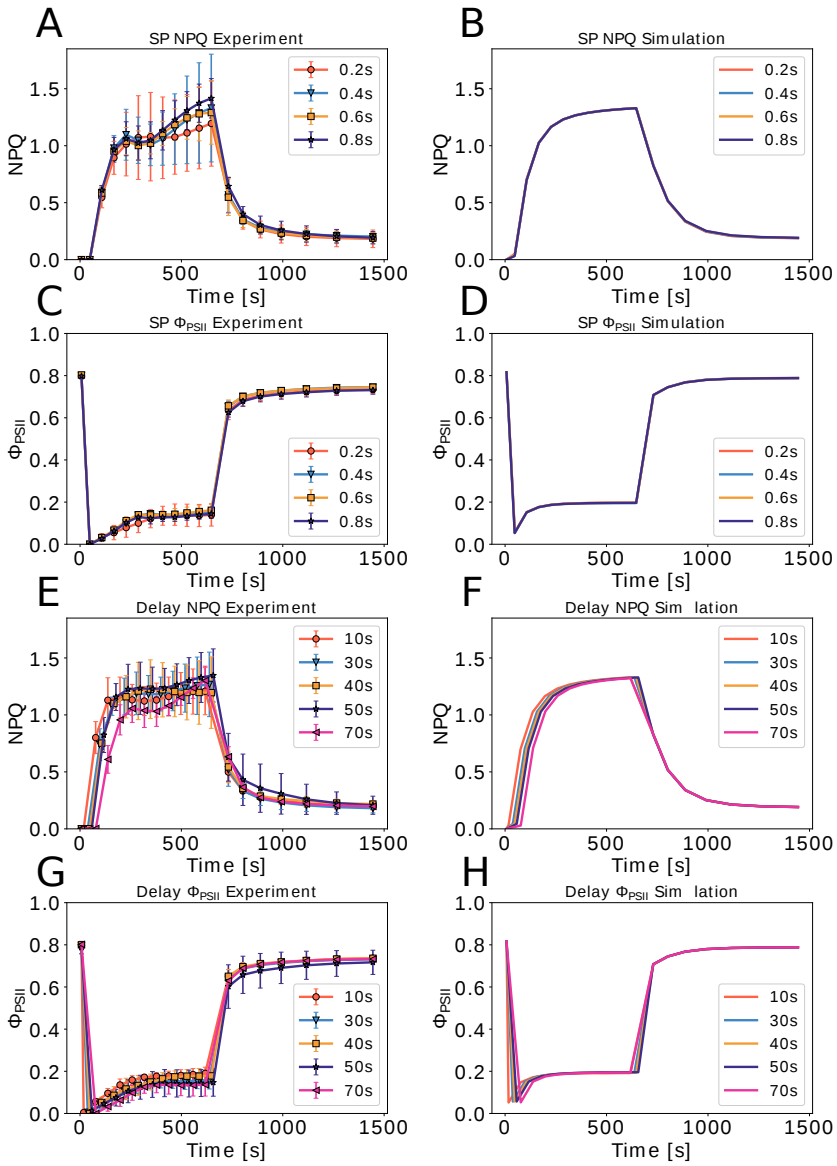

FIGURE 6.8: Comparison of the experimental and simulated NPQ and Φ_{PSII} induction and relaxation. figs. 6.8A to 6.8D: SP experiment with varying duration of the saturation pulse between 0.2 and 0.8 s. The delay was 40 s for all measurements. figs. 6.8E to 6.8H: Delay experiment with varying delay to switch on the actinic light 10s, 30 s, 40 s, 50 s and 70 s after the F_m measurement. The duration of saturation pulse was 0.8 s for all measurements. Error bars indicate standard deviation (n=4).

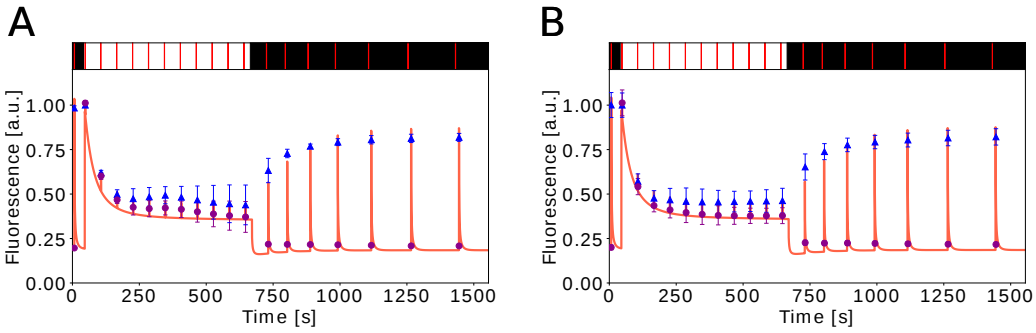

FIGURE 6.9: Comparison of the experimental data and simulated fluorescence traces. 6.9A: SP experiment with SP duration of 0.8 s and delay of 40 s. 6.9B: Delay experiment with a delay of 40 s and SP duration of 0.8 s. Blue symbols, mean values of F_m and F_m'; purple symbols, mean values of F_o and F_s ; line, simulation. Error bars indicate standard deviation (n=4). Black and white bars above the fluorescence data show dark periods and actinic light illumination, respectively. Vertical red lines inside these bars indicate the time points of saturation pulse application.

6.4 Discussion and Outlook

For decades now, PAM fluorescence measurements are widely used in plant research to assess e.g., plant health, genotypic variation, and effects of mutations. Due to their minimally invasive nature, fluorescence measurements provide a convenient method to assess photosynthetic dynamics *in vivo*. The power of this spectrometric technique lies in the connection between the yield of fluorescence and numerous intrinsic processes such as NPQ, making it a method of choice for many researchers to study oxygenic photosynthesis (Stirbet et al., 2011). Detailed understanding of the underlying mechanisms and regulating circuits of the photosynthetic machinery is essential for the improvement of agricultural and horticultural productivity and sustainability, such as better designing of greenhouses, and tailored plant breeding, as well as biotechnological exploitation. It is hence expected that the interest in applying fluorescence techniques will further increase in the future. In fact, more and more advanced technical devices and methods have been and are being invented that use fluorescence emission to obtain knowledge about the photosynthetic capacities of organisms, ranging from clip-on, leaf-level measurements, using for instance the MultispeQ device (Kuhlgert et al., 2016), to canopy-level measurements with the LIFT technique (Kolber et al., 2005) and proximal or remote sensing of solar-induced fluorescence (Aasen et al., 2019; Mohammed et al., 2019).

In parallel to the experimental efforts, numerous mathematical models simulating the dynamics of photosynthesis, often calibrated to PAM results, have been developed (for a review see Stirbet et al., 2014; Stirbet et al., 2019). It was during one of such attempts to reproduce published results of PAM experiments *in silico*, where it came to our attention that a number of publications using the PAM technique do not provide all technical parameters of the experiments that are needed to simulate the results. Concerned about possible consequences of such omission, we carried out a systematic investigation of the effects of several key technical parameters on the output of PAM measurements. Using NPQ and Φ_{PSII}, which are derived from the calculated fluorescence, we have quantified and visualised the differences between our computational experiments where such parameters have been varied. The exact time point of switching on and off the AL, combined with fixed time points of SPs, considerably affects the observed induction and relaxation kinetics of NPQ (Figs. 6.3 and 6.4). Because the kinetic information is often used to derive conclusions about photoacclimation and NPQ mechanisms, our simulations underline the importance of reporting the time points of AL and SPs applied in PAM experiments. We also examined the effects of the SP duration and the interval between those on fluorescence traces. While the former seems to have little direct influence on NPQ or PSII yield (Fig. 6.7), the latter had small but detectable effects on NPQ in low AL regimes (Fig. 6.6). Importantly, the combination of SP and AL intensities can influence the outcome of experiments substantially, as visualised by the steady-state NPQ landscape in Fig. 6.5. These mathematical simulations clearly demonstrate the importance of full disclosure of technical details. In fact, this conclusion holds true for many experimental studies, not only for PAM measurements. To exclude the possibility that it is the structure of the model that causes the observed differences, we repeated our simulations with another model of photosynthesis (Ebenhöh et al., 2014). Using this model, which has been developed with a focus on state transitions, another acclimation mechanism, still obtained similar results, suggesting that the simulated effects are not attributable to model structure (the analysis can be found in the same repository https://gitlab.com/qtb-hhu/fluopam). Moreover, we validated the *in silico* findings by conducting PAM experiments focusing on variations of the

time point of switching on AL and the duration of the SP (Fig. 6.8). The predicted impact of these variations was largely in accordance with the experimental results. Although some level of reproducibility may be achieved between experiments by simply using the default settings of commercial instruments, this does not justify the omission of the details of experimental protocols. Especially, mathematical models and computational simulations have no default values, hence any missing information hinders further replication of studies. Without the necessary information, even a basic experiment cannot be properly simulated. The analysis presented above highlights the particular consequences of not providing detailed technical information about experimental protocols on the results of computational simulations of PAM Chl fluorescence traces of a photosynthetic organism. We hope that this chapter — our response to the "reproducibility crisis" — will reach a broad plant science community. We strongly encourage all readers, not only PAM users, to carefully and critically assess reporting practice to ensure independent replicability of experiments and to enable exploitation of results in the era of data science. As many have stated before us, the first step to increase reproducibility is to "increase the quality of protocol reporting " (Jessop-Fabre and Sonnenschein, 2019). We will not solve the problem of unreproducible and unreplicable research unless we provide and share all required information, even those seemingly minor and irrelevant ones. Finally, it is critical to reach an agreement on the minimal information that should be mandatorily given in the description of PAM experiments. This kind of agreements have already been made in the field of proteomics (MIAPE, Taylor et al., 2007), next-generation sequencing (MINSEQE, http://fged.org/projects/minseqe/, accessed on: 16th April 2021) and microarray analysis (MIAME, Brazma et al., 2001), in which databases are used extensively to analyse results of individual studies or selected sets of studies in form of Open Science. Also in the field of photosynthesis, PhotoSynQ is exploring a worldwide data sharing and analysis platform by creating low-cost devices and web-linked tools to collect and analyse data, exchange measurement protocols, or perform meta-analysis for registered users (https://www.photosynq.com/, accessed on: 6th May 2021). A similar platform and database, where users can freely share experimental results and protocols, even including model algorithms for simulation, can be envisaged to promote the exploitation of PAM data and to accelerate knowledge exchange. For the realisation of such platforms, the

data stored there must fulfill the minimal requirements to provide the information necessary for reproducing the experiments. Obviously, the information would comprise technical details of measurement protocols, as shown by the experiments and computational analyses in this chapter, as well as descriptions of plant materials, growth conditions, and treatments (Materials and Methods). Albeit outside the focus of this chapter, the importance of the latter information and the challenge to reproduce experimental results in plant research have been demonstrated by the joint experiments of 10 laboratories in the European AGRON-OMICS project (Massonnet et al., 2010). As was done in the aforementioned omics communities, a concrete and practical list of minimum information needs to be elaborated for PAM experiments by a consortium involving experimental and data scientists. By committing to such common standards and open databases, we will both contribute to and benefit from transparent, integrative, and interactive science in our research fields.

6.5 Concluding remarks

This chapter tackled the experiment-theory gap using qE non-photochemical quenching, a photosynthetic process on a moderate temporal scale. In contrast to physical sciences, biology only came recently (in the last forty years) to the understanding that experimental work, combined with theory and computational simulation, can result in fruitful research projects. However, due to the relatively long separation of the theoretical and experimental community, different kinds of scientific languages exist. These different languages make communication and exchange sometimes challenging. Nevertheless, biological sciences can only advance when the theory-experiment gap becomes smaller. With this chapter, I wanted to contribute to closing the gap in photosynthesis research (using PAM instruments) from a theoretical standpoint.

Chapter 7

Understanding LIFT through mathematical modeling

Fluorescence spectroscopy has become an essential tool in photosynthesis research. Multiple techniques exist to study photosynthetic fluorescence signals originating from the electron transport chain, particularly from processes associated with photosystem II. The light-induced fluorescence transient method (LIFT) is a procedure that rapidly yields fluorometric parameters, approximating classical values obtained by standard techniques for measuring chlorophyll *a* fluorescence (ChlF). The LIFT method is fast and can be used without a prolonged dark-adaptation phase and is thus suited for high-throughput phenotyping of photosynthetic organisms. In the past and present, researchers have conducted considerable efforts to infer the mechanistic reasons for the shape of fluorescence traces obtained by spectroscopic experiments, especially for fluorescence induction (FI). Mathematical models helped to elucidate the importance of processes in photosystem II. In this chapter we present a mathematical model to study the shape of fluorescence traces obtained from experiments using the LIFT method that is based on rapid processes in PSII. We demonstrate that our model can qualitatively replicate the features of fluorescence traces obtained by fluorescence induction and LIFT experiments and discuss which processes in photosystem II are relevant for the different sections of the LIFT fluorescence traces. Finally, we investigate the importance of non-photochemical quenching to LIFT fluorescence traces in light conditions and discuss how we can iteratively refine the model using a comparison with experimental data in the future

7.1 Introduction

The utilization of light energy via photosynthesis is essential for many life forms. Collected by antenna complexes, light energy drives the photosynthetic electron transport chain (PETC), eventually storing energy in ATP and NADPH. Therefore, photosynthesis is also considered an energy storage phenomenon (Blankenship, 2021). To monitor molecular processes mediated by the protein complexes in the PETC, chlorophyll *a* fluorescence (ChlF) spectroscopic techniques became the method of choice (Papageorgiou, 2004; Lakowicz, 2006). As a quick and non-invasive way to monitor the physiological status of photosynthetic organisms, many spectroscopy techniques employed in plant physiological investigations use ChlF as standard.

ChlF, primarily related to the redox state of the first electron acceptor (Q_A) in photosystem II (PSII), is used to derive photosynthetic parameters that give information about, e.g., the quantum efficiency of photochemistry, non-photochemical quenching, and cross-section of the antenna complexes associated with PSII (Kautsky, Hirsch, and Davidshöfer, 1932; Butler and Kitajima, 1975; Genty et al., 1990). Parameters like these are used extensively to study the effects of stressors and abiotic factors, such as irradiance, on photosynthetic performance (compare, e.g., Matuszyńska et al., 2016; Rungrat et al., 2016) using various experimental techniques. Fluorescence induction (FI), the rapid exposure of dark-adapted samples to (high) light, produces a characteristic polyphasic fluorescence rise. Classically these phases are denoted with the letters OJIP(SMT) and provide information about the processes in photosystem II and the following processes in the PETC (Stirbet et al., 2011). Other techniques can be broadly classified as using single turnover (ST) or multiple turnovers (MT) flashes. Both reduce the Q_A pool but use different light intensities and flash durations leading, when long, to additional causes of the fluorescence signal (Kalaji et al., 2017), such as the reduction state of the plastoquinone pool. The differences between the maximum fluorescence measured with ST or MT techniques is assumed to be caused by a quencher that decays during the prolonged application of light in MT experiments. Frequently, oxidized plastoquinone is hypothesized to be this quencher (Samson, Prášil, and Yaakoubd, 1999).

Some techniques, like the pulse amplitude modulation method (PAM), combined with saturating light pulses for a quenching analysis (Schreiber, 2004), require the sample to be dark-adapted, and established protocols last several minutes, affecting processes after PSII in the PETC. The duration of

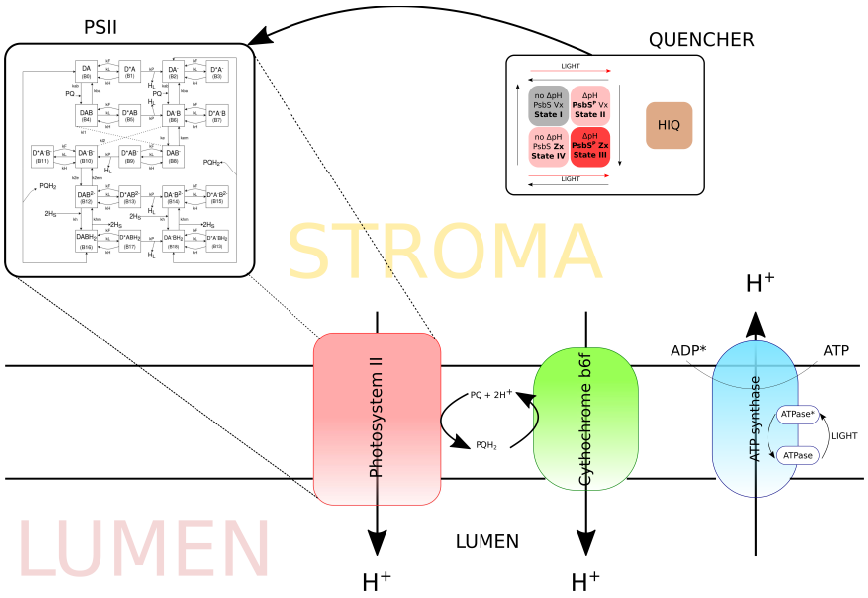

FIGURE 7.1: Schematic representation of the model used to simulate LIFT fluorescence traces. The model includes a detailed description of photosystem II and downstream processes. Additionally, it contains a module representing a quencher that is activated by the protonation of PsbS and the xanthophyll cycle and a simplified description of a high-intensity quencher. An enlarged version of the reactions involved in photosystem II is shown in Fig. 7.2.

the protocols and the dark-adaption requirement are inconvenient if the aim is to observe fast dynamic changes in the photosynthetic parameters. Fast repetition rate (FRR) technique and, consequently, the light-induced fluorescence transient technique overcome these shortcomings using subsaturating flashlets of high excitation power and rate (Kolber, Prášil, and Falkowski, 1998; Kolber et al., 2005). LIFT has been successfully applied to monitor the photosynthesis of microorganisms, canopies, and individual plants (Kolber, Prášil, and Falkowski, 1998; Kolber et al., 2005; Keller et al., 2019). Parameters derived from LIFT experiments approximate those obtained from conventional techniques in different conditions, such as various light intensities, nitrogen gas concentrations, and treatments with inhibitors (Keller et al., 2019). The short duration of the LIFT experiments (<1 s) makes it an optimal method for large phenotyping projects that require many measurements in a short time.

Interpretation of ChlF signals with mathematical models has a long history (Joliot, 1964; Malkin and Kok, 1966; Bouges-Bocquet, 1973; Butler and Kitajima, 1975; Paillotin, 1976; Butler, 1978; Genty, Briantais, and Baker, 1989; Lavergne and Trissl, 1995; Stirbet et al., 2019). Mathematical modeling is a powerful tool for studying the behavior of processes in the photosynthetic electron transport chain and CBB cycle when experimental methods

cannot proceed due to technical limitations. Kinetic models, for example, have been applied to understand the FI fluorescence trace and its characteristic phases (Lazár et al., 1997; Zhu et al., 2005; Lazár and Schansker, 2009), non-photochemical quenching (Zaks et al., 2012; Matuszyńska et al., 2016), state-transition (Ebenhöh et al., 2014; Stirbet and Govindjee, 2016), and multiple other photosynthetic phenomena in combination with carbon fixation (Morales et al., 2018a; Matuszyńska, Saadat, and Ebenhöh, 2019; Saadat et al., 2021).

In this chapter, we present a mechanistic mathematical model based on ordinary differential equations that describe fluorescence changes using the FRR fluorescence technique LIFT applied to plants. The parameters and reaction rates were foremost extracted from the literature. In particular, we modified for the simulation of processes in photosystem II the model presented in Lazár et al., 1997, as it is less complex than more advanced representations of photosystem II while still showing the main characteristics of FI fluorescence traces. For the downstream reactions of PSII, we combined our description with the mathematical model of non-photochemical quenching by Matuszyńska et al., 2016. We demonstrate that our model can qualitatively reproduce fluorescence traces typically obtained from LIFT experiments and investigate which processes influence the relaxation phase of the LIFT fluorescence trace. Further, we explore the connection between the fluorescence output and light acclimation in plants, as LIFT can also be applied to light-adapted samples, and discuss how we can further refine the parameter space/ model structure to improve our understanding of the mechanisms behind LIFT fluorescence traces.

7.2 Model and Methods

7.2.1 Model

A mathematical model was built based on reactions in photosystem II and downstream processes. Parameters for the model were mostly taken from the literature. The model was implemented via the Python-based software modelbase (Aalst, Ebenhöh, and Matuszyńska, 2021) and subsequently integrated with Assimulo (Andersson, Führer, and Akesson, 2015). The code can be found in following repository https://gitlab.com/qtb-hhu/models/2023-lift-frr.

7.2.2 Stoichiometry of the model

The mathematical model of photosystem II and parts of the electron transport chain is represented as a system of 26 ordinary differential equations governing the temporal evolution of system variables. These variables are 1-19) states of photosystem II, 20) the reduced fraction of the plastoquinone pool (P), 21) the lumenal proton concentration (H), 22) the stromal concentrations of ATP (A), 23) the non-protonated fraction of the PsbS pool (PsbS), 24) the violaxanthin fraction of the xanthophyll pool (V), 25) an activator of the ATP synthase (E), and 26) a carotenoid quencher (CarQ).

The system of equation reads

$$\frac{dB0}{dt} = v_{\text{asPQH}_2160} - v_{\text{ex01}} - v_{\text{asPQ04}} \tag{7.1}$$
$$\frac{dB1}{dt} = v_{\text{ex01}} - v_{\text{sep12}} \tag{7.2}$$
$$\frac{dB2}{dt} = v_{\text{asPQH}_2182} + v_{\text{sep12}} - v_{\text{ex23}} - v_{\text{asPQ26}} \tag{7.3}$$
$$\frac{dB3}{dt} = v_{\text{ex23}} \tag{7.4}$$
$$\frac{dB4}{dt} = v_{\text{asPQ04}} - v_{\text{ex45}} + -v_{\text{l84}} \tag{7.5}$$
$$\frac{dB5}{dt} = v_{\text{ex45}} - v_{\text{sep56}} \tag{7.6}$$
$$\frac{dB6}{dt} = v_{\text{sep56}} + v_{\text{asPQ26}} + v_{\text{l106}} - v_{\text{ex67}} - v_{\text{1e68}} \tag{7.7}$$
$$\frac{dB7}{dt} = v_{\text{ex67}} \tag{7.8}$$
$$\frac{dB8}{dt} = v_{\text{1e68}} - v_{\text{l84}} - v_{\text{ex89}} \tag{7.9}$$
$$\frac{dB9}{dt} = v_{\text{ex89}} - v_{\text{sep910}} \tag{7.10}$$
$$\frac{dB10}{dt} = v_{\text{sep910}} - v_{\text{ex1011}} - v_{\text{l106}} - v_{\text{2e1012}} \tag{7.11}$$
$$\frac{dB11}{dt} = v_{\text{ex1011}} \tag{7.12}$$
$$\frac{dB13}{dt} = v_{\text{ex1213}} - v_{\text{sep1314}} \tag{7.13}$$
$$\frac{dB14}{dt} = v_{\text{sep1314}} - v_{\text{ex1415}} - v_{\text{h1418}} \tag{7.14}$$
$$\frac{dB15}{dt} = v_{\text{ex1415}} \tag{7.15}$$
$$\frac{dB16}{dt} = v_{\text{ex1617}} - v_{\text{h1216}} - v_{\text{asPQH}_2160} \tag{7.16}$$
$$\frac{dB17}{dt} = v_{\text{ex1617}} - v_{\text{sep1718}} \tag{7.17}$$

$$\frac{dB18}{dt} = v_{\text{h1418}} + v_{\text{sep1718}} - v_{\text{ex1819}} - v_{\text{asPQH}_2\text{182}} \tag{7.18}$$

$$\frac{dB19}{dt} = v_{\text{ex1819}} \tag{7.19}$$

$$\frac{dP}{dt} = v_{\text{asPQH}_2\text{160}} + v_{\text{asPQH}_2\text{182}} - v_{\text{PQox}} \tag{7.20}$$

$$\frac{dH}{dt} = \frac{1}{b_H} \cdot (v_{\text{sep12}} + v_{\text{sep56}} + v_{\text{sep910}} + v_{sep1314} + v_{\text{sep1718}} + 4 \cdot v_{\text{PQox}} - \frac{14}{3} \cdot v_{\text{ATPsynth.}} - v_{\text{Leak}}) \tag{7.21}$$

$$\frac{dE}{dt} = v_{\text{ATPact.}} \tag{7.22}$$

$$\frac{dATP}{dt} = v_{\text{ATPsynth.}} - v_{\text{ATPconsumption}} \tag{7.23}$$

$$\frac{dPsbS}{dt} = -v_{\text{PsbSP}} \tag{7.24}$$

$$\frac{dV}{dt} = -v_{\text{Xcyc}} \tag{7.25}$$

$$\frac{dCarQ}{dt} = v_{\text{CarQ}} \tag{7.26}$$

7.2.3 Photosystem II

Photosystem II is modeled as a 3-compound system (DAB) with multiple states. The donor site (D) can be excited by light (D^*). In the Q_A-site (A) of photosystem II is a non-free plastoquinone that can be singly charged (A^-). The Q_B-site of photosystem II is either empty (DA) or contains a plastoquinone (DAB) molecule. This plastoquinone can be singly, doubly charged, and protonated (DAB^-, DAB^{2-} or $DABH_2$). Together there are 20 different combinations considered in the model of photosystem II.

The amount of available photosystem II is constant ($PSII_{tot}$). This allowed us to reduce the ordinary differential equation system by removing B12 (DAB^{2-}),

$$B_{12} = PSII_{\text{tot}} - \sum_{\substack{i=0 \\ i \neq 12}}^{19} B_i. \tag{7.27}$$

To model the changes in oxidized plastoquione we use the fact that the total plastoquinone pool, consisiting of the free oxidized and reduced plastoquinone and plastoquionone that is bound to photosystem II, is constant.

$$P_{\text{ox}} = PQ^{\text{tot}} - P - \sum_{\substack{i=0 \\ i \neq [0,1,2,3]}}^{19} B_i. \tag{7.28}$$

Eight rate laws connect the 20 different combinations/states in photosystem II.

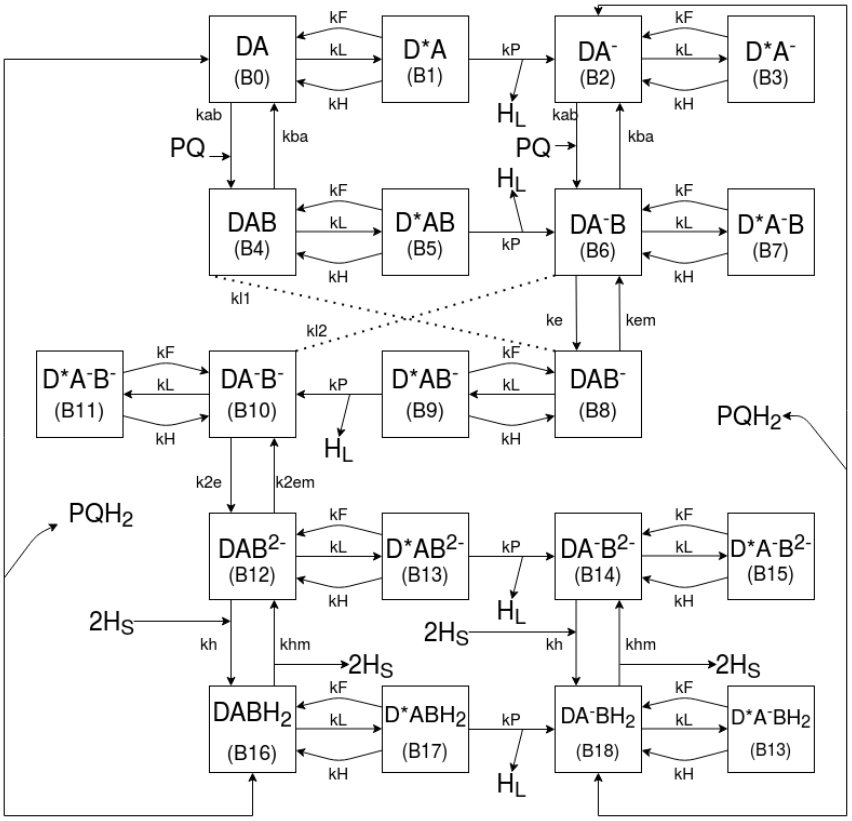

FIGURE 7.2: Schematic representation of the photosystem II submodel. Photosystem II is modeled as a 3-compound system (DAB) with multiple states. The donor site (D) can be excited by light (D^*). In the Q_A-site (A) of photosystem II is a non-free plastoquinone that can be singly charged (A^-). The Q_B-site of photosystem II is either empty (DA) or contains a plastoquinone (DAB) molecule. This plastoquinone can be singly, doubly charged, and protonated (DAB^-, DAB^{2-} or $DABH_2$). Together there are 20 different combinations considered in the model of photosystem II.

Excitation and charge separation/ stabilization: v_{ex} considers the excitation of the donor site (D) and losses of the excited state (D^*) by non-photochemical quenching (Q), fluorescence, oxidized plastoquinone and carotenoid quencher activity ($CarQ$, P_{ox}),

$$v_{ex,ij} = k_L \cdot B_i - (k_\mathrm{F} + k_\mathrm{H} \cdot Q + k_\mathrm{CarQ} \cdot Car_Q + k_\mathrm{HPQ} \cdot P_\mathrm{ox}) \cdot B_j. \tag{7.29}$$

Here and in all other equations, B_i and B_j are two states of photosystem II (see Fig. 7.2). Charge separation/ stabilization is assumed to be an irreversible process,

$$v_{sep,ij} = k_\mathrm{P} \cdot B_i. \tag{7.30}$$

Association of oxidized plastoquinone: At the Q_B-site of photosystem II attaches an oxidized plastoquinone

$$v_\mathrm{asPQ,ij} = k_\mathrm{ab} \cdot P_\mathrm{ox} \cdot B_i - \frac{k_\mathrm{ab}}{K_\mathrm{eq,ab}} \cdot B_j. \tag{7.31}$$

First electron transport in PSII: After the transfer of one electron on the non-free plastoquinone in the Q_A-site of photosystem II, the electron is transferred to the plastoquinone associated with PSII in the Q_B-site,

$$v_\mathrm{1e,ij} = k_\mathrm{e1} \cdot B_i - \frac{k_\mathrm{e1}}{K_\mathrm{eq,e1}} \cdot B_j. \tag{7.32}$$

Second electron transport in PSII: Again, after the transfer of one electron on the non-free plastoquinone in the Q_A-site of photosystem II, the electron is transferred to the singly charged plastoquinone associated with PSII in the Q_B-site,

$$v_\mathrm{2e,ij} = k_\mathrm{e2} \cdot B_i - \frac{k_\mathrm{e2}}{K_\mathrm{eq,e2}} \cdot B_j. \tag{7.33}$$

Protonation: Once the plastoquinone in the Q_B-site of photosystem II is doubly charged, it is protonated,

$$v_\mathrm{h,ij} = k_\mathrm{h} \cdot B_i - \frac{k_\mathrm{h}}{K_\mathrm{eq,h}} \cdot B_j. \tag{7.34}$$

Disocciation of reduced plastoquinone: Protonated plastoquinone in the Q_B-site can detach from PSII and is used in further downstream processes of the PETC,

$$v_{\mathrm{asPQH_2,ij}} = k_{\mathrm{PQ_{dis}}} \cdot B_i - \frac{k_{\mathrm{PQ_{dis}}}}{K_{\mathrm{eq,PQ_{dis}}}} \cdot B_j \cdot P. \tag{7.35}$$

Charge loss: Following examples of other photosystem II models e.g. Lazár et al., 1997, we included charge losses (presumably due to oxygen). These charge losses are irreversible,

$$v_{\mathrm{l}} = k_{\mathrm{l,ij}} \cdot B_i. \tag{7.36}$$

Fluorescence: Similar to Ebenhöh et al., 2014, we calculate fluorescence as the probability that an excited state is reverting to a ground state by fluorescence (Butler, 1978). Thus the fluorescence signal resulting from B_0, B_4, B_8, B_{12}, and B_{16} is proportional to $k_F/(k_F + k_H \cdot Q + k_P + k_{CarQ} \cdot CarQ + k_{HPQ} \cdot P_{ox})$ and the fluorescence signal resulting from B_2, B_6, B_{10}, B_{14}, and B_{18} is proportional to $k_F/(k_F + k_H \cdot Q + k_{CarQ} \cdot CarQ + k_{HPQ} \cdot P_{ox})$. The total fluorescence signal is calculated as

$$\begin{aligned} F = & \frac{k_F}{(k_F + k_H \cdot Q + k_P + k_{CarQ} \cdot CarQ + k_{HPQ} \cdot P_{ox})} \cdot (B_0 + B_4 + B_8 + B_{12} + B_{16}) \\ & + \frac{k_F}{(k_F + k_H \cdot Q + k_{CarQ} \cdot CarQ + k_{HPQ} \cdot P_{ox})} \cdot (B_2 + B_6 + B_{10} + B_{14} + B_{18}). \end{aligned} \tag{7.37}$$

Note that the sum of B_0, B_4, B_8, B_{12}, and B_{16} as well as the sum of B_2, B_6, B_{10}, B_{14}, and B_{18} approximate the total amount of open and closed PSII, respectively. This is because the excited states of PSII are forced to have a minor concentration in our model simulations. In contrast to the previous representation of the fluorescence signal , e.g. in Ebenhöh et al., 2014, it is necessary to assume two additional quenching pathways to reproduce the LIFT fluorescence signal. The first one is the high-intensity quenching that was found to be active when a high excitation power / light intensity is used to activate photosynthetic processes. This quenching is assumed to be associated with forming a triplet excited carotenoid state. The second is the quenching process connected to the oxidized form of plastoquinone. It is assumed that oxidized plastoquinone is a quencher in contrast to reduced plastoquinone (plastoquinol). The effect of plastoquinone might be responsible for the fluorescence difference we observe between single and multiple turnover techniques. While both close PSII, the latter reduces the plastoquinone pool, leading to a higher maximal fluorescence signal. Please note that most parameters of these quenching processes are ad-hoc estimations that must be refined in future model versions.

7.2.4 Electron transport chain

Plastoquinone oxidation: For down-stream processes of photosystem II that consume reduced plastoquinone we used the 'lumped' reaction of Cyt_{b6f} and PTOX that is presented in Matuszyńska et al., 2016.

$$v_{PQox} = \left(\frac{k_{\text{PFD}} \cdot K_{\text{eq,Cyt}b6f}(H)}{K_{\text{eq,Cyt}b6f}(H) + 1} + k_{\text{PTOX}} \right) \cdot P - \frac{k_{\text{PFD}}}{K_{\text{eq,Cyt}b6f}(H) + 1} \cdot P_{\text{ox}}, \quad (7.38)$$

where $k_{\text{PFD}} = k_{\text{Cyt}b6f} \cdot PFD$.

ATP synthase: We follow Ebenhöh et al., 2014 and Ebenhöh et al., 2011 to represent the ATP synthase. The ATP synthase is modeled with a mass-action kinetic and a lumenal pH-dependent equilibrium constant.

$$v_{\text{ATPsyntahse}} = E \cdot k_{\text{ATPsynthase}} \cdot \left(ATP^{\text{tot}} - ATP - \frac{ATP}{K_{\text{eq,ATPsynthase}}(H)} \right). \quad (7.39)$$

ATP^{tot} is the total adenosine phosphate pool. For the analyses shown in this chapter, E is fixed to one. However, for testing and future model versions, we model the activation of the ATP synthase by a simple mass-action kinetic with a switch triggered by the presence or absence of light as in Matuszyńska et al., 2016,

$$v_{\text{ATPactivity}} = k_{\text{ActATPase}} \cdot H(PFD) \cdot (1 - E) - k_{\text{DeactATPase}} \cdot (1 - H(PFD)) \cdot E, \quad (7.40)$$

where H is the Heaveside function. Note that we found that a dynamic E makes the model in simulations over large time intervals unstable. This instability must be clarified in future model versions.

Non-photochemical quenching: The representation of non-photochemical quenching follows the implementation of Matuszyńska et al., 2016. The non-photochemical quenching module implemented in the model is assumed to be a two-variables-four-states system. Included are the protonation of the PsbS protein and the Xanthophyll cycle. The equations for both processes are

$$v_{\text{Xanth}} = k_{\text{Deepox}} \cdot \frac{H^{\text{nH}_\text{X}}}{H^{\text{n}_\text{HX}} + pH_{\text{inv}} \left(K_{\text{pHsatz}}\right)^{\text{nH}_\text{X}}} \cdot V - k_{\text{Epox}} \cdot (X^{\text{tot}} - V), \quad (7.41)$$

$$v_{PsbS} = k_{\text{Prot}} \cdot \frac{H^{\text{nH}_\text{L}}}{H^{\text{n}_\text{HL}} + pH_{\text{inv}} \left(K_{\text{pHsatLHC}}\right)^{nH_L}} \cdot PsbS - k_{\text{Deprot}} \cdot (PsbS^{tot} - PsbS), \quad (7.42)$$

where pH_{inv} is a function transforming lumenal pH to lumenal proton concentration.

The quenching activity is determined as

$$\begin{aligned} Q = \gamma_0 \cdot (1 - \frac{Zx}{Zx + K_{\text{Zsat}}}) \cdot PsbS + \gamma_1 \cdot (1 - \frac{Zx}{Zx + K_{\text{Zsat}}}) \cdot PsbS^p \\ + \gamma_2 \cdot \frac{Zx}{Zx + K_{\text{Zsat}}} \cdot PsbS^p + \gamma_3 \cdot \frac{Zx}{Zx + K_{\text{Zsat}}} \cdot PsbS. \end{aligned} \quad (7.43)$$

Carotenoid quenching: Under high light intensities a quenching activity by carotenoid molecules was reported. In the fluorescence traces obtained by LIFT experiments this high intensity quenching (HIQ) appears as jump in the fluorescence signal between induction and relaxation phase. The carotenoid quenching is modeled as mass-action kinetic that includes an activation term triggered when the light intensity surpasses a threshold,

$$v_{\text{CarQ}} = k_{\text{Car,p}} \cdot (1 - CarQ) \cdot \frac{PFD}{K_{\text{CarActive}} + PFD} - k_{\text{Car,m}} \cdot CarQ. \quad (7.44)$$

Please note that this is just a rough approximation of the HIQ activity. In future model versions the activity of HIQ must be modeled more realistically and potentially be combined with the already existing quencher activity that is formulated based on the protonation of PsbS and the xanthophyll cycle.

Proton leak: The existence of a small leak current of protons over the thylakoid membrane is assumed. The leak current is modeled with a mass-action kinetic.

$$v_{\text{leak}} = k_{\text{leak}} \cdot (H - H^+_{\text{stroma}}). \quad (7.45)$$

ATP consuming reaction: Because down-stream processes of the electron transport chain are not considered, the ATP consuming reactions are collectively modeled as mass-action kinetic,

$$v_{\text{ATPconsumption}} = k_{\text{ATPconsumption}} \cdot ATP. \quad (7.46)$$

7.2.5 Light-induced fluorescence transient method protocol

For the *in silico* analyses, a generic LIFT protocol was used based on the description in Keller et al., 2019. The induction phases consisted of 300 flashlets with 40000 µmol m^{-2} s^{-1} , light intensity and a length of 1.6 µs. The interval between the flashlets was 2.5 µs. 128 flashlets with the same length and intensity were applied in the relaxation phase. The time interval between the flashlets varied in the relaxation phase according to

$$j_i = 10^{1.28+0.021 \cdot i} \text{ µs}. \tag{7.47}$$

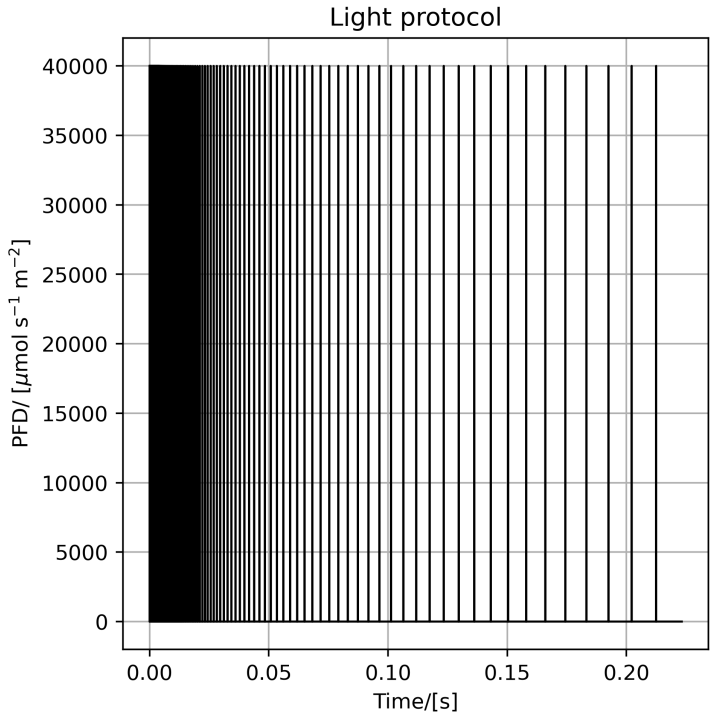

FIGURE 7.3: Visualization of the light protocol for *in silico* experiments using the LIFT method. The induction phases consists of 300 flashlets with 40000 µmol m^{-2} s^{-1} light intensity and a length of 1.6 µs. The interval between the flashlets is 2.5 µs. 128 flashlets with the same length and intensity are applied in the relaxation phase. The intervals between flashlets in the relaxation phase varies exponentially.

7.2.6 Sensitivity analysis

For the investigation of the sensitivity of fluorescence signals to parameter changes, we calculated normalized time-dependent response coefficients,

$$R_p^F(t) = \frac{p}{F(t,\mathbf{p})} \frac{\partial F(t,\mathbf{p})}{\partial p}\bigg|_{p=p_0}. \tag{7.48}$$

Here F(t, **p**) is the fluorescence signal at time t; **p** is the parameter vector.

7.2.7 Curvature of relaxation phase

The curvature of the fluorescence traces in the relaxation phase of LIFT experiments was quantified as mean curvature according to

$$\kappa_i = \frac{|Fi''|}{(1+Fi'^2)^{3/2}}, \tag{7.49}$$

and

$$\kappa = \frac{1}{N}\sum_i^N \kappa_i, \tag{7.50}$$

where F_i is the ChlF yield at flashlet i, and N is the total number of flashlet in the relaxation phase. The derivatives were calculated using a central finite-difference approximation.

7.3 Results

7.3.1 Model validation

We have built a mathematical model based on our current understanding of non-photochemical quenching and processes in photosystem II to provide a theoretical framework that relates outputs of high repetition rate fluorescence experiments to processes in and around photosystem II (Fig. 7.1, see model description). The model was kept deliberately as simple as possible and aims to investigate which reactions in PSII influence the shape of the fluorescence trace in the induction and relaxation phases of LIFT experiments.

To confirm that our model can indeed be used to understand non-steady state fluorescence phenomena originating from the activities in and around photosystem II, we reproduced typical fluorescence traces observed in fluorescence induction experiments and experiments using the LIFT technique (as well as from a quenching analysis using PAM). All simulations exhibit typical fluorescence dynamics with characteristics frequently observed experimentally (compare Keller et al., 2019 and Fig. 7.4 or supplementary Figs.

7.9 and 7.10). Looking at the changes of the PSII states during the simulations, we find that the PSII-state with a singly charged Q_A-site (B6) is the predominant closed state at the onset of the simulated FI or LIFT experiments (FI: O-J phase and LIFT: induction phase, see supplementary Fig. 7.11). At the end of the FI O-J phase and the induction phase of the LIFT experiments also other PSII-states gain importance especially those downstream of B6, such as B8, B10, and B14. The FI measurement exhibits a higher F_m than the LIFT measurement. This is due to the quenching activity of the oxidized plastoquinone pool, which is reduced during a multiple turnover flash (FI, saturating light flash with a duration of 1 s) experiment. In the later relaxation phase of the LIFT experiment, the closed PSII states B4, B6, B14, and B18 show the most significant changes. The same applies to the fluorescence induction experiment, with additionally B2 increasing when reaching the P point of the fluorescence trace. Please note that the dynamics of closed states, such as B2, B6, B10, B14, and B18, are more influential for the fluorescence signal than the open states.

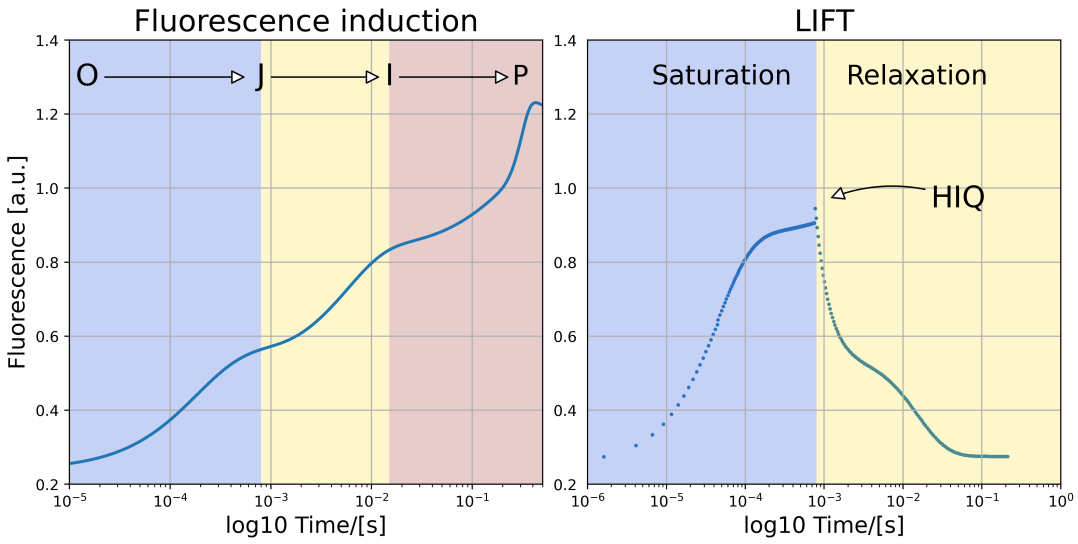

FIGURE 7.4: Simulated fluorescence traces of a fluorescence induction (left panel) and a LIFT (right panel) experiment. For the fluorescence induction experiment, the light intensity was 3000 µmol m^{-2} s^{-1}. The LIFT experiment followed the standard protocol for *in silico* LIFT experiments (see methods). The light intensities of the 1.6 µs flashlets were 40000 µmol m^{-2} s^{-1}. Both simulated fluorescence curves exhibit well-known dynamics, such as the OJIP phases of fluorescence induction and LIFT experiments' saturation/ relaxation phases.

In LIFT experiments, there is no additional measuring pulse to the subsaturating flashlet. However, our model also allows monitoring changes in the fluorescence yield between flashlets (without activating photosynthetic processes). We found that frequently, the fluorescence still rises slightly after

the subsaturating flashlet was applied (well visible in the relaxation phase), suggesting that the maximum effect of the subsaturating (measuring) flashlet is only reached after the measuring window already closed (see supplementary Fig. 7.12). It must be clarified in future model versions if this is a model artifact or an actual physical effect.

It is important to state that while our model can qualitatively replicate experimental observations, it is still in the process of being refined. This circumstance leads to some quantitative deviations between experiments and simulations, especially in the relaxation phase of LIFT experiments. With that being said, we are, nonetheless, confident in the model's ability to provide mechanistic descriptions of all phases of the LIFT fluorescence traces and suggestions for further model improvements in this analysis.

7.3.2 Sensitivity analysis

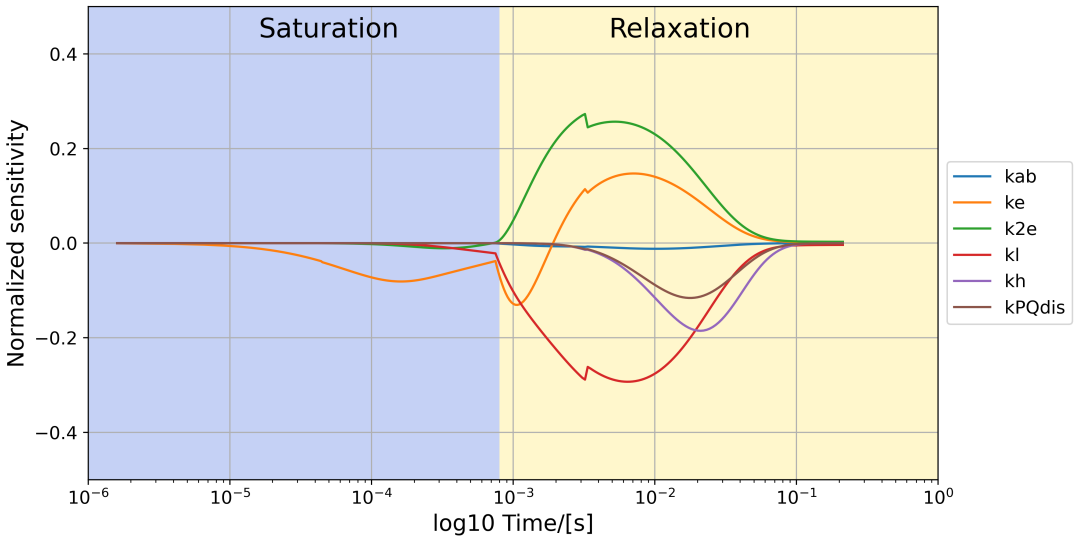

FIGURE 7.5: Local sensitivity analysis for LIFT fluorescence traces obtained with the standard *in silico* LIFT protocol. The following processes were included in the analysis: association of oxidized plastoquinone (k_{ab}), first and second electron transport between Q_A-site and Q_B-site (k_e, k_{2e}), charge loss (k_l), protonation of double-charged plastoquinone in the Q_B-site, dissociation of reduced plastoquinone (k_{PQdis}).

The LIFT and the FI fluorescence traces are transient phenomena induced by changes in light conditions. Transient phenomena are challenging to investigate mathematically, and the theory to understand them is still constructed. This lack of theory for transients contrasts with steady

state changes, where frameworks such as metabolic control theory are well-developed and regularly applied to study the behavior of metabolic models (Fell, 1992). We here used local sensitivity analysis in each time step to investigate to which processes the LIFT and FI fluorescence signal is most sensitive in its transient phases, thus extending our previous investigation of the predominant PSII states during the time course of the fluorescence traces. Fig. 7.5 shows the sensitivity of the LIFT fluorescence signal to several PSII-related processes. In the induction phase, the most influential under the investigated processes is the first electron transport between the Q_A-site and Q_B-site (k_e). The charge loss (k_l) and second electron transport (k_{2e}) gain a minor influence at the end of the induction phase. In the first part of the relaxation phase, charge loss and first/ second electron transport still most impact the LIFT transient. Interestingly, in our model simulations, the first electron transport (k_e) changes the sign of its impact (sensitivity), first having a negative (changes in the parameter lead to a decrease of the fluorescence signal) to a positive effect. In the later stages, when the two electron transport processes and the charge loss start to have reduced importance, the protonation of the double-charged plastoquinone in the Q_B-site and the dissociation of protonated plastoquinone increasingly influences the LIFT fluorescence trace. It remains to speculate why there is a jump in the sensitivities during the relaxation phase. One explanation is that the effect of the high-intensity quencher deactivation is delayed in our model. We can see the same pattern as for LIFT fluorescence traces for the sensitivities in the FI curves (supplementary Fig. 7.13). In the O-J phase, the most influential process is the first electron transport process in PSII. Later in the J-I phase, the charge loss and the second electron transport gain influence while the sensitivity for the first electron transport slowly decreases. When the FI trace eventually approaches the "P" point, the protonation at Q_B-site and the dissociation of reduced plastoquinone gain influence. In contrast to the LIFT sensitivity analysis, we see no change in the sign of sensitivity associated with the first electron transport.

7.3.3 The plastoquinone reduction-oxidation cycle influences fluorescence traces

While the previous analyses were focused to understand the fluorescence traces of LIFT experiments under standard conditions, following investigations aim to explain natural variations in the fluorescence dynamics. These

variations can be caused by the natural variations between ecotypes of plants or by external conditions, i.e. irradiance. In LIFT experiments, the intermediate to late relaxation phase is assumed to be connected to the electron transfer between plastoquinone in photosystem II's Q_A-site and Q_B-site and other downstream processes, such as the dissociation of plastoquinone from PSII. Our simulations show that the total pool size and plastoquinone's association with photosystem II strongly affect the fluorescence output of FI and LIFT experiments (Fig. 7.6).

A decrease in the plastoquinone pool size results in a less pronounced waveform of the LIFT fluorescence curves in the relaxation phase of the experiment and a loss of the I-P phase of the fluorescence induction traces. Additionally with increasing plastoquinone pool the fluorescence in the the OJI phases decreases. This can be explained by the stronger quenching of oxidized plastoquinone due to its increased amount during these phases. Interestingly, the waveform of the LIFT experiment persists in all tested plastoquinone pool sizes, Fig. 7.6 A, indicating that the pool size of plastoquinone is an influential factor for the LIFT relaxation waveform but not the reason for it.

The association of oxidized plastoquinone is an essential step in the electron transport processes in photosystem II, Fig. 7.6 B. An incomplete fluorescence relaxation is visible when lowering the association rate of oxidized plastoquinone. Additionally, the FI fluorescence traces lose the I-P phase almost entirely. In our model simulation, these changes can be explained by a shift of the PSII states that are most influential in the corresponding phases of the LIFT and FI experiments (see supplementary Fig. 7.14) . While usually the late phases of both experiments are dominated by the $DQ_A^-Q_B^{-2}$ (B14) and $DQ_A^-Q_BH_2$ (B18) PSII states (see supplemtary Fig. 7.11), a decrease in the association of oxidized plastoquinone pool leads to an increase of the DQ_A^- (B2) state.

The effect that we observe in the later phase of both experimental setups (FI and LIFT) are, thus, not primarily caused by the protonation of doubly charged plastoquinone in the Q_B-site and following dissociation from PSII, as would be normally the case, but by the accumulated B2 pool. In the LIFT experiment, a slow reduction of the accumulated B2 pool leads to a prolonged relaxation phase. This is not the case for the FI experiment, where only the induction and concomitant increases of the PSII states are observed. Here the reduction of the association rate of the oxidized plastoquinone pool leads to a considerable flux into the B2 state, making it the most dominant state in the

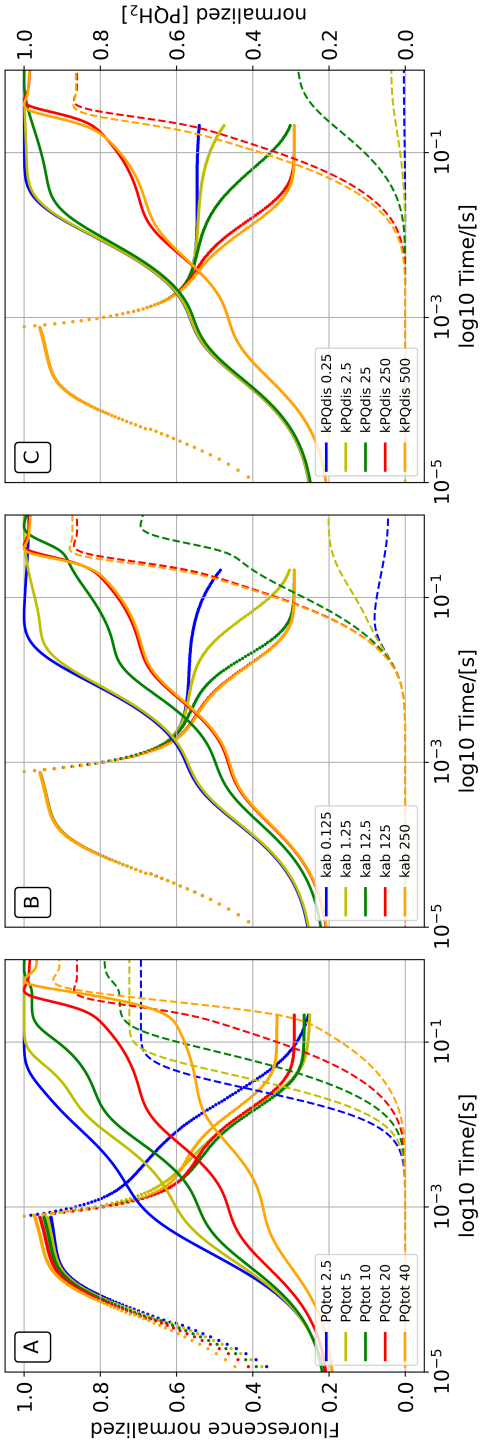

FIGURE 7.6: Effect of total plastoquinone pool size (PQpool) and the rate of association and dissociation for oxidized plastoquinone (kab) and reduced plastoquinone (kPQdis) to photosystem II, respectively, on fluorescence traces from LIFT and FI experiments (left y-axis) and redox state of the plastoquinone pool (right y-axis). *In silico* experiments were conducted with the same protocols as described in Fig. 7.4.

I-P phase. However, because the kinetics of B2 does neither experience any influence by the limiting electrons transfer between the Q_A-site and Q_B-site (k_e and k_{2e}) nor the protonation of doubly charged plastoquinone associated with PSII, we do not see any inflection in the I-P phase.

We see the same effects on fluorescence signals as when lowering the association rate of oxidized plastoquinone when lowering the dissociation rate of reduced plastoquinone from PSII (Fig. 7.6 C). However, the cause is different in contrast to lowering the association rate of oxidized plastoquinone. Here both B14 and B18 are the dominant factors in the later phases of the experiments (see supplementary Fig. 7.14), as would be observed under standard parameters. A slow dissociation merely prolongs the relaxation phase of the LIFT trace. In the FI curve, the I-P phase is normally caused by a balance of the different processes in PSII, leading to phases that look as if they were transiently in a steady state. However, lowering the dissociation rate introduces an imbalance that results in a continuous increase in the fluorescence signal.

7.3.4 Balance between first and second electron transfer contributes to curvature in relaxation phase

Our previous analysis indicated that the attachment of reduced and oxidized plastoquinone has an influential role in the LIFT fluorescence traces' relaxation phase. However, especially after the change from the induction to the relaxation phase, the shape of the fluorescence trace is primarily influenced by electron transport processes in PSII. We determined the curvature/waveform in the relaxation phase to quantify the effect of balancing first and second electron transport between the primary (Q_A) and secondary (Q_B) electron acceptor in PSII.

Fig. 7.7 displays the curvature of fluorescence traces obtained by simulated LIFT experiments as a function of the first ($Q_A^- \rightarrow Q_B$, k_e) and second ($Q_A^- \rightarrow Q_B^-$, $k2e$) electron transfer rate constants. The curvature of LIFT fluorescence traces shows three different characteristics. 1), with increasing both electron transfer rate constants, the curvature increases. 2), the curvature increases when the first or second electron transfer rate constant is increased while keeping the other one fixed. 3), an increase in the first electron transfer rate constant affects the curvature more drastically than in the second.

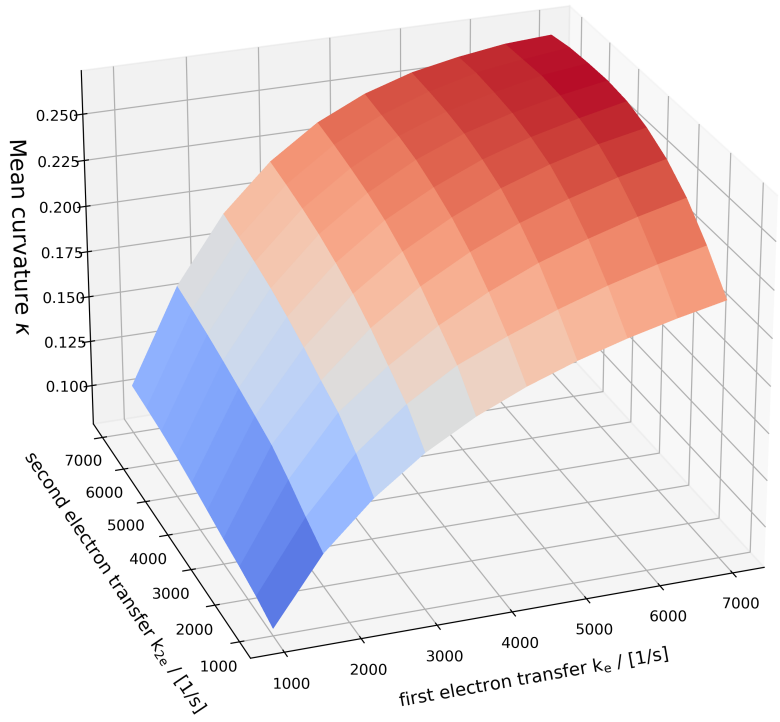

FIGURE 7.7: Predicted curvature (z-axis) in the relaxation phase of LIFT fluorescence traces varying the electron transfers between $Q_A^- \rightarrow Q_B$ (k_e, x-axis) and $Q_A^- \rightarrow Q_B^-$ ($k2e$, y-axis). For these predictions, 100 combinations of rates for the first and second electron transfer in PSII were used to conduct *in silico* experiment using the LIFT method with the standard protocol. The curvature smoothly changes between the lowest to the highest value. Changes in the direction of increasing k_e are steeper than in the direction of k_2e, indicating that the first electron transfer has a stronger influence on the curvature in the relaxation phase of LIFT experiments.

The waveform in the relaxation phase of LIFT fluorescence traces is caused by an accumulation of high fluorescence emitting (closed) states of photosystem II due to an imbalance in the rate constants. Under normal circumstances, the PSII states predominantly determining the fluorescence trace of the relaxation phase are B4, B6, B8, B14, and B18. Here B6, B14, and B18 are closed states and thus contribute to the fluorescence signal approximately five times (based on parameters used in this model) more than the

open states (B4 and B8). The "wobble" that we see in standard conditions during the relaxation phase (see Fig. 7.4) can be explained by a shift from B6 being the most abundant closed PSII state to B14, the latter reaching a maximum after a slight delay. The maximum of B14 coincides with the "wobble" in the LIFT fluorescence trace (see supplementary Figs. 7.11 and 7.15). Changes in one of the electron transport rates, while keeping the other constant, generally lead to an increased abundance of the B14 state in the relaxation phase. Thus, making the waveform in the relaxation phase more pronounced.

When having a low first but a high second electron transport, the B4, B6, and B14 PSII states determine the relaxation phase fluorescence (Fig. 7.15) . The combined contribution of the closed B6 and B14 state to the relaxation phase fluorescence signal leads to a fluorescence signal with low curvature. In contrast, when increasing the first electron transport while keeping the second low, we can see that the B6 state decreases at the end of the induction phase while the abundance of B10 increases. Both states rapidly converge to zero abundance once the relaxation phase starts, leaving only B14 and B4 as dominant factors in the relaxation phase. Since no combined effect of B6 and B14 reduces the curvature in the fluorescence trace and the contribution of the B4 state to the fluorescence signal is low, the "wobbliness" of the fluorescence trace is more pronounced. However, the total fluorescence signal might be generally lower compared to a scenario with low first and high second electron transfer rates, because the closed B6 state does not contribute anymore to the fluorescence signal. If both transfer rates are high, the abundance of B14 drastically increases, leading to a relaxation phase with a considerable curvature.

7.3.5 Connections between non-photochemical quenching and LIFT fluorescence traces in light conditions

In a natural environment, plants are exposed to changing light conditions. Extreme light intensity changes, such as in the canopy of, e.g., poplar trees (Way and Pearcy, 2012), or prolonged high illumination in open fields and clearings are not rare. Plants, thus, experience extreme fluctuations or oversupply in light energy.

Because the LIFT method does not require a dark-adaption phase before measuring, it is well suited to study the effects of light conditions on photosynthetic efficiency by comparing fluorescence traces. Comparing simulated fluorescence traces from *in silico* LIFT experiments using different

values for the parameter representing the pKa value for the protonation of PsbS, it becomes apparent that non-photochemical quenching is highly influential for the separation of LIFT fluorescence traces measured in different background light conditions (see Fig. 7.16). Using the standard parameters for non-photochemical quenching, which have been used successfully to replicate quenching analyses (Matuszyńska et al., 2016), the fluorescence traces were not separated, and two groups formed, consisting of high (300, 700 µmol m^{-2} s^{-1}) and low light background intensities (0, 30, 100 µmol m^{-2} s^{-1}).

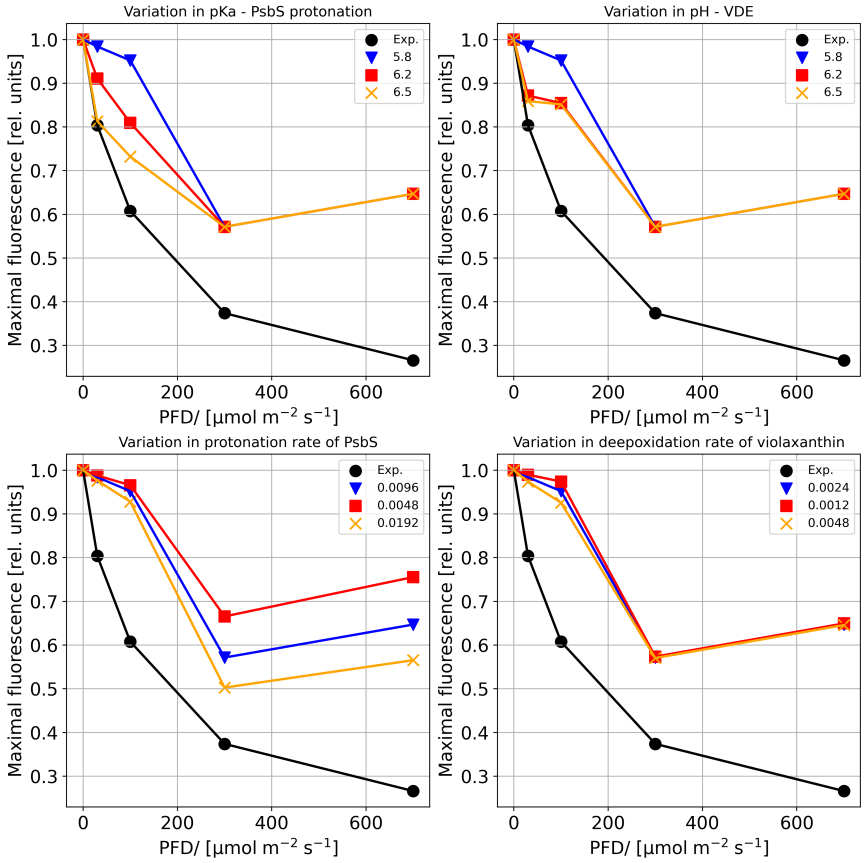

FIGURE 7.8: Changes in F_m of LIFT fluorescence traces after light acclimation in different background light intensities. Parameters that relate to non-photochemical quenching were systematically varied: kProt — protonation of PsbS, kDeepoxV — deepoxidation of violaxanthin, KphSatLHC — pKa of PsbS protonation, KphSatZ — half-saturation pH for violaxanthin de-epoxidase activity in the xanthophyll cycle. The *in silico* samples were light acclimated before the standard LIFT protocol started. Background lights were varied to be 0, 30, 100, 300, and 700 µmol m^{-2} s^{-1} . Experimental data was extracted from Keller et al., 2019.

When we increased the pKa value of PsbS protonation from 5.8 to 6.5 in our model, we could separate fluorescence traces in different background

light conditions that resemble experimental data (compare Keller et al., 2019). However, in contrast to experimental measurements, the fluorescence trace, which belongs to a background intensity of 700 µmol m^{-2} s^{-1} , is higher than for 300 µmol m^{-2} s^{-1} . Motivated by this we hypothesized that other parameters associated with non-photochemical quenching strongly influences the separation of LIFT experiments in background light conditions. We simulated multiple *in silico* LIFT experiments, varying parameters that relate to non-photochemical quenching, e.g., protonation of PsbS (kProt), deepoxidation of violaxanthin, and pKa values/ half-saturation pH for the violaxanthin de-epoxidase activity and for the protonation of PsbS. We compared the differences in maximal fluorescence (F_m) at the end of the induction phase.

As shown in Fig. 7.8, the standard parameters of our kinetic model (blue) lead to changes in F_m that do not resemble the experimentally measured data (black). Especially the last F_m value for light intensities around 700 µmol m^{-2} s^{-1} , is off, indicating that the quencher is already saturated in our model at values lower than 700 µmol m^{-2} s^{-1} . Changes in the protonation rate of PsbS, the deepoxidaion rate of violaxanthin, or the half-saturation pH for deepoxidase activity only lead to minor improvements. In contrast, an increase in the pKa value (pH value at which the PsbS protonation activation reaches half its maximum) of PsbS protonation results in a seemingly exponential decay of F_m with increasing light intensities (yellow line, the upper left panel in Fig. 7.8), before it saturates. This indicates that the pKa value of PsbS protonation might play an essential role in the differences we observe in LIFT fluorescence traces for samples acclimated to different background intensities.

7.4 Discussion and Outlook

We have constructed a mechanistic yet straightforward model of photosystem II and downstream processes to investigate fast repetition rate fluorescence measurements. The model includes intra-PSII processes like charge separation/ stabilization, electron transfer, and fluorescence emittance. Downstream processes in the PETC are represented as a lumped reaction. We further included a module for non-photochemical and an approximation of high-intensity quenching. Through the investigation of multiple processes, such as the association and dissociation of plastoquinone or the electron transfer between the Q_A-site and Q_B-site, by *in silico* analyses, we

could discern and elucidate effects determining the fluorescence trace of LIFT experiments.

Analyzing photosynthesis through fluorescence has become the preferred method for evaluating physiological properties quickly and easily. However, the interpretation of fluorescence signals can be complicated due to various factors in the PETC, such as non-photochemical quenching, influencing them. Moreover, our computational simulations reveal that different alterations in the rate of processes governing electron transfer or interactions with plastoquinone in and around PSII yield identical fluorescence signals in LIFT experiments. This observation indicates that explaining why we see certain characteristic phases in the output of spectroscopic measurements is challenging.

For instance, changes in the association of oxidized and dissociation of reduced plastoquinone results in a prolonged relaxation phase in the LIFT experiment, with the fluorescence yield being high compared to standard parameters (Fig. 7.6). Although we see the same effect in the LIFT fluorescence traces for both cases, different PSII states accumulate (B2 for lower oxidized plastoquinone attachment or B18 for lower reduced plastoquinone dissociation). According to our fluorescence yield model (Eq. 7.37), these closed PSII states contribute similarly to the final fluorescence signal (having identical quantum yields). That being said, whether B2 or B18 accumulates in the end phase of the LIFT experiment does not matter. The differences may only become apparent when simulating a prolonged LIFT experiment, eventually leading to the dark-adapted state (accumulation of B4 PSII state) since electrons starting in the B2 and B18 state have a different pathway to fulfill until they are transferred on plastoquinone (see supplementary Fig. 7.17).

The extent of the fluorescence signal ambiguity is also evident when investigating the underlying factors contributing to the curvature within the relaxation phase of LIFT experiments (refer to Fig. 7.7). This curvature arises from an intricate interplay of various closed and open PSII states, each transiently appearing (see Fig. supplementary 7.15). Our simulations reveal that the curvature primarily stems from the dynamic presence or absence of the PSII states B6 and B14. Nevertheless, while we have pinpointed the most influential PSII states in our model, more is needed to provide insight into how the combined abundances of these states give rise to the observed curvature in the experimental outcomes of a LIFT experiment. Changes in the electron transport rate could lead to variations in the combination of PSII states. However, due to the equal quantum yields of all closed and open PSII states,

distinguishing between, for instance, a mix of 0.7% B6 and 0.3¸% B14 and the reverse at any specific point in the fluorescence signal is challenging. It might be tempting to speculate that the positioning of the "wobble" could indicate the dominant states during different segments of the relaxation phase. However, initial attempts in this direction, as shown in the supplementary (compare supplementary Fig. 7.15 and Fig. 7.18), indicate otherwise.

An advantage of the LIFT technique is its applicability under background light conditions. However, the light-induced presence or absence of non-photochemical quenching influences the LIFT fluorescence traces (Keller et al., 2019). Initially, our model could not distinguish between LIFT experiment outputs in different background light intensities. The differences only became visible when we increased the half-saturation pH value to activate PsbS protonation in the NPQ module (Fig. 7.16). This necessary change in the half-saturation pH value does not drastically influence other simulated fluorescence spectroscopic measurements, such as a quencher analysis using PAM, see Fig. 7.19. It is reasonable to assume that a change in the half-saturation pH can increase the differences between the LIFT fluorescence traces. If the value is too small, differences in photon flux densities will only have a minor influence on the protonation rate of PsbS (due to changes in the luminal pH). Increasing the value leads to more drastic changes in the activation of the protonation rate in the low-light / high-luminal pH regime (supplementary Fig. 7.20). Changes in the activation of the protonation rate result in changes in the PsbS concentration at a specific light intensity and, thus, NPQ differences.

We can foresee several improvements to our model. Antenna size is assumed to influence the induction phase of LIFT experiments. As a simplification, we assumed that all the light falling on the photosynthetic tissue is used in PSII, effectively disregarding the effects of smaller or larger antennae. To improve the model fit in the future to experimental data in the induction phase, including antennae size according to Ebenhöh et al., 2014 might be a necessary step. We also did not consider the effects on the light intensity that result from the spatial distance between the LIFT device and photosynthetic tissue, which might be necessary for an improved replication of LIFT experiments. These changes are due to the spread of the excitation light beam coming from the LIFT device. Because we believe that the terrestrial-LIFT system is built to focus the excitation beam at a particular position on the photosynthetic tissue while reducing the spread of the beam as much as possible, we

assumed no loss of light intensity as simplification. Both previously mentioned effects could be easily implemented using factors that tune the "physiologically" active part of the light coming from a light source. However, preliminary experiments testing different flashlet light intensities allowed us to reduce the intensity to one-fifth of the highest intensity without considerable effects when observing a normalized fluorescence trace (supplementary Fig. 7.21).

The size of our representation of PSII is drastically reduced compared to other model implementations. This is due to the neglect of the OEC S-state cycle and of the reduction of the P680 (D) after an electron was transferred to the Q_A-site. Both could influence the mix of states that are present during the various phases of LIFT fluorescence traces. We checked if our model output drastically deviates from a model, including the S-state influence or the reduction of D (see supplementary text and supplementary figure 7.22). We could not see essential differences, and all previous interpretations of the simulated data seem to be still valid. However, future model version should explore what happens when the processes of charge separation, charge stabilization, reduction of $P680^+$ by Y_z, and reduction of $Y_z{}^+$ by electrons from the OEC are explicitly implemented in the model.

To sum up, we constructed a mathematical model of PSII and downstream processes to elucidate the cause of the fluorescence signal obtained by LIFT experiments. We found that the abundance of certain PSII states can explain the different phases of the fluorescence signal. According to our simulations, the states B4, B6, B14, and B18 are the primary agents causing the form of the fluorescence signal. However, investigating the fluorescence signal made it apparent that different combinations of these PSII states lead to similar changes in the fluorescence signal, making it challenging to interpret the LIFT experiment in terms of PSII states. With our model, we made an initial step to build a mechanistic framework that, combined with experimental data, can help to increase our understanding of the intra-PSII processes during LIFT experiments. With the model, hypotheses can be generated about the dominant PSII state in the phases of LIFT experiments. Thus, after its refinement, we can envisage that the model may help to understand and interpret LIFT-derived fluorescence traces, especially when different background light conditions are used.

7.5 Concluding remarks

In this chapter, we elucidated the rapid processes in PSII during a FRR protocol. Regarding the overall outcome, one might ask why we should bother to look into these rapid processes when we are only interested in the outcome of photosynthesis in terms of ATP and NADPH, for which we can assume the PSII processes are in a steady state. The reasons for the interest in PSII states is twofold: 1) It has become common knowledge that plants and other photosynthetic organisms live in constantly changing environments with extremely fast-changing light conditions. The assumption that the intra-PSII processes are, thus, constantly in a steady state can be challenged, making its mathematical treatments as a fast part of a fast-slow dynamic system (as we did in the other chapters) questionable. Changes in the abundance of PSII states, as modeled here, could turn out to be important. 2) The fluorescence changes mediated by changes in the abundance of different PSII states provide valuable information with which plant physiologists can monitor what processes in PSII are affected due to sickness or mutation. Effects of different processes can be determined by looking at changes in various fluorescence phases, e.g., OJIPSMT or induction/ relaxation, defined by their chronological order. Having a clear understanding of what PSII states are most abundant at which phase can help derive new hypotheses about how to treat certain diseases that change the PSII efficiency.

7.6 Supplementary figures

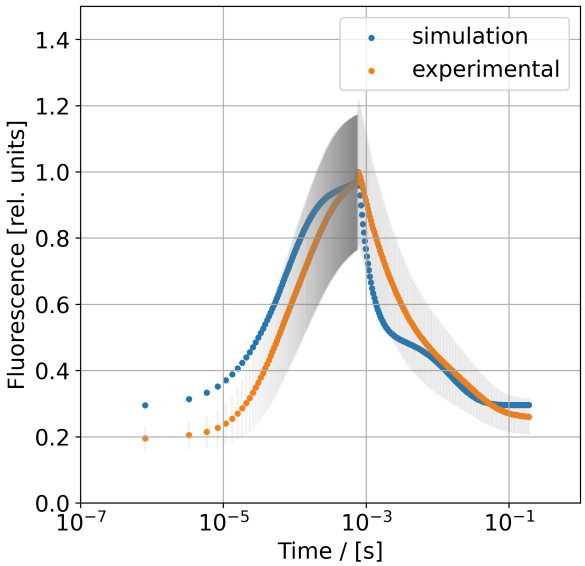

FIGURE 7.9: A comparison between experimental and simulated LIFT fluorescence traces. Errors bars (n=3) belong to experimental measurements. The data was recorded on *A.thaliana* plants predawn. The data was provided by Ana Carolina dos Santos Sá. Please note that the relaxation phase "wobble" seen in the simulated LIFT fluorescence trace is more pronounced in other experimental measurements; see, for example, Keller et al., 2019. Also note that the model parameters were not fitted to match the experimental data but were extracted from previous publications about PSII.

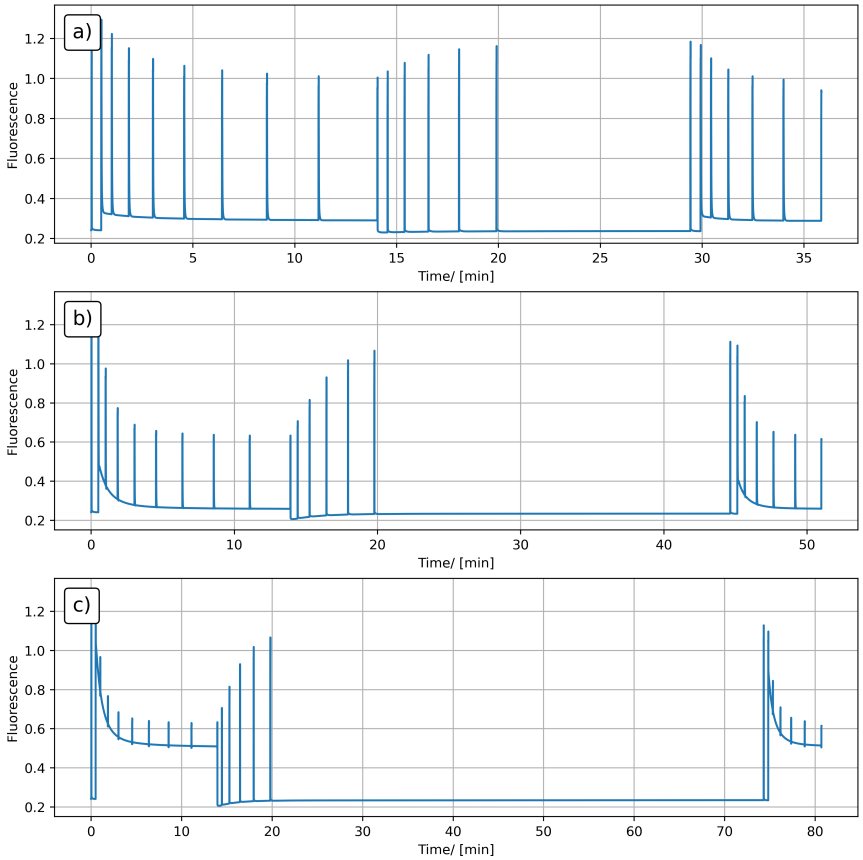

FIGURE 7.10: *In silico* replications of quenching analyses shown in Matuszyńska et al., 2016 using the pulse amplitude modulation technique. The differences between the analysis shown in Matuszyńska et al., 2016 and here are due to the constant activation of the ATPsynthase that is assumed in the PETC model (LIFT) of this study.

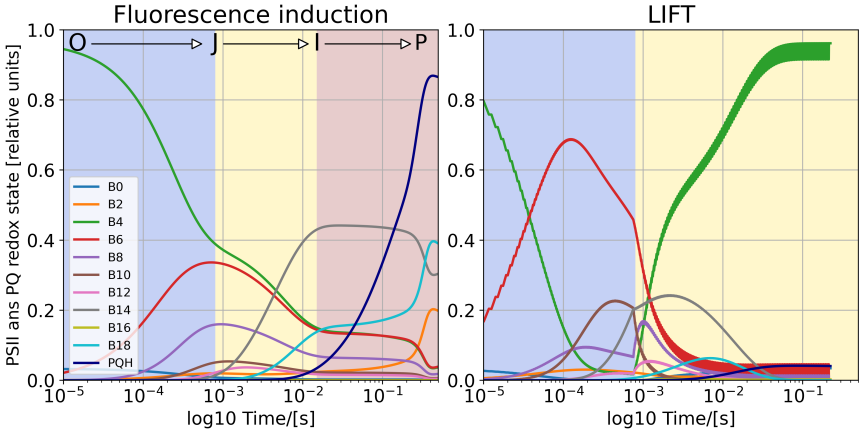

FIGURE 7.11: Changes in the PSII states during a standard FI experiment (left, 3000 µmol m^{-2} s^{-1}) and LIFT experiment (right, *in silico* protocol).

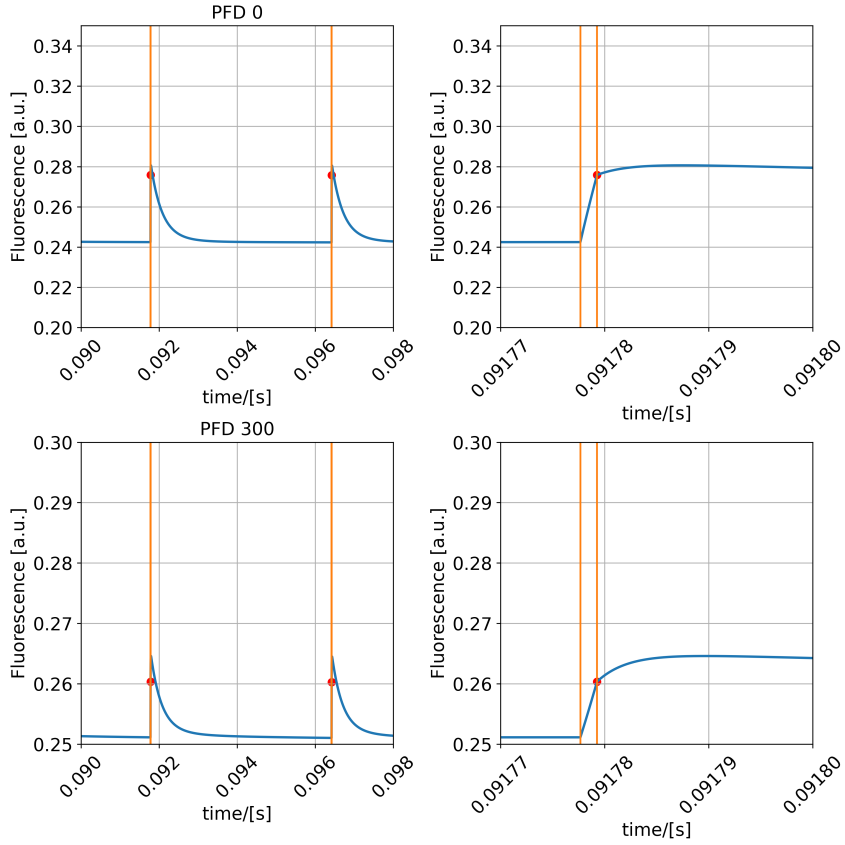

FIGURE 7.12: Fluorescence yield changes during the application of subsaturating flashlets in the relaxation phase of LIFT experiments. The right panel is a zoom into the first peak of the fluorescence yield. Upper row background light 0 µmol m^{-2} s^{-1}. Lower row background light 300 µmol m^{-2} s^{-1}.

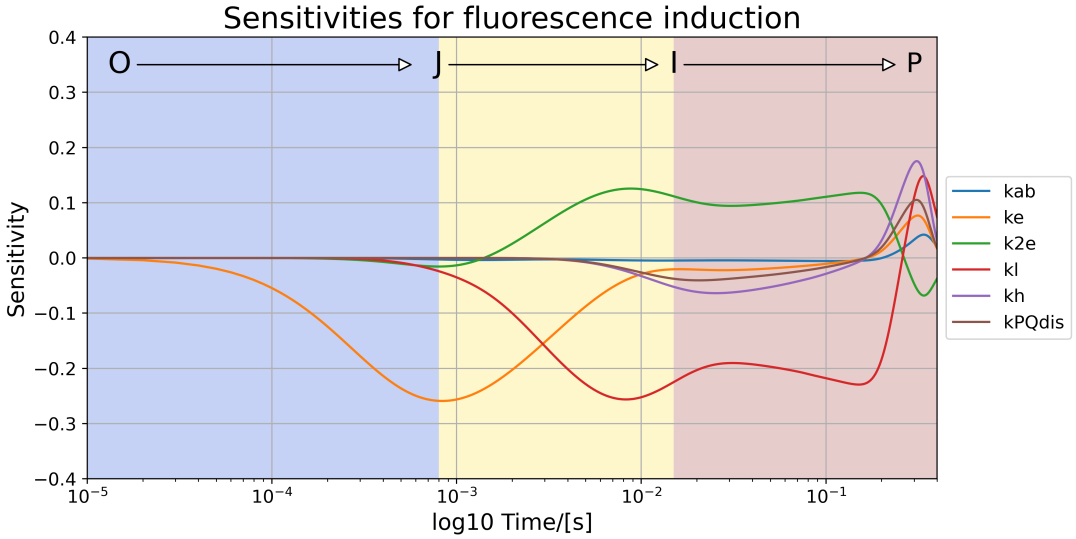

FIGURE 7.13: Local sensitivity analysis for FI fluorescence traces. The following processes were included in the analysis: association of oxidized plastoquinone (k_{ab}), first and second electron transport between Q_A-site and Q_B-site (k_e, k_{2e}), charge loss (k_l), protonation of double-charged plastoquinone in the Q_B-site, dissociation of reduced plastoquinone (k_{PQdis}).

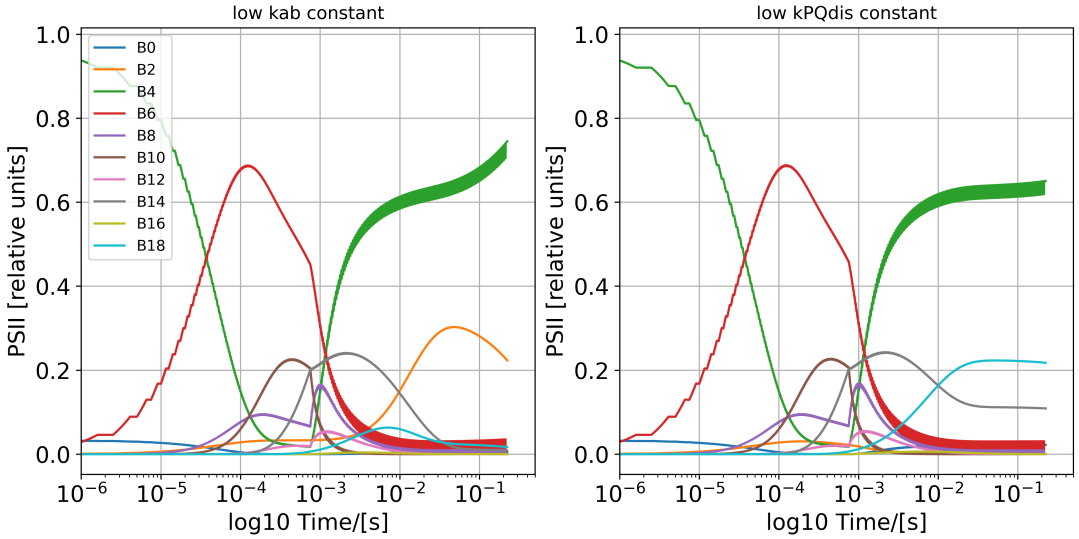

FIGURE 7.14: Changes in the PSII states during a LIFT experiment using the standard *in silico* LIFT protocol. Association rate of oxidized plastoquinone was set to k_{ab}=0.125 molChl$(\text{mmol} \cdot \text{s})^{-1}$ Dissociation rate of reduced plastoquinone was set to k_{PQdis} = 0.250 s^{-1} (left pannel).

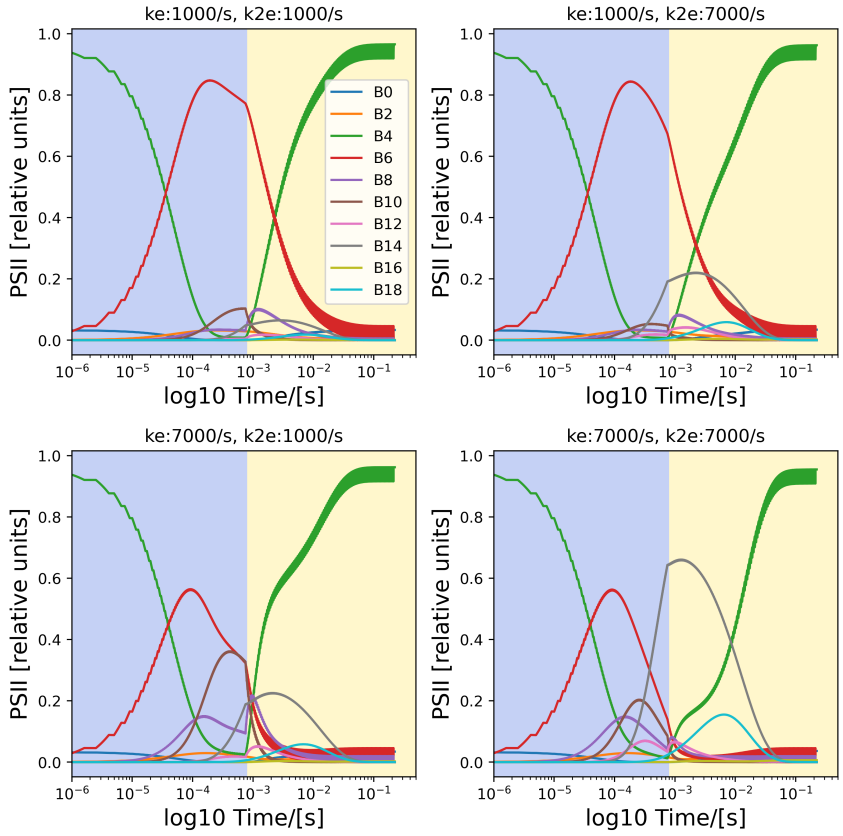

FIGURE 7.15: Changes in PSII states during a LIFT experiment using the standarad protocol. Four different model version with various rate constants for the first and second electron transport in PSII were simulated.

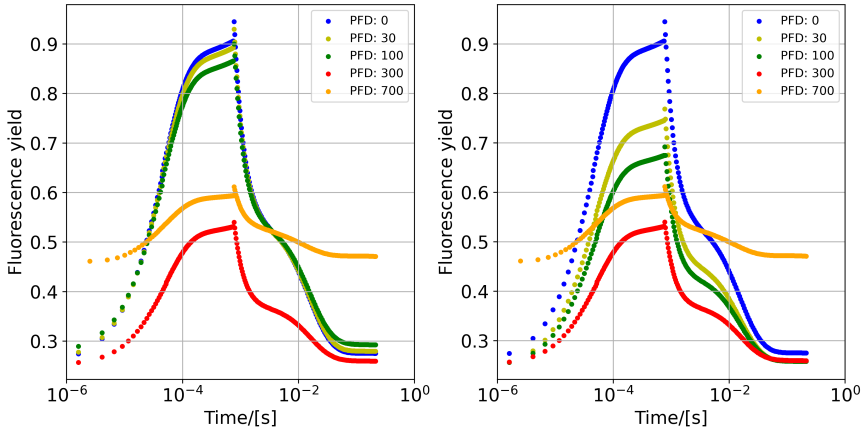

FIGURE 7.16: Simulated fluorescence traces from experiments using the LIFT method using the standard protocol. The *in silico* samples were light acclimated before the LIFT protocol started. Background light were varied to be 0, 30, 100, 300, and 700 µmol m^{-2} s^{-1} . Left half-saturation pH for PsbS activation set to 5.8 (standard, according to (Matuszyńska et al., 2016)), right set to 6.5.

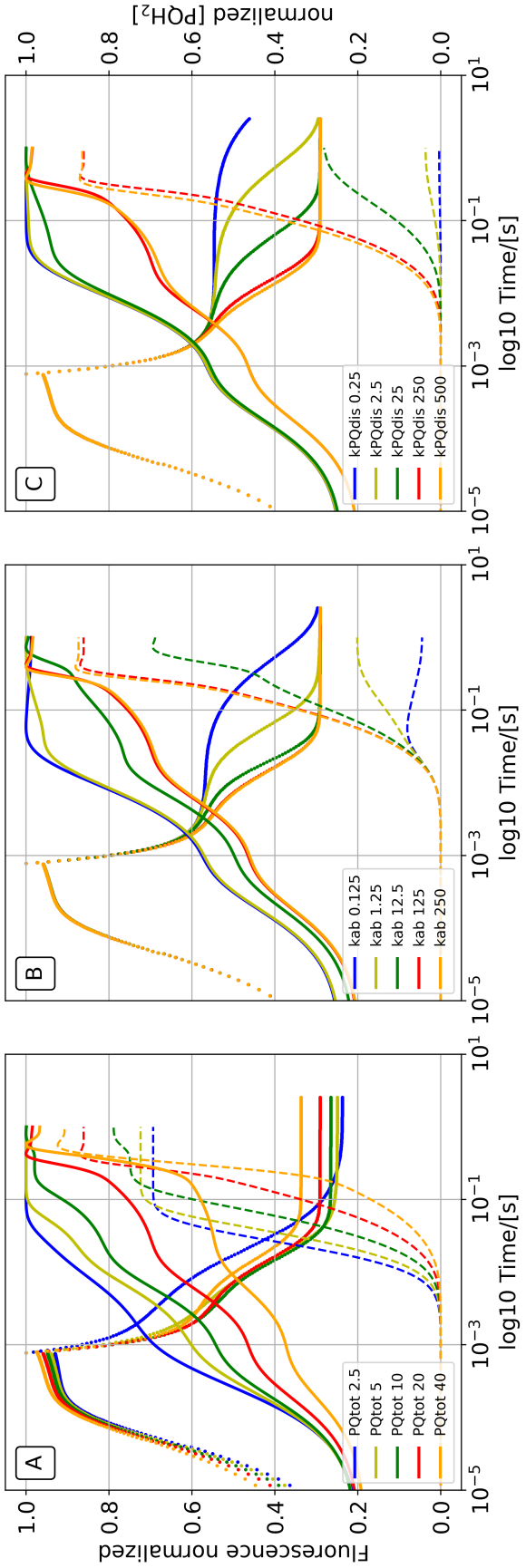

FIGURE 7.17: Effect of total plastoquinone pool size (PQpool) and the rate of association and dissociation for oxidized plastoquinone (kab) and reduced plastoquinone (kPQdis) to photosystem II, respectively, on fluorescence traces from LIFT and FI experiments (left y-axis) and redox state of the plastoquinone pool (right y-axis). *In silico* experiments were conducted with the same protocols as described in Fig. 7.4. Relaxation phase was set to 178 instead of 128 flashlets.

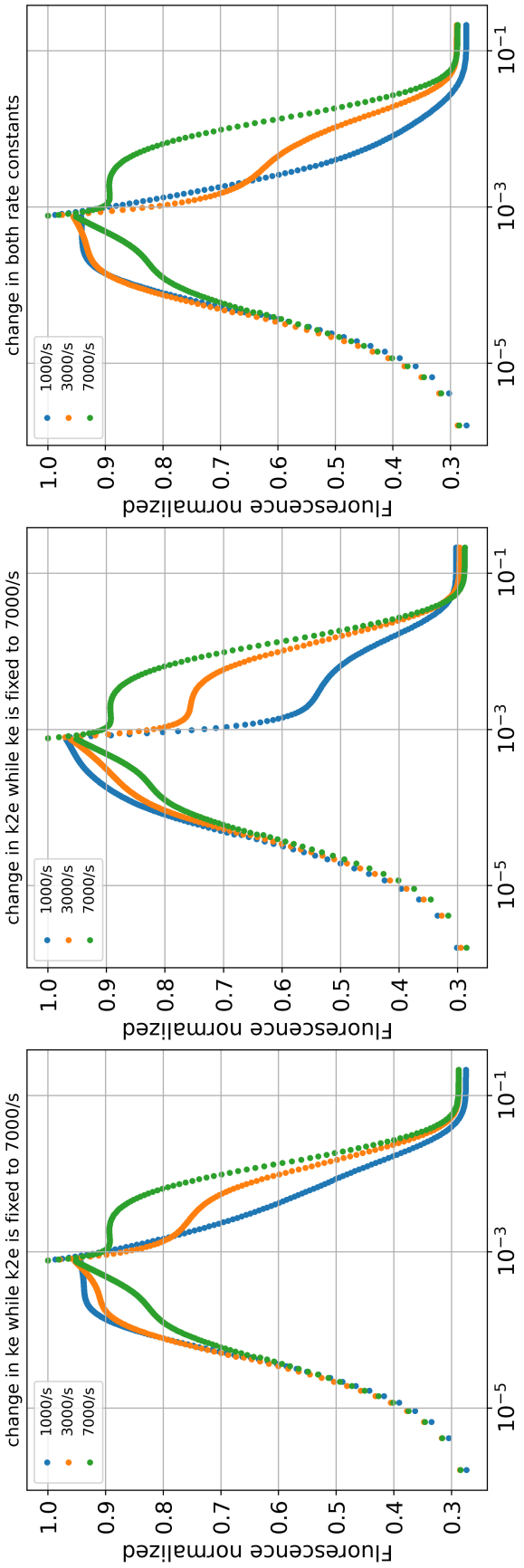

FIGURE 7.18: LIFT fluorescence traces using the standard *in silico* protocol. The rate constants of the first and second electron have been varied (compare also Fig. 7.7.

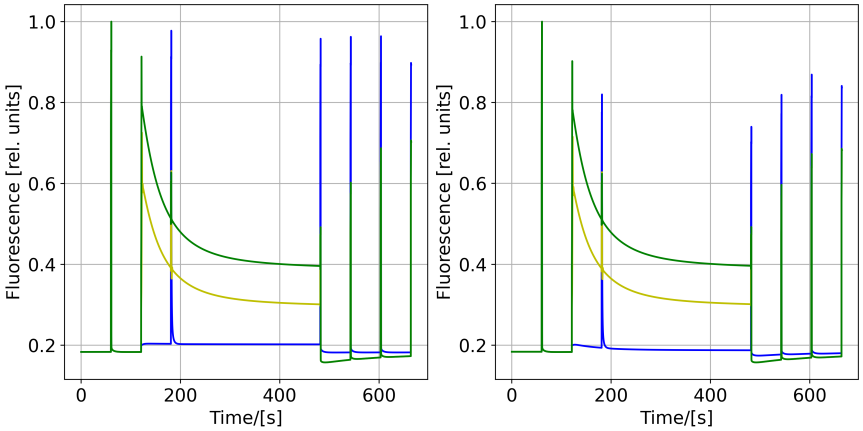

FIGURE 7.19: Quenching induction and relaxation analysis using the PAM technique foe 100, 300, and 900µmol m^{-2} s^{-1} (blue, yellow, green). Left half-saturation pH for PsbS activation set to 5.8 (standard, according to (Matuszyńska et al., 2016)), right set to 6.5.

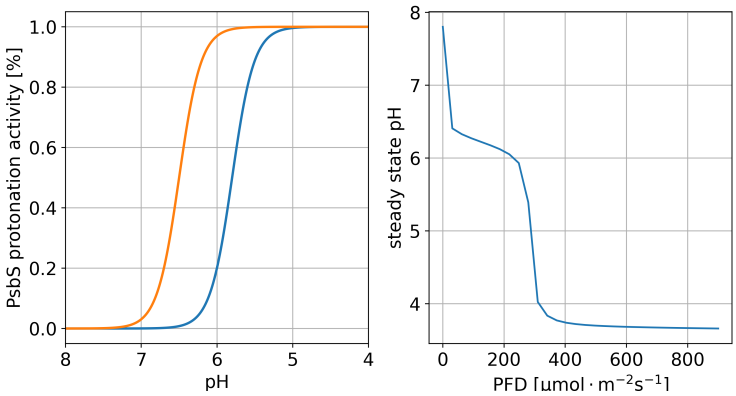

FIGURE 7.20: Left panel: differences in the activity of the PsbS protonation as function of pH for two different values of KpHSatLHC (blue, 5.8; orange, 6.5). Right panel: steady state pH as function of different light intensities.

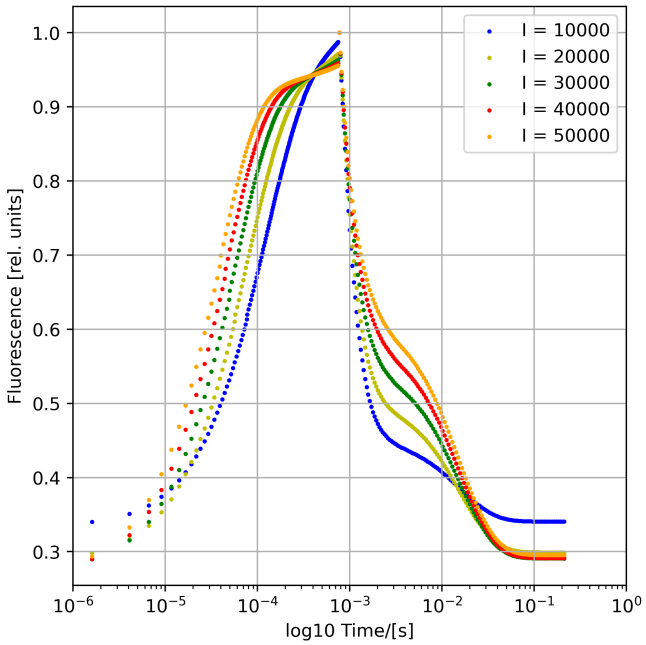

FIGURE 7.21: Effect of different flashlet light intensities in LIFT experiments using the *in silico* standard protocol. Excitation power give as µmol m^{-2} s^{-1}.

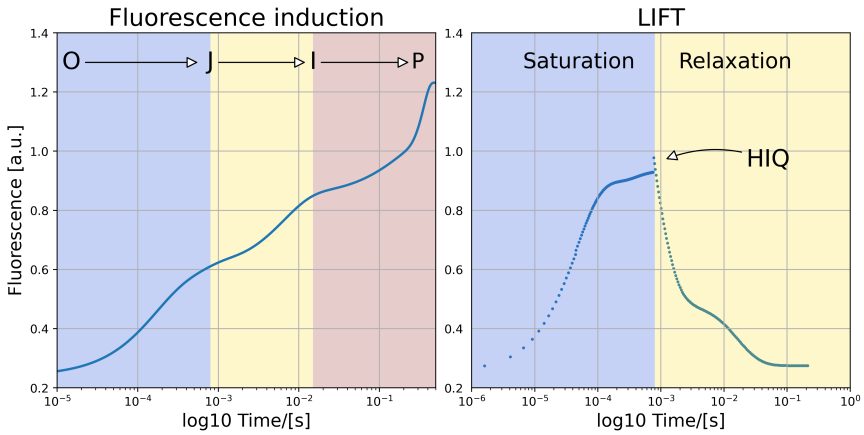

FIGURE 7.22: Simulated fluorescence traces of a fluorescence induction (left panel) and a LIFT (right panel) experiment with the expanded model, including the influence of the S-states. For the fluorescence induction experiment, the light intensity was 3000 µmol m^{-2} s^{-1}. The LIFT experiment followed the standard protocol for *in silico* LIFT experiments (see methods). The light intensities of the 1.6 µs flashlets were 40000 µmol m^{-2} s^{-1}. Both simulated fluorescence curves exhibit well-known dynamics, such as the OJIP phases of fluorescence induction and LIFT experiments' saturation/ relaxation phases.

TABLE 7.1: Parameters used throughout the *in silico* analyses

parameter	value	reference/comment
Pool sizes		
PQ^{tot}	20 mmol $(\text{mol Chl})^{-1}$	total plastoquinone pool, after Matuszyńska et al., 2016
ATP^{tot}	50 mmol $(\text{mol Chl})^{-1}$	total adenosine phosphate pool, after Matuszyńska et al., 2016
$PSII^{tot}$	2.5 mmol $(\text{mol Chl})^{-1}$	PSII reaction centers, after Matuszyńska et al., 2016
$PsbS^{tot}$	1	normalized PsbS pool, after Matuszyńska et al., 2016
X^{tot}	1	normalized total pool of xanthophylls, after Matuszyńska et al., 2016
Rate constants		
k_{ab}	125 mmol^{-1} (mol Chl) s^{-1}	association of PQ at B-site, modified from Lazár et al., 1997
k_{ba}	75 s^{-1}	dissociation of PQ from B-site, modified from Lazár et al., 1997
k_{e}	3500 s^{-1}	first electron transfer in PSII, after Lazár et al., 1997
k_{em}	175 s^{-1}	reverse first electron transfer in PSII, after Lazár et al., 1997
k_{2e}	1750 s^{-1}	second electron transfer in PSII, after Lazár et al., 1997
k_{2em}	35 s^{-1}	revers second electron transfer in PSII, after Lazár et al., 1997
k_{l}	5000 s^{-1}	charge loss, after Lazár et al., 1997
k_{h}	100 s^{-1}	protonation of Q_B^{-2}modified from Lazár et al., 1997
k_{hm}	50 s^{-1}	deprotonation of Q_B^{-2}modified from Lazár et al., 1997
$k_{Cyt_{b6f}}$	0.0018 mmol^{-2} $(\text{mol Chl})^2$ s^{-1}	
$k_{ActATPase}$	0.01 s^{-1}	activation of ATP synthase Matuszyńska et al., 2016
$k_{DeactATPase}$	0.002 s^{-1}	deactivation of ATP synthase Matuszyńska et al., 2016
$k_{ATPsynthase}$	10 s^{-1}	estimated but based on Ebenhöh et al., 2014

Table 7.1 – *Continued from previous page*

parameter	value	reference/comment
$k_{\mathrm{ATPconsumption}}$	$2.2\ \mathrm{s}^{-1}$	estimated but based on Ebenhöh et al., 2014
k_{PQas}	$25\ \mathrm{mmol}^{-1}\ (\mathrm{mol\,Chl})\ \mathrm{s}^{-1}$	association of PQH_2 at B-site
k_{PQdis}	$250\ \mathrm{s}^{-1}$	dissociation of PQH_2 at B-site Ebenhöh et al., 2014
k_{H}	$5 \cdot 10^{9}\ \mathrm{s}^{-1}$	rate of non-radiative decay Matuszyńska et al., 2016
k_{F}	$6.25 \cdot 10^{8}\ \mathrm{s}^{-1}$	rate of fluorescence Matuszyńska et al., 2016
k_{P}	$5 \cdot 10^{9}\ \mathrm{s}^{-1}$	rate of photochemistry Matuszyńska et al., 2016
k_{CarQ}	$3 \cdot 10^{9}\ \mathrm{s}^{-1}$	rate of quenching by carotenoid, estimated
k_{PTOX}	$0.01\ \mathrm{mmol}^{-1}\ (\mathrm{mol\,Chl})\ \mathrm{s}^{-1}$	after Ebenhöh et al., 2014
k_{Leak}	$100\ \mathrm{s}^{-1}$	after Matuszyńska et al., 2016
k_{Deepox}	$0.0024\ \mathrm{s}^{-1}$	rate of de-epoxidation, after Matuszyńska et al., 2016
k_{Epox}	$0.00024\ \mathrm{s}^{-1}$	rate of epoxidation, after Matuszyńska et al., 2016
k_{Deprot}	$0.0096\ \mathrm{s}^{-1}$	rate of PsbS de-protonation, after Matuszyńska et al., 2016
k_{Prot}	$0.0096\ \mathrm{s}^{-1}$	rate of PsbS protonation, after Matuszyńska et al., 2016
k_{CarQp}	$3 \cdot 10^{4}\ \mathrm{s}^{-1}$	estimated
k_{CarQm}	$3.47 \cdot 10^{5}\ \mathrm{s}^{-1}$	based on half-decay time of 2µs for $^{3}Car^{*}$ Schreiber, Klughammer, and Schansker, 2019
k_{HPQ}	$2 \cdot 10^{7}\ \mathrm{s}^{-1}$	plastoquinone quenching. Ad-hoc estimation
k_{S01}	$20000\ \mathrm{s}^{-1}$	$S_0 \longrightarrow S_1\ Q_AQ_BH_2 \longrightarrow Q_A^{-}Q_BH_2$, after Lazár and Schansker, 2009
k_{S12}	$20000\ \mathrm{s}^{-1}$	$S_1 \longrightarrow S_2\ Q_AQ_B \longrightarrow Q_A^{-}Q_B$, after Lazár and Schansker, 2009
k_{S23}	$3330\ \mathrm{s}^{-1}$	$S_2 \longrightarrow S_3\ Q_AQ_B^{-} \longrightarrow Q_A^{-}Q_B^{-}$, after Lazár and Schansker, 2009
k_{S30}	$1000\ \mathrm{s}^{-1}$	$S_3 \longrightarrow S_0\ Q_AQ_B^{2-} \longrightarrow Q_A^{-}Q_B^{2-}$ after Lazár and Schansker, 2009
k_{y}	$7 \cdot 10^{6}\ \mathrm{s}^{-1}$	after Lazár and Schansker, 2009
k_{ym}	$1 \cdot 10^{6}\ \mathrm{s}^{-1}$	after Lazár and Schansker, 2009

Table 7.1 – *Continued from previous page*

parameter	value	reference/comment
Michaelis constants		
K_{pHsatz}	5.8	half-saturation pH for deepoxidase activity, after Matuszyńska et al., 2016
K_{pHsatLHC}	5.8	pKa of PsbS activation, after Matuszyńska et al., 2016
$K_{\text{CarActive}}$	15000 µmol m^{-2} s^{-1}	half-saturation light intensity for which the carotenoid quencher becomes active
K_{Zsat}	0.12	after Matuszyńska et al., 2016
External concentrations		
O_2^{ex}	8 mmol $(\text{mol Chl})^{-1}$	external oxygen pool
P_i	0.01	internal pool of phosphates
Other constants		
F	96.485 kJ	Farraday constant
R	$8.3 \cdot 10^{-3}$ kJ K^{-1} mol^{-1}	universal gas constant
T	298 K	temperature
γ_0	0.1	base quenching Matuszyńska et al., 2016
γ_1	0.25	fast quenching due to protonation Matuszyńska et al., 2016
γ_2	0.6	fastest possible quenching Matuszyńska et al., 2016
γ_3	0.15	slow quenching by Zx Matuszyńska et al., 2016
n_{HL}	3	Hill-coefficient for activity of deprotonation, after Matuszyńska et al., 2016
n_{HX}	5	Hill-coefficient for deepoxidase activity, after Matuszyńska et al., 2016
$\Delta G_0 ATP$	30.6 kJ/mol/RT	
b_H	100	protonation buffering constant Zaks et al., 2012
Standard potentials		

Table 7.1 – *Continued from previous page*

parameter	value	reference/comment
$E_0(Q_A/Q_A^-)$	-0.140 V	Allakhverdiev et al., 2011, after Ebenhöh et al., 2014
$E_0(PQ/PQH_2)$	0.354 V	Okayama, 1976, after Ebenhöh et al., 2014
$E_m(Q_B/Q_B^-)$	0.093 V	Kato, Nagao, and Noguchi, 2016
$E_0(PC/PC^-)$	0.380 V	Suzuki, Sakurai, and Nakajima, 1987, after Ebenhöh et al., 2014

7.6.1 Equilibrium constants

For the attachment of oxidized plastoquinone, the release of reduced plastoquinone, the protonation of double-charged plastoquinone at the Q_B, and the second electron transfer, we estimated equilibrium constants based on the parameters given in the parameter table, according to

$$K_{eq} = \frac{k_f}{k_r}. \tag{7.51}$$

This rough approximation must be refined as the model gets more elaborated. The equilibrium constant for the first electron transfer was calculated according to Ebenhöh et al., 2014

7.6.2 Extension of model

Modeling photosystem II is challenging due to its many possible PSII states. A state of photosystem II is determined by the reduction/excitation of its components S_i-Y_z-P680-Pheo-Q_A-Q_B. Here "S" denotes the states of the OEC, Y_z the redox state of the tyrosin transferring electrons from the OEC to P680, which previously lost an electron to Pheophytin (Pheo), Q_A and Q_B symbolizes the plastoquinone in the A-site and the B-site, respectively. Our standard model assumes that charge separation, charge stabilization, and the reduction of the oxidized Donor site (P680 + Pheo, D) is rapid. However, this rapid reduction of the donor site might be an oversimplification because the transfer of electrons by the OEC via Y_z might be relatively slow compared to the other processes in PSII. We developed an additional model version to check if including this slow delivery of electrons to the donor site might influence our interpretations of the simulated LIFT fluorescence traces. In this

version, each row in the scheme Fig. 7.2 is extended by two additional states, for instance,

$$Y_zDQ_AQ_B \longleftrightarrow Y_zD^*Q_AQ_B \longrightarrow Y_zD^+Q_A^-Q_B \underset{k_{ym}}{\overset{k_y}{\longleftrightarrow}} Y_z^+DQ_A^-Q_B \xrightarrow{k_{Sij}} Y_zDQ_A^-Q_B$$

here k_{Sij} denotes the rate constant of the reduction of Y_z^+ by the OEC and k_y/k_{ym} the rate constants for the reversible reduction of the donor site by Y_z.

Chapter 8

Conclusion

In this thesis, I aimed to analyze photosynthesis on various temporal scales. Understanding the workings of photosynthesis in different timeframes is crucial for advancing strategies of crop enhancement or plant-based biofuel sources. However, conducting a comprehensive analysis of photosynthesis on all its time scales poses experimental challenges due to the diverse instrumentation requirements. In such cases, mathematical models are a valuable tool. My research focused on several aspects of photosynthetic processes across previous chapters, employing kinetic modeling to span the spectrum from long-term steady-state phenomena to rapid electron transfer in PSII.

By constructing mathematical models, scientists attempt to distill the complexity of a natural phenomenon to its fundamental components. Thus, model building allows us to formulate hypotheses about the minimal requirements to replicate experimental observations. Additionally, mathematical modeling is an invaluable resource when experimental approaches reach limitations. Particularly intriguing is when the model simulations yield results that diverge from experimental measurements, creating an exciting tension field in which modelers strive to devise new hypotheses to bridge the gaps in the model. This often challenging and tension-filled process can lead to a profound understanding of natural phenomena. I followed this way of modeling in chapter 5, where we iteratively refined our model of photoinhibition and deciphered the differences between active and inactive PSII during high light-induced stress. I showed that according to our calculation, the heat dissipation between inactive and active PSII should differ so that the maximal and minimal fluorescence signals fit the experimental measurement. Also, energy transfer might be necessary. These findings contribute to understanding how photodamage unfolds in high light conditions and what molecular mechanisms try to prevent the extent of photoinhibition. The theoretical results fit well in the debate on whether inactive PSII can have a photoprotective function and serve as a new impetus to the photoprotection

discussion. The devised model can also serve as a platform for analyzing quenching phenomena during high-light treatments.

There are instances where biological phenomena prove too complex to comprehend by experiments alone. A prime example is the rapid electron transport in photosystem II using fluorescence spectroscopy. Photosystem II comprises several components that can be excited, reduced, or oxidized, resulting in a combinatorial explosion of the actual PSII states responsible for different phases of fluorescence traces. While a simple mental model aids in interpreting measured fluorescence traces, a deeper understanding of the present states necessitates a more sophisticated mathematical treatment. This becomes especially evident when employing rapid, short light pulses to record fluorescence traces, where additional measurements to identify the predominant PSII states become challenging. In chapter 7, I endeavored to construct a mathematical PSII model combined with non-photochemical quenching to simulate the FRR technique LIFT. By simulations, I could pinpoint various PSII states that might be pivotal in LIFT fluorescence traces' induction and relaxation phase. Knowing these states is essential for devising new hypotheses about how new inhibitors and physiological processes, such as, e.g. temperature or immune response, change the fluorescence signals. The model could serve as a framework that enables researchers to interpret their experimental data in more detail and thus gain a deeper understanding of natural phenomena.

Another area where modeling proves beneficial is understanding the long-term steady-state behavior and control of photosynthesis. Analyzing control, as defined in MCA, and maintaining a biological system in an actual steady state poses experimental challenges, whereas achieving this *in silico* is relatively straightforward. I could, therefore, use mathematical modeling to identify shifts in the control, as defined by MCA, exerted by parts of the PETC and CBB cycle on carbon fixation (Chapter 4). These shifts might be important for designing experiments to improve crop yield. It is necessary to characterize in which control state (PETC- or CBB-dominant) the photosynthetic organism is under natural conditions to enhance carbon sequestration. For instance, modifying RuBisCO and SBPase in a natural environment in which the control relies on the PETC would result only in a minutely higher output of the photosynthetic organism. Additionally, when extrapolating the findings in chapter 4, it might be possible that the control varies along a plant stand in a crop field or vertical dimension of canopies, depending on

the height of the leaves. In the future, the model could serve as a tool to investigate the control defined by MCA on carbon sequestration in an *in silico* plant stand or canopies in which light conditions can vary.

Every scientific method has its limitations. A model is the mathematical encoding of the modeler's knowledge. Consequently, vital components of the natural phenomenon may be inadvertently overlooked and omitted in a mathematical description due to the inherent boundaries of the modeler's understanding. To mitigate this potential gap in comprehension, good communication with experimental working scientists is paramount.

However, in contrast to physical sciences, life sciences only recently (within the past approx. 40 years in comparison to several hundred years) recognized the potential for a fruitful collaboration between experiment and theory. As a result, separate theoretical and experimental communities developed in various fields of biology. Each community has its own language while discussing the same things, leading to miscommunication and the so-called experiment-theory gap. In chapter 6, as I investigated non-photochemical quenching (qE part), a moderately fast process of photosynthesis, I found it hard to reproduce experimental results *in silico* because the simulation required other or additional information than what was provided in publications. This serves as a prime example of the theory-experiment gap. By modeling, I showed what consequences this gap has on the *in silico* reproduction of quencher induction-relaxation experiments using PAM by varying technical parameters. My intention with this chapter is not to criticize but rather to stimulate improvements in communication within photosynthesis research. It shows which parameters are more critical for *in silico* reproduction. It thus communicates to the experimental community which technical details they should emphasize when collaborating with theoreticians. On the other hand, the chapter sensitizes theoreticians to the information that must be considered when working with experimentalists to successfully perform *in silico* replications, as theoreticians may not be aware of the limitations of a technique to the same extent as experimentalists.

I covered most of the time scales on which photosynthetic processes are unfolding. Most of the models used in this thesis even combine multiple timeframes. This is especially evident when looking at PSII. Typically, the processes in PSII are assumed to be much faster than the actions in the rest of the PETC, allowing treating the PETC as a fast-slow system. Although a thorough mathematical treatment of this fact is out of the scope of this thesis, it would be interesting for a future project. Another instance in which

the applied models combined various temporal levels is the activation of the non-photochemical quenching that includes the long-term effect of zeaxanthin and the short-term impact of qE. By combining NPQ with the different representations of PSII, I could investigate its impact on the steady-state (quencher saturation in chapter 4), long-term (photoinhibition in chapter 5), moderate (quenching analysis depending on technical parameters in chapter 6), and very rapid (FRR in chapter 7) procedures in the PETC. For all these processes, I used different PETC models that vary in complexity. This approach is convenient as it allows us to focus on the essential parts of each investigated process. However, it would be interesting to see if one could combine all the previous descriptions of the PETC into one model. Here, caution must be taken, as when a model becomes too complex, such that it cannot be investigated anymore by simple simulations and mathematical analysis, one must ask whether the model is still useful.

To conclude, this thesis provides several models and analysis techniques to understand photosynthesis on many of its time scales. I used these models to answer intriguing questions about photosynthesis by simulations and computational analysis. The outcomes of the investigations serve as an impetus for further research and motivate to refine and modify the models according to future scientific questions.

Bibliography

Aalst, Marvin van, Oliver Ebenhöh, and Anna Matuszyńska (2021). "Constructing and analysing dynamic models with modelbase v1. 2.3: a software update". In: *BMC bioinformatics* 22.1, pp. 1–15. DOI: https://doi.org/10.1186/s12859-021-04122-7.

Aasen, Helge et al. (2019). "Sun-induced chlorophyll fluorescence II: review of passive measurement setups, protocols, and their application at the leaf to canopy level". In: *Remote Sensing* 11.8, p. 927. DOI: https://doi.org/10.3390/rs11080927.

Allakhverdiev, Suleyman I et al. (2011). "Redox potentials of primary electron acceptor quinone molecule (QA)- and conserved energetics of photosystem II in cyanobacteria with chlorophyll a and chlorophyll d". In: *Proceedings of the National Academy of Sciences* 108.19, pp. 8054–8058. DOI: https://doi.org/10.1073/pnas.1100173108.

Anderson, Jan M (2002). "Changing concepts about the distribution of Photosystems I and II between grana-appressed and stroma-exposed thylakoid membranes". In: *Photosynthesis research* 73, pp. 157–164. DOI: https://doi.org/10.1023/A:1020426525648.

Andersson, Christian, Claus Führer, and Johan Akesson (2015). "ScienceDirect Assimulo: A unified framework for ODE solvers". In: *Mathematics and Computers in Simulation* 116, pp. 26–43. DOI: https://doi.org/10.1016/j.matcom.2015.04.007.

Andersson, Inger (2008). "Catalysis and regulation in Rubisco". In: *Journal of experimental botany* 59.7, pp. 1555–1568. DOI: https://doi.org/10.1093/jxb/ern091.

Arnon, Daniel I, Mary Belle Allen, and F Robert Whatley (1954). "Photosynthesis by isolated chloroplasts". In: *Nature* 174, pp. 394–396. DOI: https://doi.org/10.1038/174394a0.

Aro, Eva-Mari, Reetta Kettunen, and Esa Tyystjärvi (1992). "ATP and light regulate D1 protein modification and degradation Role of D1*in photoinhibition". In: *FEBS letters* 297.1-2, pp. 29–33. DOI: https://doi.org/10.1016/0014-5793(92)80320-G.

Arrivault, Stephanie et al. (2009). "Use of reverse-phase liquid chromatography, linked to tandem mass spectrometry, to profile the Calvin cycle and other metabolic intermediates in Arabidopsis rosettes at different carbon dioxide concentrations". In: *The Plant Journal* 59.5, pp. 826–839. DOI: https://doi.org/10.1111/j.1365-313X.2009.03902.x.

Baker, Monya (2016). "1,500 scientists lift the lid on reproducibility". In: *Nature* 533.7604, pp. 452–454. DOI: https://doi.org/10.1038/533452a.

Baker, Neil R (2008). "Chlorophyll fluorescence: a probe of photosynthesis in vivo". In: *Annu. Rev. Plant Biol.* 59, pp. 89–113. DOI: https://doi.org/10.1146/annurev.arplant.59.032607.092759.

Bassham, James A, Andrew A Benson, and Melvin Calvin (1950). "The path of carbon in photosynthesis VIII. The role of malic acid". In.

Bassham, James Alan et al. (1954). "The path of carbon in photosynthesis. XXI. The cyclic regeneration of carbon dioxide acceptor1". In: *Journal of the American chemical society* 76.7, pp. 1760–1770.

Belyaeva, Natalya E et al. (2016). "Thylakoid membrane model of the Chl a fluorescence transient and P700 induction kinetics in plant leaves". In: *Photosynthesis research* 130, pp. 491–515. DOI: https://doi.org/10.1007/s11120-016-0289-z.

Bernhardt, Karen and Hans-Wilhelm Trissl (1999). "Theories for kinetics and yields of fluorescence and photochemistry: how, if at all, can different models of antenna organization be distinguished experimentally?" In: *Biochimica et Biophysica Acta (BBA)-Bioenergetics* 1409.3, pp. 125–142. DOI: https://doi.org/10.1016/S0005-2728(98)00149-2.

Black, Michael T, Trevor H Brearley, and Peter Horton (1986). "Heterogeneity in chloroplast photosystem II". In: *Photosynthesis research* 8, pp. 193–207. DOI: https://doi.org/10.1007/BF00037128.

Blankenship, Robert E (2021). *Molecular mechanisms of photosynthesis*. John Wiley & Sons.

Böhme, Herbert (1978). "Quantitative Determination of Ferredoxin, Ferredoxin-NADP+ Reductase and Plastocyanin in Spinach Chloroplasts". In: *European Journal of Biochemistry* 83.1, pp. 137–141. DOI: https://doi.org/10.1111/j.1432-1033.1978.tb12077.x.

Bouges-Bocquet, B (1973). "Electron transfer between the two photosystems in spinach chloroplasts". In: *Biochimica et Biophysica Acta (BBA)-Bioenergetics* 314.2, pp. 250–256. DOI: https://doi.org/10.1016/0005-2728(73)90140-0.

Boyer, Paul D (2000). "Catalytic site forms and controls in ATP synthase catalysis". In: *Biochimica et Biophysica Acta (BBA)-Bioenergetics* 1458.2-3, pp. 252–262. DOI: https://doi.org/10.1016/S0005-2728(00)00077-3.

Brazma, Alvis et al. (2001). "Minimum information about a microarray experiment (MIAME)–toward standards for microarray data". In: *Nature genetics* 29.4, pp. 365–371. DOI: https://doi.org/10.1038/ng1201-365.

Britton, George (1995). "Structure and properties of carotenoids in relation to function". In: *The FASEB Journal* 9.15, pp. 1551–1558. DOI: https://doi.org/10.1096/fasebj.9.15.8529834.

Butler, Warren L (1978). "Energy distribution in the photochemical apparatus of photosynthesis". In: *Annual Review of Plant Physiology* 29.1, pp. 345–378.

Butler, Warren L and Masao Kitajima (1975). "Fluorescence quenching in photosystem II of chloroplasts". In: *Biochimica et Biophysica Acta (BBA)-Bioenergetics* 376.1, pp. 116–125. DOI: https://doi.org/10.1016/0005-2728(75)90210-8.

Cammack, Richard et al. (1977). "Midpoint redox potentials of plant and algal ferredoxins". In: *Biochemical Journal* 168.2, pp. 205–209. DOI: https://doi.org/10.1042/bj1680205.

Cazzaniga, Stefano et al. (2013). "Interaction between avoidance of photon absorption, excess energy dissipation and zeaxanthin synthesis against photooxidative stress in Arabidopsis". In: *The plant journal* 76.4, pp. 568–579. DOI: https://doi.org/10.1111/tpj.12314.

Chotewutmontri, Prakitchai and Alice Barkan (2020). "Light-induced psbA translation in plants is triggered by photosystem II damage via an assembly-linked autoregulatory circuit". In: *Proceedings of the National Academy of Sciences* 117.35, pp. 21775–21784. DOI: https://doi.org/10.1073/pnas.2007833117.

Cleland, William W (1963). "The kinetics of enzyme-catalyzed reactions with two or more substrates or products: I. Nomenclature and rate equations". In: *Biochimica et Biophysica Acta (BBA)-Specialized Section on Enzymological Subjects* 67, pp. 104–137. DOI: https://doi.org/10.1016/0926-6569(63)90211-6.

Colón, Amy Marshall et al. (2010). "A kinetic model describes metabolic response to perturbations and distribution of flux control in the benzenoid network of Petunia hybrida". In: *The Plant Journal* 62.1, pp. 64–76. DOI: https://doi.org/10.1111/j.1365-313X.2010.04127.x.

Cushman, John C (2001). "Crassulacean acid metabolism. A plastic photosynthetic adaptation to arid environments". In: *Plant physiology* 127.4, pp. 1439–1448. DOI: https://doi.org/10.1104/pp.010818.

Demmig-Adams, Barbara and William W Adams III (1996). "The role of xanthophyll cycle carotenoids in the protection of photosynthesis". In: *Trends in Plant science* 1.1, pp. 21–26. DOI: https://doi.org/10.1016/S1360-1385(96)80019-7.

Dourado, Hugo and Martin J. Lercher (2020). "An analytical theory of balanced cellular growth". In: *Nature Communications* 11.1. DOI: https://doi.org/10.1038/s41467-020-14751-w.

Duysens, Louis NM, Jan Amesz, and BM Kamp (1961). "Two photochemical systems in photosynthesis". In: *Nature* 190, pp. 510–511. DOI: https://doi.org/10.1038/190510a0.

Ebenhöh, Oliver et al. (2011). "A minimal mathematical model of nonphotochemical quenching of chlorophyll fluorescence". In: *Biosystems* 103.2, pp. 196–204. DOI: https://doi.org/10.1016/j.biosystems.2010.10.011.

Ebenhöh, Oliver et al. (2014). "Short-term acclimation of the photosynthetic electron transfer chain to changing light: a mathematical model". In: *Philosophical Transactions of the Royal Society B: Biological Sciences* 369.1640, p. 20130223. DOI: https://doi.org/10.1098/rstb.2013.0223.

Emerson, Robert and William Arnold (1932a). "A separation of the reactions in photosynthesis by means of intermittent light". In: *The Journal of general physiology* 15.4, p. 391.

— (1932b). "The photochemical reaction in photosynthesis". In: *The Journal of general physiology* 16.2, pp. 191–205.

Emerson, Robert, Ruth Chalmers, and Carl Cederstrand (1957). "Some factors influencing the long-wave limit of photosynthesis". In: *Proceedings of the National Academy of Sciences* 43.1, pp. 133–143. DOI: https://doi.org/10.1073/pnas.43.1.133.

Erb, Tobias J and Jan Zarzycki (2016). "Biochemical and synthetic biology approaches to improve photosynthetic CO2-fixation". In: *Current opinion in chemical biology* 34, pp. 72–79. DOI: https://doi.org/10.1016/j.cbpa.2016.06.026.

Evans, Michael CW and P Heathcote (1980). "Effects of glycerol on the redox properties of the electron acceptor complex in spinach photosystem I particles". In: *Biochimica et Biophysica Acta (BBA)-Bioenergetics* 590.1, pp. 89–96. DOI: https://doi.org/10.1016/0005-2728(80)90148-6.

Farquhar, Graham D, Susanne von von Caemmerer, and Joseph A Berry (1980). "A biochemical model of photosynthetic CO 2 assimilation in leaves of C 3 species". In: *planta* 149, pp. 78–90. DOI: https://doi.org/10.1007/BF00386231.

Farquhar, Graham D and Thomas D Sharkey (1982). "Stomatal conductance and photosynthesis". In: *Annual review of plant physiology* 33.1, pp. 317–345. DOI: https://doi.org/10.1146/annurev.pp.33.060182.001533.

Feinberg, Martin (2019). "Foundations of chemical reaction network theory". In: DOI: https://doi.org/10.1007/978-3-030-03858-8.

Fell, David A (1992). "Metabolic control analysis: a survey of its theoretical and experimental development." In: *Biochemical Journal* 286.Pt 2, p. 313. DOI: https://doi.org/10.1042/bj2860313.

Flexas, Jaume and Marc Carriquí (2020). "Photosynthesis and photosynthetic efficiencies along the terrestrial plant's phylogeny: lessons for improving crop photosynthesis". In: *The Plant Journal* 101.4, pp. 964–978. DOI: https://doi.org/10.1111/tpj.14651.

Flexas, Jaume et al. (2012). "Mesophyll diffusion conductance to CO2: an unappreciated central player in photosynthesis". In: *Plant Science* 193, pp. 70–84. DOI: https://doi.org/10.1016/j.plantsci.2012.05.009.

Flügel, Franziska et al. (2017). "The Photorespiratory Metabolite 2-Phosphoglycolate Regulates Photosynthesis and Starch Accumulation in Arabidopsis". In: *The Plant Cell* 29.10, pp. 2537–2551. DOI: https://doi.org/10.1105/tpc.17.00256.

Forster, Theodor (1965). "Delocalization excitation and excitation transfer". In: *Modern quantum chemistry*.

Fuchs, Georg (2011). "Alternative pathways of carbon dioxide fixation: insights into the early evolution of life?" In: *Annual review of microbiology* 65, pp. 631–658. DOI: https://doi.org/10.1146/annurev-micro-090110-102801.

Gaffron, Hans and Kurt Wohl (1936). "Zur Theorie der Assimilation". In: *Naturwissenschaften* 24.6, pp. 81–90.

Geigenberger, Peter et al. (2017). "The unprecedented versatility of the plant thioredoxin system". In: *Trends in plant science* 22.3, pp. 249–262. DOI: https://doi.org/10.1016/j.tplants.2016.12.008.

Genty, Bernard, Jean-Marie Briantais, and Neil R Baker (1989). "The relationship between the quantum yield of photosynthetic electron transport and quenching of chlorophyll fluorescence". In: *Biochimica et Biophysica Acta*

(BBA)-General Subjects 990.1, pp. 87–92. DOI: https://doi.org/10.1016/S0304-4165(89)80016-9.

Genty, Bernard et al. (1990). "The relationship between non-photochemical quenching of chlorophyll fluorescence and the rate of photosystem 2 photochemistry in leaves". In: *Photosynthesis research* 25, pp. 249–257. DOI: https://doi.org/10.1007/BF00033166.

Giersch, Christoph and G Heinrich Krause (1991). "A simple model relating photoinhibitory fluorescence quenching in chloroplasts to a population of altered photosystem II reaction centers". In: *Photosynthesis research* 30, pp. 115–121. DOI: https://doi.org/10.1007/BF00042009.

Gillespie, Daniel T (2007). "Stochastic simulation of chemical kinetics". In: *Annu. Rev. Phys. Chem.* 58, pp. 35–55. DOI: https://doi.org/10.1146/annurev.physchem.58.032806.104637.

Gilmore, Adam M (1997). "Mechanistic aspects of xanthophyll cycle-dependent photoprotection in higher plant chloroplasts and leaves". In: *Physiologia Plantarum* 99.1, pp. 197–209. DOI: https://doi.org/10.1111/j.1399-3054.1997.tb03449.x.

Govindjee, Dmitriy Shevela, and Lars Olof Björn (2017). "Evolution of the Z-scheme of photosynthesis: a perspective". In: *Photosynthesis research* 133, pp. 5–15. DOI: https://doi.org/10.1007/s11120-016-0333-z.

Hahn, Brian D (1986). "A mathematical model of the Calvin cycle: analysis of the steady state". In: *Annals of botany* 57.5, pp. 639–653. DOI: https://doi.org/10.1093/oxfordjournals.aob.a087147.

— (1987). "A mathematical model of photorespiration and photosynthesis". In: *Annals of Botany* 60.2, pp. 157–169. DOI: https://doi.org/10.1093/oxfordjournals.aob.a087432.

Heineke, Dieter et al. (1991). "Redox transfer across the inner chloroplast envelope membrane". In: *Plant Physiology* 95.4, pp. 1131–1137. DOI: https://doi.org/10.1104/pp.95.4.1131.

Heinrich, Reinhart and Tom A Rapoport (1974). "A linear steady-state treatment of enzymatic chains: general properties, control and effector strength". In: *European journal of biochemistry* 42.1, pp. 89–95. DOI: https://doi.org/10.1111/j.1432-1033.1974.tb03318.x.

Heinrich, Reinhart and Stefan Schuster (1996). *The Regulation of Cellular Systems*. London: Chapman & Hall.

Hill, Robert (1939). "Oxygen produced by isolated chloroplasts". In: *Proceedings of the Royal Society of London. Series B-Biological Sciences* 127.847, pp. 192–210.

Hill, Robin and Fay Bendall (1960). "Function of the two cytochrome components in chloroplasts: a working hypothesis". In: *Nature* 186, pp. 136–137. DOI: https://doi.org/10.1038/186136a0.

Hoefnagel, Marcel HN, Owen K Atkin, and Joseph T Wiskich (1998). "Interdependence between chloroplasts and mitochondria in the light and the dark". In: *Biochimica et Biophysica Acta (BBA)-Bioenergetics* 1366.3, pp. 235–255. DOI: https://doi.org/10.1016/s0005-2728(98)00126-1.

Hörtensteiner, Stefan (2013). "Update on the biochemistry of chlorophyll breakdown". In: *Plant Molecular Biology* 82, pp. 505–517. DOI: https://doi.org/10.1007/s11103-012-9940-z.

Horton, Peter and Alan Hague (1988). "Studies on the induction of chlorophyll fluorescence in isolated barley protoplasts. IV. Resolution of non-photochemical quenching". In: *Biochimica et Biophysica Acta (BBA)-Bioenergetics* 932, pp. 107–115. DOI: https://doi.org/10.1016/0005-2728(88)90144-2.

Horton, Peter et al. (2008). "Photosynthetic acclimation: does the dynamic structure and macro-organisation of photosystem II in higher plant grana membranes regulate light harvesting states?" In: *The FEBS journal* 275.6, pp. 1069–1079. DOI: https://doi.org/10.1111/j.1742-4658.2008.06263.x.

Jablonsky, Jiri, Hermann Bauwe, and Olaf Wolkenhauer (2011). "Modeling the Calvin-Benson cycle". In: *BMC Systems Biology* 5.1, pp. 1–13. DOI: https://doi.org/10.1186/1752-0509-5-185.

Jessop-Fabre, Mathew M and Nikolaus Sonnenschein (2019). "Improving Reproducibility in Synthetic Biology". In: *Frontiers in Bioengineering and Biotechnology* 7, p. 18. DOI: https://doi.org/10.3389/fbioe.2019.00018.

Johnson, Jennifer E and Joseph A Berry (2021). "The role of cytochrome b6f in the control of steady-state photosynthesis: a conceptual and quantitative model". In: *Photosynthesis Research* 148.3, pp. 101–136. DOI: https://doi.org/10.1007/s11120-021-00840-4.

Joliot, Pierre (1964). "Etude cinetique de la reaction photochimique liberant l'oxygene au cours de la photosynthese." In: *CR Acad. Sci.* 258, pp. 4622–4625.

Junge, Wolfgang and Nathan Nelson (2015). "ATP synthase". In: *Annual review of biochemistry* 84, pp. 631–657. DOI: https://doi.org/10.1146/annurev-biochem-060614-034124.

Kacser, Henrik et al. (1995). "The control of flux". In: *Biochemical Society Transactions* 23.2, pp. 341–366.

Kaiser, Elias, Viviana Correa Galvis, and Ute Armbruster (2019). "Efficient photosynthesis in dynamic light environments: a chloroplast's perspective". In: *Biochemical Journal* 476.19, pp. 2725–2741. DOI: https://doi.org/10.1042/BCJ20190134.

Kaiser, Elias, Alejandro Morales, and Jeremy Harbinson (2018). "Fluctuating light takes crop photosynthesis on a rollercoaster ride". In: *Plant Physiology* 176.2, pp. 977–989. DOI: https://doi.org/10.1104/pp.17.01250.

Kalaji, Hazem M et al. (2012). "Experimental in vivo measurements of light emission in plants: a perspective dedicated to David Walker". In: *Photosynthesis Research* 114, pp. 69–96. DOI: https://doi.org/10.1007/s11120-012-9780-3.

Kalaji, Hazem M. et al. (2014). "Frequently asked questions about in vivo chlorophyll fluorescence: practical issues". In: *Photosynthesis Research* 122.2, pp. 121–158. DOI: https://doi.org/10.1007/s11120-014-0024-6.

Kalaji, Hazem M. et al. (2017). "Frequently asked questions about chlorophyll fluorescence, the sequel". In: *Photosynthesis Research* 132.1, pp. 13–66. DOI: https://doi.org/10.1007/s11120-016-0318-y.

Kalmatskaya, Olesya A. et al. (2020). "Electron transport in Tradescantia leaves acclimated to high and low light: thermoluminescence, PAM-fluorometry, and EPR studies". In: *Photosynthesis Research*. DOI: https://doi.org/10.1007/s11120-020-00767-2.

Kaňa, Radek (2013). "Mobility of photosynthetic proteins". In: *Photosynthesis Research* 116, pp. 465–479. DOI: https://doi.org/10.1007/s11120-013-9898-y.

Kato, Yuki, Ryo Nagao, and Takumi Noguchi (2016). "Redox potential of the terminal quinone electron acceptor QB in photosystem II reveals the mechanism of electron transfer regulation". In: *Proceedings of the National Academy of Sciences* 113.3, pp. 620–625. DOI: https://doi.org/10.1073/pnas.1520211113.

Kato, Yusuke and Wataru Sakamoto (June 2018). "FtsH Protease in the Thylakoid Membrane: Physiological Functions and the Regulation of Protease Activity". In: *Frontiers in Plant Science* 9, p. 855. DOI: https://doi.org/10.3389/fpls.2018.00855.

Kautsky, Hans and A Hirsch (1931). "Neue versuche zur kohlensäureassimilation". In: *Naturwissenschaften* 19.48, pp. 964–964.

Kautsky, Hans, A Hirsch, and F Davidshöfer (1932). "Energie-Umwandlungen an Grenzflächen, VI. Mitteil.: Kohlensäure-Assimilation (1.)" In: *Berichte der deutschen chemischen Gesellschaft (A and B Series)* 65.10, pp. 1762–1770.

Keller, Beat et al. (2019). "Maximum fluorescence and electron transport kinetics determined by light-induced fluorescence transients (LIFT) for photosynthesis phenotyping". In: *Photosynthesis Research* 140, pp. 221–233. DOI: https://doi.org/10.1007/s11120-018-0594-9.

Kelly, G.J. and E. Latzko (1976). "Inhibition of spinach-leaf phosphofructokinase by 2-phosphoglycollate". In: *FEBS Letters* 68.1, pp. 55–58. DOI: https://doi.org/10.1016/0014-5793(76)80403-6.

Khorobrykh, Sergey et al. (2020). "Oxygen and ROS in photosynthesis". In: *Plants* 9.1, p. 91. DOI: https://doi.org/10.3390/plants9010091.

King, Edward L and Carl Altman (1956). "A schematic method of deriving the rate laws for enzyme-catalyzed reactions". In: *The Journal of physical chemistry* 60.10, pp. 1375–1378. DOI: https://doi.org/10.1021/j150544a010.

Kirchhoff, Helmut (2013). "Architectural switches in plant thylakoid membranes". In: *Photosynthesis research* 116, pp. 481–487. DOI: https://doi.org/10.1007/s11120-013-9843-0.

Kirchhoff, Helmut, Uttama Mukherjee, and Hans-Joachim Galla (2002). "Molecular architecture of the thylakoid membrane: lipid diffusion space for plastoquinone". In: *Biochemistry* 41.15, pp. 4872–4882. DOI: https://doi.org/10.1021/bi011650y.

Kitajima, Masao and Warren L Butler (1975). "Quenching of chlorophyll fluorescence and primary photochemistry in chloroplasts by dibromothymoquinone". In: *Biochimica et Biophysica Acta (BBA)-Bioenergetics* 376.1, pp. 105–115. DOI: https://doi.org/10.1016/0005-2728(75)90209-1.

Klipp, Edda et al. (2016). *Systems biology: a textbook*. John Wiley & Sons.

Kolber, Zbigniew et al. (2005). "Measuring photosynthetic parameters at a distance: laser induced fluorescence transient (LIFT) method for remote measurements of photosynthesis in terrestrial vegetation". In: *Photosynthesis research* 84, pp. 121–129. DOI: https://doi.org/10.1007/s11120-005-5092-1.

Kolber, Zbigniew S, Ondřej Prášil, and Paul G Falkowski (1998). "Measurements of variable chlorophyll fluorescence using fast repetition rate techniques: defining methodology and experimental protocols". In: *Biochimica et Biophysica Acta (BBA)-Bioenergetics* 1367.1-3, pp. 88–106. DOI: https://doi.org/10.1016/S0005-2728(98)00135-2.

Kou, Jiancun et al. (2012). "The time course of photoinactivation of photosystem II in leaves revisited". In: *Photosynthesis research* 113, pp. 157–164. DOI: https://doi.org/10.1007/s11120-012-9743-8.

Kromdijk, Johannes et al. (2016). "Improving photosynthesis and crop productivity by accelerating recovery from photoprotection". In: *Science* 354.6314, pp. 857–861. DOI: https://doi.org/10.1126/science.aai8878.

Ksenzhek, Octavian S and Alexander G Volkov (1998). *Plant energetics*. Elsevier.

Kühlbrandt, Werner (2019). "Structure and mechanisms of F-type ATP synthases". In: *Annual Review of Biochemistry* 88, pp. 515–549. DOI: https://doi.org/10.1146/annurev-biochem-013118-110903.

Kuhlgert, Sebastian et al. (2016). "MultispeQ Beta: a tool for large-scale plant phenotyping connected to the open PhotosynQ network". In: *Royal Society Open Science* 3, p. 160592. DOI: https://doi.org/10.1098/rsos.160592.

Lakowicz, Joseph R (2006). *Principles of fluorescence spectroscopy*. Springer.

Lavergne, Jerome and Hans-Wilhelm Trissl (1995). "Theory of fluorescence induction in photosystem II: derivation of analytical expressions in a model including exciton-radical-pair equilibrium and restricted energy transfer between photosynthetic units". In: *Biophysical journal* 68.6, pp. 2474–2492. DOI: https://doi.org/10.1016/S0006-3495(95)80429-7.

Lazár, Dušan and Gert Schansker (2009). "Models of chlorophyll a fluorescence transients". In: *Photosynthesis in silico: understanding complexity from molecules to ecosystems*, pp. 85–123.

Lazár, Dušan et al. (1997). "Mathematical modeling of changes in chlorophyll fluorescence induction caused by herbicides". In: *Pesticide Biochemistry and Physiology* 57.3, pp. 200–210. DOI: https://doi.org/10.1006/pest.1997.2277.

Lee, H-Y, Y-N Hong, and WS Chow (2001). "Photoinactivation of photosystem II complexes and photoprotection by non-functional neighbours in Capsicum annuum L. leaves". In: *Planta* 212, pp. 332–342. DOI: https://doi.org/10.1007/s004250000398.

Li, Lei, Eva-Mari Aro, and A Harvey Millar (2018). "Mechanisms of photodamage and protein turnover in photoinhibition". In: *Trends in plant science* 23.8, pp. 667–676. DOI: https://doi.org/10.1016/j.tplants.2018.05.004.

Lichtman, Jeff and José Angel Conchello (2006). "Fluorescence Microscopy". In: *Nature Methods* 2, pp. 910–919. DOI: https://doi.org/10.1038/nmeth817.

Liebermeister, Wolfram and Edda Klipp (2006). "Bringing metabolic networks to life: convenience rate law and thermodynamic constraints". In: *Theoretical Biology and Medical Modelling* 3.1, p. 41. DOI: https://doi.org/10.1186/1742-4682-3-41.

Long, Stephen P. et al. (2006). "Can improvement in photosynthesis increase crop yields?" In: *Plant, Cell & Environment* 29.3, pp. 315–330. DOI: https://doi.org/10.1111/j.1365-3040.2005.01493.x.

Malkin, Shmuel and Bessel Kok (1966). "Fluorescence induction studies in isolated chloroplasts I. Number of components involved in the reaction and quantum yields". In: *Biochimica et Biophysica Acta (BBA)-Biophysics including Photosynthesis* 126.3, pp. 413–432. DOI: https://doi.org/10.1016/0926-6585(66)90001-X.

Malnoë, Alizée (2018). "Photoinhibition or photoprotection of photosynthesis? Update on the (newly termed) sustained quenching component qH". In: *Environmental and Experimental Botany* 154, pp. 123–133. DOI: https://doi.org/10.1016/j.envexpbot.2018.05.005.

Massonnet, Catherine et al. (2010). "Probing the reproducibility of leaf growth and molecular phenotypes: a comparison of three Arabidopsis accessions cultivated in ten laboratories". In: *Plant Physiology* 152.4, pp. 2142–2157. DOI: https://doi.org/10.1104/pp.109.148338.

Matsubara, Shizue and Wah Soon Chow (2004). "Populations of photoinactivated photosystem II reaction centers characterized by chlorophyll a fluorescence lifetime in vivo". In: *Proceedings of the National Academy of Sciences* 101.52, pp. 18234–18239. DOI: https://doi.org/10.1073/pnas.0403857102.

Matuszyńska, Anna, Nima P Saadat, and Oliver Ebenhöh (2019). "Balancing energy supply during photosynthesis–a theoretical perspective". In: *Physiologia plantarum* 166.1, pp. 392–402. DOI: https://doi.org/10.1111/ppl.12962.

Matuszyńska, Anna et al. (2016). "A mathematical model of non-photochemical quenching to study short-term light memory in plants".

In: *Biochimica et Biophysica Acta (BBA)-Bioenergetics* 1857.12, pp. 1860–1869. DOI: https://doi.org/10.1016/j.bbabio.2016.09.003.

Maxwell, Kate and Giles N. Johnson (2000). "Chlorophyll fluorescence–a practical guide". In: *Journal of Experimental Botany* 51.345, pp. 659–668. DOI: 10.1093/jexbot/51.345.659.

Melis, Anastasios (1985). "Functional properties of photosystem IIβ in spinach chloroplasts". In: *Biochimica et Biophysica Acta (BBA)-Bioenergetics* 808.2, pp. 334–342. DOI: https://doi.org/10.1016/0005-2728(85)90017-9.

Meurer, Aaron et al. (2017). "SymPy: symbolic computing in Python". In: *PeerJ Computer Science* 3, e103. DOI: https://doi.org/10.7717/peerj-cs.103.

Minagawa, Jun (2011). "State transitions–the molecular remodeling of photosynthetic supercomplexes that controls energy flow in the chloroplast". In: *Biochimica et Biophysica Acta (BBA)-Bioenergetics* 1807.8, pp. 897–905. DOI: https://doi.org/10.1016/j.bbabio.2010.11.005.

Mitchell, Peter (1979). "Keilin's respiratory chain concept and its chemiosmotic consequences". In: *Science* 206.4423, pp. 1148–1159. DOI: https://doi.org/10.1126/science.388618.

Mohammed, Gina H et al. (2019). "Remote sensing of solar-induced chlorophyll fluorescence (SIF) in vegetation: 50 years of progress". In: *Remote sensing of environment* 231, p. 111177. DOI: https://doi.org/10.1016/j.rse.2019.04.030.

Morales, Alejandro et al. (2018a). "Dynamic modelling of limitations on improving leaf CO2 assimilation under fluctuating irradiance". In: *Plant, cell & environment* 41.3, pp. 589–604. DOI: https://doi.org/10.1111/pce.13119.

Morales, Alejandro et al. (2018b). "In silico analysis of the regulation of the photosynthetic electron transport chain in C3 plants". In: *Plant physiology* 176.2, pp. 1247–1261. DOI: https://doi.org/10.1104/pp.17.00779.

Muller, Patricia, Xiao-Ping Li, and Krishna K Niyogi (2001). "Non-photochemical quenching. A response to excess light energy". In: *Plant physiology* 125.4, pp. 1558–1566. DOI: https://doi.org/10.1104/pp.125.4.1558.

Murata, Norio and Yoshitaka Nishiyama (2018). "ATP is a driving force in the repair of photosystem II during photoinhibition". In: *Plant, cell & environment* 41.2, pp. 285–299. DOI: https://doi.org/10.1111/pce.13108.

Murchie, Erik H and Tracy Lawson (2013). "Chlorophyll fluorescence analysis: a guide to good practice and understanding some new applications". In: *Journal of Experimental Botany* 64.13, pp. 3983–3998. DOI: https://doi.org/10.1093/jxb/ert208.

National Academies of Sciences, Engineering, and Medicine (2019). *Reproducibility and Replicability in Science*. The National Academies Press. Chap. 5. DOI: https://doi.org/10.17226/25303.

Nevo, Reinat et al. (2012). "Composition, architecture and dynamics of the photosynthetic apparatus in higher plants". In: *The Plant Journal* 70.1, pp. 157–176. DOI: https://doi.org/10.1111/j.1365-313X.2011.04876.x.

Nicholls, David G (2013). *Bioenergetics*. Academic press. DOI: https://doi.org/10.1016/B978-012518121-1/50000-2.

Nickelsen, Kärin and G Govindjee (2011). "The Maximum Quantum Yield Controversy". In: *Otto Warburg and the "Midwest-Gang". Bern: Bern Studies in History and Philosophy of Science*.

Nies, Tim, Shizue Matsubara, and Oliver Ebenhoeh (2023). "A mathematical model of photoinhibition: exploring the impact of quenching processes". In: *bioRxiv*. DOI: 10.1101/2023.09.12.557336.

Nies, Tim et al. (2021). "Chlorophyll fluorescence: How the quality of information about PAM instrument parameters may affect our research". In: *bioRxiv*. DOI: https://doi.org/10.1101/2021.05.12.443801.

Nies, Tim et al. (2023). "What controls carbon sequestration in plants under which conditions?" In: *Biosystems* 231, p. 104968. DOI: https://doi.org/10.1016/j.biosystems.2023.104968.

Nilkens, Manuela et al. (2010). "Identification of a slowly inducible zeaxanthin-dependent component of non-photochemical quenching of chlorophyll fluorescence generated under steady-state conditions in Arabidopsis". In: *Biochimica et Biophysica Acta (BBA)-Bioenergetics* 1797.4, pp. 466–475. DOI: https://doi.org/10.1016/j.bbabio.2010.01.001.

Oguchi, Riichi et al. (2011). "Intra-leaf gradients of photoinhibition induced by different color lights: implications for the dual mechanisms of photoinhibition and for the application of conventional chlorophyll fluorometers". In: *New Phytologist* 191.1, pp. 146–159. DOI: https://doi.org/10.1111/j.1469-8137.2011.03669.x.

Okayama, Shigeki (1976). "Redox potential of plastoquinone A in spinach chloroplasts". In: *Biochimica et Biophysica Acta (BBA)-Bioenergetics* 440.2, pp. 331–336. DOI: https://doi.org/10.1016/0005-2728(76)90067-0.

Ort, Donald R. et al. (2015). "Redesigning photosynthesis to sustainably meet global food and bioenergy demand". In: *Proceedings of the National Academy of Sciences* 112.28, pp. 8529–8536. DOI: https://doi.org/10.1073/pnas.1424031112.

Osmond, Charles B (1978). "Crassulacean acid metabolism: a curiosity in context". In: *Annual Review of Plant Physiology* 29.1, pp. 379–414. DOI: https://doi.org/10.1146/annurev.pp.29.060178.002115.

Paillotin, Guy (1976). "Capture frequency of excitations and energy transfer between photosynthetic units in the photosystem II". In: *Journal of theoretical biology* 58.1, pp. 219–235. DOI: https://doi.org/10.1016/0022-5193(76)90149-1.

Palsson, Bø (2015). *Systems biology: constraint-based reconstruction and analysis*.

Papageorgiou, George and Govindjee (1968). "Light-Induced Changes in the Fluorescence Yield of Chlorophyll a In Vivo". In: *Biophysical Journal* 8.11, pp. 1316–1328. DOI: https://doi.org/10.1016/s0006-3495(68)86558-0.

Papageorgiou, George Christos (2004). *Chlorophyll a fluorescence: a signature of photosynthesis*. Springer.

Parry, Martin AJ et al. (2008). "Rubisco regulation: a role for inhibitors". In: *Journal of experimental botany* 59.7, pp. 1569–1580. DOI: https://doi.org/10.1093/jxb/ern084.

Pätsikkä, Eija, Eva-Mari Aro, and Esa Tyystjärvi (1998). "Increase in the Quantum Yield of Photoinhibition Contributes to Copper Toxicity in Vivo1". In: *Plant Physiology* 117.2, pp. 619–627. DOI: https://doi.org/10.1104/pp.117.2.619.

Pettersson, Gosta and Ulf Ryde-Pettersson (1988). "A mathematical model of the Calvin photosynthesis cycle". In: *European Journal of Biochemistry* 175.3, pp. 661–672. DOI: https://doi.org/10.1111/j.1432-1033.1988.tb14242.x.

Pfundel, Erhard E and Richard A Dilley (1993). "The pH dependence of violaxanthin deepoxidation in isolated pea chloroplasts". In: *Plant Physiology* 101.1, pp. 65–71. DOI: https://doi.org/10.1104/pp.101.1.65.

Poolman, Mark G, David A Fell, and Simon Thomas (2000). "Modelling photosynthesis and its control". In: *Journal of Experimental Botany* 51.suppl_1, pp. 319–328. DOI: https://doi.org/10.1093/jexbot/51.suppl_1.319.

Poolman, Mark G et al. (2007). "Modular decomposition of metabolic systems via null-space analysis". In: *Journal of theoretical biology* 249.4, pp. 691–705. DOI: https://doi.org/10.1016/j.jtbi.2007.08.005.

Quero, Gastón et al. (2020). "Genetic architecture of photosynthesis energy partitioning as revealed by a genome-wide association approach". In: *Photosynthesis Research*. DOI: https://doi.org/10.1007/s11120-020-00721-2.

Raesch, Anna R et al. (2014). "Field observations with laser-induced fluorescence transient (LIFT) method in barley and sugar beet". In: *Agriculture* 4.2, pp. 159–169. DOI: https://doi.org/10.3390/agriculture4020159.

Raines, Christine A et al. (2000). "Investigating the role of the thiol-regulated enzyme sedoheptulose-1, 7-bisphosphatase in the control of photosynthesis". In: *Physiologia Plantarum* 110.3, pp. 303–308. DOI: https://doi.org/10.1111/j.1399-3054.2000.1100303.x.

Raven, John A (2009). "Contributions of anoxygenic and oxygenic phototrophy and chemolithotrophy to carbon and oxygen fluxes in aquatic environments". In: *Aquatic Microbial Ecology* 56.2-3, pp. 177–192. DOI: https://doi.org/10.3354/ame01315.

— (2011). "The cost of photoinhibition". In: *Physiologia plantarum* 142.1, pp. 87–104. DOI: https://doi.org/10.1111/j.1399-3054.2011.01465.x.

Rochaix, Jean-David (2011). "Regulation of photosynthetic electron transport". In: *Biochimica et Biophysica Acta (BBA) - Bioenergetics* 1807.3 (3), pp. 375–383. DOI: https://doi.org/10.1016/j.bbabio.2010.11.010.

Rohwer, Johann M (2012). "Kinetic modelling of plant metabolic pathways". In: *Journal of Experimental Botany* 63.6, pp. 2275–2292. DOI: https://doi.org/10.1093/jxb/ers080.

Ruban, Alexander V. (2016). "Nonphotochemical Chlorophyll Fluorescence Quenching: Mechanism and Effectiveness in Protecting Plants from Photodamage". In: *Plant Physiology* 170.4, pp. 1903–1916. DOI: https://doi.org/10.1104/pp.15.01935.

Rüdiger, Wolfhart and Bernhard Grimm (2006). "Chlorophyll metabolism, an overview". In: *Chlorophylls and Bacteriochlorophylls: biochemistry, biophysics, functions and applications*, pp. 133–146.

Rungrat, Tepsuda et al. (2016). "Using phenomic analysis of photosynthetic function for abiotic stress response gene discovery". In: *The Arabidopsis Book/American Society of Plant Biologists* 14. DOI: https://doi.org/10.1199/tab.0185.

Rungrat, Tepsuda et al. (2019). "A genome-wide association study of non-photochemical quenching in response to local seasonal climates in Arabidopsis thaliana". In: *Plant Direct* 3.5, e00138. DOI: https://doi.org/10.1002/pld3.138.

Saadat, Nima P et al. (2021). "Computational analysis of alternative photosynthetic electron flows linked with oxidative stress". In: *Frontiers in plant science* 12, p. 750580. DOI: https://doi.org/10.3389/fpls.2021.750580.

Sage, Rowan F (2004). "The evolution of C4 photosynthesis". In: *New phytologist* 161.2, pp. 341–370. DOI: https://doi.org/10.1111/j.1469-8137.2004.00974.x.

Samson, G, O Prášil, and B Yaakoubd (1999). "Photochemical and thermal phases of chlorophyll a fluorescence". In: *Photosynthetica* 37, pp. 163–182. DOI: https://doi.org/10.1023/A:1007095619317.

Sarvikas, Päivi, Taina Tyystjärvi, and Esa Tyystjärvi (2010). "Kinetics of prolonged photoinhibition revisited: photoinhibited photosystem II centres do not protect the active ones against loss of oxygen evolution". In: *Photosynthesis research* 103, pp. 7–17. DOI: https://doi.org/10.1007/s11120-009-9496-1.

Schöttler, Mark Aurel, Helmut Kirchhoff, and Engelbert Weis (2004). "The role of plastocyanin in the adjustment of the photosynthetic electron transport to the carbon metabolism in tobacco". In: *Plant Physiology* 136.4, pp. 4265–4274. DOI: https://doi.org/10.1104/pp.104.052324.

Schreiber, Ulrich (2004). "Pulse-amplitude-modulation (PAM) fluorometry and saturation pulse method: an overview". In: Springer, pp. 279–319. DOI: https://doi.org/10.1007/978-1-4020-3218-9_11.

Schreiber, Ulrich, Christof Klughammer, and Gert Schansker (2019). "Rapidly reversible chlorophyll fluorescence quenching induced by pulses of supersaturating light in vivo". In: *Photosynthesis Research* 142, pp. 35–50. DOI: https://doi.org/10.1007/s11120-019-00644-7.

Schreiber, Ulrich, U. Schliwa, and W. Bilger (1986). "Continuous recording of photochemical and non-photochemical chlorophyll fluorescence quenching with a new type of modulation fluorometer". In: *Photosynth Res.* 10, pp. 51–62. DOI: https://doi.org/10.1007/bf00024185.

Sekulska-Nalewajko, Joanna et al. (2019). "Spatial referencing of chlorophyll fluorescence images for quantitative assessment of infection propagation in leaves demonstrated on the ice plant: Botrytis cinerea pathosystem". In: *Plant Methods*. 15. DOI: https://doi.org/10.1186/s13007-019-0401-4.

Sharkey, Thomas D. (1988). "Estimating the rate of photorespiration in leaves". In: *Physiologia Plantarum* 73.1, pp. 147–152. DOI: https://doi.org/10.1111/j.1399-3054.1988.tb09205.x.

Steuer, Ralf et al. (2006). "Structural kinetic modeling of metabolic networks". In: *Proceedings of the National Academy of Sciences* 103.32, pp. 11868–11873. DOI: https://doi.org/10.1073/pnas.0600013103.

Stiehl, HH and Horst T Witt (1969). "Quantitative treatment of the function of plastoquinone in photosynthesis". In: *Zeitschrift für Naturforschung B* 24.12, pp. 1588–1598. DOI: https://doi.org/10.1515/znb-1969-1219.

Stirbet, Alexandrina and Govindjee (2016). "The slow phase of chlorophyll a fluorescence induction in silico: origin of the S–M fluorescence rise". In: *Photosynthesis research* 130, pp. 193–213. DOI: https://doi.org/10.1007/s11120-016-0243-0.

Stirbet, Alexandrina et al. (2011). "On the relation between the Kautsky effect (chlorophyll a fluorescence induction) and photosystem II: basics and applications of the OJIP fluorescence transient". In: *Journal of Photochemistry and Photobiology B: Biology* 104.1-2, pp. 236–257. DOI: https://doi.org/10.1016/j.jphotobiol.2010.12.010.

Stirbet, Alexandrina et al. (2014). "Modeling Chlorophyll *a* Fluorescence transient: Relation to Photosynthesis". In: *Biochemistry (Moscow)* 79, pp. 291–323. DOI: https://doi.org/10.1134/s0006297914040014.

Stirbet, Alexandrina et al. (2019). "Photosynthesis: Basics, History, and Modeling". In: *Annals of Botany* 126.4, mcz171. DOI: https://doi.org/10.1093/aob/mcz171.

Stitt, Mark, Ross McC. Lilley, and Hans W. Heldt (Oct. 1982). "Adenine Nucleotide Levels in the Cytosol, Chloroplasts, and Mitochondria of Wheat Leaf Protoplasts". In: *Plant Physiology* 70.4, pp. 971–977. DOI: https://doi.org/10.1104/pp.70.4.971.

Stitt, Mark and D Schulze (1994). "Does Rubisco control the rate of photosynthesis and plant growth? An exercise in molecular ecophysiology". In: *Plant, cell & environment* 17.5, pp. 465–487. DOI: https://doi.org/10.1111/j.1365-3040.1994.tb00144.x.

Suzuki, Shinnichiro, Takeshi Sakurai, and Takuo Nakajima (1987). "Characterization of plastocyanin isolated from Brazilian elodea". In: *Plant and cell physiology* 28.5, pp. 825–831. DOI: https://doi.org/10.1093/oxfordjournals.pcp.a077363.

Taiz, Lincoln et al. (2015). *Plant physiology and development*. Ed. 6. Sinauer Associates Incorporated.

Taylor, Chris F et al. (2007). "The minimum information about a proteomics experiment (MIAPE)". In: *Nature biotechnology* 25.8, pp. 887–893. DOI: https://doi.org/10.1038/nbt1329.

Tikkanen, Mikko et al. (2008). "Core protein phosphorylation facilitates the repair of photodamaged photosystem II at high light". In: *Biochimica et Biophysica Acta (BBA)-Bioenergetics* 1777.11, pp. 1432–1437. DOI: https://doi.org/10.1016/j.bbabio.2008.08.004.

Tyystjärvi, Esa, Pirkko Mäenpää, and Eva-Mari Aro (1994). "Mathematical modelling of photoinhibition and Photosystem II repair cycle. I. Photoinhibition and D1 protein degradation in vitro and in the absence of chloroplast protein synthesis in vivo". In: *Photosynthesis Research* 41, pp. 439–449. DOI: https://doi.org/10.1007/bf02183046.

Uys, Lafras et al. (2007). "Kinetic model of sucrose accumulation in maturing sugarcane culm tissue". In: *Phytochemistry* 68.16-18, pp. 2375–2392. DOI: https://doi.org/10.1016/j.phytochem.2007.04.023.

Van Niel, CB (1941). "The bacterial photosyntheses and their importance for the general problem of photosynthesis". In: *Advances in enzymology* 1, pp. 263–328.

Vieira, Sónia et al. (2013). "Photosynthesis Assessment in Microphytobenthos Using Conventionaland Imaging Pulse Amplitude Modulation Fluorometry". In: *Photochemistry and Photobiology* 89, pp. 97–102. DOI: https://doi.org/0.1111/j.1751-1097.2012.01224.x.

Virtanen, Pauli et al. (2020). "SciPy 1.0: Fundamental Algorithms for Scientific Computing in Python". In: *Nature Methods*. DOI: https://doi.org/10.1038/s41592-019-0686-2.

Von Caemmerer, Susanne von and Graham D Farquhar (1981). "Some relationships between the biochemistry of photosynthesis and the gas exchange of leaves". In: *Planta* 153, pp. 376–387. DOI: https://doi.org/10.1007/BF00384257.

Walker, Berkley J. et al. (2016). "The Costs of Photorespiration to Food Production Now and in the Future". In: *Annual Review of Plant Biology* 67.1, pp. 107–129. DOI: https://doi.org/10.1146/annurev-arplant-043015-111709.

Wang, Rui-Sheng, Assieh Saadatpour, and Reka Albert (2012). "Boolean modeling in systems biology: an overview of methodology and applications". In: *Physical biology* 9.5, p. 055001. DOI: https://doi.org/10.1088/1478-3975/9/5/055001.

Watanabe, Chihiro KA et al. (2016). "Mitochondrial alternative pathway-associated photoprotection of photosystem II is related to the photorespiratory pathway". In: *Plant and Cell Physiology* 57.7, pp. 1426–1431. DOI: https://doi.org/10.1093/pcp/pcw036.

Way, Danielle A and Robert W Pearcy (2012). "Sunflecks in trees and forests: from photosynthetic physiology to global change biology". In: *Tree Physiology* 32.9, pp. 1066–1081. DOI: https://doi.org/10.1093/treephys/tps064.

Wilken, St. Elmo et al. (2022). "Interrogating the effect of enzyme kinetics on metabolism using differentiable constraint-based models". In: *Metabolic Engineering* 74, pp. 72–82. DOI: https://doi.org/10.1016/j.ymben.2022.09.002.

Witt, Heike et al. (2003). "Species-specific differences of the spectroscopic properties of P700: analysis of the influence of non-conserved amino acid residues by site-directed mutagenesis of photosystem I from Chlamydomonas reinhardtii". In: *Journal of Biological Chemistry* 278.47, pp. 46760–46771. DOI: https://doi.org/10.1074/jbc.M304776200.

Witzel, Franziska, Jan Götze, and Oliver Ebenhöh (2010). "Slow deactivation of ribulose 1, 5-bisphosphate carboxylase/oxygenase elucidated by mathematical models". In: *The FEBS Journal* 277.4, pp. 931–950. DOI: https://doi.org/10.1111/j.1742-4658.2009.07541.x.

Yamada, Shoya, Hiroshi Ozaki, and Ko Noguchi (2020). "The mitochondrial respiratory chain maintains the photosynthetic electron flow in Arabidopsis thaliana leaves under high-light stress". In: *Plant and Cell Physiology* 61.2, pp. 283–295. DOI: https://doi.org/10.1093/pcp/pcz193.

Zaks, Julia et al. (2012). "A kinetic model of rapidly reversible nonphotochemical quenching". In: *Proceedings of the National Academy of Sciences* 109.39, pp. 15757–15762. DOI: https://doi.org/10.1073/pnas.1211017109.

Zavafer, Alonso (2021). "A theoretical framework of the hybrid mechanism of photosystem II photodamage". In: *Photosynthesis Research* 149.1-2, pp. 107–120. DOI: https://doi.org/10.1007/s11120-021-00843-1.

Zhao, Honglong et al. (2020). "Why an increase in activity of an enzyme in the Calvin–Benson cycle does not always lead to an increased photosynthetic CO2 uptake rate?–a theoretical analysis". In: *in silico Plants* 3.1. DOI: https://doi.org/10.1093/insilicoplants/diaa009.

Zhu, Xin-Guang et al. (2005). "Chlorophyll a fluorescence induction kinetics in leaves predicted from a model describing each discrete step of excitation energy and electron transfer associated with photosystem II". In: *Planta* 223, pp. 114–133. DOI: https://doi.org/10.1007/s00425-005-0064-4.